L. I. KARBIVSKA
V. L. KARBIVSKII

APATITES AND TETRAOXIDE COMPOUNDS

PROJECT
«UKRAINIAN SCIENTIFIC BOOK
IN A FOREIGN LANGUAGE»

KYIV
AKADEMPERIODYKA
2019

UDK [53+54]:549.753.1
K 21

doi: http://org/10.15407/akademperiodyka.390.232

Reviewers:

BRIK Aleksandr B.,
Corresponding Member of NAS of Ukraine (Nanophysics of Minerals),
Professor, Doctor of Physical and Mathematical Sciences

VASYLYEV Mykhailo O.,
Professor, Doctor of Physical and Mathematical Sciences

Approved for publication by G.V. Kurdyumov Institute
for Metal Physics of the NAS of Ukraine
(June, 26, 2018, Protocol No. 6)

Publication was funded in the frame of the Target Complex
Program "Creation and Development of Scientific Publishing Complex
of the National Academy of Sciences of Ukraine"

Karbivska L.I.

K 21 Apatites and tetraoxide compounds / L. I. Karbivska, V. L. Karbivskii; G.V. Kurdyumov Institute for Metal Physics of the NAS of Ukraine. – Kyiv : Akademperiodyka, 2019. — 232 p.

ISBN 978-966-360-390-2

The monograph is devoted to the electronic structure, synthesis, properties and applications of apatites. Contains extensive factual material on the study of the atomic and electronic structure of specific systems. Modern concepts of the structure of crystalline and disordered apatite-like structures, as well as physico-chemical, medical-biological, ecological and technological aspects of application are considered. Particular attention is paid to theoretical and applied developments in the field of functional apatite-like nanomaterials. Features of the electronic structure of natural apatites are described.

For specialists in the field of physics and chemistry of apatites who have deal with the research, development and application of new materials, as well as teachers, postgraduates and students of relevant specialties.

UDK [53+54]:549.753.1

ISBN 978-966-360-390-2

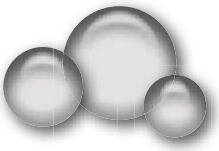

INTRODUCTION

Problems of ecology and health of a man, life prolongation and its distribution beyond the limits of the planet become main points of the beginning of the third millenium for mankind. Thus one of basic problems on this way is research and working out of technologies of obtaining of materials of medical-biological and ecological application. Apatite materials are in the lead on publishing degree and volume of spent researches in this direction.

Minerals and synthetic compounds with structural type of apatite form the big family: $A_{10}(XO_4)_6Y_2$ (A = Ca, Sr, Ba, Pb, Na, Mn, Cd, Fe, K, Li, rare-earth elements (REE); X = P, Si, Ge, As, Cr, N, V, S; Y = F, Cl, OH, O, Br, J, CO_3).

Wide circulation in bio- and a lithosphere along with features of electronic and crystal structure define their direct influence on various aspects of technical, ecological and biological application. Under the condition of the decision of some scientific and technical problems on creation of apatite-like materials with necessary parameters, their use in a science and practice promises revolutionary changes.

Materials on a basis of apatite-like compounds can find and already find their application in computer engineering, at creation of quantum generators, in the field of communication means, smart biosensors and bioelectronic devices, in energetics, in nano-medicine, in nanobionics and space researches.

The programme Advanced Life Support (ALS) was recenty approved by the space agency NASA. Within the limits of the program complex researches of apatite-like compounds with the purpose of their use, as source of soil phosphorus and oxygen, for long-term space missions and settlements on the Moon and Mars are conducted. Today it is possible to conclude with confidence that in modern materials technology the new direction — *apatite science* was generated.

Expansion of physical properties of apatites, no less than other compounds, is defined mainly by isomorphic replacements. The wide spectrum of iso- and heterovalency replacements of compounds of apatite series, determined by anomalous limits of nonstoichiometry composition, causes their use as luminescent and laser materials, and also matrixes of a burial place of a radioactive and toxic waste. Mechanical, optical, thermodynamic, catalytic and a number of other characteristics of such objects possess the unusual properties which parameters can be operated effectively by isomorphic replacements both in cation, and anion sublattice.

Establishment of fundamental principles of the structural organization and management of physicochemical properties of apatite-like structures by means of isomorphic replacements is possible only under the condition of an establishment of laws of formation of electronic structure depending on the composition, condition of synthesis, changes in dimention and topology of key elements, binding between features of composition and structure of apatite-like compounds and electronic structure.

One of the important factors, which is influencing on properties is the structural condition of substance. Formation of methodology of studying of properties and synthesis of apatite-like nanostructures has led to considerable progress in this vast area. The substance in nanometer scale gets new properties in comparison both with separate atoms and with a massive firm body. Besides special properies of isolated nanoclusters, unusual qualities of substance arise at association of clusters in nanostructure or at formation of matrix nanosystems. Real or potential practical applications of apatites are caused, mainly, by features of their nanostructure. Novelty of properties of nanodisperse apatite-like compouns puts these materials abreast the most perspective ones in creation of a wide range of applications.

Nanostructured materials as functional superadsorbents are potentially significant for high-sensitivity methods of control and clearing of environment. Their anomalous reactionary ability is caused by a considerable quantity of the torn off chemical bonds and the high specific surface reaching of several hundreds of square meters on gram. Such a structure is created in materials with big positive (nanopowders) and negative curvature of a surface (nano- and mesoporous systems). In this number of materials apatite-like nanosystems occupy one of the leading positions as possess a wide spectrum of adsorbtional properties, absorbing both light elements (H, O, C) and heavy metals (Sr, Pb, transuranium elements).

Apatite-like materials are represented by difficult objects, formation conditions, stability, physical and chemical properties of which are defined not only by a nuclear skeleton and type of crystal structure, but also by the presence of imperfections of vrious kinds of crystals: defects, impurity centers, superficial states, etc. Therefore, methods applying for the adequate strict description of a real material, should consider all variety of the factors influencing on finding of properties. In this sense, physical methods of research are one of the major tools of studying of substance structure. Creation of new materials with the set properties is impossible without wide use of new physical

methods of research of substances and methods of quantum-mechanical modeling of their electronic structure. The arsenal of modern physical methods is so extensive, and their application is so various that regular considerations along with theoretical principles and perfection of a technical embodiment of possibilities of their practical use is required. In first three chapters questions on methods of research and physicochemical properties of apatite materials contain. In view of that these chapters have mostly a review character they don't contain a final part with conclusions.

Our previous book — ***Apatites***, got out in 2002 was mostly realization of necessity of ordering of collected by that time in the scientific literature array of different aspects data on apatite materials and consequently contained insignificant part of a research material of authors. The present monography summarizes twenty years' experience of authors in this area. Results of research of an electronic structure of stoichometric apatites, isomorphically substituted in cation and anion sublattice, biogene and artificial nanocrytalls of apatites are given. Properties and morphological features of compounds depending on the structural organization are described. Questions of practical application of apatite materials are considered.

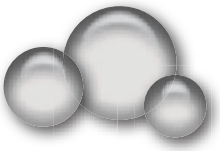

ABBREVIATIONS

HAP — hydroxyapatite
FAP — fluorapatite
ClAP — chlorapatite
OCP — octacalcium phosphate
2DHAP — two-dimensional crystalline hydroxyapatite
TCP — tricalcium phosphate
ASP — amorphous strontium phosphate
α-TCP — α-tricalcium phosphate (α-$Ca_3(PO_4)_2$)
β-TCP — β-tricalcium phosphate (β-$Ca_3(PO_4)_2$)
TTCP — tetracalcium phosphate
EXAFS — extended X-ray absorption fine structure
XANES — X-ray absorption near edge structure
Pb-HAP — lead hydroxyapatite $Pb_{10}(PO_4)_6(OH)_2$
Sr-HAP — strontium hydroxyapatite $Sr_{10}(PO_4)_6(OH)_2$
X_α-SW — X_α-SW cluster calculation
ACP — amorphous calcium phosphate
IR — infrared spectroscopy
LMTO — linear method of MT-orbitals
TDOS — total densities of states
REM — rare-earth metal
XPS — X-ray photoelectron spectroscopy
Ca-HAP — calcium hydroxyapatite $Ca_{10}(PO_4)_6(OH)_2$
Ca-FAP — calcium fluorapatite $Ca_{10}(PO_4)_6 F_2$
Ca-ClAP — calcium chlorapatite $Ca_{10}(PO_4)_6Cl_2$
FTIR — Fourier transform infrared spectroscopy
NMR — nuclear magnetic resonance
EPR — electron paramagnetic resonance
DENR — double electron-nuclear resonance
SEM — scanning electron microscopy

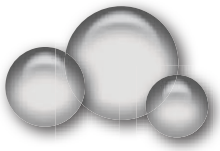

CHAPTER 1

STRUCTURE AND SYNTHESIS OF APATITES. FUNDAMENTAL ASPECT

The industrial production of synthetical apatites is determined by the increase of their use in different forms, for example, in form of porous and dense ceramic, powders and films. The increase of number of techniques of apatite synthesis gives a possibility to change their characteristics purposefully. There are two chemical approaches to date: waterless ("dry") and "wet". The most prevailing waterless methods including mechanochemical one, are realized in solid-state reactions between compounds of calcium and phosphorus and have along with the disadvantages a number of preferences when obtaining stoichiometric powders (Ca/P = 1.67). Apatite film coatings are deposited on the metallic and ceramic supports. Bulk monocrystals find a practical application as lasing medium, and also in the basic research.

The work of T. Kanazawa [1] summarizes well-known by the end of eighties the apatites synthesis techniques and information about morphology of produced apatites.

In the given chapter the structure and features of crystal chemistry of apatites data are presented, and also the production technology of monocrystals, thin films, powders and ceramics with the prescribed characteristics (particularly porosity, mechanical strength and others). Also the fundamental problems of nanotechnology of these structures are discussed.

1.1. Structure and synthesis of stoichiometric apatites

Apatites is the class of compounds with the structure that belongs generally to the hexagonal spatial group $P6_3/m$ (figure 1.1) and have the common chemical composition:

$$Me_{10}(ZO_4)_6X_2,$$

where Me^{n+}, n = 1 ÷ 3; Z^{m+}, m = 1 ÷ 3; X^{k-} — anion with k = 1 ÷ 3 or vacancy (□, k = 0), for example:

Me^{n+}	Ca	Pb	Cd	Sr	Ni	Eu	Al	Y	La	Ce	Na	K
Z^{m+}	P	As	V	Cr	Si	C	Al	S	Re			
X^{k-}	OH	F	Cl	Br	I	O	N	CO_3	□			

The main and the most prevailing apatite family representative is calcium hydroxyapatite ($Ca_{10}(PO_4)_6(OH)_2$, Ca-HAP), where metal ions occupy two different crystallographic positions: the column of calcium atoms by z = 0, 1/2 (Ca^{2+}) and screw axis with z = 1/4, 3/4 (Ca^{2+}). The projections of such three screw axes of Ca^{2+} ions form triangles on the mirror plain, which is located along sextic screw axis. The position of OH^- along the axis *c* is specified with the neutron diffraction method [1].

The crystal structure of $M_{10}(PO_4)_6X_2$ samples, where M = Pb, Ca and X = OH, F, Cl or Br, was determined with the method of synchrotron X-ray analysis of powders and neutronography [2]. The lattice of all the compounds is hexagonal and belongs to the $P6_3/m$ spatial group (Table 1.1)

In the concerned compounds, anion with $M_{(2)}$ atoms the most strongly, which is determined by their position in the triangular fragment. In $Ca_{10}(PO_4)_6X_2$ ion F^- is located in the triangle plane, whereas large OH^- and Cl^--anions are located above and

Table 1.1. **Unit cell parameters (Å) of synthetical hydroxyapatite.**

Compound	*a, Å*	*c, Å*	*c/a*	rM^{2+}
$Ca_{10}(PO_4)_6(OH)_2$	9.430	6.891	0.7308	1.12
$Ca_{10}(PO_4)_6F_2$	9.348	6.865	0.7344	1.12
$Ca_{10}(PO_4)_6Cl_2$	9.590	6.767	0.7056	1.12
$Ca_{10}(PO_4)_6Br_2$	9.648	6.779	0.7026	1.12
$Pb_{10}(PO_4)_6(OH)_2$	9.861	7.424	0.7529	1.29
$Pb_{10}(PO_4)_6F_2$	9.755	7.283	0.7466	1.29
$Pb_{10}(PO_4)_6Cl_2$	9.977	7.326	0.7343	1.29
$Pb_{10}(PO_4)_6Br_2$	10.062	7.359	0.7314	1.29
$Cd_5(PO_4)_3(OH)$	9.335	6.664	0.7139	1.10
$Sr_5(PO_4)_3(OH)$	9.745	7.265	0.7455	1.26
$Cd_5(PO_4)_3Cl$	9.633	6.484	0.6731	1.10
$Ca_3(PO_4)_3Cl$	9.52	6.85	0.7200	1.12
$Sr_5(PO_4)_3Cl$	9.859	7.206	0.7309	1.26
$Pb_5(PO_4)_3Cl$	9.990	7.377	0.7345	1.29
$Ba_5(PO_4)_3Cl$	10.284	7.651	0.7487	1.38

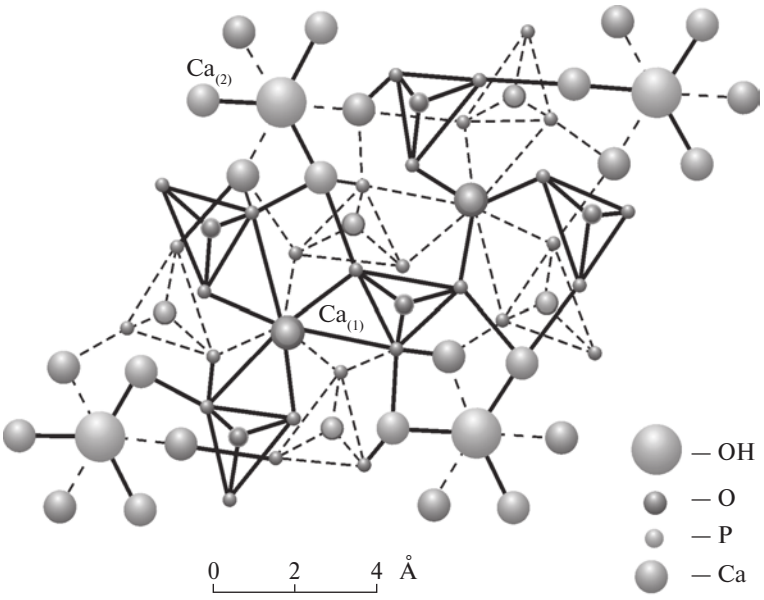

Fig. 1.1. Apatite structure

below the $M_{(2)}$ triangles. A large Br^--ion is located between two triangles (0, 0, z). In spite of the large unit cell volume of the elementary cells of isostructural lead compound, anions inside of them are not located outside the $Pb_{(2)}$ triangles plane. Such distinction in the structure is probably caused by 6*s* electrons of lead.

$Ca_{10}(PO_4)_6(OH)_2$ ***monocrystalls*** can be grown with stream method using hot isostatic compression of β-tricalcium phosphate (β-TCP) and $Ca(OH)_2$ mixture [3]. After chemical etching with 0.05 M HCl water solution, the surface of crystall of Ca-HAP was investigated using atomic force microscopy (AFM). It turned out that it was presented as steps with the altitude corresponding to the size of lattice d(100). Carboxylic acid films formed on the monocrystal surface of Ca-HAP were described using Langmuir approach. Using AFM data the distance between carboxylic acid groups and surface of Ca-HAP was determined. It appeared ~40 μm, which is enough for realization of chemical interaction.

Synthesis of $Ca_{10}(PO_4)_6(OH)_2$ with the monoclinic structure by "wet" method with the consequent annealing during 1 hour in air under 1473 K is described in work [4]. The Ca/P ratio in carbonate-free product was equal to 1.65, which is insignificantly less than theoretical value (1.67). The crystal structure of samples was determined by X-ray diffraction method and conformed on 98% to monoclinic symmetry with the spatial group $P2_1/b$, ρ = 3.14 g/cm^3 and parameters of crystal lattice a = 9.426(3) Å, b = 18.856(5) Å, c = 6.887(1) Å and γ = 119.97(1)°.

The description of the growth condition of monocrystals of carbonate-containing HAP in hydrothermal conditions is given in work [5]. Synthesis was carried out

by the heating in the thermal gradient, applied to the vessel, containing reactionary mixture: $CaHPO_4$, H_2O and carbon dioxide (dry ice). The optimal conditions for obtaining large monocrystals proved to be: $CaHPO_4$ concentration — 10 g/l; temperature gradient — 33.5 °C/cm; heating rate — 0.005 °C/min; carbon dioxide content — 55 g/l. The largest from obtained crystals was about 12 mm × 200 μm × 400 μm. The relation of Ca/P and the content of CO_2 in monocrystals were found within the limits of 1.60 ÷ 1.67 and 0.09 ÷ 0.65 wt. % correspondingly. In such conditions carbonate ions replaced only OH groups.

The work [6] informs of synthesis and structure determination of four new apatite-like phases. The structure of $Ca_{10}(PO_4)_6S$ is specified by means of monocrystaline X-ray data, and the structure of $Sr_{10}(PO_4)_6S$, $Ba_{10}(PO_4)_6S$ and $Ca_{10}(PO_4)_6Se$ is specified from the X-ray photograph of powders. All four compounds are isostructural and have their crystals with the trigonal spatial group $P_{\bar{3}}$ and arrangement of chalcogenide ion (0, 0, and 1/2). Sulfoapatite samples didn't reveal the H_2S absorptivity, whereas oxyapatite absorbs H_2O by the high temperature, which is attributed to the position of the sulphide ion in the lattice and its impact on the crystal structure around the lattice vacancy (000).

The formation of the ***microcrystalline*** $Ca_{10}(PO_4)_6(OH)_2$ in alkaline solutions at pH 9.5—12.0 is investigated in the work [7]. The primary solid phase was amorphous calcium phosphate (ACP) which transformed into microcrystalline Ca-HAP after the period of induction. The results obtained using radioisotopic tracer technique confirmed that in that case the transformation occured by means of ACP dissolution with the consequent Ca-HAP crystallization. The observed decrease of induction period with the increase of pH, temperature and concentration of reagent correlates with the decrease of HPO_4^{2-} concentration and indicates that deeper deprotonation of phosphate anion is the stage antecedent to Ca-HAP crystallization. Polycrystals of strontium hydroxyapatite ($Sr_{10}(PO_4)_6(OH)_2$, Sr-HAP) can be prepared using homogeneous deposition method [8] using $SrCl_2$, NaH_2PO_4 solution and carbamide (molar ratio Sr/P = 1.67). Both $Sr_{10}(PO_4)_6(OH)_2$ and α-$SrHPO_4$, β-$SrHPO_4$, $Sr_3(PO_4)_2$ and $SrCO_3$ used for comparative structural research are generated at 97 (±1) C° depending on the concentrations of the reagents and the time of heating. α-$SrHPO_4$ emerges at the initial stage of synthesis. $SrCO_3$ is generated and remains in the composition of the reaction product even after ageing of the precipitate.

Such admixtures as Cl^- or CO_3^{2-} are inevitably present in Sr-HAP crystal during the hydrolytic deposition using carbamide. Their quantity can be minimized with the meticulous observance of the concentration regime of precipitation.

The preparation of $Sr_5(PO_4)_3Br$ using solid-state reaction is described in [9]. The structure of the polycrystalline $Sr_5(PO_4)_3Br$ was determined using X-ray powder diffraction data. It was found, that $Sr_5(PO_4)_3Br$ and $Sr_5(PO_4)_3)Cl$ were isomorphic: the spatial group $P6_3/m$; the parameters of lattice: a = 9.9641(1) Å, c = 7.2070(1) Å, α = β = 90 °, γ = 120 °, Z = 2, ρ_{calc} = 4.27 g/cm^3 and ρ_{expt} = 4.10 g/cm^3 were identical.

Stoichiometric Ca-HAP (Ca/P = 1.66) can be prepared of alkaline solutions by 95 °C using slow acid titration method in nitrogen atmosphere [10]. As the result there are generated apatite samples with the strictly stoichiometric ratio Ca/P. Phase composition of the prepared powders remained constant after heating during 2 hours at 900 °C. The lattice parameters of the mentioned crystal powders were in the excellent accordance with the diffractional data of card-file in case with Ca-HAP (ASTM9-432). The synthesis under moulding allows reaching maximum ordering of lattice, but doesn't influence on Ca/P ratio. The size of crystallites and their morphology were changing considerably during the twenty-four hours after obtaining optimum relationship of the components in the reaction mixture.

The synthesis of the pure Ca-HAP using the orthophosphoric acid and calcite was carried out in the work [11]. The physicochemical study of the precipitation peculiarities shows that the method using calcium hydroxide results in the obtaining of the apatite and tricalcium phosphate (TCP) mixture after calcination of the precipitate by 900 °C. At the presence of calcite first the apatite and calcite mixture is generated. The reaction between them passes the stage of the carbonate apatite formation (*B*-type). However, as a result of long keeping of nitrogen in the atmosphere Ca-HAP is formed.

Stoichiometric $Ca_{10}(PO_4)_6(OH)_2$ with the relation Ca/P = 5/3 is synthesized using gel-technology in water solution, inclusive besides citric acid also calcium nitrate and phosphorous acetic acid [12]. Using X-ray powder diffraction, infrared spectroscopy (IR) and TGA methods it was ascertained that the stoichiometry of the powder obtained in that way met the composition (Ca/P = 5/3 realation) and didn't contain carbonate ions.

The interest in the investigation of similar compounds of bivalent lead including different oxoanions is connected with the search for new non-linear optical materials. An example of such crystals are PbB_4O_7 and $Pb_3(PO_4)_3$. The quantum- generating characteristics of these materials are generated with Pb^{2+}-cations, whose unshared electron pair promotes the formation of the asymmetrical Pb-polyhedrons that finally leads to the polarization of the polyhedral frames.

$Pb_{10}(PO_4)_6(OH)_2$ (Pb-HAP) can be prepared by means of hydrolysis of lead hydrophosphate $PbHPO_4$ or reaction between $(NH_4)_2HPO_4$ and lead nitrate [13]. The enthalpy of the resultant formation of these transformations was determined using calorimetric method: -8258.4 kJ/mole (for the hydrolysis reaction) and —8261.4 kJ/mole (for the substitution reaction).

Pb-HAP can be prepared also with H_3PO_4 and $Pb(NO_3)_2{\cdot}5PbO$ (1), obtained using dehydration of $2Pb(NO_3)_2{\cdot}5Pb(OH)_2$ (2) or $Pb(NO_3)_2{\cdot}5Pb(OH)_2$ (3) [14]. The quantity of the product (2) relatively to (3) as with the quantity of the unidentified water-soluble product (4) was decreasing in the reaction mixture gradually with time. The dehydration of (2) and (3) but not of (4) led to the desired product with the typical roentgenograms and IR spectra. After keeping of Pb-HAP samples at temperatures 773, 973 and 1173 K during 3 hours, X-ray diffraction confirmed the apatite structure. However, after heating of Pb-HAP to 1173 K, it has partially transformed into

the amorphous product. At 1473 K Pb-HAP was melting. X-ray diffraction analysis has shown that the shortest distance of Pb-O in Pb-HAP is 2.18 Å, which is shorter than the bond length of Ca-O and Sr-O for corresponding HAP.

Similarly to hydroxyapatites where bivalent cations are represented with Cd, Ca and Sr, hydroxypyromorphite is characterized with unusual PO_4-tetrahedron distortion, in which $P\text{-}O_{(3)}$ bonds are shortened (1.536 Å) and form the sharpest angles O-P-O = 104.4(4)°. Such a peculiarity is also typical for $Pb_9(PO_4)_6$.

In the majority of other investigated phosphates the P-O bonds with the minimal length form the biggest O-P-O angles. Another peculiarity of synthetical F- and OH-containing the pyromorphite similarities consists in much larger distance of these anions (~1.8 Å) away from the triangle plane, formed by $Pb_{(2)}$ atoms; in (Ca, OH)- and (Cd, OH)- apatite-like structures this distance is equal to ~0.4 Å.

The stoichiometric calcium fluorapatite (Ca-FAP) samples can be prepared using solid phase reaction in argon current at 1370 °C during 60 minutes [15]. For of Ca-, P- and F-content test the next methods are used: titration with DTA (differential thermal analysis) for the determination of Ca^{2+} content (accuracy: 0.8%), spectrophotometric method for the determination of PO_4^{3-} (accuracy: 0.6%) and potentiometric measurements using the fluoride-selective electrode (accuracy +5.4%) for the determination of F^- content.

In the work [16] big crystals of barium chlorapatite ($Ba_5(PO_4)_3Cl$, Ba-ClAP) are grown for the first time. The solubility of $Ba_5(PO_4)_3Cl$ in NaCl melt was increasing with the increase of temperature, obtaining value 1.9 mol. % at 1100 °C. $Ba_5(PO_4)_3Cl$ crystal growth took place when the temperature of the solute mixture was kept at 1100 °C, during 10 hours and consequently was lowered to 500 °C with the speed 5 °C/h. There were obtained colorless and transparent prismatic crystals with the length up to 12 mm and width 3 mm. The optimal content of solute for prismatic crystals growth is 1.2 mol. %. Prismatic crystals are limited with the $\{10\bar{1}0\}$ and $\{10\bar{1}0\}$ faces. Relational elongations of crystals ranged from 1.1 to 4.8. Needle-shaped crystals with length up to 4 mm and width 60 μm appeared at the initial stage of growth, further their growth occurred only in [0001] direction with the relational elongation in the range 43 up to 56.

1.2. Synthesis of apatites with nonstoichiometric composition

The unique Ca-HAP characteristic is the nonstoichiometry of its composition. Ca/P ratio is used as the index of nonstoichiometry. The majority of Ca-HAP powders synthesized by "wet" method are nonstoichiometric. As the result of detailed research there were several variants of interpretation of such phenomenon [1] suggested, and at the present time for the describtion of nonstoichiometry is used the next formula:

$Ca_{10-x}(HPO_4)_x(PO_4)_{6-x}(OH)_{2-x}nH_2O$; $0<x<1$, n = 0-2.5, presupposing calcium deficit. It is supposed that the local negative charge is balanced with introduction of H^+ ions resulting in formation of H_2O molecules and holding OH^- positions. There are reasons to believe that besides Ca^{2+}, PO_4^{3-} and OH^- ions such ions as H_3O^+, $H_4O_4^{4-}$ and HPO_4^{2-}, which replace Ca^{2+} and PO_4^{3-} in Ca-HAP crystal lattice, respectively, also take part in phase formation by "wet" synthesis.

Many studies were dedicated to the preparation Ca-HAP with the different Ca/P ratio. Nonstoichiometric Ca-HAP can be formed in heterophasic system in the presence of soluted formamide and chlorides [17]. The composition of crystal phase and grain morphology is often defined with the reagent concentration in the mother solutions. Spherical particles of Ca-deficit Ca-HAP with a diameter of less than 800 μm are obtained from 3-7 M formamide solution. Cl^- ions facilitate Ca-HAP crystals growth in the form of needle-shaped grain.

Keeping of apatite structure while changing the molar ratio Ca/P over the range 1.502-1.717 in samples, prepared with wet method [18] with the posterior thermal treatment by 1250 °C, was shown using X-ray diffraction method and FTIR.

A new method of Ca-HAP synthesis is suggested at [19]. Ethylene-glycol solution of $Ca(OAC)_2 \cdot H_2O$ and P_2O_5 solution in butanol were used as parent compounds for Ca-HAP synthesis. Acetic acid and ammonium nitrate (NH_4NO_3) were used as stabilizer and oxidant, respectively. After input of the solution mixture on the hot surface for solvent evaporation, the polymeric composit is prepared. The calcinations of this composite at 500 °C resulted in dark powder formation, and only after consequent annealing at 1000 °C white powders of Ca-HAP crystalline phase with stoichiometrically understated calcium amount were obtained: $Ca_{10-x}(HPO_4)_x(PO_4)_{3-x}O$. The described way of Ca-HAP synthesis has a potential application for the functional coatings deposition.

Cadmium apatites $Cd_5(PO_4)_3Br$ and $Cd_5(VO_4)_3I$ are halogenide deficient [20]. Ordering unsuiTable to stoichiometric one is discovered in planes perpendicular to *c*. The structure of monocrystal $Cd_5(PO_4)_3Br$ is determined from X-ray diffraction data in four-dimensional superspatial group $R:P_{(\bar{3})}:(0\ 0\ \gamma)$: a = 16.932(2) Å = 6.451(1) Å, Z = 6, R = 0.043. The structure changes happen because of misfit between large halogenide-ions and ambient rigid substructure Ca-PO_4. $Cd_5(PO_4)_3Br$ "chain" model structure is confirmed on the basis of equality of Br-Br 3.466 Å distance.

1.3. Synthesis of crystals of mixed apatites

The monocrystals of substituted strontium HAP ($Ca_{9.42}Sr_{0.18}H_{0.8}(PO_4)_6(OH)_2$) with the dimension $0.2 \times 0.2 \times 5$ mm^3 were grown hydrothermaly in the long tube autoclave, using $CaHPO_4$, $SrHPO_4$ and the method of thermal gradient [21]. The monocrystal with the dimensions $165 \times 165 \times 231$ μm, Sr

content of 1.92 mol. %, with (Sr+Ca)/P atomic ratio equal to 1.60 and with the density 3.207 g/cm^3, had hexagonal prismatic structure, what is consistent with the spatial group $P6_3/m$ and a = 9.3920(7) Å, c = 6.890(1) Å. Primary calcium substitution with the strontium is noticed for $Ca_{(1)}$ positions.

The preparation of Sr-Ba-HAP and the definition of their characteristics are realized in [22]. Sr-Ba-HAP with the different mole ratio Ba/(Ba+Sr) is synthesized using wet method. The particles are obtained under mole ratio variation over the range from 0 up to 1 and the probability of ions Ba^{2+} inclusion into the HAP crystals structure is less than Sr^{2+}. Particles that are precipitated in conditions of the increasing content of Ba^{2+} except of Sr-HAP are agglomerates consisting of the small particles. The relations (Ba+Sr)/P in all samples always exceed stoicheometric relation 1.67.

$Ca_{10-x}Pb_x(PO_4)_6F_2$ with $0 \le x \le 10$, precipitated in the medium with pH = 10, comprising besides ammonia also fluoride-ions [23]. The standard enthalpy of formation are calculated. The enthalpy of formation was changing linearly with the increase of introduced lead quantity from —13550 kJ/mole up to —8466 kJ/mole for the fraction with the change of lead content from x = 0 до x = 10, respectively. The change of standard enthalpy of mixing has inverse relationship with the lead concentration.

The carbonate apatite monocrystall is grown under the pressure 50 MPa of argon in the system with $CaCO_3$ [24]. The obtained crystals are 1 mm long and 200 μm in diameter. Carbonate ions held both A(OH) and $B(PO_4)$-positions. It was shown from the angular dependence of polarized IR spectra for in-plane and out-of-plane fluctuations of CO_3^{2-} ions that CO_3^{2-} ion plane was parallel to c axis for A-substitution and perpendicular to c axis for B-substitution.

The crystal structure of carbonate apatite is determined also with X-ray diffraction analysis using monocrystal, grown with $CaCO_3$-flux method [25] and having composition of $Ca_{9.75}[(PO_4)_{5.5}(CO_3)_{0.5}]CO_3$, in which all OH-clusters are substituted with carbonate ions. Spatial group conformed to the hexagonal one with the constants of crystal lattice a = 9.480(3) Å and c = 6.898(1) Å. The quantitative relation between CO_3^{2-} ions in A(OH) and $B(PO_4)$- clusters of crystal is calculated through the lack of Ca.

In aqueous medium trimetal phosphates transform into HAP. The work [26] covers the evolution of the mixed phosphate of calcium and strontium. Reaction is carried out in hydrothermal conditions (770 °C, 90 MPa, 24 hours). The formation of HAP $Me_{10}(PO_4)_6(OH)_2$ with the relation Sr/(Sr+Ca), corresponding to the composition of the initial mixture was observed.

Synthesis of Na^+- and CO_3^{2-}- containing apatites during the process of monetite hydrolysis ($CaHPO_4$) at 95 °C in solutions with the concentration Na_2CO_3 in the range of 0.001 M and 0.250 M was investigated in the work [27]. The presence of unreacted $CaHPO_4$ in precipitates at relatively low pH values (<9) indicated that it was necessary to keep high pH values for the complete transformation of monetite into apatite. Besides, low Na_2CO_3 (<0.005 M) concentrations are optimal even at high pH level (~10) when HPO_4^{2-}-ions suppress CO_3^{2-} incorporation into the apatite lattice certifying the

competition between CO_3^{2-} and HPO_4^{2-} during structure formation. It's also found that $CaCO_3$ appears in precipitate's composition already after the short time as reaction starts. However, after the lapse of at least 5 hours after hydrolysis there is no calcite in the precipitate anymore. It is concluded that uncontaminated high-crystal and monophase apatites may be obtained by means of $CaHPO_4$ hydrolysis in solutions with the Na_2CO_3 concentration of $0.010 \div 0.250$ M minimum after 5 hours.

The stoichiometry of Na^+- and CO_3^{2-}-containing apatites obtained by monetite hydrolysis is studied in [28], where Ca-HAP is synthesized using $CaHPO_4$ hydrolysis in Na_2CO_3 solutions under the same precipitation conditions. The analysis has shown that precipitations are monophase and well crystallized. *B*-type is presented with apatites with carbonate content of $8 \div 20$ wt. %. Even after long-term vacuum drying at 25 °C samples included a great amount of water. On the basis of compound data it is found that the prevailing mechanism of substitution, responsible for incorporation Na^+ and CO_3^{2-} in $Ca_{10}(PO_4)_6O_2$ are: $Ca^{2+}+PO_4^{3-}+OH^- \leftrightarrow V_{Ca}+CO_3^{2-}+V_O$ and $Ca^{2+}+PO_4^{3-} \leftrightarrow Na^+ + CO_3^{2-}$, where V_X means free place in X-sublattice.

Pb-Ag stoichiometric apatites were obtained using hydrothermal reaction of lead phosphate $Pb_3(PO_4)_2$ and silver phosphate Ag_3PO_4 at 215 C° and 100 atm. in the work [29].

1.4. The influence of medium factors on the compound and structure of apatites

Ca-HAP-collagen system. Among the important problems is the study of interaction nature between Ca-HAP, composing the inorganic matter of bone tissue and the organic matter of bone, presented almost completely by collagen. The specific feature of collagen is that every third aminoacid residue of its molecule is an anion of the simplest aminoacid — glycine. In this connection the study of Ca-HAP interaction with glycine (NH_2CH_2COOH) is of interest.

Synthesis and physicochemical analysis of glycine-containing Ca-HAP is carried out in [30]. The system $CaCl_2$-$(NH_4)_2HPO_4$-NH_3-H_2O-NH_2CH_2COOH at 25 °C was studied using the methods of solubility (determination of residual concentration) and pH measuring. The conditions of glycine-containing Ca-HAP (glycine hydroxyapatite) precipitation were found. It was shown that anionic form of glycine $NH_2CH_2COO^-$ isomorphically substituted OH^- ions in Ca-HAP lattice with the formation of glycine hydroxyapatite $Ca_{10}(PO_4)_6(OH)_{2-x}(NH_2CH_2COO)_x$. Values *x* are increasing from 0.07 up to 0.4 when the concentration of glycine in the initial solutions is increased. It must be noted that entering of small amount of glycine in apatite's lattice channels is determined with the precipitation of Pb-HAP crystals in the presence of glycine.

It is known that in the $CaCl_2$-$(NH_4)_2HPO_4$-NH_3-H_2O system (at 25 °C and at constant content of $(NH_4)_2HPO_4$ (0.025 mol./l) and with the ammonia excess (pH 10.7)

the initial ratio Ca^{2+}/PO_4^{3-} = 1.67-1.75 and stirring for 14 days are necessary for Ca-HAP formation without TCP phase inclusions.

According to X-ray diffraction data the degree of glycine-containing Ca-HAP crystallinity is increasing with the increase of the time of storage in contact with the mother solution. As the result of stirring for 14 days amorphizing fine-crystalline powder forms and after another 30 days solid phase has accurate diffraction pattern typical for Ca-HAP structure. TCP lines are absent. After calcination (950 °C) in air glycine-hydroxyapatite loses glycine and turns into Ca-HAP with the diffraction pattern typical for crystalline Ca-HAP.

IR spectra indicate that the products of interaction Ca-HAP and glycine obtained with the precipitation from solutions are not mechanical mixtures of mentioned substances and are not the result of glycine adsorption on the Ca-HAP surface, but represent glycine-hydroxyapatite of variable composition.

On the basis of the IR spectra analysis it is established that from three known forms of glycine $NH_3^+CH_2COOH$ (I), $NH_3^+CH_2COO^-$ (II) and $NH_2CH_2COO^-$ (III) in glycine-hydroxyapatite anion form III is present.

The role of metals in Ca-HAP crystallization process. It is shown in work [31] that the presence of zinc in the initial solution strongly slows down the crystallization of Ca-HAP which can be synthesized as monophase only when zinc concentration doesn't exceed approximately 25 at. %. In the forming phase with the increase of zinc concentration the decrease of both molar Ca/P relation and crystals size is observed. At the same time Ca/Zn relation in solid phase and solution remain the same. The values of cell parameters of apatite phase indicate that zinc can not fill place of calcium in Ca-HAP structure. Therefore zinc can be adsorbed with the apatite crystal surface or be present in amorphous phase. The range of Ca-HAP thermal transformation into β-TCP broadens with the increase of zinc concentration in the solid phase compound. The decrease of β-TCP lattice constants with the increase of zinc content in solid phase indicates that zinc partly substitutes calcium in this structure. The effect of slowing down the Ca-HAP crystalisation with zinc and its preference for β-TCP structure resembles the effect that was observed in the presence of magnesium.

The role of magnesium in synthetic apatite degradation using FTIR analysis is investigated in details in [32]. Synthetic apatites precipitated in the presence of magnesium cations and carbonate anions at the room temperature with subsequent maturation. Crystallinity index for each sample is calculated according to FTIR data. It is shown that the synergism of Mg^{2+} and CO_3^{2-} interference appears as a delay of crystallinity index increase.

Also the inhibitory effect of magnesium and zinc ions on HAP surface (0001) growth kinetics in pseudophysiological solutions is investigated in [33]. As it was ascertained, (0001) surface was increasing not according to helical mechanism but by means of multiple bidimensional nucleations. It was shown that lateral growth of bidimensional islands on (0001) surface was inhibited with addition of magnesium

and zinc compounds. Though both cations delayed the growth, zinc delayed it 1000 times more efficiently than magnesium.

The influence of nickel on the formation of calcium phosphate from water solutions is examined in [34]. Samples, which were formed under different conditions (pH, temperature and nickel concentration), were described using X-ray diffraction, FTIR spectroscopy and thermogravimetry methods. As evidenced by the results nickel facilitates brushite and ACP formation. Also it is shown that the presence of nickel in the solution slows down the formation of Ca-HAP and OCP phases. However, at pH>7 and 95 °C, Ca-HAP can be nevertheless obtained. These results indicate that nickel presence gives a possibility to manage the calcium phosphates precipitation.

Other factors of influence on nucleation and Ca-HAP crystal growth. In the work [35] the influence of Langmuir monolayers of stearic acid on the nucleation and Ca-HAP crystal growth from the solutions is investigated. Monolayers of surfactant increased the probability of Ca-HAP nucleation. It is shown that Ca-HAP crystals were nucleating and growing epitaxially on the monolayer interface.

The effect of ethanol on the calcium phosphates is investigated in [36]. Initially, ACP with Ca/P relation increasing from 1.28 at pH 7.4 up to 1.50 at pH 10.2 precipitated from oversaturated both water and water ethanol solutions of calcium phosphate with pH 7.4 and higher. In water solutions at pH 7.4 ACP was quickly transforming into Ca-HAP. In water-ethanol solution this process slowed down at pH 7.4 but sped up with the addition of 8.9 ppm of fluoride and at significantly lower values pH 7.1. Ethanol favours ACP formatiom by means of increasing the oversaturation and deposition rate, and also speeds up drying of solid precipiations. Fluoride ions and low pH values favour apatite formation through shortening time of ACP existence.

The effect of vanadocenes on Ca-HAP crystal growth is investigated in conditions of steady oversaturation of solutions [37]. All dichloric vanadocenes were found to be inhibitors of Ca-HAP crystal growth, possibly due to blocking of crystal regions with active growth, that indicates the surface-diffused crystallization mechanism.

The influence of chondroitin sulphate (CS) templates on Ca-HAP crystal growth is studied in [38]. Ca-HAP-particles and 60 HAP/40 CS (in wt. %) specimens were synthesized using method of precipitation from the suspensions obtained with pouring of calcium hydroxide and phosphoric acid solutions. The dimensions of Ca-HAP crystals formed without CS were about 75×10 nm, while CS-containing complexes had dimensions about 12×6 nm. The inhibitory effect of CS on the Ca-HAP crystal growth can be explained with regulating effect of organic matrix on the Ca-HAP formation because of steric inhibition.

There is a number of publications on the creation of sTable composites of hydroxyapatite/plastic alginete, particularly [39]. The influence of several polymer admixtures on nucleation, crystal growth and morphology of Ca-HAP obtained from solutions is studied in [40]. It is shown that polymer of asparcam acid is the most effective inhibitor of Ca-HAP scales growth.

The effects of increasing of the speed of calcium phosphate crystallization in presence of $Pb(Ti,Zr)O_3$ (PZT) are studied using PZT dipping into saturated solutions of $Ca_{10}(PO_4)_6(OH)_2$ [41]. It is shown that electric field affected the orientation of the forming crystal because OCP layers were found on the negative PZT surfaces.

In connection with the fact that bile acids lead to pathological calcinosis [42], the role of folic acid salts in Ca-HAP growth stimulation was studied. It was found that Ca-HAP precipitation is controlled with this organic molecule. Kinetic analysis of nucleus formation speed as a function of solution oversaturation indicates that the amount of ions forming critical nucleus is equal to two. Obviously Ca-HAP formation is initiated by interaction of calcium ions with the negative oxygen atom of C = O fragment. Middle-range order found from kinetic data was equal to 1.7±0.4, indicating the surface mechanism guided with the product diffusion.

The effect of electromagnetic fields on the apatite crystal growth. Low-frequency electromagnetic fields of 3 mTl and with frequency 1300 Hz were used during the processes of spontaneous precipitation of phosphates admixtures from their oversaturated water solutions of calcium chloride and sodium phosphate [43]. At the temperature 37 °C in water solution with pH 7.4 for any total time of precipitation (from 15 minutes to 5 hours), precipitated solid phase is formed with OCP and nonstoichopmetric Ca-HAP. Electromagnetic exposure doesn't effect on the composition change of the precipitated mixture. For any time of precipitation powders, obtained under the influence of fields are characterized with the specific values of surface parameters which are lower than those one which correspond to the samples obtained without influence of fields. Crystal sizes of both samples are within the limits of 10 and 20 nm, however, middle size of crystallite obtained in field, are characterized on 40% bigger size than those samples which are precipitated without electromagnetic field influence. It is shown that influence of electromagnetic field is active on the beginning of the process of precipitation, when calcium phosphate particles are mainly in colloidal state It is determined that particles sizes which are affected with external field have order 0.1 nm.

Gravitation and growth of Ca-HAP crystals. In work [44] the characteristics of calcium phosphate crystals grown on the Earth and in the space are compared. When using $CaCl_2$ and KH_2PO_4+K_2HPO_4 solutions with the same pH value, it was found out that on the Earth only Ca-HAP crystals grew whereas in the process of experiment both Ca-HAP and OCP crystals grew in the space. Grown in the space OCP crystals reached the size 100 times more than crystals grown on the surface of the Earth. Also it was found that the crystallites grown in space are more perfect than those which were grown on the Earth, they are more resistant to electronic beam exposure. Ca-HAP spherolites consist/are composed of little and thin Ca-HAP needle-like crystals with different orientations. Crystals that grew in the space and contained almost pure OCP phase had deep grooves along direction *c*. OCP crystals which are grown on the Earth at the lowest oversaturation had the same sizes with crystals grown in the space. However, they included massive regions of Ca-HAP structure. During electron microscopy investigation

of these crystals electronic emission stimulates therein transformation of crystal phase in amorphous one. Such transformation in crystals grown in the space requires long-term irradiation. The conclusion is that the distinctions described above proceed from the lower degree of oversaturation and difference of local pH values for crystals, that nucleated and grew in the space comparing with those that formed on the Earth.

Calcium phosphate powders grown in earth and space conditions (EURECA 1992-1993) were analysed and compared using optical and electrical microscopy (scanning and on transmission), electronic and X-ray microdiffraction and micro-analysis [45]. Only little microsized Ca-HAP spherolites are grown on the Earth. In the space Ca-HAP spherolites reach the dimensions of hundreds of micrometers. Also OCP spherolites as large as 3mm were obtained. Computer simulation of diffusion in real camera gave possibility to assume higher spatial gradients of oversaturation at zero gravitation than on the earth's surface where convection takes place.

1.5. Disordered and nanodispersed apatite structures

Nucleation. In a number of works, in particular, in [46] Ca-HAP crystal growth kinetics is studied. Step speeds of Ca-HAP growth in physiological conditions as step height functions, its special placement and local oversaturation of solution were measured using AFM. It was shown that the character of growth did't depend on diffusion and dehydration but only on incorporation of a fragment on the front of step. Kinetic coefficient of step growing turned out to be of the same order as of macromolecular viruses and protein crystals, and was few times less than in the case of inorganic ion crystals. Relying on this it was suggested that the «unit of growth» of Ca-HAP crystal represented a claster but not an ion associate. It is supposed [47] that the velocity of nucleation is a function of average ion activity, and the transverse velocity of the nucleus growth is controlled with calcium ions concentration. Comparatively slow formation of functional OH groups of water molecules captured with the crystal surface is also taken into account. Using the frequency of diffusive jumps of calcium ions the theoretical value of the process speed equal to $1.6 \cdot 10^5\ c^{-1}$ is obtained.

Heterogenic nucleation of calcium phosphate in the monolayer of pseudophisiological solution was studied using AFM. Calcium phosphate nanoparticles with a diameter of 5-10 nm were forming already at the initial stage of nucleation (less than 3 hours) [48]. After this stage the surface was covered with the seeds of calcium phosphate with a diameter of 20-30 nm. Data interpretation on Ca-HAP precipitation during "wet" synthesis is complicated with absence of classic approach to the description of nucleation. The mechanism of particles formation was suggested including nuclei aggregation and controlled with the excess of surface energy compensating repulsive forces between the particles [49]. The combination of agglomerates forms cross bridges and growth in the separate particles continues due to repulsive forces.

Some new aspects of surface nucleation, revealed by growth and mdissolution of Ca-FAP and Ca-HAP [50] resulted in revision of mechanism of these processes and formulation of new conception that uses calcium ions concentration instead of average ion activities. Coefficient of limitation of surface growth and Ca-FAP and Ca-HAP dissolution is hypothetically connected therewith that calcium ions make diffusive jump at simultaneous partial dehydration. For such processes experimental values $\nu_{in} = 10^5\ c^{-1}$, which conform theoretical ones except for the case with the FAP growth at pH 5.0. Mononuclear mechanism in the minor axis direction and multinuclear in the main axis direction are suggested for the explanation of FAP growth.

In the work [51] synthesis of amorphous calcium polyphosphate is described and the changes of its molecular composition during dehydration are studied. It was shown that by heating substance wass hydrolysed first under influence of water contained in it with the formation of acid mono- and diphosphates of calcium which at higher temperature transformed back into polyphosphate. Synthesis of amorpous calcium polyphosphate was realized by means of pouring of 10% water solutions of high-molecular natrium polyphosphate $(NaPO_3)_n$ and calcium chloride. $(NaPO_3)_n$ solution was slowly added with intensive stirring to $CaCl_2$ solution, which amount exceeded the level needed for substitution of ions Na^+ to Ca^{2+} 2-fold. Obtained white precipitate was rinsed with cold water twice.

NMR ^{31}P method showed that freshly obtained, not yet swept from chlorides precipitate had the molecular composition that did't differ from natrium polyphosphate, used for synthesis — it had no cyclic phosphates, instead it had a little amount of mono- and diphosphates. During the washing chlorides off the precipitate there is no changes of it's composition in spite of long duration of the process.

The substance with chlorides washed off, segregates gradually at room temperature during 100-120 hours with the formation of transparent gel and layer of liquid above it. Lamination occurs due to emission of excess water involved during precipitation. The drying process is accompanied with the change of molecular composition manifested in the increase of low-molecular forms content in the gel. During dehydration gel starts to be more and more adherent and with the lapse time it solidifies. In the dried state it resembles glass in outward appearance, however it's very fragile and can be easily triturated.

Solution precipitation of Ca-HAP is a mass crystallization with the formation of many small crystals as a result of chemical reaction between phosphate and calcium ions. Ca-HAP is the least soluble at pH>4 among four modifications of calcium phosphate salts (Ca-HAP, OCP, brushite, monetite). The mechanizm of nucleation and growth of Ca-HAP crystals still is the subject of numerous experimental and theoretical investigations considering great interest in creation of effective bioimplants and artificial bone tissue.

Particles-films-coatings. Hollow Ca-HAP particles can be prepared using spray hydrolysis of $CaCl_2$-$(NH_4)H_2PO_4$ solution after exposure to UHF electromagnetic ra-

diation [52]. The derived particles need to be annealed. It was discovered that the heating to 1050 °C lead to crystal growth on the particles surface. The crystallite dimensions for polycrystal particles is controlled as the function of the time of annealing.

In the work [53] the method of synthesis of spherical calcium phosphate particles during the process of ageing of the solution, including $CaSO_4$, NaH_2PO_4, carbamide (1 mole/dm^3) and surfactant at 80 and 100°C was suggested. The size and form of the obtained particles depend strictly on the reagents concentration and temperature. Spherical Ca-HAP particles were precipitated only in the narrow range of concentration of reagents, for example, at $[CaSO_4] = 2.0 \cdot 10^{-3}$ mole/dm^3 and $[NaH_2PO_4] = 7.9 \cdot 10^{-4}$ mole/dm^3 at 100 °C during 3 hours and appeared as agglomerates of small particles, which composition belongs to *B*-type of carbonate Ca-HAP, in which PO_4^{3-}-ions are substituted 4.8 wt. % with CO_3^{2}-ions. The results of elemental analysis and TG allowed to write down the formula of particle as $Ca_{8.5}Na_{1.5}(PO_4)_{5.4}(CO_3)_{0.8}(OH)_{0.7} \cdot 1.2H_2O$. The texture and crystallinity of spherical Ca-HAP particles remained intact up to 1000 °C. It was found out that particles showed ability to selective absorption of H_2O molecules, increasing after samples heating on the air.

In case with spherical particles of apatite prepared using the method of homogeneous precipitation in the presence of 5 wt. % of magnesium ions, ion-exchange test on toxical ions (Pb^{2+}, Cd^{2+} *и* Ni^{2+}) showed that apatite powders containing magnesium ions had better ability to toxin elimination than powders of magnesium-free apatite [54]. Quantity of subtitutional ions in magnesium-containing powders of apatite is decreasing in a following order: $Pb^{2+} >> Cd^{2+} > Ni^{2+}$.

The peparation of Ca-HAP powder using ultrasound [55] gives the possibility to control microstructure and characteristics of Ca-HAP pores [56]. The samples were prepared using different given powders and sintering at different temperatures and constant pressure. The volume and distribution of pores by size depend considerably on the temperature of sintering and morphology of initial Ca-HAP powders. The fraction of the opened pores of whisker-like powder sintered at 900 and 1000°C accounted 100 and 96%, respectively. The diameter and volume of pores during Ca-HAP preparation from whisker-like powder were larger as compared with the spherical and rod-like powders.

The possibility of obtaining of Ca-HAP "whiskers", streched along the crystallographic axis *c* using the method with the citric acid use is presented in work [57]. Initial solutions with the two different concentrations of the components 1.7 and 4.4 wt. %, which stoichiometry corresponded Ca-HAP composition, were prepared using the method of precipitation and reformed to the operation solution with the addition of citric acid amount required for Ca-HAP precipitate. The solution's volumes of 1.0 dm^3 were heated in the autoclave at the temperatures from 180 up to 220°C during 0, 1, 2, 3, 5 and 10 hours. According to the data of the X-ray powder diffraction the yield of crystalline phase of the products was determined with the concentration of reacting components in the solution, temperature and heating duration. The formed Ca-HAP whiskers had the length from 10 to 30 μm and diameter of ~0.5 μm.

Plasma spraying of suspension (PSS) of Ca-HAP powder is described in the work [58]. The essence of PSS is to obtain hard-grained powders of spherical particles of the suspension of fine (<10 μm) or even ultra fine (<100 nm) powders. PSS precursor is plasma-atomized gas. Liquid evaporation, consolidation and sintering occurs during the plasma thermotreatment process.

Ca-HAP precipitation during the process of microwave heating of Ca/citrate/phosphate solution is presented in [59]. There were obtained calcium deficient nanodimensional (<100 nm) HAP particles with the needle morphology. Chemical and morphological characteristics of Ca-HAP don't change in time and are similar to those obtained with microwave heating of Ca/citrate/phosphate solution. At that sTable states are reached faster than while Ca-Hap precipitation in reactor with standard heating.

Synthetic analogues of natural Ca-HAP (bones) are widely used in biomedical applications for substitution, grafting and regeneration of bone. Many strict criterions for biomaterials should be kept including the possibility of combining with the tissues of organism without any side effects. The approach developed in the work [60] includes spontaneous growth of Ca-HAP film with micron porosity under optimal conditions on the oriented TiO_2 surface layer, sprayed on a Ti base.

Bidimensional crystal Ca-HAP. By now many various methods of Ca-HAP synthesis with the different form and size of crystals are worked out. However the possibilities of synthesis of new forms appeared not to be spent: with the method of speed mixing of reagent solutions under certain temperature and hydrodynamical conditions Ca-HAP in bidimensional crystal form [61] was obtained.

Particles were taken from the reactor at a different times t after acid supply and subjected to sublimation drying. As X-Ray diffraction analysis proved to be not informative, further examination of particles were carried out using transmission electron microscopy. It was found out that at $t = 10^4$ c all particles are nanoplates and have Ca-HAP crystal lattice. Electron-diffraction pattern of each single nanoparticle is point, and aggregates of such particles give diffusive pattern of electron diffraction with 2 wide rings.

According to analysis data the phase after air-drying at 293 K untill the fixed mass had a composition $Ca_{10}(PO_4)_6(OH)_2 \cdot 3H_2O$. Its irreversible dehydration occurs at 400 K. Moreover, water molecules don't enter Ca-HAP crystal lattice and are chemisorbed with nanoplates. Thanks to the nanoparticles thickness which is equal to 1-3 parameters of cell, synthesized substance can be called as bidimensional crystal pseudocrystalhydrate with Ca-HAP or 2DHAP structure.

Obtained data allow to hypothesize that calcium phosphates can be in boundary bidimensional-crystal state where all crystals have thickness $h = b$ at $l >> b$.

Obtained 2DHAP ($b = 0.82$ nm) wasn't in such state because of nanoplates' coalescence with bases of crystal faces. The role of coalescence is confirmed with the found in special experiments dependence of OCP and 2DHAP properties on presence of collagen in reactor. It is established that if we inject tropocollagen ($M = 5 \cdot 10^3$) into the reactor together with $Ca(OH)_2$ solution, then we will be able to define specific surface

area of nanoplates using the collagen amount, gone off with the solid phase while its extraction from the reactor. Under experiment conditions at t = 40 s the specific surface area appeared to be 900±50 m^2/g and close to the surface 920±20 m^2/g, calculated on the assumption that all nanoplates allocated by size have the same thickness and $h = b$. This means that OCP immediately after formation was in boundary bidimensional-crystal state which was stabilized by collagen.

By the results of research the technology of 2DHAP synthesis has been developed. It appeared to be high-performance medicine, stimulating osteogenesis after implantation in bone tissue lesions in living organisms.

1.6. Mechano-chemical synthesis of apatites

Mechano-chemical synthesis (MCS) of compounds with the apatite structure are of interest not only as an ecologically clean production method but also as a model for research of peculiarities of passing such process of MCS in multicomponent systems. Apatites of general formula $Me_{10}(ZO_4)X_2$ possess the wide spectrum of isomorphic substitutions, what allows mechanochemical synthesis of the one-type matrix of the initial compounds with the different chemical properties and very differing values of ionic radii of their components [62].

The absence in some cases of another way of synthesis of the given composition and structure, but MCS, determines significance of this method.

Investigations of MCS phosphates allowed to ascertain that the character of resulting phases and their similarity with the water or condenced systems are determined with the amount of energy supplied to the reaction zone. By the increase of Ca/P relation acid-base interaction between calcium oxide and hydrophosphates is speeding up and is completed with the formation of the compounds with apatite's structure.

For the reveal of peculiarities of passing of mechano-chemically initiated solid phase reaction of $Ca_{10}(PO_4)_6(OH)_2$ formation the dry dispersion of mixtures of $Ca(OH)_2$-P_2O_5 and CaO-$Ca(OH)_2$-P_2O_5 was carried out [63]. It turned out that Ca-HAP formation in $Ca(OH)_2$-P_2O_5 mixture is more favorable than in CaO-$Ca(OH)_2$-P_2O_5 system. H_2O presence and its amount contained in the initial mixtures plays the key role in the increase of efficiency of Ca-HAP formation.

By MCS of apatites, if after the formation of the final crystal product energy supply was going on, the inverse process was starting, i.e., the mechanical activation of synthesized product took place.

MCS allows obtaining compounds with the localization of ions in the structure, which are impossible to get using some other methods. The example of this can be Ca-HAP synthesis with the insertion of organic acids into the structure. According to the IRS data, these fragments take two positions — they substitute phosphate (adsorption bands in the range of 1400-1470 cm^{-1}) and also are localized on 6_3 axis (ad-

sorption bands of carboxylic groups' oscillations in the range of 1555-1595 cm^{-1}). At that structures with the substitution on the 6_3 axis are less sTable and are hydrolysed during water treatment of the samples.

While long-time storage of mechanically activated mixtures in samples the chemical transformations can go on even at room temperature. This nonordinary fact requires further systematic researches.

1.7. The preparation of hydroxyapatite ceramics

There are several methods of sintering of HAP ceramics with the controllable porosity. Bonding admixtures are rarely used because Ca-HAP solid state reactions with the different compounds at high temperatures lead to decomposition of HAP phase on α- and β-TCP. Using of HAP powders as a source material is preferable because of their bigger specific surface that promotes increase of reactivity and is effective while sintering. HAP-ceramics porosity is controlled as a rule with hydrogen peroxide solution. Water suspension of Ca-HAP powder inclusive H_2O_2, is gradually dried and consequently sintered. While thermal decomposition of H_2O_2 gaseous products are formed, which expansion in the volume of solid matrix gives the possibility to reach porosity right up to 60%.

To decrease the temperature of HAP sintering the hot isostatic pressing (HIP) is used. Using this procedure HAP powders encapsulated in golden capsules were compressed isostatically under the pressure 140 MPa at 550 °C during 3 hours. The density obtained in this way was increasing appoximately up to 74% of the theoretical one [1].

The hydrothermal method of HAP powder synthesis is described in [64]. The heating of $Ca(OH)_2$, $Ca(H_2PO_4)_2 \cdot H_2O$ powders in the presence of distilled water in a sealed reservoir at 109 °C during 1-3 hours resulted in formation of needle-shaped HAP crystalls (130-170 nm lengthwise and 15-25 nm in width) which have specific surface area 31-43 m^2/g and Ca/P ratio equal to 1.640-1.643. HAP powder obtained at 1200-1300 °C may have high density. The optimally sintered ceramics has porousless structure with the flexural strength 120 Mpa, Vickers microhardness 5.1 GPa and impact strength 1.2 $MPa \cdot m^{1/2}$. The synthetic method is simple; scale production is economically sound and allows obtaining high quality powders and make them perspective for live bone tissue regeneration.

Depending on molar ratio Ca/P of original precipitations that is determined with precipitation conditions (with molar ratio of Ca/P-containing reagents and pH of the medium), after sintering at 1250 °C monophase, biphase and triphase ceramics including Ca-HAP, β-TCP and calx were obtained [65]. The phase and elemental compositions and properties were determined: density, shrinkage, hardness, flexural strength and character of cracking of isostatic compressed ceramics.

Synthesis of biphase ceramics of HAP and β-TCP with controlled phase-content and porosity is described in [66]. The process is based on solid-state reactions of brushite with calcium carbonate. The optimal conditions of the thermotreatment for the formation of stoichiometric pure HAP, β-TCP and biphase HAP and β-TCP compound with the certain phase composition are defined with thermal analysis method, X-ray diffraction and IR absorption spectroscopy. For the preparation of ceramics with the different microporosity, a deal of non-calcined powder as a gas forming agent is mixed with the preliminary sintered powder. Foam-like ceramics with macropores is prepared using immersion technique. The structure of pores formed is described using REM data. It is ascertained that HAP-ceramics can be prepared using sintering and emulsion fractionating [67]. Usual precipitation process leads to the formation of agglomerates of solid particles, which presence lowers both compactness and possibility of the final product powder densifying. Obtained using emulsive fractionating the powder-like product has higher density while sintering at >800 °C. It is ascertained that density, reached after sintering of traditionally processed materials is limited with the presence of variously sized agglomerates of powder that are not coincided under the pressure of 200 MPa. Solid agglomerates of powder forming highly compacted areas in sintered ceramical sample start compacting in and around 400 °C, what is 100 °C lower than temperature of the start of emulsion fractionated powder compact sealing with the rate of its heating 5 °C/min. Inner hollow space of agglometares appearing by differential sintering, lead to the formation of large crack-like pores which operate as strength-limiting microstructure defects in traditionally processed HAP. After sintering of both during 2h. at 1100 °C breaking strength for emulsive fractionated material comparing with 70±15.4 MPa for traditionally processed material amounted to 170±12.3 MPa.

For the first time transparent HAP ceramics was made using microwave processing [68], what is reached thanks to the use as an initial material crystal HAP powder, synthesized hydrothermally. HAP ceramics obtained using sintering is single-phase and has average grain size 0.2 mkm. Similar characteristics of ceramics sintered in this way are also obtained in [69, 70].

The comparative study of annealing and agglomeration processes of hydroxyfluorapatite powders of $Ca_{10}(PO_4)_6(OH)_xF_{2-x}$ composition was carried out in [71]. The annealing led to the decrease of specific surface at the expense of particle binding. The surface diffusion and gas-phase transfer appear as main mechanisms of the surface decrease. Minimun of density is reached at $x = 1$ that corresponds to the minimum of FAP-HAP admixture enthalpy. Sintering is limited with the diffusion of hydroxyl and fluorine ions.

The compressive strength assessment of the prepared porous ceramics with the framework of fibers was conducted in [72]. High-strength fibers of β-$Ca(PO_3)_2$, which, as it is expected, have good biocompatibility, were derived from the crystallization products of ultraphosphate glasses with water lixiviation. Porous ceramics with almost 70% porosity with the framework from β-$Ca(PO_3)_2$ fibers for biomedical use is prepared using agglomeration of fibers. Its compression test showed that for

the fracture large deformations (0.2-0.3) are needed; phosphatecalcium porous ceramics showed much higher plasticity comparing to the common one.

Silver particles were used as a hardware for the bioceramic Ca-HAP hardening [73]. Such composites are made of HAP powders and silver oxide. Sintering of system components is dilatometrically studied. For the density increase, inhibition of HAP matrix decomposition and silver evaporation the program of sintering optimization was developed. High density was reached both for small cylindrical and large block samples with sintering without pressure. Density of composites — more than 92.4% of theoretical one was reached with the inclusion up to 30 wt. %. of silver, and their strenghth (by four-point bending) >80 MPa. The inclusion of silver refines impact strength from 0.70 MPa·$m^{1/2}$ for monolite HAP up to 2.45 MPa·$m^{1/2}$ by silver content 30 wt. %. The study of strengthening mechanism showed that sequential alternation of cracks in silver plates is the cause of hardening.

In work [74] the preparation of dense HAP bioceramics and also formation of highly porous structure with the communicating pores is described. Porous structure is formed using 1—3% of H_2O_2. The integral porosity 63—74%, with the mechanical properties: E-module 1.7—3.7 GPa, flexural strength — 7—14 MPa and ultimate strength 3.5—8.4 MPa is obtained. On the basis of porosity interconnectivity and some other mechanical properties, the given bioactive material can be potentially used in medicine.

In work [75] the characteristics of multilayer ceramics with HAP gradient structure, partly stabilized with zirconium (PSZ) are studied. There is a difficulty while preparing of samples with two-layer structure, composed of separated layers of HAP and PSZ because these layers can't merge with each other by means of standard procedure of sintering. Because of the flaking it is also difficult to prepare threelayer structures composed of the monolithic HAP layer, HAP and PSZ layer with the mass ratio 1/1. Five- and sevenlayer HAP/PSZ structures were prepared using heating in the atmosphere of electric furnace (1450 °C, 2 hours). In this case HAP reacted with PSZ at high temperature and the resulting products were zirconium oxide and calcium oxide ($Ca_{0.15}Zr_{0.85}O_{1.85}$). Seven- and eightlayer HAP/PSZ samples with gradient structure are prepared using hot-pressing (1150 °C, 1350 °C). In this case layers were combined chemically and there were no separation even after cutting and refinement operations. At the temperature of sintering (1350 °C) there appeared small cracks in the layer of monolithic HAP, parallel to the direction of compressing. Cracks were not found in any layer after sintering at 1150 °C. In the multilayer structure, prepared using hot pressing method between HAP and PSZ no chemical reactions were founded. Gradient structure was confirmed with the results of elemental analysis. Flexural strength of triplewall HAP/PSZ sample was much higher than of the monolite HAP. Vickers hardness of the layer composed of monolithic HAP was 4.3 GPa and increased with the increase of PSZ degree of refinement reaching 12.0 GPa in monolithic PSZ layer.

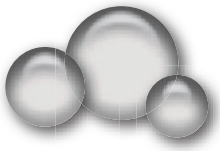

CHAPTER 2

METHODS OF INVESTIGATION OF STRUCTURE AND PHYSICOCHEMICAL PROPERTIES OF APATITE

Here the review of literature on experimental research of physicochemical properties of apatites is given. The physical and chemical properties of apatites are being discussed in connection with potential and real practical application.

2.1. Diffraction methods

Diffraction methods as a rule are used for phase's identification and more exact definition of structure parameters. Thereby neutron powder diffraction data for $Pb_{10}(PO_4)_6(OH)_2$, obtained at room temperature and 10 K, were used in [76] for the refinement of structure parameters. Compounds have hexagonal structure at both temperatures, $P6_3/m$, $z = 1$, $a = 9.8828(4)$, $9.8355(3)$ and $c = 7.4406(2)$, $7.4100(1)$ Å at 295 and 10 K, respectively. It was found that displacement of OH group from the point of structural localization appeared to be larger that it was expected from topological considerations.

The accuracy of determination of Ca/P ratio in apatites for medicinal application is a question of principle, to which individual research [77] is devoted, where quantitative X-ray diffraction analysis for Ca/P ratio determination within the range from 1.5 up to 2 is applied. High accuracy for the interval $1.5<Ca/P<1.667$ with the relative error of Ca/P ratio determination in the range of $0.1 \div 0.4\%$ was obtained. In this range of values of Ca/P ratio the X-ray diffraction method is more accurate than other methods. For the range of values $1.667<Ca/P<2$ the precision of reaction methods appeared to be higher.

The neutron diffraction analysis of synthetical calcium phosphates is examined in work [78]. As often as not the vibrational modes of hydroxyl groups don't appear because of overlapping with the oscillation of other oxygen-containing anions

like carbonate. In inelastic neutron scattering spectra oscillations of proton-containing groups is prevailing. The inelastic neutron scattering of Ca-HAP and brushite gives new opportunities for determining the number of aspects of biomaterials structure inaccessible for standart vibrational methods.

2.2. Atomic-force and electron microscopy

Various methods of microscopy are used for investigation of apatite-like compounds to determine micro- and nanostructure of these compounds. Thereby in work [79] electron microscopy was used for the description of microstructure of sintered pure Ca-HAP. The analysis of electron diffraction results with the convergent beam allowed to identificate Ca-HAP spatial group as $P6_3/m$. The compaction of material has been carried out using agglomeration without compression at 1250 °C for 30 minutes. Pure sample consisted of apatite — single crystal phase. Generally the observed microstructure was homogeneous and consisted of apatite grains with the mean diameter of about 1—2 μm. There was no residual amorphous phase observed, which could be formed during agglomeration on the grain boundaries. The investigations on the grain boundaries also have shown that intergranular amorphous film is absent along the two-granular compound, what confirming that compaction occurs without liquid phase. There was weakly disarranged area on the surface indicating widened structure of grain boundaries.

The investigation of stages of formation of Ca-HAP, obtained using sol-gel method was carried out using scanning electron microscopy (SEM) [80], which allows to study gel samples, treated at different temperatures and during different time slices, and also to define the morphology and size of grains along with the degree of porosity of samples surface. Therefore, the phase evolution could be analysed as the function of time of thermal treatment and temperature. The gel was prepared using calcium acetate and triethylphosphate, added with Ca/P molar ratio equal to 1.67. The determination of samples characteristics using transmission electron spectroscopy (TES) gave the possibility to investigate more precisely the interaction between separate particles, and also reveal the peculiarities of much lesser scale. The obtained results were compared with those obtained with X-ray diffractional method and FTIR spectroscopy.

The growth rate of crystal face (0001) of Ca-HAP in pseudophysiological solution was studied for the first time with phase shift interferometry. Recently engineered signal processing device used in phase shift technique gave the possibility to precise measuring of the growth rate. It is determined [81] that growth rate depends on the time, decreasing gradually and becaming constant soon. The maximum layer thickness, which was growing on the seed crystal, was equal to 500—700 nm, whereas growth rate during the initial stage of growth was of order of 10^{-2} nm/s. The detailed surface morphology is described using atomic-force microscopy method (AFM), certifying two-dimensional type of nucleation.

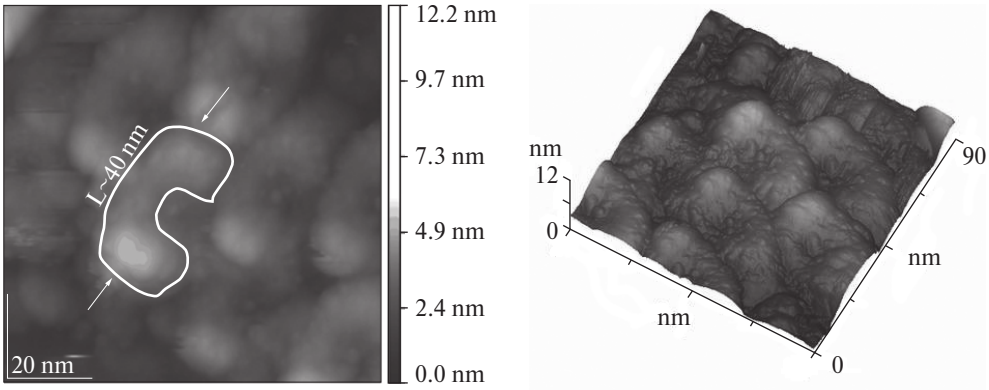

Fig. 2.1. The morphology of nanodisperse hydroxyapatite: a) two-dimensional image, b) three-dimensional image

The nanodisperse samples of calcium apatite were synthesized of water solutions of calcium nitrate and ammonium phosphate ("wet" chemical synthesis). The chemical composition and structure of obtained samples were determined using methods of chemical analysis and X-ray diffraction.

The morphology of nanodispersed samples of apatites was investigated with the method of atomic force microscopy (AFM) using scanning probe microscope JSPM-4500/4610 (JEOL). The parameters of imaging were the following: the size of image was 90.0 × 90.0 nm; the image height 12.2 nm; the time of exposure in point 83.33 μs. The morphology of the examined nanodisperse calcium hydroxyapatite is shown at the fig. 2.1. The average size of particles is 40 nm what corresponds to the specific surface area of about 500 m^2/g. The features of particles were the monomodal distribution of particles size and specific ordering.

2.3. Radiospectroscopy

As a rule radiospectoscropy is applied for structural-chemical atom state specification.

In work [82] it is shown using EPR method, that there is always an oxygen in O^- form on 6_3 axes of natural apatites, which is paramagnetic ($S = 1/2$), and carries out the function of probe in complexation process. There are coplexes F^--O^--F registered in a triplet form 1:2:1in EPR in a most widespread fluoroapatites in nature.

The occurance of chlorine in F- apatites in small quantities (0.03—0.4%) is also accompanied by the occurance of F^--O^--$C1^-$ complexes. Carbonate-containing Ca-HAP powder synthesized under high temperatures is tested [83] with EPR methods and double electron-nuclear resonance (DENR). There is intensive signal assigned to O^- ion radical observed in EPR spectra. Interactions of O^--radical with three non equivalent

sets of ^{31}P nuclei and also with one set of protons are resolved in spectra of DENR powders. After detailed analysis, based on "orientation selection principle", a detailed model for O^- ion radical and its surrounding was obtained. Thus, O^- location in hydroxyl position was unambiguously defined. Besides, there was found an experimental evidence of the carbonate group being the source of O^-, but not the OH group. Together with ion radical O^- resonances of another paramagnetic center were observed. As a result of spectra analysis and comparison with previous results this radical was identified as ion radical CO_3^{3-}, placed in the position of phosphate ion.

The observation ^{31}P-^{19}F-rotary echo was carried out in work [84]. The obtained data showed dipole coupling that happens only at the smallest distances ^{31}P-^{19}F in fluoroapatite. The use of fluorinated HAP, the main non organic enamel and dentine component showed the formation of fluorohydroxyapatite, covering the material with a layer smaller than one unit cell.

The work [85] demonstrates the ability of radiospectroscopy methods to determine spin space allocation in dissimilar system. The study is carried out with F—treated HAP and F-substituted (for 25%) apatite. The correlations of intesities by full echo and with different periods of dephasing were measured. After this the results were compared with calculated values for the models with different stages of flourating and orientation. The modelling included the calculation of ^{31}P dephasing (in the form of phosphate-ions) with a help of additional ^{19}F and then, with summing of ^{31}P-^{19}F clusters by all spins. The data has shown that OH^- ions in the unit cell on the (001) face are substituted with fluoride-ions. This result presupposes that fluorination occurs during ion exchange process faster than in the diffusion process or by dissolution — precipitation.

Lately the results of intense research of carbonate-ion state in biological (bones, enamel) and synthetical apatites, represented by hydroxyl-holding difference and used for medical purposes (implantes, pastes and cementes in stomatology) were reflected in literature [82, 86]. In the first study of biological apatites with EPR method the spectrum observed in g = 2.00 area was attributed to CO_3^{3-}-radical. The following studies initiated the discussion of many years on the nature of the radical observed in bioapatite: different authors identified the observed EPR spectrum with CO_2^- and CO_3^{3-}-radicals or with both. While discussing of interpretation of EPR spectrum observed in bioapatite some remarks on the CO_3^{3-}-radicals orientation in natural appatites were made and also the presence of CO_3^--radical in their composition was brought into question because of its recombining characteristics.

The parallel investigation of synthetic carbonapatites, enriched in some cases with ^{13}C isotope, the appliance of NMR and DEPR methods along with EPR has led to the identification of CO_2^--, CO_3^-- and CO_3^{3-}-radicals in it. The comparative analysis allowed to conclude, that in bioapatites the signal in $g = 2.00$ area is the result mainly of CO_2^--radical and the contribution of CO_3^{3-} in intensity of observed spectrum makes up to 10%.

Talking about localization of the most intensive signal of CO_2^--radical, there is still no agreement. Bioapatites that are studied intensively make only a little part of apatite's group,

which is polygenic mineral with the complex structure and composition. Particularly, carbonate-containing species (FHAP, O^{-}-F^{-}, F^{-}-O^{-}-Cl^{-}, P_3^{2-}, CO^{-}_3, CO_3^{3-} and HFAP, HAP, FAP) are typical both for magmatic and sedimentary apatites (biological ones). There are various genetic types that are distinguished among sedimentary apatites: marine (micrograin, granular, nodular, shell) and hypergene (continental, insular), which have different chemical characteristics of crystals. Using the method of EPR for each genetic type individual set of centers is registered, among which are ions: H^{+}, Mn^{2+}, Pb^{3+}, VO^{2+}, inorganic F^{-} — organic $\dot{P}(OR)_2$, $\dot{P}(OR)_3$, $H\dot{C}O$, $\dot{C}H_3$, $(\dot{C}H_3)_2$ C — R — radicals identified. Besides, during the processes of apatites catagenesis, metamorphism and weathering, their transformation — change of composition occurs and, as a result, change of structural features of matrix, sometimes very significant also takes place. Thus, using EPR method PO_3^{2-}-centres formed as a result of entering of ions U^{4+} and Th^{4+} in the position Ca^{2+} (II) (introduction of U and Th or transformation of surface complexes U(VI) and U(IV)) are registered in metamorphized and catagenetically processed apatites. By meamorphism and catagenesis the removal of CO_2 and introduction of Cl^{-} with the formation of paramagnetic F^{-}-O^{-}-Cl^{-} centres takes place. Weathering is accompanied with oxygen diffusion along 6_3 axis with the formation of F^{-}-O^{-}-F^{-} complexes and so on.

The reason for the steady interest of researchers in the problem of carbon introduction into the apatite structure is in the substantial change of apatite properties by carbonate ions: crystallinity has deteriorated, solubility has improved, reactivity has increased, thermal resistance has decreased. Taking into account great practical significance of apatite, the necessity to understand and to learn how to control its properties emerges. One may assume that the explanation of difference in assimilability of phosphate fertilizer made of phosphorites of different genetic types by plants, problems of teeth caries and pathologic formations in human organism, problems of single-minded/purposeful synthesis of apatites for technical and medical aims is being hampered by misunderstanding of crystal chemical peculiarities caused with carbon occurrence in the apatite structure.

The characteristic of $Ca_5(PO_4)_3$(F, Cl, OH) apatite structure is the occurrence of several halogens, placed on the 6_3 axis. In natural apatites they are present as a rule simultaneously with the preferences of one over another two (or one): F>Cl, OH; F>OH; OH>F, Cl. The most widespread one of finite forms (with one halogen) in nature is FAP, while ClAP and Ca-HAP rarely occurre in nature. They are crystallized in different crystal systems: FAP — in hexagonal one with the spatial group $P6_3/m$, HAP and CAP — in monocline with the spatial group $P2_1/b$. Carbonate-containing apatites are presented as the FAP-containing differences: francolites (F>1%) and dahllites (F<1%).

Carbonate ion is considered to be able to substitute PO_4^{3-} anion (*B* type), OH-groups (*A* type) and be adsorbed by the surface. In this division of carbonate apatites to *A* and *B* types on the basis of chemical, X-ray diffraction and IR spectra analysis there are elements of conditionality and contradictions. There are still no definite arguments for CO_3^{-}-ion location in place of OH-group on 6_3 axis, though the presence

of such methods as NMR, DENR and others in the arsenal of researchers allows to localize ions in the unit cell. It should be noted that the A type substitution is registered by now only for synthetical apatites.

It is well known that water occurrs in sedimentary and biological apatites in two forms: in the form of OH-groups, placed on the axis in the 6_3-position of halogens and in the form of molecules H_2O.

Depending on the formation conditions carbonate-ion forms part of apatite structure substituting PO_4^{3-}-anion in complex with the combined water or without it. In the absence of H_2O carbonate is bound firmer with the structure. In the presence of H_2O whole apatite surface, or a part of it (depending on the amount of H_2O), is presented with water which adsorbs CO_2 from the air. In such samples/specimens CO_2^--radicals are registered after the irradiation with correlation of their intensity with the amount of bound water. Moreover, the established specific character of CO_2^--radicals behavior allows suggesting the presence of CO_2 and H_2O amorphous layer or phase on the apatite surface (and maybe cations), which play a greater role in the definition of its properties.

The similar assumption of presence of «amorphous-like» carbonate on the surface or in the excited sites inside the crystal is stated after studying a NMR ^{13}C and ^{1}H and the mass spectra observed for different conditions of existence of synthetic and biological apatites [82, 86, and 87]. About presence of two positions a carbonate-ions in CO_3^{2-}-form instead of PO_4^{3-} and on a surface in the form of HCO_3 in synthetic (60 and 40%) and biological (70 and 30%) apatites are revealed by means of a radioisotope ^{14}C when it has been shown, that in exchange processes participate only superficial a carbonate-ions. The presence of water was also specified, as a necessary condition for CO_2^--radicals formation in synthetic apatites. By studying CO_2^--radicals in corals, aragonites, synthetic $CaCO_3$ and $CaHPO_4 \cdot 2H_2O$ the role of water in their stabilization was noted. The opportunity of formation of metal-water complexes, in particular $[Ca^{2+}(H_2O)n]$, $[Mg^{2+}\text{-}(H_2O)n]$, where molecules of water isolate CO_2^--radical from cations of structure is supposed. Meanwhile the isotropic spectrum with $g = 2.0007$, caused by complexes with rotating fragments is observed.

Thus, the authors have shown, that the bonding of surface-adsorbed CO_2 with the water in apatite exists, as it was also revealed in other minerals. However, no resolved superfine structures for ^{1}H nuclei of water molecules was observed anyway. Only the size of ΔH lines of CO_2^- spectrum is a little bit greater than those for CO_3^-- and CO_3^{3-}-radicals in PO_4^{3-} position. Using the NMR and DEPR methods it is established by now, that around the CO_2^- -center within a radius of 6 Å there are no ^{31}P nuclei, and the minimal distance up to ^{1}H proton is 9 Å. This distance is great enough to observe the resolved superthin splitting in EPR spectra. The further investigation is necessary to define “structure” of surface formation (probably, the phase) on the surface of apatite as its properties are caused with it.

The investigation of CO_3^{3-}-center in synthetic apatites, enriched with ^{13}C isotope, using NMR and DEPR methods has led to the conclusion about its localization in PO_4^{3-}-anion position with vacancies in the adjacent positions of Ca and OH and with arrangement of the plane of three atoms of oxygen parallel to the *c* axis. There is also another variant of arrangement of the molecular plane, namely at an angle of 90 degrees to the *c* axis, what is ill-founded and is out of keeping with the real structure.

The absence of natural monocrystals of francolites, small quantity of CO_2 in monocrystals of the magmatic origin has not allowed carrying out detailed investigation.

The question on charge balance by $CO_3^{2-} \leftrightarrow PO_4^{3-}$ replacement has also "long" history. It was considered not less than 11 mechanisms summarized in a number of publications. Offered almost 60 years ago for francolites the mechanism of $PO_4^{3-} \leftrightarrow (CO_3\text{-}F)^{3-}$, $(CO_3\text{-}V)$ and $(CO_3OH)^{3-}$ compensation for HAP with F and OH positions in the place of oxygen vacancy and preservation of tetrahedral structure was widely enough applied by researchers alongside with more logical $Ca^{2+}+PO_4^{3-} \leftrightarrow Na^{+}+CO_3^{2-}$ or $Ca^{2+}+PO_4^{3-}+OH^{-} \leftrightarrow \leftrightarrow V_{Ca}+CO_3+V_{OH}$. Some researchers explained anomalies in the behaviour of peaks on thermograms with the presence of different (CO_3F) and $(CO_3\text{-}V)$ complexes. However in recent years the application of magnetic resonant spectroscopy methods in addition to EPR-research investigation of apatite has solved the problem of this mechanism in a short time. Using the NMR method of the direct bonding between CO_3 and F was not revealed, as well as the presence of (CO_3OH)-ion after EPR and DENR investigation of Ca-HAP. And quantum-mechanical calculation has shown that hypothetical tetrahedral ion (CO_3P) cannot be stabilized in the apatite lattice. Ion F^- should be placed in interstice, that is more consistent with the results of other investigations, in particular of FTIR. For Ca-HAP the mechanism with vacancies in adjacent Ca- and OH-positions more particularly is applied, i.e. the opportunity for localization of structural water in the matrix is available.

It is known, that C-radicals have various factors of stabilization. In such situation the estimation of the dependence of their intensity on the quantity of CO_2 (%) becomes problematic. Directly proportional dependence is observed in the groups of apatites with identical conditions of formations of minerals (or synthesis). Quite often lines of CO_3^{3-}-radical "are absorbed" by the intensive line of CO_2^{-}. In this case reliable criterion of presence of CO_3^{3-} is the change of intensity of a registered line even for 5—10 days after irradiation. As CO_2^{-} is unaltered, the character of a kinetic curve is determined only with the presence of CO_3^{3-}. In addition computer modelling of spectra allows to register the CO_3^{3-}-radical contribution.

The investigation of equilibria in phosphate-calcium water systems at $T = 25$ °C has shown, that depending on pH of the equilibrium solution isomorphic versions of apatite (15 types) with the characteristic ratio of chemical constituents (Ca/P = 1.44-2.0), among which there also analogues of natural ones are formed. Depending on pH sedimentary apatites are conventionally divided into three groups: «acid» (pH = 2-7),

«neutral» (pH = 7) and «alkaline» (pH>7) which contain different quantity of bound water and have the solubility increasing from «acid» to «alkaline».

The change of density, specific surface and other parameters of calcium phosphates, phosphorites depending on the isomorphic impurity content, mainly CO_2 and H_2O, is studied.

The results indicate, that apatites of marine nodular phosphorites, essentially not changed by processes of catagenesis and aerations, with the greatest quantity of these impurities have the minimal density (2.877 g/cm^3), greater specific surface (21 m^2/g) and solubility. Just in these apatites the most intensive EPR spectrum of CO_2^--radical, is registered, that in light of the presented results indicates a plenty of [CO_2-nH_2O] complexes on a surface.

Thus, the investigation of natural carbonate apatites of various genesis, type and structure (HAP, FHAP, HFAP, and FAP) has allowed understanding the peculiarities of carbon ocurrence in its structure, allowed to show and to explain a variety of observable EPR spectra which can be used as indicators of formation conditions, and also the fact of presence of imposed, secondary processes. The application of crystal-chemical approach for solving the problem of carbon ocurrence in the structure of apatite has appeared quite successful, has led to the establishment of important regularities. The received results demand to continue research, in particular to define concretely the "structure" of complexes and to estimate their quantity on the apatite surface with which presence some properties of apatite correlate. It is necessary to establish boundary H_2O and CO_2 proportions on the surface, to connect them with specific properties of apatite.

Thus, the behaviour of carbon impurity in all forms of natural carbonate apatite and experimental results allow making the following conclusions.

— Stable CO_2^-, CO_3^- and CO_3^{3-}-radicals (8 versions) in the structure of carbonate apatite have different nature and stability. Radicals are indicators of carbon localization caused with formation (synthesis) conditions, surface and structure condition: a) CO_3^- and CO_3^{3-} are formed of carbonate-ion CO_3^{2-} in PO_4^{3-}-position; b) CO_2^- is formed of CO_2, adsorbed on the surface through the bound water.

— Factors of radicals stabilization in structure are different: surface CO_2^- -radical is stabilized the water connected by molecules; structural CO_3^--radicals with F^- ions, and CO_3^{3-} with F^- and Mg^{2+} ions. Bound water (H_2O) and Na^+-ions are destabilizing factors for CO_3^--radical.

— The special role belongs to the molecular form of water, which: a) stabilizes surface CO_2^--radical and defines its quantity; b) influences on kinetic and dynamic characteristics of structural CO_3^- and CO_3^{3-}-radicals; c) defines the ratio of intensities of surface and structural C-radicals; d) participates together with CO_2 in formation of amorphous layer on the surface that correlates with apatite properties, in particular with its solubility.

— In the structure the interfaced isomorphic replacements occur, namely: $NaCO_3$, $MgCO_3 \leftrightarrow CaPO_4$, influencing on stabilization of structural radicals.

— The ration between structural (CO_3^-, CO_3^{3-} in PO_4^{3-}-position) and surface (CO_2^-, CO_3^-)-radicals for each genetic type of natural carbonate apatite individually: intensive CO_2^--radical is characteristic for marine, biological and synthetic (obtained using precipitation) apatites. In hypergenic samples there are all variants of ratio depending on the structure and mainly quantities of the bound water in molecular form H_2O.

— In magmatic and sedimentary samples transformed with weathering and catagenesis, isotropic spectra of these radicals are registered.

— CO_3^-- and CO_3^{3-}-radicals arise after irradiation of fluorine-containing HAP samples. They are particularly intensive in samples without appreciable quantities of isomorphic impurities. In pure HAP they are absent or are present in very small quantities, and CO_2^--radical makes the main contribution to the spectrum intensity.

— CO_2^--radical is present in apatites of all types studied, but only in samples that according to the results of chemical analysis and NMR investigation contain structurally bound water; thus CO_2^--signal intensity correlates with its quantity. Influences of other admixtures on signal strength of CO_2^- are not detected. Isomorphic impurities essentially affect the observable picture. So, CO_3^--radical signal strength in samples with Na^+ is less, than without it. It can be caused with $CaPO_4$ substitution for $NaCO_3$. Its intensity decreases (to disappearance) in samples with a great amount of bound water. The presence of Mg^{2+} admixture is accompanied with the existence of not only intensive, but also more stable CO_3^{3-}-radical. This also can be caused with the presence of $MgCO_3$ complexes, replacing Ca-PO_4.

2.4. Optical methods and vibrational spectroscopy

Very often Raman spectroscopy is used for the quantitative analysis of apatite compostition [88]. The relations of relative intensities of Raman bands corresponding to Ca-HAP and calcium oxalate monohydrate (COM) were used for calibration curve construction. There were lines at 960 cm^{-1} (I_RCa-HAP) and 1462 cm^{-1} (I_RCOM) used. The linear dependence of I_RCa-HAP/I_RCOM ratio by inversion of the concentration in solid body, in binary mixtures was found. The comparison of this data with the data of quantitative analysis of Ca-HAP-COM system with X-ray diffractional method using relative intensities (002) reflections off Ca-HAP and (020) reflections of COM, has shown that Raman spectroscopy gives the relative advantage of investigations without samples polishing, thereby providing the possibility of layered minerals analysis.

According to the data of IR and Raman spectroscopy of FAP, Ca-HAP and Ca-ClAP [89], it is found that the displacement of the anion columns relatively to the mirror surface leads to the increase of PO_4 tetrahedron deformation both in terms of quadratic elongation and in terms of tetrahedral angle modification, and promotes systematic decrease of frequency of vibrational modes ν_1, ν_3 and explicit increase of splitting of ν_3, ν_4 Raman and IR modes. Existing results indicate that the displacement of vibrational

frequencies in apatites is not a direct consequence of modification of bonds length or voluentary unit; as also modification of splitting value is not only a result of dipole-dipole interaction between phosphate ions in elementary cell, but the concequence of vibrational interaction between tetrahedron and structural column.

The comparison of Raman spectra of polycrystal Ca-HAP and β-TCP is presented in work [90]. Both compounds have generally similar Raman spectra, which is the consequence of manifestations of internal modes of PO_4^{3-} tetrahedrons. However, certain characteristic features of Raman spectra gave the possibility to define the difference between these phosphates. In the determination of differences between $Ca_{10}(PO_4)_6(OH)_2$ and β-$Ca_3(PO_4)_2$, as for example, width of internal PO_4^{3-}-bands, as it was made in work [91], where the comparative study of Raman spectra of polycrystal β-TCP and Ca-HAP in all optical range is presented. Raman scattering allows finding structural distinction of these two calcium phosphates not only by means of finding of vibrational modes relating to OH-group of Ca-HAP but also by means of bands comparison, which are the result of internal PO_4^{3-} modes distortion. The band widths of Raman scattering are interrelated with the modes of bondings flexure in PO_4^{3-}-groups, and the frequency difference is the characterictic feature which can be used for the distinction beetween β-TCP and Ca-HAP. This method was used for the controlled formation of Ca-HAP layer of micron thickness which is precipitated on the surface of TCP-volastonite from SBF.

Raman spectroscopy is also used in a number of biomedical investigations, especially, [92], including those which study human tissues, single cells, implantants and the presence of exogenic inclusions and also while introduction and interaction of chemical reagents with tissues. That work underlines the advantages of Raman spectroscopy application in biomedical research.

The analysis of Ca-HAP based powder coatings on the metal medical implantants using Raman spectroscopy and FTIR was conducted in [93]. In spite of numerous studies of structure and vibrational Raman and IR spectra of FAP, the problem of correlation of observed and predicted bands still remains. IR spectroscopy of FAP powders together with micro-Raman polarization investigation of FAP monocrystal in the area $45 \div 1100$ cm^{-1} was carried out in [94]. The presence of E_{2g} band for mode ν_1 is rather doubtful. For ν_2 mode two A_g bands were observed, which demonstrated different response relatively to the direction of polarization. Raman and IRthe S provide dynamic information relatively to molecular structure, unlike the diffraction data which carry the information on the average atom position in the crystal lattice.

Deuteration of synthetic Ca-HAP and properties of fluoride-deuterationed samples were studied with FTIR method in [95]. Deuteration of column of OH^- ions in Ca-HAP structure was carried out at different degree of fluorination. The band at 2680 cm^{-1} observed in deuterationed Ca-HAP is attributed to the surface OD-groups which react with CO_2 molecules. The band at 2633 cm^{-1} for the column of OD^--groups is not influenced by CO_2^- adsorption. As it was expected Ca-HAP fluorination doesn't result in the increase of surface OD^- band.

Laser ablation with excimer laser for Ca-HAP targets was analyzed in [96]. For this purpose pulsed laser Kr-F_2 (248 nm) with two different flux densities 4.8 and 2.1 J/cm^2 was used, directed on two targets of different densities (1.3 and 1.7 g/cm^3) providing evaporation of target material and formation of characteristic plasma torch. For torch analysis the high-speed representing device with the charge coupling and band-pass filters was used. Obtained results showed the occurance of three species of plasma emission: atomic component, molecular and hot particles spreading from the target. Velocity dependence on laser flux intensity shows that mechanism of molecular component formation differs from other species. The analysis of dependence on target density shows that the mechanism which controls the velocity of ablation at a given flux is the evaporation of hot particles from the target.

Flares, initiated with laser ablation of Ca-HAP by different irradiation conditions, are analysed using CCD-photographing and optical spectroscopy [97]. The images obtained by four different laser intensities of flux (1, 1.5, 2.6 and 3.5 J/cm^2) revealed the presence of two separate emission components in flare after laser impulse up to 1 mks. The relative intensity of emission of both components depends strongly on the flux density value and determines in such a way the observable velocity of the propagation. Spectra have shown that by low flux densities, molecular variety dominates atomic one, and at high flux densities atomic variety is predominant. Images obtained using band-pass filter showed that the nature of high-velocity emission component in flare is mostly atomic; taking into consideration that emission for the second one is a result of molecular radicals' excitation.

The results of Ca-HAP irradiation with Nd:YAG laser are discussed in [98]. The research is carried out using high-speed CCD-mapping with band-pass interference filters which allow extracting the following species: neutral calcium, calcium oxide radicals and neutral oxygen. The results, obtained in vacuum, show that expansion occurs by constant velocity (~$2 \cdot 10^4$ m/s for atoms and ~$3 \cdot 10^3$ m/s for molecules) and emission is completely determinded with neutral calcium emission. After ablation carried out in the atmosphere of water vapor, background gas contained angular varieties of flares that resulted in the formation of plane shock wave by 0.1 mBar and spherical shock wave by 0.2 mBar. The comparison of images obtained at 0.1 mBar showed the existence of chemical reactions resulting in formation of calcium oxide radicals. In this case flare emission depends on the molecular individuality.

Laser-induced spectroscopy (with temporal resolution) of natural apatites, scheelite, zircon, calcite and fluorite allows disclosing luminescence centers which can't be spectroscopically resolved by stationery conditions [99]. Application of spectroscopy with temporal resolution allowed to determine rare-earth elements, which luminescence was hidden with stronger bands of Eu^{2+}, Mn^{2+}, $(WO_4)^{4-}$, $(MoO_4)^{4-}$ and radiative centers. Luminescence of Pr^{3+}, Tm^{3+} and Er^{3+} is discovered for the first time in the same way in minerals over ions (Sm^{3+}, Dy^{3+} and Tb^{3+}) with the similar emission spectra.

2.5. EXAFS and XANES study

Natural apatites used in industry for fertilizer production often contain residual quantities of Cd^{2+} which can reach concentration from several tens up to several hundreds particles for a million. Cd^{2+} isn't eliminated during phosphate fertilizer production and its concentration in the final product can exceed ecologically safe norms. Knowledge of standart Cd^{2+} content in apatite ores is a prerequisite for the development of effective technological processes of its extraction. Extended X-ray absorption fine structure at the *K*-edge of cadmium is used in work [100] for the determination of Cd^{2+} presence. The structural environment of Cd in sedimentary apatite ores from western Africa was investigated. These apatites are fluorinated and contain goethite, quartz and crandallite as auxiliary phases, what is established with X-ray diffraction and EXAFS spectroscopy. Cd *K*-edge EXAFS spectra of two natural samples were analyzed and compared with the spectra of corresponding Cd-containing minerals, including HAP, goethite and crandallite. There was good spectral similarity between natural samples and synthetical apatite containing small quantities of Cd observed. The spectral similarity indicates that the majority of Cd atomes in apatite structure forms $Cd_{10}(PO_4)_6(OH, F)_2$ clasters what is certified with the quantitative analysis of EXAFS spectra. It was shown that Cd atoms are surrounded with O atoms at the distance 2.33 Å, then — atoms of phosphorus lie at the distance 3.53 Å, and the third coordination sphere is presented with calcium atoms at the distance 4.02 Å. The comparison of this data with those obtained for the synthetical apatites allowed assuming that Cd occupies two Ca crystallographic positions with the minor preference of $Ca_{(2)}$ positions.

Посилання на р нок у те ???

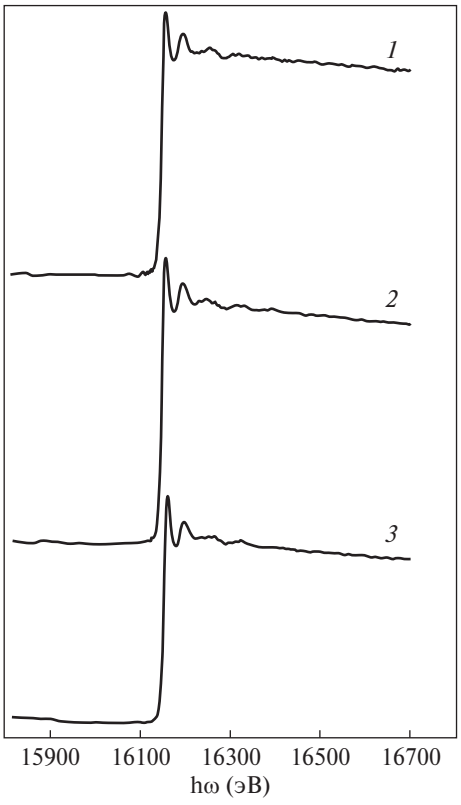

Fig. 2.2. Strontium EXAFS spectra in: *1* — crystalline $Sr_{10}(PO_4)_6(OH)_2$; *2* — amorphous strontium phosphate; *3* — isomorphically substituted $Sr_{10-2x}Na_xLa_x(PO_4)_6(OH)_2$ ($x = 1.0$)

Electronic structure of phosphates and sulphates of 3*d* transition metals was investigated using XANES spectroscopy method in [101]. There are two peaks by 3*d* electrons amount in cations less than 9 and one peak by 10 electrons in P and S *K*—edges of XANES spectra, which describe electron transfer from P and S 1s to P and S 3*d* vacant states. With the increase 3*d* electrons quantity, the intensity of the peak, corre-

sponding to lower energy (pre-edge peak) decreases and the shift to the region of lower energy with the discontinuity by five 3*d* electrons occurs, and the peak corresponding to higher energy (main peak) moves to the region of lower energy. Pre-edge peak changes indicate that electron density and energy level of P or S 3*p* vacant states depend on the number of 3*d* electrons what indicates that P and S 3*p* states are hybridized with 3*d* states of cations. The displacement of the main peak which is connected with P or S 3*p* states hybrisization with the 4*s* states of cations can be explained with the lowering of energetic levels of cations with the increase of the number of electrons.

Fourier analysis of EXAFS-spectra of strontium in disordered apatites [102].

We have studied short-range order in strontium phosphate systems with different degree of disorder: in isomorphically substituted Sr-HAP — the case of cellular disorder and in amorphous strontium phosphate (APS) — the extreme case of disordering. As an independent method of investigation EXAFS-spectroscopy method was used, which is the most applicable for the short-range order investigation of disordered phosphate systems because of ineffectiveness of other structural methods.

The investigations were carried out using EXAFS-spectrometer of V.D. Dobrovolskiy construction [103], which allows to carry out precise measurement of X-ray absorption coefficient with relative error not exceeding 0.2%. EXAFS-spectra are obtained (fig. 2.2) using quartz crystal analyzer with the reflection plane (1010) and arched according to Koshua method. Bending radius of crystal R = 890 mm.

Initial processing of experimental spectra was carried out using traditional technique/procedure [104]. EXAFS spectrum was extracted following the formula:

$$\chi(k) = (\mu(k) — \mu_0(k))/(\mu_0(k) — \mu_1(k)),$$

where $\mu(k)$ — experimental absorption coefficient of a sample; $\mu_1(k)$ — absorption coefficient appearing because of all other processes with the exception of photoionization of the studied atomic shell (ionization of outer electronic levels, ionization of other chemical elements, scattering); $\mu_0(k)$ — absorption coefficient, which was observed in the case of absence of adjacent atoms close to absorbing one; k — module of wave photoelectron vector which is specified using relation: $k = [(2m_e/h^2)(h\nu—E_0)]^{1/2}$.

$\mu_1(k)$, $\mu_0(k)$ — were determined using Victorin polynomials. At the same time polynomial coefficients were determined using least square (LS) method in subthreshold and far spectral region.

Radial distribution curve of g(r) atoms around absorbing atom in this method was determined based on Fourier transformation $\chi(k)$:

$$g(r) = \int_{-\infty}^{\infty} \chi(k)k^nP(k)e^{-2ikr}dk.$$

For all studied spectra the limits of integration were selected from 2 $Å^{-1}$ up to 12 $Å^{-1}$, and n = 1.

Window function P(k) was used as Gauss and Hamming functions [104], what/which allowed certain analyzing of experimental data up to 4.5 Å.

Посилання на рисунок у тексті ???

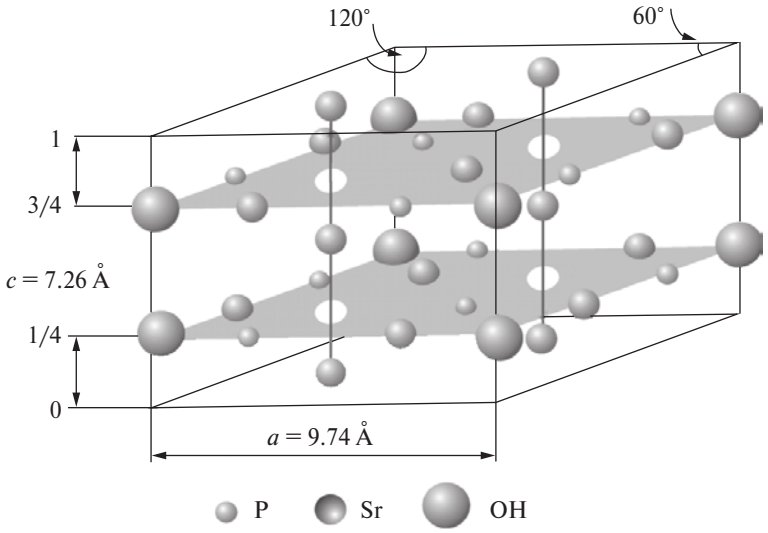

Fig. 2.3. Unit cell of Sr-HAP (oxygen atoms from tetrahedrons are not listed)

In single-electron approximation and presentation of discrete spheres of EXAFS — oscillations are described using the following formule:

$$\chi(k) = \frac{1}{k}\sum_{j}^{\infty}\frac{N_j}{r_j^2} f_j(k,\pi)\sin(2kr_j + \varphi_j(k))e^{-2\sigma_j^2 k^2}e^{-2r_j/\gamma(k)}$$

N_j, r_j, σ_j — parameters of coordination sphere;
γ — the length of free path of an electron;
$f_j(k, \pi)$ — amplitude of probability of photoelectron 180° scattering (backscattering factor);
$\phi_j(k)$ — photoelectron phase change by its emission and scattering.

For the analysis of experimental results Fourier transform method, with theoretical values of phase shift function and scattering amplitude (phase Fourier transform) was used. McKale functions were used as theoretically calculated amplitude and phase functions [105].

Stoichiometric Sr-HAP was chosen as model compound, which structure is presented on the fig. 2.3. There are two unequivalent lattice sites for Sr, notably — $Sr_{(1)}$ (Sr in column) by z = 0 and ½, and $Sr_{(2)}$ (screw axis Sr) at z = 1/4 and 3/4. Each $Sr_{(1)}$ ion is surrounded with 9 oxygen atoms of 6 PO_4-groups, and ion $Sr_{(2)}$ — with 7 oxygen atoms of 5 PO_4-groups and 1 of OH group. Thus, the apatite composition can be also expressed as: $[Sr_{(1)}]_4[Sr_{(2)}]_6(PO_4)_6(OH)_2$.

Radial atom distribution around different types of strontium atoms in Sr-HAP according to the reference crystallographic data [106] is given in table 2.1, and its graphic visualization is represented in fig. 2.4. The main curve features of stoichiometric Sr-HAP can be with comparison of positions of maximum module of Fourier transformant with the given atom distribution around strontium atoms.

It can be seen that the main function maximum of radial atom distribution is determined only with oxygen environment of strontium. The small shoulder in the region around 2.8 Å (fig. 2.4) is determined by the hydroxyl group neighborhood of strontium. At the same time the similar feature observable at small R (~1.8 Å), is caused with experimental data interval limitation in k-space.

The absence of the feature in the region around 2.8 Å on curves of radial distribution of amorphous strontium phosphate atoms and isomorphically substituted Sr-HAP indicates the absence or significant reduction of OH-groups contribution to the environment of Sr atoms (fig. 2.5).

Since backscattering functions for Sr atoms have the greatest value, it is possible to assert confidently, that peaks B and C are determined with metal-metal coordination.

It can be seen that the transition to ASP (fig. 2.5) transforms both peaks to one and indicates the leveling of two various structural positions of Sr atoms. At the same time wide enough peak not allowing to judge the existence of only one structural position for Sr atoms in ASP is observed.

ASP of $Sr_3(PO_4)_2 \cdot nH_2O$ (n = 3-4.5; 15-20 wt. % H_2O) composition that correspons to strontium-deficient HAP is in amorphous state.

ASP is formed mainly as a spherical particles approximately 300-1000 Å in diameter and with a specific surface area of approximately 50-150 m^2/g.

Table 2.1. **Radial distribution of atoms around various types of strontium atoms in Sr-HAP.**

Atom	The quantity of atoms in the coordination sphere	R, Å	Atom	The quantity of atoms in the coordination sphere	R, Å
$Sr_{(1)}$			$O_{(4)}$	1	2.388
$O_{(1)}$	3	2.409	$O_{(3)}$	2	2.512
$O_{(2)}$	3	2.459	$O_{(1)}$	1	2.714
$O_{(3)}$	3	2.809	H	2	2.768
P	3	3.218	P	1	3.083
$Sr_{(1)}$	1	3.420	H	2	3.091
$Sr_{(1)}$	1	3.460	P	1	3.292
$Sr_{(2)}$	2	3.954	$O_{(3)}$	2	3.390
$Sr_{(2)}$			$O_{(1)}$	1	3.455
$O_{(3)}$	2	2.345	P	1	3.465
$O_{(2)}$	2	2.357	$Sr_{(2)}$	2	3.569

$O_{(1)}$, $O_{(2)}$, $O_{(3)}$ — oxygen of phosphate tetrahedrons; $O_{(4)}$ — oxygen of OH-groups.

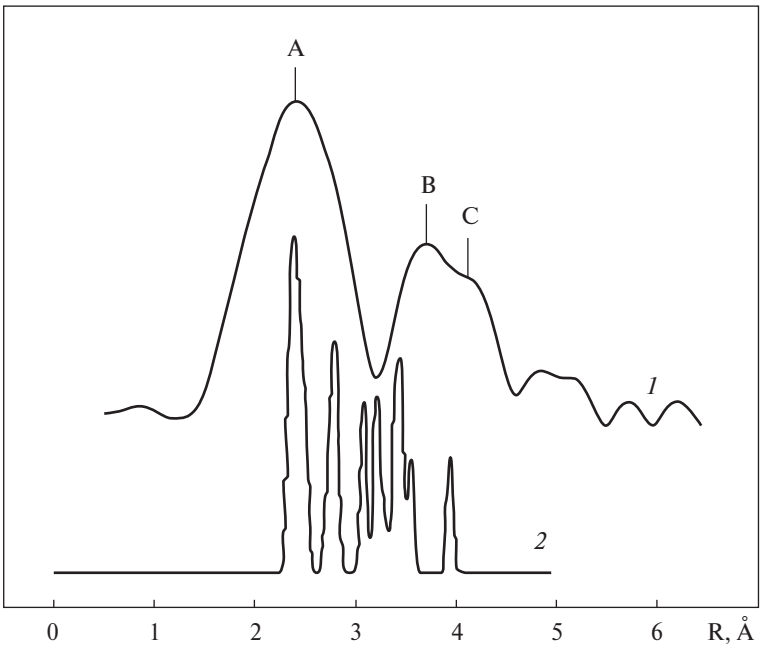

Fig. 2.4. *1* — Partial function of radial distribution of atoms around strontium atoms in $Sr_{10}(PO_4)_6(OH)_2$; *2* — Graphic visualization of coordination sphere around strontium atoms in $Sr_{10}(PO_4)_6(OH)_2$ using Gaussian broadening (table 2.1)

For the explanation of structure of amorphous phosphates of alkaline-earth metals several models [1] were offered. However uncertainty concerning structure nevertheless remains. IR and the NMR-investigation of amorphous phosphates of alkaline-earth metals, carried out in [107], show the reduction of PO_4-tethraedrons symmetry and the absence of strong crystal field in such substances.

Hence, ASP cannot be a simple cluster of HAP-Sr cell units and it is necessary to consider the nanoassembly in ASP in approaches of polycluster structure. Most likely, ASP consists of clasters, in which the nearest oxygen environment of strontium is close to crystal Sr-HAP except for OH-groups. Every such cluster most likely has a cell unit of $Sr_3(PO_4)_2$ composition with the size approximately equal to double metal-metal distance, i.e. about 8-10 Å, centered by the $Sr_{(1)}$ site of apatite crystal lattice structure. The result of Fourier transformant EXAFS-spectra of crystal and amorphous samples comparison which shows correlation of an oxygen environment of strontium, without taking into account hydroxil groups in ASP, and a relative positioning of metal atoms in ASP, close to $Sr_3(PO_4)_2$ serves as conformation of such arguments.

Relative reduction of feature C intensity (fig. 2.5) in isomorphically substituted strontium phosphate indicates that strontium atoms substitution for atoms of alkaline and rare-earth elements occurs mainly in $Sr_{(2)}$-positions. Narrower peak A, and

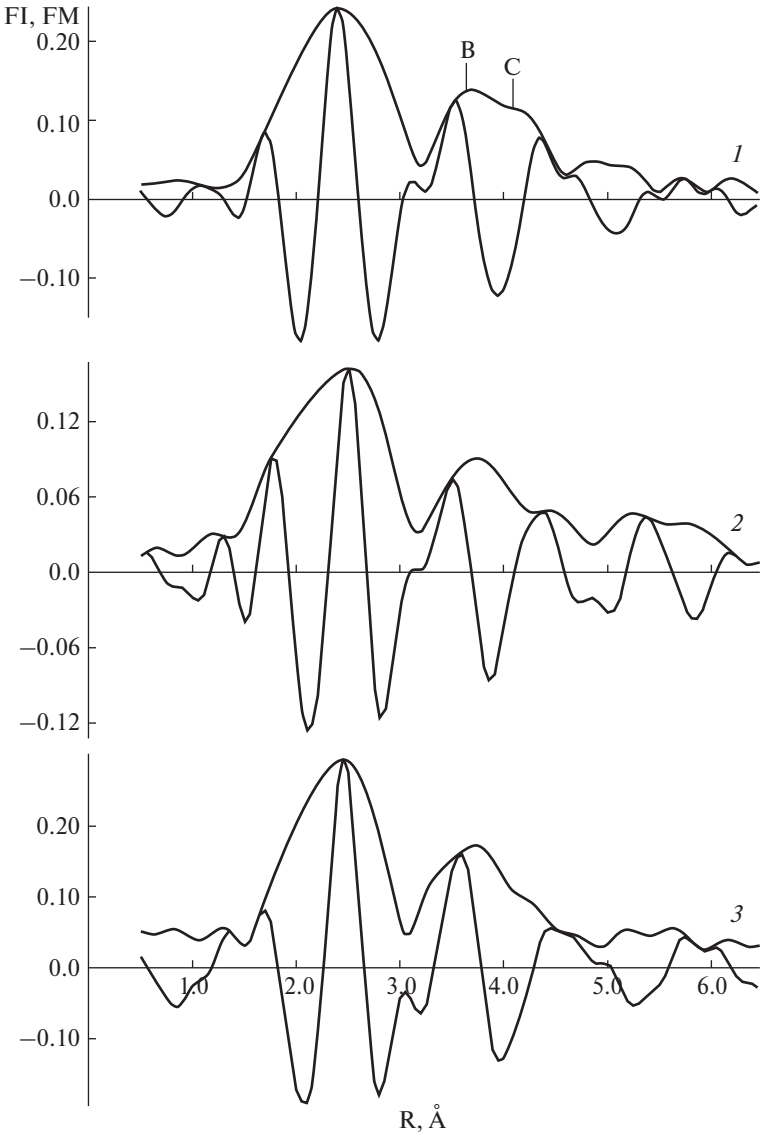

Fig. 2.5. Fourier-transformants of Sr EXAFS-spectra: *1* — $Sr_{10}(PO_4)_6(OH)_2$; *2* — ASP; 3 — $Sr_{10-2x}Na_xLa_x(PO_4)_6(OH)_2$ ($x = 1.0$).

also manifestation of additional feature of about 3.3 Å, associated, most likely, with P atoms, points to the changes of PO_4^{3-} tetrahedrons geometry.

Differences of investigated curves in the range up to 2 Å (fig. 2.5) can be related as well to the fact that the charge compensation within the cell unit, occuring on the channel $2Sr^{2+} = Na^{+}+La^{3+}$ is carried out topologically heterogeneous and it determines the change of a crystal field near Sr atoms-leading to various processes of pho-

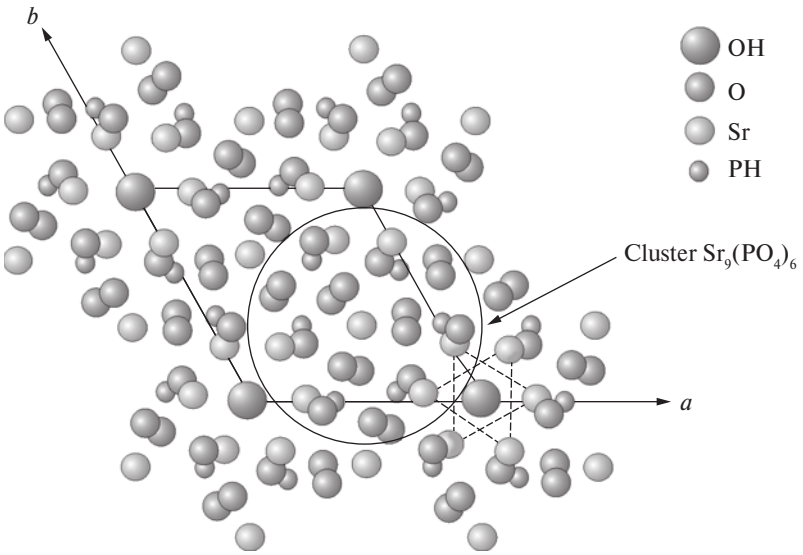

Fig. 2.6. Atomic structure of amorphous strontium phosphate

toelectron scattering and contributing to the structural information being received in the interval up to 2 Å.

Fourier-analysis of Sr EXAFS-spectra in isomorphically substituted $Sr_{10-2-x}Na_xLa_x(PO_4)_6(OH)_2$ ($x = 1$) and ASP using functions, amplitudes and phases calculated theoretically has allowed to describe radial distribution of atoms around of Sr atoms up to 4.5 Å.

It is shown that of strontium atoms substitution for atoms of alkaline and rare-earth elements occurs mainly in $Sr_{(2)}$-positions.

Isomorphous substitution in Sr-HAP metal sublattice results in substantial modifications in oxygen environment of strontium atoms appearing in the PO_4-tetrahedrons symmetry reduction and in OH-groups leaving the nearest environment of strontium.

Experimentally observed radial distribution of metal atoms environment in amorfous strontium phosphate is well described using polyclaster structure approach with the possible local structural motif close to the tristrontium phosphate (fig. 2.6).

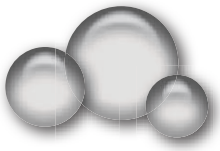

CHAPTER 3

PHYSICOCHEMICAL PROPERTIES AND APPLICATION OF APATITES

3.1. Thermodynamics of apatites

Thermodynamic values for stochiometric apatites and vitlokite are obtained in work [108]. In table 3.1 values for enthalpy formation per one atom (ΔH^{A}_{298}), and characterizing average bond energy are given. Minerals of apatite group with the increase of interatomic bond form the series: hydroxyapatite-chlorapatite-vitlokite-fluorapatite. The series reflects the special position of fluorapatite as the most stable chemical compound of this class.

The thermometric method of fluorine detection based on fluoride-ions interaction with Ca-HAP is developed in work [109]. Detecting consists in enthalpy measurement by adsorption of Ca-HAP fluorine by means of temperature measurement, using thermistor calorimeter. The detection limit of fluorine made 5 micrometers (0.1 ppm). The method can be applied for fluorine detection in water solution and gives highly reproducible results, at least, within 6 months without the need for replacement or regeneration of ceramic Ca-HAP tablet.

Expressity of operations of thermal reading and the analysis of injective mapping stream provides cheapness and speed of the fluorine detection method.

Thermochemistry of fluorapatites and volatility of components are investigated in work [110]. Theoretical compositions of apatites are characterized with high maintenances of volatile components: fluorapatite $Ca_5(PO_4)_3F$ contains 3.8 weight. % of fluorine, chlorine apatite $Ca_5(PO_4)_3C1$ — 6.8 weight. % of chlorine, hydroxyapatite $Ca_5(PO_4)_3OH$ — 1.8 weight. % of water. However natural isomorphic mixtures of apatites with such high content of volatile components are rarely formed though their examples are given in special mineralogical collatings.

This specific character of apatites has attracted attention of researchers and was explained with excess oxygen entering

Table 3.1. **Enthalpy and free energy of formation of minerals, kJ.**

Compound	$-\Delta H^{A}_{298}$	$-\Delta H^{0}_{298}$	$-\Delta G^{0}_{T}$	
			298 K	1000 K
$Ca_5(PO_4)_3F$ (FAP)	327.25	6872.20	6508.12	5684.10
$Ca_5(PO_4)_3C1$ (ClAP)	315.72	6630.15	6271.47	5426.52
$Ca_5(PO_4)_3OH$ (HAP)	305.53	6721.60	6338.43	5471.66
$Ca_9P_6O_{24}$	316.99	12362.46	11686.96	10156.67
CaF_2	409.75	1229.26	1176.92	1060.49
$CaCl_2$	265.27	795.80	748.06	642.12
$Ca(OH)_2$	197.22	986.09	898.41	691.14
H_2O	95.28	285.83	237.14	192.56
NiO	119.87	239.74	211.58	149.22
Fe_3O_4	159.39	1115.73	1012.73	789.43
Fe_2SiO_4	211.34	1479.36	1379.38	1150.82
SiO_2	303.57	910.70	856.29	729.98

apatite structure, replacing fluoride-, chloride- and hydroxid-ions, with the formation of a hypothetical mineral — oxyapatite (voelckerite) $Ca_{10}P_6O_{25}$, though its existence is discussed.

Hence, by thermochemical substantiation of a new theory of isomorphism of minerals of apatite group necessity of wider interpretation of belonging of some intermediate solid solutions to more general isomorphic system with theoretical composition of $Ca_9P_6O_{24}$-$Ca(F, Cl, OH)_2$, which is formed in the reaction: $Ca_9P_6O_{24}$+$Ca(F, C1, OH)_2$=$Ca_{10}P_6O_{24}(F, C1, OH)_2$, being carried out at minimally possible temperature. With temperature increase lesser quantity of $Ca(F, Cl, OH)_2$ is involved in the reaction and the series of solid solutions with composition close to vitlokite are generated. It is possible to judge the influence of temperature by change of volatile components (F_2, Cl_2, H_2O) output.

3.2. Thermal stability

Ca-HAP behaviour by sintering depends not only on characteristics and impurities of pure materials, but also on the thermal conditions of manufacturing process. The work [111] concerns the influence of the size of Ca-HAP particles on relative density and hardness of the final matrix. Ca-HAP powder has been isostatically pressed at 200 MPa and a room temperature, then sintered at the temperature from 1000 °C up to 1450 °C with 2 hours retention.

It was found, that at the temperature of 1250 °C the material is phase-homogeneous and it is represented by Ca-HAP which samples have density of >99% of the theoretical value and possess hardness of 6.08 HPa.

Ca-HAP decomposition begins at 1400 °C and is accompanied with the formation of TCP phase. Hardness change depends on relative density and of certain average grain size.

$Ca_5(PO_4)_3OH$ and $Ca_5(PO_4)_3(F_{1-x},OH_x)$ powders with x=0.025 and $Ca_5(PO_4)_3(Cl_{0.7},OH_{0.3})$ were investigated using X-ray diffraction at a pressure of 19.9 HPa 18.3 HPa and 51.9 HPa in work [112]. The change of the unit cell volume was determined for 962°C and 907 °C versus 25 °C.

The revealed law is described by expression for hydroxy- and FAP:

$$V(T)/V_{293}=1+\alpha_1(T-293)+\alpha_2(T-293)^2,$$

where $\alpha_1(OH)=2.4(\pm0.1)\cdot10^{-5}$ K^{-1}, $\alpha_2(OH)=2.7(\pm0.1)\cdot10^{-8}$ K^{-2} and $\alpha_1(F)=3.4(\pm0.1)\times$ $\times10^{-5}$ K^{-1}, $\alpha_2(F)=1.6(\pm0.1)\cdot10^{-8}$ K^{-2} respectively.

Significant thermal expansion was observed already at ≈550 °C, however it clearly appeared on the roentgenogram at a temperature above 790 °C. These features are interpreted as progressive dehydration of Ca- deficient HAP (Ca/P<1.67).

With the purpose of investigation of reconstruction process of Ca-HAP hardened in air, the powders were annealed and hardened by temperature difference from 1500 °C up to room temperature and is iteratively heated up properly chosen temperature [113]. X-ray diffraction and FTIR analyses are used for investigation of changes in crystal phases and functional groups of Ca-HAP powders hardened at various temperatures.

The results of investigations have shown, that hardened Ca-HAP powder consists of TTCP and α-TCP crystal phases. By repeated heating of hardened Ca-HAP powders, TTCP is gradually transformed to Ca-HAP at 500 °C with simultaneous formation of $Ca(OH)_2$. α-TCP didn't transform to Ca-HAP at temperatures below 700 °C, however transformation of α-TCP to β-TCP was observed.

α-TCP reacts with a $Ca(OH)_2$, a product of TTCP reconstruction transforming to Ca-HAP at temperatures above 700 °C. Inclusion of carbonate ions into Ca-HAP lattice is observed at 500 °C, however, the intensity of CO_3^{2-} line decreases with the increase of temperature and completely disappears at 900 °C. At a temperature >1000 °C, Ca-HAP loses OH-ions and turns into oxyhydroapatite.

Influence of annealing conditions on evolution of Ca-HAP morphology is investigated in work [114]. Heating was carried out in the atmosphere with controllable water vapour pressure at temperatures from 100 °C up to 900 °C. It is known, that below 780 °C, surface mechanisms of phase transformation work. Grain size distribution depends on conditions of annealing, which can be the consequence of small particles aggregation due to surface diffusion while formation of greater grains occurs during volume diffusion.

Thermal stability and proton conductivity of ceramic Ca-HAP at high temperatures is investigated in [115]. High-temperature ionic conductivity is determined with hydroxide-ion. Considering the fact, that Ca-HAP ceramics is synthesized above 1200 °C without destruction of apatite structure, dehydration is represented as the phenomenon of ageing. Using measurements of hydrogen atoms content in unit cell it is shown, that conductivity is completely determined with proton component. The phenomenon of ageing is reversable, which was determined during deuteration of "old" Ca-HAP; absorption of OD^- by the sample is confirmed with infrared spectral analysis after exposure to vapours of deuterium oxide. Relying on these results the model of conductivity, fitting the phenomenon of ageing is offered. The conducted research has shown the importance of presence of H_2O vapour during sintering.

The mechanism and kinetics of thermal decomposition of Ca-HAP ceramics are investigated at temperatures above 1400 K in work [116, 117] when of Ca-HAP decomposition to α-TCP, H_2O and CaO occurs. Ca-HAP decomposition begins on the surface of Ca-HAP ceramics samples. The kinetic analysis of dependence of time of Ca-HAP transformation to TCP has shown, that thermal decomposition of Ca-HAP ceramics is controlled with diffusion of water from the reaction zone to the surface of the ceramic sample. Activation energy of thermal decomposition of Ca-HAP ceramics was 283.5 kJ/mole.

For apatite/aluminium oxide composites, sintered in air, Ca-HAP decomposition to TCP is revealed already at temperatures ~1000 °C and finishes at 1200 °C [118]. Composites of aluminium oxide and various apatites (Ca-HAP, ClAP and FAP), and also separate components have been isostatically (at pressure 160 MPa) pressed at 1200 °C for 1 hour. For investigation of stability of phases, samples after attrition were heated in air at the certain temperature. FAP and ClAP samples reacted with water vapour and partially turned into oxyhydroxyapatite. The phase structure of materials was estimated with X-ray powder diffraction.

The new approach in using of ultra-violet Raman spectroscopy for Ca-HAP samples at temperatures up to 1200 °C for the first time was carried out in work [119]. With temperature increase the spectrum intensity in the range of longitudinal fluctuations of OH-ion decreased. Full intensity of the line in the range of 3300-3800 cm^{-1} changed slightly up to ~800 °C, however then it has sharply decreased at temperatures > 800 °C. These results can be interpreted as the formation of oxy-hydroxyapatite because of Ca-HAP dehydration above 800 °C. Water generation entails defects formation.

3.3. Hydrolysis

In view of good biocompatibility with living tissues inorganic salts of calcium (mainly phosphates) are widely used for medical purposes [120]. However all materials should be exposed to preliminary sterilization for medical application.

For this purpose various methods of disinfecting and clearing are developed: use of ultra-violet or γ-radiation, sterilization in autoclave using superheated water vapour, and also treatment with some chemical reagents (chloric lime, ethylene oxide, ethanol, etc.). However influence of sterilization conditions on properties and chemical transformations of calcium phosphates practically is not investigated. It was found, that the surface of pure stoichiometric $Ca_{10}(PO_4)_6(OH)_2$ does not change during the sterilization using superheated vapour, while sterilization of Ca-HAP with γ-radiation leads to removal of the adsorbed water and destruction of surface phosphate groups.

Chemical processes of interaction of three calcium phosphates with water are studied at temperature of 121 °C (autoclave sterilization). As initial ones calcium hydrophosphate $CaHPO_4 \cdot 2H_2O$ (CHP), non stoichiometric hydroxyapatite (NHAP, approximate formula $Ca_{10-x}(HPO_4)_x(PO_4)_{6-x}(OH)_{2-x}$) and biphase calcium phosphate (BCP), consisting of β-$Ca_3(PO_4)_2$ (~40%) and stoichiometric Ca-HAP (~60%) and also containing ~0.7% of CaO impurity were chosen. The choice of compounds is caused with their wide application in stomatology and other areas of medicine.

Based on results of electron microscopy investigation, it is possible to assume stoichiometric Ca-HAP-formation in the sterilized suspension of HPCD-water. Detected solution acidation is explained with hydrolysis:

$$5(CaHPO_4 \cdot 2H_2O) = Ca_5(PO_4)_3OH + 2H_3PO_4 + 9H_2O.$$

Formation of Ca-HAP traces (or NHAP) in experimental conditions is quite possible since in CaO-P_2O_5-H_2O system Ca-HAP is the least soluble calcium phosphate at pH> 4.5. According to [120] by 0.064% transformation of initial CHP to Ca-HAP, pH of the solution decreases from 7.2 down to 5.4. This value is close to experimentally found pH values of 5.5-5.6. Such small HAP content in the solid phase (~0.05 weight. %) is beyond detection limits of IRS and XPA methods and consequently isn't detected experimentally.

The found difference in acidity of NHAP suspensions (pH 8.0-8.6) and BCP (pH~10.6), possibly, is explained with the chemical processes occuring during BCP synthesis of NHAP at 1050 °C. The results of the thermogravimetric analysis (TGA) show that by BCP synthesis of NHAP the total weight loss of the sample is 8.70%. The most of the mass loss (8.15%) occurs at temperatures below 350 °C, and the reminder (0.55%) at 650-700 °C. At the temperatures below 350 °C evaporation of water traces (both sorbed and crystalline hydrate) and at 650-700 °C thermal decomposition of carbonates occurs:

$$Ca_{10-x}HPO_4(CO_3)_x(PO_4)_{6-x}(OH)_{2-x} = \\ = Ca_5(PO_4)_3OH + Ca_3(PO_4)_2 + CaO + CO_2 + H_2O.$$

The admixture of carbonates in the synthesized samples of NHAP is quite possible, as according to marking of the reagents used in the work the carbonates content in CPH is not normalized, and solid NaOH contains up to 1% of Na_2CO_3. The

presence of carbonates in investigated NHAP samples is so negligible, that it was not possible to find them using XPA method. Nevertheless, the carbonate admixture in NHAP was registered using IRS method: by absorption in the range of characteristic fluctuations of CO_3^{2-} groups at 1400 and 870 cm^{-1}.

Considering the aforesaid, the difference between acidity of NHAP and BCP suspensions can be explained with the presence of 0.7% of CaO impurity in BCP. By contact with water CaO is rapidly hydrated with the formation of hydroxide that leads to a pH increase in solution.

Constant and slow pH decrease of solutions which are being in equilibrium with BCP, corresponds to data arguing the gradual pH decrease of water solutions being in equilibrium with BCP and β-$Ca_3(PO_4)_2$ while pH of the solutions which are in equilibrium with stoichiometric Ca-HAP, does not change. Besides it was found , that the increase in duration of BCP suspension ageing leads to the increase of Ca-HAP/β-$Ca_3(PO_4)_2$ ratio in the solid phase of BCP owing to hydrolysis of β-$Ca_3(PO_4)_2$:

$$10Ca_3(PO_4)_2+6H_2O=3Ca_{10}(PO_4)_6(OH)_2+2H_3PO_4.$$

Since investigated BCP is composed of Ca-HAP and β-$Ca_3(PO_4)_2$ mixture and contained 0.7% of CaO impurity, by interaction of BCP with water two processes occurred simultaneously: CaO hydration up to hydroxide and hydrolysis of β-$Ca_3(PO_4)_2$. It was found, that cinetics of these processes is different: CaO hydration occurs quickly, and β-$Ca_3(PO_4)_2$ hydrolysis — slowly. Therefore, firstly pH of suspension rapidly increases till the conversion of the total CaO in $Ca(OH)_2$, and then only β-$Ca_3(PO_4)_2$ hydrolysis occurs in BCP suspension that leads to the increase of acidity of a solution.

As it was noted previously by sterilization of NHAP, no changes of NHAP chemical and phase structure using methods of IRS and XPA was revealed. However using SEM method it was found, that crystals of non-sterilized NHAP are a little bit more minute than initial ones, owing to transformations in NHAP suspensions. On the other hand, the difference between sterilized and non-sterilized NHAP suspensions appears as a small pH decrease of solution (from 8.6 till 8.2—8.0) during the sterilization process.

The cinetics of Ca-HAP powder dissolution was analyzed at 37 °C at constant pH 5 and pH 6 by the fluorine ions content of 1 and 10 ppm [121]. The experiments were carried out using the device which continuously registered proton absorption and concentration of calcium and fluorine in the solution. The presence of fluorine ions at the surface reduces apatite solubility, and as consequence, the equilibrium is reached earlier. However, adsorption of fluorine ions at the surface of apatite speeds up the process of initial dissolution. Both processes are completely interpreted using recently offered quantitative model for Ca-HAP dissolution according to which dissolution of apatite is controlled with adsorption of calcium ions on the interface with the formation of cationic semipermeable layer. Fluorine ions interact with this layer and reduce its ability to dissolution, especially in the case of higher concentration of fluorine when surface CaF_2 is formed.

pH changes during $CaHPO_4$ hydrolysis in water and in 18.75—600 mM NaF, KF and NH_4F solutions were determined by the weight relation of liquid/solid matter equal to 20.0 and at the temperature of 37.4 °C; equilibrium composition of solutions and morphology of deposits 3 months after preparation [122] were determined too. In all fluorine-containing solutions hydrolysis rate increased. pH variations in time indicate complex kinetic behaviour of systems. The presence of fluoride-ions changes the mechanism of reaction in the range of analyzed concentrations. $CaHPO_4$ solubility changes from incongruent up to congruent one, when the concentration of cation-phosphatic complexes increases irrespective of the nature of cation (Na^+, K^+ or NH_4^+). By fluoride concentrations less than 75 mM FAP hydrolysis is slowed down, $CaHPO_4$ and FAP coexist in equilibrium. FAP forms discrete needles on surface of $CaHPO_4$. At that the density of these FAP needles on surfaces and faces of $CaHPO_4$ is various. The single phase existing in the system by the fluoride concentration in solution of 75 mM is FAP so it can be concluded that hydrolysis does not occur.

By fluoride concentration above 75 mM FAP and CaF_2 coexist in equilibrium. Thus, the evolution of phases in systems with increasing concentration of fluoride-ions is the following: $CaHPO_4$+FAP, FAP and FAP+CaF_2. FAP and CaF_2 coexist as components of pseudo-morphs of initial $CaHPO_4$ crystallites. By $CaHPO_4$ hydrolysis in 600 mM fluoride solution pseudo-morphs of initial $CaHPO_4$ crystallites were observable only morphologically.

Work [123] describes bicalciumphosphate ($CaHPO_4$, BCP) hydrolysis in deionized water at 37 °C as a function of time, with large liquid/solid matter ratio (2500 ml/g) in order to avoid reaching the limits of solubility [123]. Investigation of the liquid have shown that BCP dissolution occurs incongruent. Though solutions were not saturated, in regard to solubility, dissolution has stopped after 4 days, and the formation of a film with a thickness of several tens of Å was observed. It was not possible to determine film composition using common volumetry methods. XPS data indicated that the film consists of calcium phosphate with Ca/P ratio close to 1.50. Changing of Ca/P ratio in the solution over time indicates that some processes occur there. The first one is BCP dissolution and the second one corresponds to entering the monetite surface of a portion of Ca ions released by dissolution, leading to the formation of apatite film. The formation of this film, probably by heteroepitaxy with BCP, explains low solubility in deionized water.

Using X-ray diffraction and IR spectroscopy the activity of TTCP ($Ca_4(PO_4)_2OH$), at 37 °C is defined, and also its hydrolysis in 0.01—0.1 M solutions of H_3PO_4 and KH_2PO_4 [124] is investigated.

TTCP is easily hydrolyzed with formation of calcium deficient apatite (Ca-def. HAP, $Ca_{5-x}(HPO_4)_x(PO_4)_{3-x}(OH)_{1-x}$) or bicalciumphosphate ($CaHPO_4 \cdot 2H_2O$). By H_3PO_4 concentration of 0.1 M TTCP is hydrolysed with formation of bicalciumphosphate within several minutes. By H_3PO_4 concentration of 0.025 M and KH_2PO_4 concentration of 0.025 M, TTCP hydrolizes with the formation of HAP-def. In the latter

solution insignificant quantity of OCP ($Ca_8(H_2PO_4)_2(PO_4)_4 \cdot 5H_2O$) as intermediate product is found. By KH_2PO_4 concentration of 0.025 M, TTCP hydrolizes directly with the formation of Ca-def. HAP. By H_3PO_4 concentration of 0.01 M TTCP hydrolysis comes to the end. Thus, the end product composition and hydrolysis degree depend on pH and general Ca/P ratio in the reaction system. Process of Ca-def. HAP formation is determined with TTCP dissolution rate.

In work [125] non stoichiometric dissolution of Ca-HAP in water solutions NaCl, Na_2SO_4 and natrium dodecyl sulfate (SDS) was investigated. Molar ratios of Ca^{2+} and phosphate-ion (PI), released from HAP, changed depending on the nature and concentration of the added salt. The order of salts effect on Ca-HAP dissolution with the increase of PI concentrations was the following: SDS>Na_2SO_4>NaCl, while Ca^{2+} concentration increased as follows NaCl>Na_2SO_4>SDS with SDS concentration lower than the critical concentration of micelle formation. These results are explained in the following way: PI the HAP surface is easier replaced with SO_4^{2-} ions, than with Cl^--ions, by isomorphic substitution mechanism, since dimensions of SO_4^{2-} and PO_4^{3-} ions are similar; on the other hand, the chemical structure of dodecyl sulfate-ion is formed with covalent bond between polar group and hydrocarbon chain ($C_{12}H_{25}$). Adsorption of organic dodecyl sulfate -ion is more extensive, than of inorganic SO_4^{2-}-ion and in both cases occurs due to hydrophobic/cooperative effect of hydrocarbon chain and isomorphic substitution on the HAP surface. The amount of uncompensated negative charge in the case of adsorbed dodecyl sulfate accelerated PI release from HAP, leading to the reduction of electrochemical potential of the surface. This mechanism causes greater quantity of PI in presence of sodium dodecyl sulfate, than in presence of Na_2SO_4.

Growth and dissolution kinetics of Ca-HAP by constant pH (6.0 and 7.2) and variable values Ca/P ratio in a solution is presented in work [126]. As it was shown both processes are controlled with the polynuclear surface mechanism in which nucleation is expressed as ion activity function. By dissolution, transverse velocity of nuclei growth is proportional to the difference between the general concentration calcium ions in the saturated solution and in the local area of a solution, and the rate constant is connected with the frequency calcium ions do diffuse jump in kink and simultaneously become partially dehydrated. The model of transverse velocity of growth has recently been developed. This model is based on hydroxyl-ion settlement somewhat below growing surface due to trapped water molecules dissociation. Thus, transverse velocity of growth is determined with successive processes: calcium ions entering the positions of calcium, accompanied with phosphate-ions, and retardation caused with sufficiently slow production of hydroxyl ions in the corresponding positions. The frequency of substitution, equal $1.6 \cdot 10^5$ s^{-1} was found. As this frequency is approximately constant, the frequency calcium ion escape from a kink decreases with the decrease of the dissolved calcium concentration. This reflects the important changes of a crystal surface dynamics: the values calculated from kinetic data for the surface tension were σ_{growth}=100 mJ/m^2 and $\sigma_{dissolution}$=40 mJ/m^2.

Growth of Ca-HAP crystals, which is thermodynamically the most stable phase of calcium phosphate, at 37 °C, pH 7.40 and ionic strength of 0.15 M in the presence of ferrocene complexes was investigated using the constant composition method [127]. Kinetic results indicated the surface mechanism of diffusion control. The presence of ferrocene salts slowed down Ca-HAP crystals growth probably due to adsorption on active areas of crystal growth. Kinetic results coincide with Langmuir-type isotherm, assuming high affinity of ferrocene salts to Ca-HAP surface.

3.4. Mechanical properties

Investigation of mechanical properties of Ca-HAP are carried out with the purpose of fragility overcoming inherent in polycrystalline ceramics, and for realization of practical use of Ca-HAP as biologically active implantation materials. In addition to the excellent biological compatibility with various bone tissues, mechanical durability of Ca-HAP constantly improves, reaching values comparable or surpassing the durability of human bone and teeth. The dense Ca-HAP-ceramics with ultimate compression, tensile and torsional strengths several times greater, than of bone and teeth has already been obtained. On the other hand, porous sintered Ca-HAP samples have an advantage that the will be completely transformed to natural bone. Such porous materials usually have lower tensile strength. Porous materials can function as implantation ones, however, considering the fact, that their applicability application is limited with areas where there is no tension. Thus, both dense, and porous Ca-HAP-ceramics will be improved for the further biological applications. However there are still some problems connected with such mechanical properties as fracture resistance and impact elasticity which have to be resolved.

In work [1] it is shown, that fracture resistance of ceramics samples usually worsens with the increase of microstructural distortions, such as impurities, other phases and pores.

On the other hand addition of some compounds can increase durability. From this point of view effective admixtures are glasses of calcium phosphate. The flexure strength value of 205.8 MPa is reached by adding 5% of glass containing 46 mol. % P_2O_5, 20 mol. % CaO, 32 mol. % BaO and 2 mol. % Al_2O_3 to Ca-HAP. This effect of hardening is connected with a role of admixtures which simultaneously suppress growth of grains and promote sintering. Layers of TCP formed as a result of chemical reaction between Ca-HAP and the glass melted during sintering at 1250 °C, limit mass transfer on the interface and by that suppress growth of grains. As the material with large grains has low durability, suppression of growth of grains is effective for mechanical durability augmentation. It is obsereved, that the contribution of the main crystal phase of Ca-HAP with the addition of phosphatic glasses changes symbatically with the value of Ca/P ratio; the main phase by the large ratio (> 1.60) is Ca-HAP, by the smaller ratio (<1.59) TCP dominates. Partially stabilized zirconium

oxide (PSZO), usually used as the addition to Al_2O_3 is also studied with the purpose of Ca-HAP break resistance increasing.

Solid-state Ca-HAP reaction with ZrO_2 or with PSZO in air at temperatures above 1200 °C leads to Ca-HAP decomposition under the scheme: $Ca_{10}(PO_4)_6(OH)_2 \rightarrow$ $\rightarrow 3Ca_3(PO_4)_2 + H_2O$ (vapours) which can be to a large degree suppressed in the water vapour jet. In biological applications it is necessary to pay special attention to the influence of the environment, such as physiologically active solutions, on mechanical properties of Ca-HAP.

In connection with the above, mechanical properties of porous Ca-HAP represent greater interest, than of dense Ca-HAP. According to work [1] some samples of porous Ca-HAP show compressive strength sufficient for implanted materials; however their impact elasticity makes less than half of the demanded value.

The role of pores in destruction mechanics is obvious. Using fractographic method (investigation of fracture surface with scanning electron microscopy) it was found, that the fracture of porous samples with the porosity ranging from 9% up to 20% occurs mainly on grain boundaries, and for dense samples with porosity ranging from 2% up to 4% transgrain break is observed.

The composites consisting of Ca-HAP (0—30%) and hydroxyapatite whiskers (HAP (w)) (0—30%) are obtained with agglomeration, hot pressing and HIP [128]. The composites obtained at 1000—1100 °C (2 h., 190 MPa) have density of 97.0—99.5% and fracture resistance 1.4—2.0 MPa $m^{1/2}$ in comparison with 1.0 MPa $\cdot m^{1/2}$ for not reinforced Ca-HAP-matrix. It is shown, that growth of grains and/or instability of HAP (w) depend on the conditions of processing, and HAP (w) are also responsible for microstructural changes in the composites. Ca-HAP/HAP (w) composites are characterized with sufficiently high values of mechanical parameters alongside with bioactivity and biocompatibility.

3.5. Radiation properties

Local changes of Ca-HAP crystal structure during electron microscopic study are revealed in work [129]. The transition from hexagonal ($P6_3/m$) to monocline (with $b=2a$) structure occurs as a consequence of stoichiometry change, or after electronic beam exposure. Such order-disorder transformations are probably caused with local rotations of fragments of a crystal lattice.

The work [130] is devoted to investigation of transition between monocline ($P2_1/b$) and hexagonal ($P6_3/m$) phases in Ca-HAP $Ca_5(PO_4)_3OH$ using X-ray diffraction and a differential scanning calorimetery methods. Intensities of peaks in a X-ray diffraction pattern of low temperature monocline phase are constant up to 473 K, but sharply decreased to zero at temperatures > 483 K. At the same time differential scanning calorimeter registers endo- and exothermal effects, having allowed to estimate enthalpy and entropy of transition as 630±25 J/mole and 1.30±0.05 J/mole K respectively.

Phase segregation in crystalline and amorphous apatite, caused with electronic irradiation is investigated in work [131]. F-containing apatite monocrystals and apatite amorphised with 800 keV Kr^{2+} ion beam have been exposed to irradiation in electron microscope in a range of energies and currents of an electron beam. The irradiation of the matrix of crystalline apatite by high-density current (16 A/cm^2) has caused the formation of cubic CaO. When using lower current (16 A/cm^2) the formation of nanosized lacunas was observed, however CaO was not generated even after long irradiation. Amorphous apatite transformed into coarse-grained formations of apatite crystallites at 85—200 keV. The increase in a current has caused the formation of fine-grained cubic CaO. In each case blisters formed with sizes increasing to the beam edge. Thermal annealing at 450 °C has led to epitaxial crystallization and to the formation of a monocrystal with high density of defects. Electron beam irradiation at 300 °C has confirmed that the difference in microstructural evolution is controlled with doze parameters as function of current density. Actually, the temperature and doze rate are competing parameters of CaO phase formation.

Investigation of defects in irradiated Ca-HAP was carried out using EPR method [132]. CO_3^--radicals are found almost in all investigated samples, however isotropic CO_3^- is obtained only in water-containing Ca-HAP with low crystallity. H-O doublet signal is obtained in Ca-defficient Ca-HAP. The results of EPR and FTIR indicate that water molecules in Ca-HAP are not on the surface, but are embedded in the lattice.

3.6. Electrical properties

Mass transfer in Ca-HAP makes the essential contribution to electric conductivity, and also determines biological phenomena: degradation and growth of bones, and Ca^{2+}-exchange in solutions. However, because of data limitation, concrete conclusions about mass transfer in connection with electric properties are not made yet. It is necessary to consider electric and dielectric properties and also possible mechanisms of mass transfer in connection with practical and potential applications.

Currently there is a consensus view that electric charges in Ca-HAP move mainly by diffusion of hydroxide-ion [1] through crystal lattice sites located along the *c* axis. It is confirmed with a number of experimental results. For OH^--conductivity vacancies for relay-race change of positions in an electric field are required. Such mechanism is plausible since a certain quantity of OH^--vacancies is introduced into Ca-HAP not only when using methods of solution-phase synthesis, but also by sintering while at temperatures > 1100 °C $Ca_{10}(PO_4)_6(OH)_2$ decays with formation of oxyhydroxyapatites $Ca_{10}(PO_4)_6(OH)_{2-2x}O_x\square_x$, where $\square$ — vacancies.

On the other hand, it is reported about the capability of protons overjumping [1] in solid solutions of Ca-HAP and FAP as it was found out by proton conductivity study of simple ionic hydroxides. For proton migration under weak electric field influence, the specified distance of 3.44 Å between two vicinal OH^--ions will be too

large. In any case, ion transfer along *c* axis determines electric properties of Ca-HAP. Domination of these mechanisms levels the role of charge transfer with Ca^{2+}-ions.

Electric conductivity of various apatites, including Ca-HAP, was measured at temperatures above 500 °C (reached using alternating current with the frequency of 1 kHz) for the pressed powders. According to the obtained results, alternating current conductivity of Ca-HAP at temperatures 800—900 °C makes ~10^{-5} ohm/cm with the activation energy value of 0.69 eV. Apatites of cadmium, barium and strontium show OH^--conductivity ranging from 10^{-5} to 10^{-7} ohm/cm at high temperatures with activation energy ranging from 0.5 to 0.90 eV. At the same time lead apatite is the mixed conductor of OH^- ions and electrons. HAP possesses dielectric properties, mainly, because of reorientation of OH^- dipoles in columns, parallel to *c* axis in the electric field. It is offered two models: the "ordered" columns with OH^- dipoles aligned in one direction inside of the column with vicinal columns having opposite orientations; and "disordered" columns in which OH^- orientation is opposite in various places inside of one column. The model of "disordered" columns is based on investigation of dielectric relaxation when the presence of vacancies initiates reorientation of OH^- dipole.

In work [133] the influence of crystallization process on ionic conduction of poorly crystallized synthetic apatite is investigated. The tendency which is observed for Ca-HAP consists in the increase in ionic conductivity during the crystallization process. At a room temperature ionic conduction increases after 50 days of ageing which dependence on frequency gradually decreased during ageing. These results are explained with short-range order and reduction of progressive motion of ions by material ageing.

Ca-HAP ceramics with ZnO and RuO_2 electrodes shows rather high sensitivity to alcohol vapours. Such device has sensitivity to ethyl alcohol ~50, determined with the relation *(electroresistance at the presence of C_2H_5OH)/(electroresistance in the air),* at temperatures from 400 °C up to 600 °C.

Structural transition and dielectric characteristics of ultrapure Ca-HAP is resulted in work [134]. Temperature and frequency dependences of dielectric constant ε and tangent of dielectric losses tgδ are investigated in the range 20-500 °C. It is found, that in the range 20 ÷ 300 °C temperature dependences of ε and tg δ are determined with dipolar polarization of OH groups. Polarization of the spatial charge prevails at t> 300 °C owing to generation of charge carriers. The results are compared with the data of measurements of thermal capacity and thermally stimulated exoelectron emission of Ca-HAP.

In work [135] it is reported about investigation of connection between structure and conductance for apatite-like structures — $La_{9.33}Si_6O_{26}$ и $La_8Sr_2Si_6O_{26}$. High oxygen-ionic conductance was observed for $La_{9.33}Si_6O_{26}$ ($\sigma=1.2\cdot10^{-4}$ ohm/cm at 700 °C, E_a=0.73 eV) and is considerably lower for $La_8Sr_2Si_6O_{26}$ ($\sigma=3.9\cdot10^{-7}$ ohm/cm at 700 °C, E_a=1.34 eV). Refinement of structure of both compositions have hexagonal unit cell. In addition to vacancies in cation positions, $La_{9.33}Si_6O_{26}$ sample has shown key differ-

ences in the unit cells of oxygen channel in comparison with $La_8Sr_2Si_6O_{26}$. For the last one, atoms of oxygen are located close to ideal (0, 0, 0.25) position, and for $La_{9.33}Si_6O_{26}$ approximately 14% of these atoms are displaced to the new position (0, 0, 0.38). It might me suggested, that higher conductance and lower activation energy for oxygen ionic conductance in $La_{9.33}Si_6O_{26}$ comparing to $La_8Sr_2Si_6O_{26}$ follows from the observable disorder in the position of oxygen.

3.7. Laser ablation

Using high-speed CCD photographing, the analysis of flashes of Ca-HAP laser ablation during irradiation with KrF excimer laser [136] was carried out. The obtained images have shown the presence of three various areas of luminescence: the flash-like plasma was accompanied with a small cloud; freely expanding area after laser impulse; it is observed for more than 50 μs after laser impulse; it is generated by the hot particles which have left the target. The experiment was repeated under the same conditions with ArF laser wavelength. In this case only first two plasma clouds are identified. For the detection of hot Ca-HAP particles on films, deposited using pulsed laser, scanning electron microdiagrams of coatings were obtained which have shown much smaller density of droplets in the case of ArF irradiation, than in the case of KrF.

The flash induced with KrF laser irradiation of Ca-HAP-target at 0.1 mBar of water atmosphere, is also analysed using CCD and time-resolving optical spectroscopy in work [137]. The obtained images have shown the presence of three various emission components in the flash. The first and the fastest one in which distribution occurs with the speed of about 10^4 m/s, shows the development of a shock wave at its front, occuring because of interaction between discharge of a target and background gas. Water vapor slows this component down to values of approximately $3 \cdot 10^3$ m/s that can be well described using spherical shock waves dynamics. Low emission intensity of the second component has not allowed analysing its dynamics. The third and the slowest component broadens with the constant speed of $5 \cdot 10^2$ m/s and consists of hot macroparticles leaving the target. The spectra registered in the shock front, have shown the presence of the emission lines resulting from emissive Ca_I, Ca_{II}, P_I and some impurities, and two strong bands which can be attached to calcium oxide.

In work [138] images obtained during KrF eximer laser ablation of Ca-HAP objects, have shown the presence of two various luminescence areas of flashes. The first one has a pen-like shape with a speed of distribution of $\sim 2.0 \cdot 10^4$ m/s. The second one resembles a small plasma cloud near the object surface and has a speed of distribution of $\sim 2.9 \cdot 10^3$ km/s. The spectroscopic analysis of flashes has shown the presence of several atomic (Ca_I, P_I, O_I and impurity), ionic (Ca_{II}) and molecular (calcium oxides) components in plasma. The dynamics of basic nuclear and ionic impurities was analysed by spectra. The CCD-images which have been recordered through various band

filters were used, for the display of impurities distribution along flash and, thus, the character of preliminary observable luminescence areas was identified. The images obtained using this method, have shown the atomic nature of the first luminescence area while the second area consisted of molecular fragments.

3.8. Surface properties

Very often it is difficult to answer the question what is the interface. As a rule, "heterophase" or "interface" to some extent depends on the point of view.

Adsorption and its influence on the growth of HAP crystals. Orthophospho-L-serine is a component of salivary proteins, it plays an important role in teeth mineralization. For the determination of the mechanism of interaction sorption of orthophospho-L-serine from water solutions (up to 100 mmol/l) by the surface of synthetic HAP was analysed [139]. Research has shown that in diluted solutions (<12.5 mmol/l) absorption is described with Langmuir equation. At higher concentration curvature of absorption curves sharply increases, however the formation of a separate phase in apatite was not revealed. Apatite dissolution led to transition of ions of phosphate and calcium to the solution in quantities linearly depending on serine adsorption.

As it is shown in work [140] phospho-L-serine slows down the growth of HAP crystals with blocking the centres of crystal growth by adsorption. Full suppression of growth is reached by phosphor-L-serine concentration of $4 \cdot 10^{-4}$ M. The analysis of results of kinetic studies of adsorption isotherms has also revealed Langmuir type of adsorption. The quantity of phospho-L-serine, adsorbed with HAP surface has decreased by pH increase from 7.4 to 10.4. Adsorbed phospho-L-serine groups in pH interval of 7.4—10.4 are generally monoprotonated (HL^{2-}). They are localized at the internal Helmholtz plane of the double electrical layer at the HAP/electrolyte interface and interact with the surface of HAP both electrostatically and chemically. The location of negatively charged HL^{2-} group at the internal Helmholtz plane has led to ξ-potential shift toward more negative region. It was suggested phospho-L-serine adsorption model by HAP surface at pH 7.4 according to which ionic pair is formed between protonated amino-group of one HL^{2-} group and negatively charged area of HAP surface (phosphatic or hydroxyl group). Owing to the electrostatic repulsion, negatively charged deprotonated carboxylato — and phosphato-groups are in the greatest possible distance from the negatively charged HAP surface.

Injection of amino acids (serine, tyrosine and 4-hydroxyproline) with polar uncharged lateral substituents at physiological pH and 37 °C in oversaturated solution of calcium phosphate reduces growth rate of HAP crystals [141]. Depending on the nature of substituent the degree of inhibition was found to be different. Reaction rate decrease is determined with the concentration of injected reagent according to the equation obtained from Langmuir adsorption kinetic model. Crystallization rate depended on the degree of blocking of active sites of crystal surface growth. Reac-

tion order of crystal growth was n=2 that presupposes the spiral growth mechanism controlled with surface diffusion.

Kinetics of HAP crystallisation at the presence of protonated forms of amino acids (aspartic and glutamic acids) is investigated in conditions of continuous oversaturation in work [142]. In the presence of the mentioned acids, growth rate of HAP crystals considerably decreased because of adsorption of acids and subsequent blocking of active growth sites on the surface of HAP crystals. The results have shown that adsorption isotherm resembles Langmuir curve. The average order of reaction of crystal growth was equal to 2.

In work [143] the activity of four natural amino acids with hydrophobic unpolar side group (alanine, phenylalanine, proline and methionine), in HAP crystallisation is investigated. Crystallisation took place only on seed crystals of HAP injected into supersaturated calcium phosphate solutions. Extrapolation of experimental data to the Langmuir adsorption isotherm indicates inhibitory mechanism based on molecular adsorption of amino acids in active sites of HAP crystal surface growth. The effect of inhibition is characterised with a constant of adsorption equilibrium of each amino acid relating to the crystal surface which depends on the nature of side group of amino acid molecules.

Lysine, present in biological liquids, is an amino acid with basic lateral group. Its role in biological process of calcification [144] is investigated. The delay of HAP crystal growth rate in supersaturated calcium phosphate solutions has been revealed. Reaction rate decrease is due to adsorption and blocking of active sites of crystal surface growth. Crystallisation kinetics was interpreted in terms of Langmuir adsorption models. The order of crystallisation reaction is defined as n=2, assuming that surface diffusion is determined by the spiral mechanism of growth. Kinetic characteristics of HAP crystallisation are received using constant composition method when concentration of reagents in the stock solution remains constant during controllable crystal growth.

As it is known, small quantities of zinc and magnesium ions can determine mineralization kinetics. In this connection in work [145] results of-equilibrium adsorption study of these ions by HAP surface are given and electrophoretic mobility by zinc ions concentration above 1 ppm. Zinc phosphate formation dominates the growth process. In the presence of zinc and magnesium ions HAP crystal growth is considerably decreased and is characterised with Langmuir-type adsorption of these additives on active sites of HAP crystal growth.

Adsorption of inorganic compounds on HAP surface. Adsorption of fluorides-ions by hydroxyapatite powder surface from water solutions as a function of calcium ion and fluoride-phosphate-anions concentration is described in work [146]. Adsorption kinetics of fluoride, calcium and H^+ ions was measured continuously using ion-selective electrodes. In any conditions fluoride addition stimulates pH increase due to $H_2PO_4^-$ ions adsorption, accompanied with brushite formation on the reacting surface. Isotherms of fluoride systems are characterized with Langmuir-type plateau

that indicates the adsorption of fluoride, calcium and phosphate ions without association and formation of a solid phase. By higher concentration fluoride ions are adsorbed simultaneously with sedimentation of certain CaF_2 amount. By calcium concentration increase CaF_2 precipitation occures. The presence of phosphates-ions promotes fluorinated apatite formation.

The formation of tin compounds on hydroxyapatite surface is discussed in connection with use of SnF_2 as a remedy for caries prevention, introduced into toothpaste composition [147]. Pure hydroxyapatite contacted with compositions of commercially available tooth-pastes containing tin fluoride and it was analyzed using electron spectroscopy. It was concluded that on the surface of hydroxyapatite the mixture of fluoride-phosphate compounds of bivalent tin was formed. SnO was not detected in the mixture.

Adsorption of organic compounds on the HAP surface. The structure of fibrinogen, the main plasma protein adsorbed on TiO_2 and HAP, was investigated using differential scanning calorimetry (DSC), circular dichroism (CD) and fluorescent spectroscopy [148]. It is found that TiO_2 surface has reduced the degree of ordering of protein structure: fibrinogen conformation reversebly changed after desorption. The content of α-spirals during these processes gradually changed. It is essential that fibrinogen transition enthalpy has increased in case of adsorption on HAP. These results in combination with DSC-thermography data of fibrinogen for different ionic forces, indocate that electrostatic interactions are the basic mechanism controlling fibrinogen adsorption on TiO_2 and HAP.

In work [149] bovine serum albumin adsorption (BSA) on strontium-calcium hydroxyapatite (CaSr-HAP) surface with various Ca/Sr ratios and texture was investigated. The adsorption isotherms of BSA on CaSrHAP particles were pseudo-Langmuir type. The amount of adsorbed BSA (n(s)) linearly increased with Sr/(Ca+Sr) ratio increase. n(s) increased with the increase of (Ca+Sr)/P molar ratio confirming that electrostatic attractive forces between BSA molecules and CaSr-HAP particles is the key parameter defining the character of n(s) dependence. For large values of cation/P ratio, two particles, forming agglomerate with surface roughness, have determined small n(s) value. This fact has been explained with structure difference. Large needle-like particles with large surface are suitable for adsorption of negatively charged BSA molecules due to availability of a great number of positively charged sites of active adsorption. Hence, the particle structure is essential for efficiency of BSA adsorption.

Adsorption of lysozyme (LSZ) on particles of hydroxyapatites $A_{10}(PO_4)_6(OH)_2$, A=Ca, Sr and Ca+Sr has been investigated at 15 °C in $1 \cdot 10^{-4}$ mole/dm^3/0.1 mM solution of KCI (pH 6.0) in work [150]. Adsorption isotherms of LSZ were pseudo-Langmuir type. Negative electrophoretic mobility of particles is transformed into positive by adsorption of positively charged LSZ molecules. There was no appreciable relationship between maximal amount of adsorbed LSZ (n(s)) and cation/P molar ratio of particles. In the case of Sr-HAP and CaSr-HAP n(s) approaches zero by cation/P

molar ratio ~1.70. n(s) values on Ca-HAP, Sr-HAP and CaSr-HAP particles are much less for LSZ in comparison with BSA. It is shown that LSZ molecules are mainly adsorbed by phosphate-ions located on *ac* or *bc* face and/or on negatively charged sites formed with six oxygen atoms of three phosphates-ions on *ab* faces HAP crystal surface; however the probability of the latter interaction mechanism is defined as low.

Absorption and immobilization of L-lysine on the surface of electrochemically synthesised porous hydroxyapatite coatings are described as a method of preparation of the system for fine protein separation in work [151]. The nature of surface interactions between L-lysine and hydroxyapatite is investigated by FTIR spectroscopy. The formation of hydrogen-containing fragment which is located between C=O groups of L-lysine and polar OH-group of hydroxyapatite is the basic factor effecting intermolecular bonds.

Adsorption of potassium salt of N-phenologlycine on synthetic hydroxyapatite from water and ethanol solutions was analyzed at 22 °C in work [152]. The isotherm of N-phenologlycine adsorption from water solutions is of Langmuir-type. The analysis has shown that one glycinate-ion is localised by adsorption on the surface in area of two HAP unit cells. By adsorption of one glycinate-ion the water solution 3.5 of ions phosphate while calcium concentration slightly decreases. Adsorption from ethanol (99.8%) is full and irreversible from the solutions diluted to threshold concentration and in case of the concentrated solutions adsorption is of the Langmuir-type and reversible. The amount of irreversibly and reversibly adsorbed substance is equal and makes about half of the total substance's amount adsorbed from water solutions. It is shown that adsorption occurs on electrically neutral fragments. The adsorbed molecules completely occupy the surface that indicates the absence of repulsion between them.

Exact knowledge of citrate-ion concentration in soft drinks is important for controlling their cariogenic influence. Absorption of these ions (ion-exchange adsorption) from water solutions of sodium or potassium citrates by synthetic HAP surface at 22 °C is investigated in work [153]. Adsorption isotherms are of Langmuir-type curves. Interaction is completely caused by ion-exchange adsorption. The equations of ion-exchange equilibrium show that the surface is electrically charged by adsorption of salts, but remains neutral by adsorption of citric acid that determines the efficiency of different adsorbates in surface coverage.

HAP surface adsorption of citrates was analyzed at 25 and 37 °C, pH 6 and pH 8 in work [154]. Experimental results by low concentrations of citrates fit the Langmuir model of adsorption of citrate salt. Adsorption decreases with the increase of pH and temperature increase. However, positions occupied on HAP surface are identical for both pH values. Desorption at pH 8 is higher, and ξ-potential values of suspensions containing HAP with the surface adsorptionally saturated with citrate, are negative and decrease with pH increase. Adsorption occurs by a mechanism of ionic exchange between phosphate- and citrate-ions at the solid body/solution interface that is caused with higher affinity of citrate-ions for phosphate groups, and also for

Ca-sites on the HAP surface. To interpret the experimental data the model that predicts coordination of citrate anions in different ways.

Oleate adsorption by an apatite surface is investigated in work [155]. Using FTIR method the strong influence of pH on process parameters was found. At pH 8.0 and 20 °C the layer density of adsorbed oleate increases monotonously with an increase in oleate equilibrium concentration from $5 \cdot 10^{-6}$ to $1 \cdot 10^{-3}$ M. The obtained results contrast with the results obtained at pH 9.5 and 20 °C when the monomolecular layer is formed on the surface. Comparison of oleate adsorption by apatite, fluorite and calcite has shown that behaviour of the surface of these three minerals by adsorption is caused by difference in concentration of surface positions of calcium and solubility of these minerals. Spectral investigation at pH 8.0 and 20 °C has shown that the dominating form of oleic acid adsorbed on the surface of apatite is molecular one. At the same time at pH 9.5, 20 °C and by the formation of monomolecular layer oleate, possibly, is chemisorbed that is confirmed with peak at 1554 sm^{-1} and with the increase in adsorption density at higher temperatures. In the case of the monolayer coating obtained by surface precipitation of calcium dioleate, the doublet at 1575 and 1540 sm^{-1} is characteristic. At pH 9.5 and elevated temperature (65 °C) oleate chemisorption and calcium diolete sedimentation degree on the apatite surfaces increase. Wetting angles of apatite surface has been measured, and it is shown that the sorbate amount and adsorption character defines surface hydrophobicity.

Surface modification. As shown in work [156] the surface of synthetic $Ca_{10}(PO_4)_6(OH)_2$ particles can be improved with modification of hexomethyldisilazan $[(CH_3)_3Si]_2NH$, dissolved in hexane with the subsequent thermal processing. There was no changes in X-ray diffraction pattern or in the particle shape observed. FTIR results have shown that hexomethyldisilizan reacted with surface P-OH-groups of HAP with the formation of Si-$(CH_3)_3$ group on the surface. The surface of modified HAP is hydrophobic. Si-$(CH_3)_3$ groups will be transformed to three kinds of surface Si-OH groups by heating to 500 °C in air. Generated surface Si-OP groups and P-OH groups that had remained on the surface also react with hexomethyldisilizan. It was shown that the new material containing surface Si-$(CH_3)_3$ or Si-OH groups, sorbed smaller CO_2 amount, than unmodified.

The surface of the synthetic Ca-HAP modified with monohexyl or monodecyl phosphates in acetone at 25 °C is investigated in work [157]. Diffractional patterns of the materials modified by 0.1 M monohexyl or 0.15 M monodecyl, and unmodified do not differ, as well as morphology of particles. The number of alkyl groups in the modified materials has made 2 per nm^2. Alkyl groups are removed by degassing at a temperature above 300 °C. Then the concentration of surface P-OH groups in the modified materials had increased that led to the increase of negative electrophoretic mobility in comparison with unmodified material.

Synthetic colloidal Ca-HAP processed with hexyl, octyl and decyl phosphates in water-acetone solutions, was investigated and described using various methods

[158]. X-ray diffraction has shown the presence of one strong and two weak reflexes, uncharacteristic for HAP. The interplanar space linearly increased with the increase of hydrocarbon chain lenght in phosphates. With the increase of phosphates concentration in solution peaks of other phases went up, while the peaks of HAP phase, went down. After processing needle particles dominated, indicating that the surface of initial HAP particles had changed. These results show that modified HAP particles are surface-layered composition with alternation of octacalcium-phosphat-like phase and bimolecular layers containing alkyl groups. In order to obtain mesoporous materials alkyl fragments and H_2O are removed at temperatures above 200 °C.

Colloidal calcium hydroxyapatite particles were modified with Ni^{2+}, Cu^{2+}, Co^{2+} and Cr^{3+} ions using ion exchange and coprecipitation in work [159]. The metal/(Ca+metal) atomic relation in the surface phase (X_s), changed in the process of coprecipitation with Ni^{2+} and Cu^{2+} was much less, than the atomic relation for the whole particle (X_w) while X_s for the particles modified with Cr^{3+}, approached X_w. In the case of modification by ionic exchange X_s was larger than X_w and only for Ni^{2+}-substituted samples X_s was equal to X_w. The number of surface P-OH-groups decreased by replacement of protons of P-OH groups by Ni^{2+}, Cu^{2+} and Co^{2+} ions by application of both methods of modification. Besides, Cr^{3+} ions are introduced to the surface layer by anion exchange of surface phosphate-ions for hydrated anions of chrome hydroxide complex.

3.9. Catalytic properties

Hydroxyapatites catalyze selective oxidation of methane to carbon monoxide and hydrogen at temperatures above 600°C: $CH_4+O_2 \rightarrow CO_2+2H_2$ and $CH_4+O_2 \rightarrow CO+H_2+H_2O$. The reaction is catalyzed mainly on stoichiometric apatite. Nitrous oxide is applied as an active oxidizer at presence of hydroxyapatite hydrogen removal from methane. In the presence of oxygen, active sites, possibly, co-operate directly with carbon atoms.

Methane oxidation on stoichiometric Sr-HAP prepared at 873, 1048 and 1123 K was investigated in work [160] at the presence and absence of tetrachloromethane (TCM) at 973 K. In these conditions Sr-HAP, irrespective of stoichiometry, was partially transformed into $Sr_3(PO_4)_2$. By TCM injection to the stream, selectivity of reactions with carbon oxide, ethane and ethylene increased, while methane transformation was inhibited. As x-ray diffraction has shown strontium chlorapatite, synthesized of apatites and phosphates in similar oxidation reaction in the presence of TCM, also contributes to the increase in selectivity for CO and reduces methane transformation.

As shown in [161], introduction of TCM into a stream of CO and O_2 gases suppresses the formation of CO_2 on hydroxyapatite. TCM interacts with hydroxyapatite surface with the formation of its chlorinated analogue — chlorapatite which suppresses CO oxidation to CO_2. Thus, TCM addition helps to suppress CO oxidation by methane oxidation.

Comparative investigation of methane and ethane oxidation processes on calcium hydroxyapatite with a lead impurity at the presence and absence of TCM is carried out in work [162]. The effect of methane and ethane oxidation by TCM injection depended on the nature of hydrocarbon, TCM partial pressure and catalyst composition. Methane and ethane transformation in the presence of TCM decreased by small TCM partial pressure. It is shown in the given research that at higher TCM partial pressure, the level of transformation increases, especially with the increase of process time and at the same time selectivity decrease for CO_2 formation is observed.

Catalytic ethane oxidation on Sr-HAP surface in the presence and absence of TCM has been investigated in work [163] at 773 K. By TCM addition to the stream of a reaction mixture, ethane transformation and selectivity for CO_2 yield decreased with the increase of time, while oxidation degree of ethane had considerably increased. Though chlorides together with chlorapatites, generated of corresponding hydroxyapatites during oxidation, as it is believed, are products of interaction with TCM, the participation of unstructural chlorine is not excluded.

In work [164] oxidation of propane at the presence and absence of TCM on Ca-HAP, $Ca_3(PO_4)_2$, $CaSO_4$ and CaO at 723 K is investigated. In the absence of TCM, C_3H_8 transformation with Ca-HAP has made 7.7—9.2% during 6 hour process while with $Ca_3(PO_4)_2$, $CaSO_4$ and CaO it has made 0.6, 0.0 and 0.2 0.4% respectively. The main products in systems with the specified catalysts in the absence of TCM were CO and CO_2 with small selectivity for C_3H_6 and C_2H_4 (5—6%). After TCM addition, the selectivity for C_3H_6 oxidation of all catalysts and the degree of C_3H_8 transformation with $CaSO_4$ have increased, while with the increase in time of processes of change in transformation and selectivity depended on the nature of catalysts. XPS method and x-ray diffraction study have confirmed the presence of chloride-ions on the surface and in the volume of three catalysts, specifying that chlorination causes selectivity increase while in the absence of chlorine in calcium sulphate underlines the difference of catalysts in their ability to adsorb and co-operate with TCM.

Thermally steady Sr-HAP with different stoichiometric ratio can be used as a catalyst for methane oxidation by oxygen and nitrogen oxide in the presence and absence of TCM [165]. There has been occuring nonselective oxidation by oxygen of CO to CO_2 on thermally instable Sr-HAP at 873 K, at the same time selectivity for CO increased with the increase of time and in the presence of TCM it made 90% after 6 hours regardless of Sr/P ratio of catalyst. Sr/P ratio considerably effects the selectivity to CO oxidation in the presence of TCM in reactions with nitrogen oxide. In the presence of TCM, catalyst consists of complex mixture of HAP, CAP, phosphate, chloride and oxychloride, each adding its peculiarities to the catalytic process.

Methane oxidation by nitrogen protoxide on PO_4-deficient Ba-HAP is investigated in the presence and absence of TCM. There was comparison of HAP catalysts in the presence of oxygen conducted in order to increase in methane oxidation activity [166]. In the absence of an external oxidizer, TCM addition suppressed the for-

mation of oxidation products with CO and CO_2 removal and selectivity increase for C_2H_6. Selectivity for C_2H_4 is sufficiently small, indicating that TCM directly promotes the activation of structural oxygen of the catalyst. In the absence of TCM and with nitrogen oxide as oxidant maximal selectivity has reached 80% by conversion of 4.5% of methane during half an hour. CO_2 was predominatly generated in the presence of oxigen, while in the presence of nitrogen oxide and TCM with the increase in time, only CO was generated.

Methane oxidation was investigated for Pb-HAP, Sr-HAP and their binary sistems at 873 K. Pb-HAP showed no methane oxidation activity while Sr-HAP initiates carbon monoxide generation with the selectivity of 2—4% [167]. The similar synergetic effect in methane conversion and selectivity of CH_3Cl yield for binary systems was observed with TCM. Sr-HAP, probably, plays the key role in methane activation while Pb-HAP presence is required for minimisation of undesirable processes of methyl radicals formation.

3.10. Coatings and films on the basis of apatites

Methods of coatings. HAP-coatings are widely used for orthopedic and tooth prosthetics. Their chemical, biological and mechanical properties can be improved by development of new technologies.

To overcome comparatively low values of characteristics of mechanical properties of HAP, HAP film coating was deposited on biologically inert materials possessing sufficient durability and impact strength, such as polycrystalline aluminium oxide (Al_2O_3), zirconium dioxide (ZrO_2), metal titanium (Ti) and titanium carbide (TiC). There are several methods for thin HAP films preparation. It is reported in a number of works about HAP-coatings, deposited on Ti plates using electrophoretic deposition [1]. Then the coating is densified and bonded with the wafer with further sintering. It was revealed using Auger-electron spectroscopy that the interface between HAP and Ti contains phosphides of titan while the external surface of coating consists only of HAP.

HAP coatings deposition on strong ceramics and metals in order to obtain bioactive implants is one of the current problems in biomaterials science. It is reported in work [168] on apatite coating deposition on ceramic aluminium oxide using magnetron sputtering, which was carried out in mixed CO_2/Ar atmosphere. The main idea of the method is using of calcium phosphate glass with Ca/P ratio lower than at stoichiometric HAP. Surface studies with methods of X-ray diffraction and FTIR have ascertained carbonated calcium hydroxyapatite formation similar to the structure of bone tissue in which CO_3^{2-} ions occupied PO_4^{3-}-positions. Bioactivity of coatings on ceramic materials was tested *in vitro* by crystals growth in simulated body fluid (SBF). It has been established experimentally that growth rate on such coatings is much higher than on hydroxyapatite not containing carbonates-ions

Radio-frequency magnetron sputtering was used for calcium phosphate coatings deposition with various thicknesses (0.1, 1.0 and 4.0 microns) on titanium disks [169]. A part of sputtered coatings has been exposed to additional thermal processing for 2 hours at temperature 500 °C. X-ray diffraction has shown that annealing at 500 °C has caused the transformation of sputtered amorphous coatings (with thickness of 1 and 4 microns) to amorphous-crystal structure while the amorphous layer with a thickness of 0.1 micron completely transformed to crystalline apatite. REM has shown that annealing of coatings with the thickness of 1 and 4 microns has led to occurrence of small cracks. Features of dissolution of Ca-P coatings were investigated in SBF. After ageing within 4 weeks it was found that dissolution is determined with the degree of crystallinity of deposited coating. REM and Fourier-spectrometry, FTIR have shown that coatings have different stability. Amorphous coatings (0.1 and 1μm) dissolved completely in 4 weeks while amorphous (4 μm) coatings showed only signs of surface dissolution. The scratch test has shown that there is a linear correlation between critical loading and thickness of a coating. Coating thickness of 0.1 micron is enough already for displaying proper bioactivity and adhesive properties *in vitro*.

Plasma spraying. Choice of HAP as a coating for materials which are used in implantation surgery thanking its biocompatibility is quite natural. HAP-coatings can be deposited using several methods, one of which is vacuum plasma spraying (VPS). This method is used commercially for HAP deposition on titanium alloy substrates. The complete definition of characteristics of the sputtered surfaces was carried out in work [170] using REM, X-ray diffraction, and also AFM. It was shown that coatings, as a rule, were hypocrystalline and had an irregular shape. The values of surfaces imperfections were evaluated from AFM data. There were images of coatings after ageing during 28 days in a physiological solution (Ringer buffer solution) obtained, with changes in topography which can be connected with reactions of a tissue and the implanted material in a living organism.

FTIR study of plasma-sprayed HAP coatings [171] have established differences between the surface and the basic part of a coating. Coating thickness does not influence the position of infra-red bands and with the decrease in coating crystallinity band broadening is observed. The distinctive feature of surface spectra and of spectra of the basic part of a coating was higher degree of splitting of dissymetric P-O mode of valence vibrations (ν_3) the surface layer. This difference is attributed to the environment of PO_4^{3-}-ions and dehydration at the expense of condensation of hydroxide-ions that has affected apatite crystals during the process of plasma spraying.

Assessment of coating crystallinity is important, as there is a dependence between crystallinity degree and tendency to degradation. Assessment of crystallinity degree is complicated with texturing of coatings. The structure dependence on a thickness of plasma sprayed layer was investigated by calculation of texturing coefficient [172]. Experimental results have shown that texturing coefficient values for (002) and (004) peaks increased with a thickness, and texturing coefficient values for

(211) peak decreased that was caused with high temperature gradient during deposition, and also by the presence of a priority growth direction. It was established that the controllable increase in temperature during annealing did not lead to structure formation. However at a high temperature gradient large (002) structure is formed.

Various characteristics of plasma-sprayed hydroxyapatite coatings (PSHAP) were investigated *in vitro* in work [173] where the influence of coating characteristics on osteoconductivity of PSHAP *in vivo* was estimated. There were prepared three various PSHAP on Ti_6Al_4V substrata by different parametres of plasma spraying. Using of a new implant in the wolf femur and quantitative histology allowed determining PSHAP osteoconductivity, characterised by an index of bone healing in 2, 4 and 6 weeks after implantation. Results *in vitro* indicate that the microstructure, phase composition, crystallinity, hydroxyl content and Ca/P molar ratio of PSHAP depends on sputtering process parameters. TCP, TTCP and calcium oxide phases were found out in PSHAP after plasma spraying, and hydroxide-ion content in PSHAP has considerably decreased. Strength of PSHAP depends on coating microstructure. Histomorphometrical study has shown that coating characteristics does not essentially influence the values of index of bone healing by short-term implantation.

Coating by laser deposition. As an alternative to traditional plasma spraying of coatings, a pulsed laser deposition (PLD) is applied for stoichiometry preservation [174]. $Ca_{10}(PO_4)_6(OH)_2$ target is sputtered using Ar-F_2-laser in water vapour atmosphere for definition of a flux density area corresponding to stoichiometrycal transfer. Ca/P ratio in a coating and both OH^- and CO_3^{2-} content was estimated using FTIR method. The irradiated surface was analyzed using REM, and wash-out coefficient was measured by the surface roughness. By higher flux densities all target material was sputtered congruentially with stoichiometry preservation. By lower flux densities (<1.2 Dj/cm^2) washing-out of Ca and strong external diffusion of CO_3^{2-} groups took place. Increase of CO_2 partial pressure leads to PO_4^{3-} substitution for CO_3^{2-} and to Ca/P ratio increase in the coating.

Pulsed laser deposition is a perspective method of deposition of calcium phosphate thin film. In work [175] for HAP target sputtering and thin HAP film deposition on titanium wafers in vacuum ruby laser was used. Precipitation was carried out in a range of temperatures from room temperature to 800 °C. Precipitation at 400 °C has led to the formation of films with given stoichiometry, crystallinity and adhesive properties of metal-ceramics interface.

Deposition of thin films of HAP ceramics was carried out on various substrates, in particular, on Ti, α-Al_2O_3, SiO_2/Si (100) and on $SrTiO_3$ (100) by pulsed Ar-F_2-laser deposition [176]. The surface morphology of HAP films was investigated using AFM. For measurement of such electric characteristics of HAP films as inductive capacity and disruption/breakdown voltage at 25 °C (1 MHz) and 10^4 B/cm^1 respectively, Au/HAP/Nb-doped $SrTiO_3$ (100)-structures were fabricated. It was established that HAP films can be applied not only as a material for biologically compatible coatings of implants, but also as dielectric, promising for use in electric circuits and bioelectronic devices.

The excimer laser deposition technique was used for $Ca_{10}(PO_4)_6(OH)_2$ thin film preparation on tetrafluorethylene substrates [177]. The surface of tetrafluorethylene substrates has been modified with a complex of naphthalene with sodium in clay. X-ray diffraction study indicated that HAP in the films prepared at the substrate temperature lower, than the temperature of tetrafluorethylene substrates vitrifying (327 °C), is in amorphous state. Crystallization of deposited films was held by annealing at 310 °C during 10 hours. Surface structure, morphology and adhesive strength of HAP films with a substrate surface was estimated using X-ray diffraction and AFM. Tensile strength of HAP films by adhesion to the modified substrate surface has made 6.0 MPa that is 10 times more than of film deposited on unmodified surface.

Calcium phosphate coatings were deposited on Ti_6Al_4V by laser ablation (355 nm, Nd:YAG-laser) at various substrate temperatures [178]. Two types of coatings were deposited at water vapour pressure of 10 and 45 Pa and at substrate temperature of 20 up to 600 °C. To investigate the influence of deposition temperature and water vapour pressure on coating properties the characterization of their structure and adhesion dynamics was carried out. It was established that high temperature promotes synthesis of crystal phases. Calcium phases are synthesized at 10 Pa while HAP synthesized at 45 Pa contained a certain amount of α-TCP. Coating-substrate adhesion for the films deposited at 45 Pa considerably increased at substrate temperatures above 400 °C, however the greatest adhesion was observed for the amorphous coatings received at 10 Pa and 200 °C.

Calcium phosphate coatings, obtained at various rates of deposition by pulsed laser (Nd:YAG-laser, λ=355 nm) were studied in work [179]. The deposition rate was changed from 0.013 up to 1.16 Å/impulse by ablation area modification and preservation of constant local flux density. Coatings were characterized using scanning electronic microscopy, X-ray diffractometry, and also IR, micro-Raman spectroscopy and XPS. Investigations have shown that coatings possess compact surface morphology generated from grains of glass. There were only peaks of HAP and α-TCP revealed on the diffractogram. The relative amount of α-TCP decreased with the reduction of HAP deposition rate which dominates in the field of low speeds of a stream.

Sol-gel technique. The apatite layer can be generated on pure silica gel, wetted with SBF. Formation depends on characteristics of a solution and agglomeration temperature of a silica gel. In [180] silica gel texture influence on degree of hydroxyapatite formation was investigated. The product yield was controlled by FTIR, and also by measurement of ion concentration change in a liquid. Induction time of apatite nucleation on silica gel has decreased when the size and the volume of pores have increased. The substrate parameters influencing on nucleation has been discussed, and the mechanism assuming that pores to be hydroxyapatite nucleation sites is offered.

Hydroxyapatite synthesis of sol-gel precursor was investigated by X-ray diffraction in [181]. Sol-gel has been transformed to powders and thin films. The influence of a drying mode and annealing temperature on HAP phase formation was investigated. Thin HAP films with the thickness up to 1 μm were deposited on silicon

substrates covered with either glass of phosphateboric silicate or titanium films, then dried up and annealed. The rise of drying temperature has increased the annealing temperature before the beginning of HAP crystal formation. It was established that at annealing temerature of 300 up to 1000 °C, the dominating phase in powders is HAP with small amount of calcium oxide and β-TCP admixtures. When annealing temperature has increased both CaO and β-TCP amount has increased. At annealing temperature of 300 up to 500 °C only HAP crystal phase was observed.

The hydrothermal mechanism of coating formation. In work [182] hydroxyapatite films were deposited on the surfaces of titanium disks by the method of homogeneous precipitation using hydrothermal reaction between $Ca(EDTA)^{2-}$ and NaH_2PO_4 in solution at 120—200 °C and pH ranging from 4.0 up to 10.0 during 2-20 hours. When titanium disks had been directly placed in a reaction mixture at 160 °C and pH 5 for 2 hours they were uniformly covered with films consisting of a mix of big lamellar monetite particles and thin needle-like hydroxyapatite particles while at pH> 6 and at pH 4, respectively, the units consisting of needle-like and/or rod-like hydroxyapatite and lamellar monetite were deposited on the surfaces in the form of islets. Lamellar-like monetite, generated at the initial stage of reaction at pH 5.0, with time was transformed into needle-like HAP at pH>5.5. Double coating, when titanium disks have been successively dipped in 0.05 M $Ca(EDTA)^{2-}$- 0.05 M NaH_2PO_4 solution at pH 5.5 (then pH 6—9), and 160 °C for 2 hours, to completely cover the surface with the thin film of monetite and hydroxyapatite, is convenient for continuation of HAP coating formation.

Thin transparent HAP sheets consisting either of ultrathin HAP particles or of particles, increased in size by hydrothermal processing, were made using the modified method of pressure casting [183]. When heated to 1000 °C samples being very small particles have become non-transparent while samples of hydrothermally processed gels have kept the transparency. The optical transparency measurement of laminary samples during heating at a constant speed has allowed to determine the temperature interval of transition. Dilatometric measurements have indicated the increase of samples volume at a temperature above 1000 °C which is connected with pores formation which apparently has led to the sample transparency reduction at a temperature above 750 °C.

Sintered hydroxyapatite was used as a substrate. Monetite ($CaHPO_4$) was deposited on its surface at a nucleation pressure of 1.55—8.59 MPa and a temperature of 200—300 °C [184]. Speed of monetite deposition increased with the increase of temperature and reaction time. At 8.59 MPa and 300 °C small needle-like crystals of monetite were revealed after 8-hour contact. After 72 hours the diameter and the length of needle-like crystals have increased. During 120 hours at 300 °C the crystal morphology has changed and needle-like crystals have merged into granulated grains.

The multilayer material consisting of HAP and calcium titanate ($CaTiO_3$) was hydrothermally synthesised on a titanic substrate [185] which was processed at 150 °C by a solution containing $CaCl_2$ and KOH for preliminary $CaTiO_3$ layer formation. $CaTiO_3$ layer thickness changed symbatically with KOH concentration increase and

simultaneous reduction of coherence between a coat layer and a substrate. HAP layer was formed on $CaTiO_3$ layer, precipitating from the mixed solution containing $CaCl_2$, K_2HPO_4 and KOH with Ca/P ratio less than 1.67. Calcium was fed from the reacting solution and $CaTiO_3$ layer and precipitated in the form of HAP. Partial $CaTiO_3$ destruction and consecutive calcium transfer promote the formation of HAP layer strongly fixed on the substrate at 220 °C during 24 hours with pH 8-10. Adhesive strength between the substrate and $CaTiO_3$ layer did not decrease after HAP formation, however, it decreased with increase in KOH concentration in the process of synthesis of $CaTiO_3$ layer. After soaking of HAP/$CaTiO_3$ multilayer in SBF during 35 days at 37 °C, had been covered with very thin needle-like HAP particles though neither the surface of $CaTiO_3$ layer nor a titanium substrate did not change after the same processing.

Electrochemical preparation of films. Hydroxyapatite microcrystals can be precipitated on titanium oxide film formed by hydrothermal processing, containing calcium and phosphorus with typical for HAP Ca/P ratio and which is generated on the titanium metal anode in water electrolite solution of calcium acetate and β-glycerophosphate. In [186] the mechanism of formation of such film is described. Spark discharges on the titanium surface with a release of a large amount of heat, cause the crystallisation of TiO_2 matrix and simultaneous incorporation of calcium and phosphorus from these electrolits into a matrix. Thin HAP layers consisting of precipitated microcrystals using the given method can be generated uniformly even on the titanium with a complex surface profile and even porous one.

Electrophoretic precipitation of ultrapure calcium phosphates from anhydrous suspensions on metal matrixes was conducted for obtaining of coatings with variable porosity [187]. It was established that the surface of calcium phosphate particles accumulated a considerable electrostatic charge when the dense and homogeneous precipitate was formed during ageing. The addition of ionogenic surfactants allows obtaining coatings with the necessary density and microporosity.

Plasma sprayed hydroxyapatite coatings, deposited on metal implants, are biologically compatible and capable to form chemical bonds with bone tissue. However, the structural changes usually occurring in these coatings as a result of high-temperature transformation can unfavourably change their stability *in vivo*. In [188] it is reported on an electrochemical method coating at low temperatures which eliminates risk of phase transformations in such coatings.

The method of electrolytic precipitation was developed for manufacturing of HAP bioactive coatings on Ti_6Al_4 at rather low temperature [189]. Galvanostatically electroprecipitated HAP coating has Ca/P molar ratio of 1.62 and porous structure which is similar to a human bone. In [190] microstructure of HAP ceramic coating on TiNi alloy substrata with shape memory effect is investigated. From a perspective of adhesion, these coatings possess higher strength (~30 MPa). Coatings were obtained at 55, 50 and 45 V. At lower voltage, the prepared HAP coatings contained pure $Ca_{10}(PO_4)_6(OH)_2$ with Ca/P ratio of 1.65. At the highest voltage (55 V) phase

transition of $Ca_{10}(PO_4)_6(OH)_{0.5}O_{0.75}$ out was registered. Good strength was observed at the interface metal/ceramics.

The method using the effect of electric field on calcium phosphate continuously precipitated from the solution is applied in [191] for obtaining of HAP coating (1-2 μm) on stainless steel with reproducible characteristics. The influence of change of various parametres, including current strength and pressure, temperature, supersaturation and distance between electrodes, on the character of a coating was established. Mechanical properties were tested using microhardness indentation. There was offered a model for the explanation of the observable phenomena during precipitation and deposition processes. ACP is initially formed originally in the form of spheres which next merge, forming gel-like disks which were the matrix where hydroxyapatite nucleation is initiated. Gel layers under the influence of the electric field are precipitated on the cathode in the form of the cells each wall of which consists of set of nanosized (100 nm) crystals focused perpendicularly to the sample surface.

New methods of preparing films and coatings. The coating an implant surface with apatite layer has become one of most widely used methods to improve adhesion to a bone. Metal/apatite interface is the area of chemical and mechanical heterogeneity causing ambiguity in calculation of long-term integrity of implants covered with apatite. These problems are essentially connected with the coatings obtained by usual methods of plasma spraying. Recently, there have been attempts to make a coating with the improved properties, in particular, using surface modification during preparation and with use of alternative precipitation methods. Apatite precipitation from the liquid phase is one of new methods investigated for coating deposition. In [192] there was made an attempt to describe the basic chemical processes perspective for preparation of a stable metal/apatite interface, in order to form the fundamental principles for the further technological developments.

As opposed to extensive investigation of thin HAP films, there are only few works concerning thin films of carbonate-containing apatite (dahlite). In [193] synthesis and the results of characterization of highly crystalline dahlite thin film deposited using biomimetic method are described. The continuous film of calcium carbonate-phosphate precursor was initially prepared by precipitation of a inhibitor solution as amorphous phase using template method at the air-water interface. The surface stearic acid monolayer acted as a template while phosphate-carbonate solution was a binary inhibitory system. The precursor film generated at the air/water interface, heated to 900 °C also transformed into the dense crystal film which had completely kept the form of the precursor. The crystalline phase characterized with X-ray diffraction and IR, was carbonate-apatite, with CO_3^{2-} occurrence both in $A(OH^-)$, and $B(PO_4^{3-})$-position.

HAP precipitation from a water solution on titanium disks represents possibility of deposition of biologically active coatings for bone implants. While the factors acting in solution are clearly established, the studies, concerning the surface stimulation of HAP nucleation, are in the implementation phase. In [194] on the titanium surface

by Na^+ ion introduction and the subsequent thermal processing sodium titanate/Na_2TiO_3 layer was formed. Such surface with ion implantation favours nucleation and growth of HAP crystals in SBF.

In work [195] the application of ionic bombardment for consolidation of a porous ceramic film is described. Ionic implantation is a room-temperature process, and, thus, can be more preferable in comparison with the use of conventional high-temperature sintering which, as a rule, is carried out at temperatures above 1000 °C. Thin films of bioceramic hydroxyapatite $Ca_{10}(PO_4)_6OH_2$ were deposited on silicon substrates using sol-gel technique. Films with thickness of 600 nm after drying at 620 °C during 3 minutes had density of 36% of the density of monolithic HAP. The dried films were irradiated with Si^{2+} ions with energy of 1 both 2 MeV and flux densities in the range from 10^{14} up to $6{\cdot}10^{15}$ ion·s/cm^2. The samples irradiated with largest flux density reaching 83% of the density of monolithic HAP. Rutherford backscattering spectroscopy is used for a more precise definition of films composition stoichiometry and density distribution. Mechanical test (scratch test) has shown that the implantation has led to substantial improvement of mechanical characteristics determined using nano-indentation, which has shown that after irradiation the hardness has increased 15-fold. Ionic irradiation led to certain decrease of crystallinity degree of the film. The advantage of ion implantation processing over high-temperature one is shown as no secondary crystal phases resulting of such consolidation appear.

In recent years high-velocity oxy-fuel spraying technique for HAP coatings deposition is used. In [196] the influence of the condition of HAP powders on the microstructure and coating characteristics during fusion process was investigated. The results have shown that tensile strength of HAP coatings sputtered using high-velocity oxy-fuel spraying method can reach 31 MPa and substantially depends on spraying parametres. The results of X-ray diffraction show that HAP coatings depositied in this way using powders with the particle size of about 50 μm, consist of HAP crystal and α-TCP impurity. The coatings deposited using fine powders with diameter of particles of about 30 μm, consisted generally of amorphous and a small amount of crystalline HAP, and also α-TCP impurity. The results of indication indicate that crystallization temperature of the amorphous phase of coatings of approximately 703 °C. The presence of an amorphous phase in coatings spread in this way has considerably improved the adhesion strength. The structure was completely crystalline at a temperature below 750 °C. Investigation of HAP coatings fracture by REM method show that fracture occurs in partially melted powders. The surface between the melted and unmelted parts of powders is a zone of distribution of fractures. This suggests that the fully melted state of the feedstock can result in the formation of amorphous phase and simultaneously decrease the bond strength. It also suggests that the fraction of the powders melted is the most critical factor influencing the bond strength and phase composition of the coatings.

In order to obtain a biomaterial which has both biological affinity and high mechanical strength, hydroxyapatite granules were introduced into superplastic (by

heating to approximately 750 °C) $Ti_{4.5}Al_3V_2Pe_2Mo$ alloy substrates [197]. Hydroxyapatite granules (32—38 μm in diameter) were depositied on the alloy surface with the subsequent piston pressing. Granules, introduced into the substrate at 8.5 MPa and 750 °C during 10 minutes, were strongly attached to the substrate. They formed layers at the interface. Titanium alloy with implanted hydroxyapatite granules is perspective as a biomaterial for artificial bones and roots of teeth.

In [198] the introduction of HAP granules into a superplastic $Ti_{4.5}Al_3V_2Fe_2Mo$-alloy substrate was made. For improvement of Ti alloy biocompatibility pure titanium film was initially deposited on alloy substrate by sputtering. HAP granules of 32—38 μm in diameter were sputtered over the Ti-alloy substrate, and then were pressed into the substrate. After introduction of granules at temperature 750 °C, the formation of a large quantity of cracks around the introduced granules on a film coating was observed, and the HAP granules appeared to be damaged. At the same time, at 800 °C the pure titanium film became thinner near the ledge of a lateral wall nearby HAP granules; however, granules were introduced into the alloy with the shape preservation and with no defects.

Functionally gradient materials (FGM) is a new development in the field of composite materials — they consist of continuously changing interface between phases of two components. The methods of sintering [199], including gas-vapour deposition, plasma spraying, electrophoretic precipitation, controllable mixing of powders, slip casting, formation by precipitation from solutions, rotary formation, laser deposition of coatings, metal infiltration, controllable solvent evaporation and self-propagating high-temperature synthesis are considered. The new approach to FGM production, using thixotropic casting — vibrational casting of highly-concentrated thixotropic suspensions is presented. HAP- stainless steel system is a biologically compatible ceramics that was used because of affinity of values of density, factor of thermal expansion and agglomeration temperature. Solid blends with a density of 76.08—82.67% of the initial value were tested. By a density of 78.17%, the ideal continuous FGM was formed, showing gradual transition from pure ceramics to pure metal in a sample with a length of 60 mm. By the closest tested changes of density (±0.3%) the gradation was far from the optimum: the composition with a density of 77,87% had a sharp ceramics/metal interface and with a density of 78.47% — rather homogeneous sample with a small degree of gradation, from metal-containing edge to metal depleted.

There was made an attempt to deposit gradient HAP coating on titanium using plasma spraying as an alternative to direct HAP deposition on this substrate [200]. Application HAP multilayers and titanium-containing mixtures guaranteed the gradual change of structure perpendicularly to the surface. As a result, the microstructure of the area near coating-substrate interface has shown good adhesion between the coating and the substrate. Oxidation of the titanium substrate was effectively reduced by an appropriate choice the particle size and protective atmosphere. The main prod-

uct of reaction representing a separate phase of composition TiO_x ($x \approx 1.04$), in contrast to TiO_2, was formed in gradient coating layers and as it was believed, plays the important role in maintenence of adhesion between HAP and titanium.

A functionally-gradient biomaterial in a HAP-Ti system was developed by an optimised powder metallurgical process and investigated by microstructural analysis and mechanical tests for durability [201]. The constituents in sintered HAP-Ti FGM distribute gradually with the variation in chemical composition, eliminating the macroscopic interfaces such as that in HAP-Ti direct joint. Partial decomposition of HAP phase was found out in interlayers of the FGM due to the co-existence of Ti during sintering. Mechanical properties in HAP-Ti FGM also exhibit gradient distributions. Vickers hardness and Young's modulus are strongly affected by the porosity. However bending strength and fracture toughness increases with the rise of Ti content, especially in the Ti-rich region. The maximum strength and toughness (971.96 MPa and 29.691 $MPa^{1/2}$ respectively) were reached in the pure Ti layer which are far higher than those of human bone. In addition, the strengthening and toughening mechanism was discussed. In summary, HAP-Ti FGM is a promising biomaterial for use as a hard-tissue replacement implant, considering its mechanical behaviors.

Postprocessing of films and coatings. In work [202] the effect of post-deposition annealing treatment in 1 bar of oxygen and moderate temperatures (<450 °C) under illumination by vacuum ultra-violet (VUV) radiation emmited upon thin HAP films grown by the pulsed laser deposition technique was investigated. HAP layers were deposited at 650 °C and various values of oxygen partial pressure without any water vapours. The VUV treatment was also beneficial for the partially crystalline HAP layers containing tetracalcium phosphate and calcium oxide phases. It is most accurately expressed for the films which have been grown up at lower partial pressure of oxygen. After the VUV-assisted anneal, the crystalline structure and the stoichiometry greatly improved while the percentage of the other crystalline phases initially present was many times reduced. After ultra-violet annealing the layers were transformed to the high-quality crystal films of HAP, with Ca/P ratio close to the stoichiometric value of 1.67. The content of other crystal phases initially present was considerably reduced. IRS has shown that the amount of OH^--ions in films has increased after the specified influence. The combination of two low-temperature methods makes it possible to deposit high-quality HAP layers without material oxidation.

HAP plasma-sprayed coatings were treated with Nd-YAG laser [203]. The results have shown that HAP surface melted during continuous scanning when exposed to laser energy above or equal to 2 J and by an area of section of 2 mm^2. The melted material had multilayered porous structure. Pore diameter varied in the range of 30-150 microns, and pores supported osteoinduction. Results of X-ray diffraction studies of the laser treated coating have shown the increase the crystalline HAP phase content. The optimum crystalline HAP content is reached by laser impulse energy of less than 5 J and the laser spot size of 3 mm.

3.11. Disordered compounds

Cluster model of disordered apatite-like compounds. The presence of 7 to 10 Å calcium phosphate clusters in SBF was revealed in work [204]. The clusters were also observed in liquids, unsaturated with respect to octacalcium and amorphous calcium phosphates and oversaturated with respect only to hydroxyapatite. That fact that hydroxyapatite crystal grows with step of 8 or 16 Å in height and that the probability of realisation of step-by-step growth in a crystal is low-probability, specifies that a cluster is a growth unit of hydroxyapatite. The model of cluster growth of Ca-HAP can be proved using 8 Å $Ca_9(PO_4)_6$ clusters. In theory defects of clusters packaging form mirror twins of a crystal, boundary dislocations with *c*/2 slip vector and screw dislocations. The atomic image corresponding to boundary dislocations with *c*/2 slip vector has been obtained at the surface of a synthetic hydroxyapatite monocrystal.

Stability of 8 Å calcium phosphate clusters found in SBF ($CaCl_2H_3PO_4$-KCl-H_2O system) at 25 °C was investigated experimentally in work [205]. It was shown that tris-hydroxymethylaminomethane which was used as the main component of the buffer solution, did not influence cluster formation. The quantity of clusters has decreased with the reduction of solution oversaturation with respect to hydroxyapatite.

Using *ab initio* method the potential of surface energy of $Ca_3(PO_4)_2$ cluster [206], with each calcium atom surrounded by four oxygen atoms is defined. Investigation of $[Ca_3(PO_4)_2]_n$ with n=2 or 3 has given a possibility to analyze stability of so-called Pozner cluster $Ca_s(PO_4)$, which is the core of structural model of ACP.

Aggregation of HAP was investigated in the presence of potassium phosphate using centrifugal fractionation [207]. The dependence of quantity of medium-size HAP particles on potassium phosphate (K_3PO_4) concentration, and also on time, enabled researchers to determine a speed constant for bimolecular process of aggregation. By K_3PO_4 above 5.10^{-2} M HAP particles accumulation led to two-level (with different population) particle distribution that gave a possibility to separate polydisperse HAP particles into two fractions.

A novel VIMOX (volume identical metal oxidation) route to near-net-shaped calcium hydroxyapatite is demonstrated: the oxidation of machinable Ca-$Ca_2P_2O_7$ precursors [208]. Mechanically alloyed mixes of calcium and β-$Ca_2P_2O_7$ were compacted into a disk — and bar-shaped preforms. The latter preforms could be machined into cylinders using a metalworking lathe (200 rpm, hardened steel tooling. After oxidation at 600 °C in O_2 and then postoxidation annealing admixtures H_2O/O_2 mixtures at 850 °C and 1150 °C phase-pure hydroxyapatite was obtained. Because of offsetting volume changes from calcium oxidation and hydroxyapatite formation, porous hydroxyapatite bodies were produced that retained the shapes and dimensions (within 1%) of the machined precursors.

Amorphous phosphates. It is possible to obtain ACP, which is usually formed as unstable phase during the initial stage of hydroxyapatite synthesis, with fast dosed ad-

dition of ammonia hydroxide to calcium dihydrophosphate solution. When dipped in various ACP solutions (with Ca/P ratio of 1.25-1.55) easily is transformed to various crystalline calcium phosphates: DCPD, OCP and HAP. In work [209] crystallization conditions, structure and crystallographic characteristics of the new phases generated by crystallization in system of a kind — ACP with Ca/P ratio > 1.40 were determined at 0 °C during 24 hours. The compound composition fitted the formula $Ca_3(PO_4)_2 \cdot 8H_2O$. It was shown that crystallographic phase parameters correspond to monocline system with a=1.312 nm, b=1.111 nm, c=1.264 nm, β=109.0°. 3×6 μm crystallites had a lamellar shape.

The formation of a thin water film on sample surface in wet atmosphere sample transformation. Behavior of ACP with Ca/P ratio of 1.33 in wet atmosphere at 40, 60 and 80 °C was investigated in [210]. At 40 and 60 °C on the sample surface crystallization of triclinic OCP, containing structural water take place. Another deeper part of the surface is transformed into apatite OCP. Irrespective of temperature, the end-product of transformation of crystals of both types (in several stages) is a mixture of HAP and monetite.

Hydroxyapatite, prepared with precipitation in reaction of $Ca(OH)_2$ water suspension with H_3PO_4 at pH> 7 with the subsequent sintering at 700 °C, was exposed to compression [211]. FTIR and REM studies have shown that crystalline hydroxyapatite at a pressure of 2-10 HPa is in amorphous phase. Investigation of amorphous coatings [212] have shown that it consists mainly of dehydroxylated calcium phosphate. Heating of hydroxyl-containing areas of coatings leads to HAP formation. Hydroxyl-deficient amorphous areas crystallize with oxyapatite formation at 700 °C. Crystallisation occurs in wide range of temperatures and depends on the content of amorphous phase, hydroxyl and partial pressure of water steam. Activation energy of HAP crystallization, hydroxide-ions diffusion and oxoapatite crystallization is 274, 230 and 440 kJ/mol, respectively. Reduction of retention intervals of these processes leads to the formation of a network of cracks and reduces mechanical durability of a coating.

Ion-beam-induced amorphization of $Ca_2La_8(SiO_4)_6O_2$, a silicate ceramic with the apatite structure was investigated in [213]. In-situ TEM was performed during irradiation with 1 MeV Ar^+, 1.5 MeV Kr^+ and 1.5 MeV Xe^+ ions over the temperature range from 20 to 773 K to determine the ion dose required for complete amorphization of the crystal (critical amorphization dose D_c). D_c increased with increasing irradiation temperature and decreased with increasing ion mass. The residual irradiation damage after low ion doses appeared as nanometre scale amorphous domains. The images of these areas are extremely sensitive to the sample thickness. At higher temperatures the observed amorphous domains are smaller indicating thermally activated epitaxial recovery at the amorphous-crystalline interface. The amorphous domains are larger in size after irradiation with ions of higher mass.

Fibers, based on apatites. A novel method for preparing Ca-HAP fibers has been developed [214]. HAP fibers can be prepared succesfully by heating a com-

pact, consisting of β-$Ca(PO_3)_2$ fibers with $Ca(OH)_2$ particles in air at 1000°C and subsequently treating the resultant compact with dilute aqueous HCl solution. The β-$Ca(PO_3)_2$ fibres and the $Ca(OH)_2$ in the compact were converted into fibrous HAP and CaO phases by the heating. Then CaO phase was removed by acid leaching. HAP fibers obtained in this way were 40-150 μm in length and 2-10 μm in diameter.

In work [215] HAP (w) were used for preparation of fibrous, porous HAP ceramics. The fibrous microstructure remains in all cases of hot pressing of HAP (w) at 800-900 °C (1 hour, 30 MPa). Fracturing of fibrous porous HAP ceramics occurred at the grain boundary. After HAP (w) pressing at 1000-1100 °C (1 hour, 30 MPa) only big equiaxed grains appeared in HAP ceramics i.e. hardening did not occur. When using nonstoichiometric HAP (w) for the preparation of a porous body β-TCP was precipitated on HAP (w) surface without destruction of its fibrous microstructure.

Whiskerlike-shaped hydroxyapatite single crystals were hydrothermally grown under natural convection by using a temperature-gradient-applied pressure vessel [216]. The crystals grew thinner with a smaller conicity angle, than those grown under nonconvection. The maximum length of the crystals, grown under the natural convection was 8.3μm. The grown up crystals survived without fracture through the three-point bending tests, showing the maximum bending angle of 62 °. Average tensile strength of the crystals was 410.0 MPa.

HAP whiskers and platelets can be synthesized by the hydrolysis of α-TCP in H_2O system and ethanol/H_2O system at 70 °C and atmospheric pressure [217]. The effect of ethanol addition into H_2O on the hydrolysis of α-TCP to HAP was also examined. The hydrolysis rate of α-TCP to HAP was inhibited in ethanol/H_2O system. It is found that the morphology and the aspect ratio of HAP could be controlled by adding ethanol into H_2O during the hydrolysis reaction of α-TCP.

As a rule, HAP (w) were synthesised by hydrothermal crystallization of ACP with 0-5.0 M solutions of different carboxylic acid solutions such as acetic acid, malic acid and citric acid at 140-220 °C in autoclave [218]. The shape of products was controlled by the nature of carboxylic acids. The largest HAP (w) were obtained under conditions such as acetic acid of concentration 1.0 mol/dm^3, hydrothermal temperature of 200 °C and holding time of 3 hours; the resulting HAP (w) was hexagonal prisms of 100 μm in length and 4 μm in diameter and had Ca/P atomic ratio of 1.56±0.02. The formation of HAP (w) is ascribed to adsorption of dimer-carboxylic acids on the *a*-plane of HAP. Optimum conditions for HAP (w) synthesis were calculated from the dissociation constant.

HAP crystallization in the presence of synthetic polymers was investigated during synthesis of HAP/polymer composites in [219]. Side groups of polymers included carboxylate, monosubstituted acid phosphate, sulphate and primary amine. Amorphous-crystal HAP transformation at the presence and the absence of ionic polymers was analyzed. The rate of HAP crystals nucleation and growth were determined from the duration of the induction period before the beginning of crystallisation and the

subsequent distribution of HAP crystallites in bulk. Addition of anionic and cationic polymers suppressed crystallisation in concentration-dependent way with the exception of concentrated polyacrylic acid which was precipitated by formation of calcium salt for acceleration of nucleation and growth of HAP crystallites. It was shown that molecular interaction occurs between ionic chains of polymers and growing HAP crystallites. HAP, precipitated in the presence of ionic polymers, incorporated chains of polymers into microcrystalline HAP aggregates. Hence there have been compounds (HAP/(poly) acrylates) by *in situ* HAP crystallization at the presence of (poly) acrylate acid obtained. Tensile strength test and electron-microscopy of fracture surface have shown that mechanical strength of the samples prepared by "wet" method, is far good than of the samples obtained by mixing.

Foams based on HAP. HAP foams obtained by a method of gel-moulding with porosity of 0.72 up to 0.90 were investigated with the description of several parameters: pore size distribution, specific surface, permeability, modulus of elasticity [220]. According to the data of mercury porometry, the porous structure represents a massif of spherical cells interconnected with channels and with pore diameter in the range of 17-122 μm. The specific surface has increased from 1.5 to 3.8 m^2/g, with porosity increase. The ultimate compressive strength and the modulus of ealsticity was in in the range of 1.6-5.8 MPa and 3.6-21.0 HPa, respectively. Such combination of properties makes HAP foam a suitable material for use in different areas of biomedicine: bones regeneration, carriers for drug delivery and matrices for technological processing of a bone.

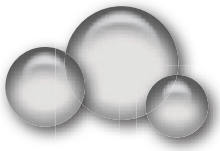

CHAPTER 4

ELECTRONIC STRUCTURE AND VIBRATION SPECTRA OF STOICHIOMETRIC APATITES

In this chapter the results of electronic structure investigation of stoichiometric calcium and strontium apatites are considered. The data on electronic structure of chlorine-, fluorine- and hydroxyapatite obtained by spectral methods and methods of quantum-mechanical calculations, are given. Vibration spectra of calcium and strontium apatites are described.

4.1. Vibration spectra of apatites

Tetrahedral XO_4^{3-} anion is a structural element of many crystalline compouds, such as garnet, spinels and apatites. In a first approximation XO_4^{3-} tetrahedrons can be considered as separate molecules, which symmetry is deformed by the action of structural factors. Generally, positional symmetry of tetrahedrons in a crystal is lower, than their symmetry in a free state. Reduction of symmetry leads to full or partial splitting of vibration levels, and also to occurrence of additional frequencies forbidden by selection rules for the symmetric configuration of a molecule. By a gradual decrease in symmetry of XO_4^{3-} anion from T_d up to C_3 the number of bands in a spectrum of such group [221] consistently increases.

Thus the influence of a crystal field will appear to some extent depending on the nature of the central atom in the anion, like for example, how strong is chemical bond X-O.

IR-spectrum of absorption of sample $Ca_3(PO_4)_2$ sample absorption is shown in Fig. 4.1. There are two intensive bands near 1028 cm^{-1} and 556 cm^{-1} observed. As it is known, nine possible vibrations of XO_4 group in the case of equivalence of all X-O bonds, i.e. tetrahedral symmetry T_d, cause only two bands in IR spectrum: one ν_3 vibration band and one of ν_4 band, ν_2 and ν_1 vibrations will be active/available only in combinational scattering spectra [221]. If only three bonds of four are equivalent (C_{3v}

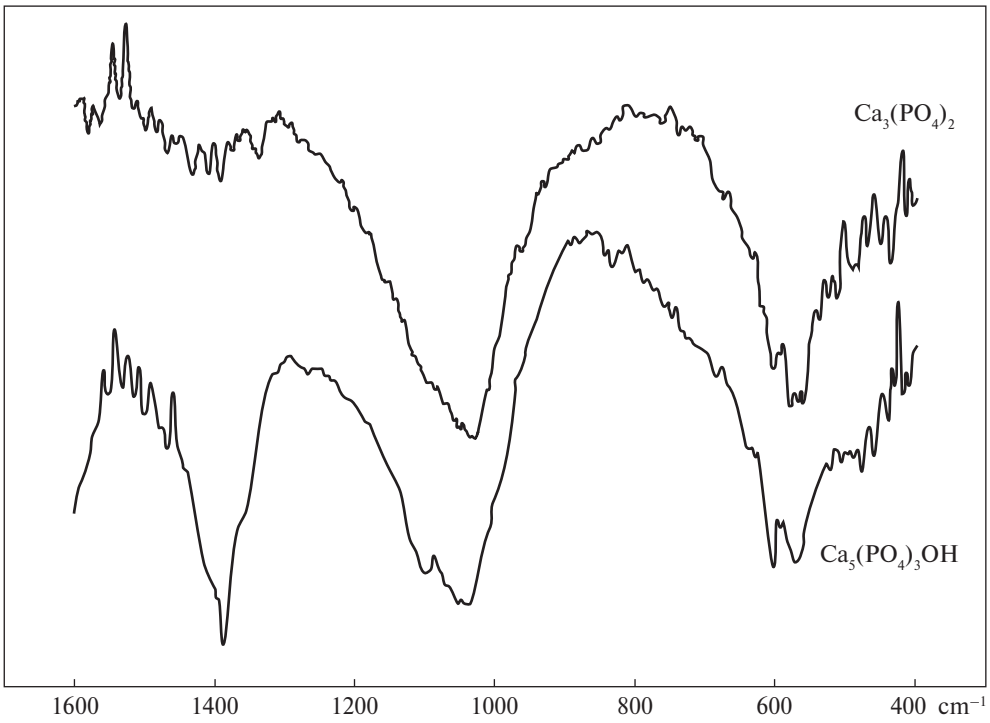

Fig. 4.1. IR-absorption spectra(1) $Ca_3(PO_4)_2$ and (2) $Ca_5(PO_4)_3OH$

symmetry), then totally symmetrical ν_1 vibration appears and partially splits triply degenerate ν_3 and ν_4 vibrations.

By non-equivalence of two X-O bonds to another two bonds ($C_{2\omega}$ point symmetry) ν_3 and ν_4 vibrations completely split. Finally, in the case, when all four bonds are various (C_3 symmetry), one more change appears in the spectrum notably the removal of doubly degenerate ν_2 vibrations [221—223].

Hence, the obtained spectrum of $Ca_3(PO_4)_2$ absorption (fig. 4.1) corresponds to PO_4-group absorption which symmetry close to T_d. In the transition to apatite (fig. 4.1) the spectrum bands corresponding to PO_4 group vibrations split. This indicates symmetry reduction of an PO_4^{3-}-anion environment in an apatite sublattice. Since ν_4 vibration ~570 cm^- splits into two components environment symmetry should correspond to C_{3v} point group. This result will agree with the fact that the quinquevalent phosphorus atom forms three single and one double bond with oxygen environment.

Totally different spectrum changes are observed for VO_4 tetrahedron. There is a wide band with a minimum near 700 cm^- in $Ca_3(VO_4)_2$ spectrum (fig. 4.2), while in apatite lattice the bands corresponding to vibrations of VO_4 group are much narrower [224]. As it is known, vibrations of free VO_4 group, active in IR spectrum,

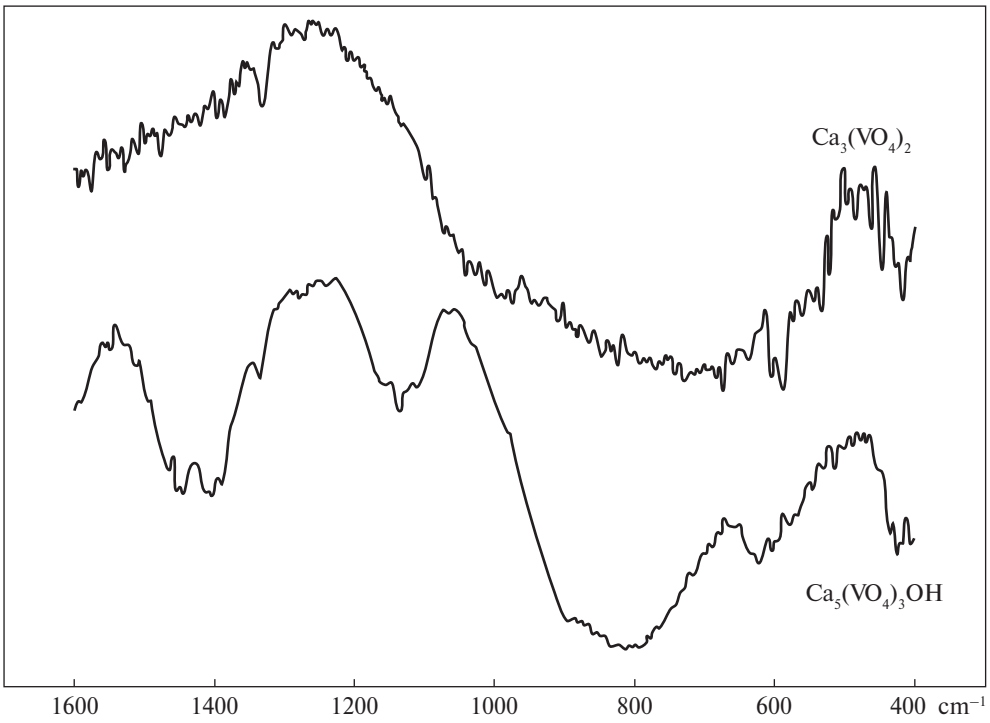

Fig. 4.2. Spectra of IR-absorption (1) $Ca_3(VO_4)_2$ and (2) $Ca_5(VO_4)_3OH$

should appear at frequencies of ν_3=825 cm$^-$ and ν_4=480 cm$^-$ [1]. The half-width of ν_3 absorption band in $Ca_5(VO_4)_3OH$ spectrum is much less than half-width of absorption band of $Ca_3(VO_4)_2$ (~520 cm$^-$). Thus, the symmetry of an environment of VO_4 group in apatite lattice is higher, than in $Ca_3(VO_4)_2$ lattice.

Comparison of $Ca_5(PO_4)_3OH$ and $Ca_5(VO_4)_3OH$ spectra shows that broadening of short-wave ν_3 absorption band of a crystal is less in $Ca_5(VO_4)_3OH$ than in $Ca_5(PO_4)_3OH$. The long-wave ν_4 absorption band is explicitely splitted into two components in $Ca_5(PO_4)_3OH$ spectrumwhile splittings for $Ca_5(VO_4)_3OH$ was not observed. Thus it may be concluded that environment symmetry of VO_4 group is higher, than of PO_4 group in crystal structure of apatite. The difference between phosphorus and vanadium atoms consists in the structure of their outer electron shells. Vanadium, as it is known [225], is transition metal with the filled inner electron shell. Therefore oxygen environment hybridization of its electron orbital is necessary for bonding with. Apparently, thereby, vanadium is known as a variable-valence element and this can lead in some cases to symmetry breaking of VO_4 group, as, for example, in $Ca_3(VO_4)_2$ which spectrum differs from $Ca_3(PO_4)_2$ spectrum. Besides, it was revealed that $Ca_5(VO_4)_3OH$ spectrum can be instable over time and depend on the conditions of a powder synthesis.

Hence, symmetry of XO_4^{3-} anion vibrations in a crystal lattice depends not only on the symmetry of its local environment, but also to a considerable extent on the nature of chemical bonds inside of anion.

IR absorption spectra of calcium and strontium apatites are presented in fig. 4.3 There are two groups of bands caused with $(PO_4)^{3-}$ tetrahedral sublattice absorption and located near 1030 cm^- and ~570 cm^-. This is consistent with the fact that elements of tetrahedral T_d symmetry are caused only two bands of IR spectrum, namely ν_3 and ν_4 [221] which position corresponds to that observed in the spectra (fig. 4.3). However the half-width of bands varies depending on the ions making apatite lattice. So, minimal broadening of absorption bands in calcium phosphateapatite was observed in the spectra of $Ca_5(PO_4)_3OH$. Substitution of OH-groups for F atoms leads to small broadening of bands, and substitution for Cl^- atoms leads to considerable broadening of absorption bands in spectra (tab. 4.1).

Another situation is observed in strontium phosphateapatites. By substitution of Ca^{2+} for Sr^{2+} minimal broadening of absorption bands was observed for fluorapatite while maximal broadening was observed for hydroxyapatite (tab. 4.1) that indicates considerable disordering and tetrahedral symmetry breakdown.

Hydrogen bond in apatites appears in IR absorption of OH^--groups. The absorption observed at 631 cm^- and 3573 cm^- (is not given) corresponds to libration and valence modes. OH^--valent band which appears as low-intensity peak indicates the weakness of hydrogen bonds of OH^--groups.

Hydrogen bond O-H----Cl is considered to be stronger than O-H----F of halogenated HAP, though F is essentially more electronegative than Cl (on the Pauling scale). It is confirmed with the results of IR-spectroscopy which indicate that by fluorine introduction HAP valence band shifts to 3514 cm^- while chlorine introduction leads to larger shift to 3495 cm^- that corresponds to conception that the more strongly hydrogen bond is, the more valence zone shifts.

Fluorine atoms in apatite are in the same planes, as the triangles of calcium atoms. According to neutron diffraction data, oxygen of hydroxyl group is shifted to 0.3 Å up or down from this plane. Therefore the distance between F and O for OH----F bond is equal to the distance between z=1/4 and z=3/4 planes minus 0.3 Å (R=3.44-03=3.14 Å).

Libration vibrations are OH-group vibrations in the direction, perpendicular to the crystal axis that is in agree with the assumption of rocking of hydrogen atom relatively

Table 4.1. **Half-width of absorption band near 1030 cm^- depending on the structure of phosphateapatite.**

Compound	Half-width of band, cm^-	Compound	Half-width of band, cm^-
$Ca_5(PO_4)_3OH$	190	$Sr_5(PO_4)_3F$	180
$Ca_5(PO_4)_3F$	210	$Sr_5(PO_4)_3Cl$	290
$Ca_5(PO_4)_3Cl$	420	$Sr_5(PO_4)_3OH$	430

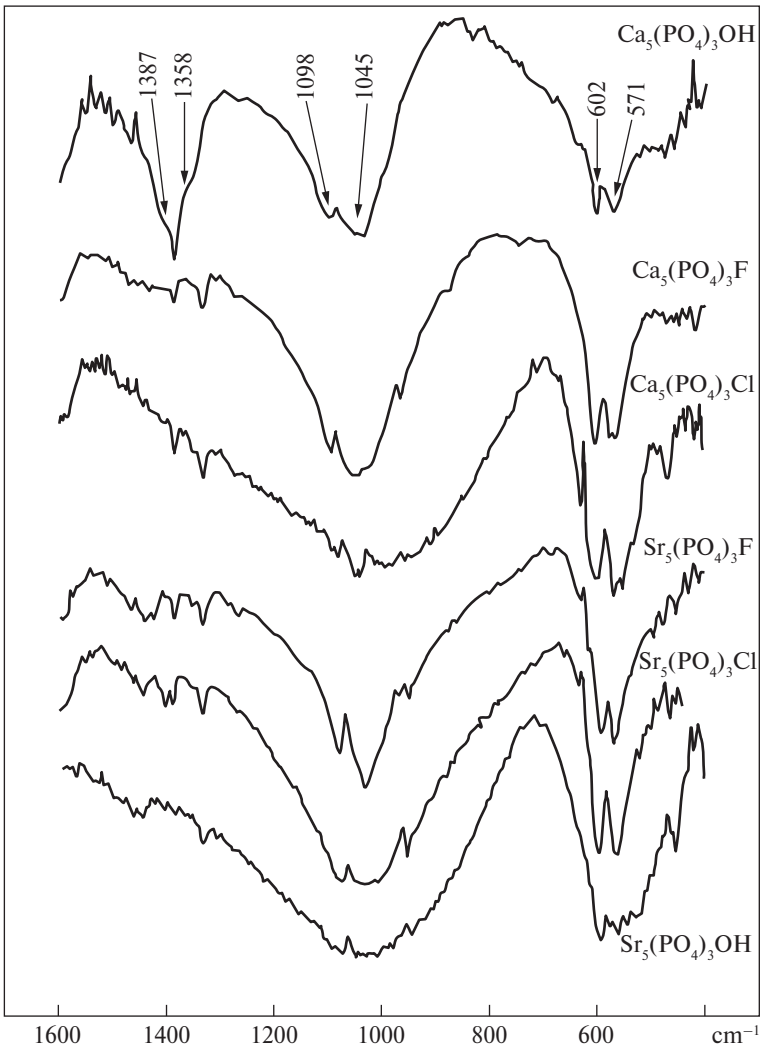

Fig. 4.3. IR-absorption spectra of apatites

to oxygen or to the centre of mass in hydroxyapatite. Hydrogen bond with fluorine (or oxygen) atom located higher or lower on a crystal axis, in a following triangle from atoms of Ca functions as the restoring force that provides a possibility of such vibrations. The frequency of such libration vibration will be the higher, the larger restoring force will be. OH....F bond in apatite is stronger than OH....O bond, therefore the frequency of libration vibrations of OH-groups, connected through hydrogen bond with F atom, should be higher than of those connected with oxygen atoms. For valence vibrations there should be an inverse relationship. The frequency of valence vibrations of hydroxyl in the case of OH....F bond should be lower, than in the case of OH….O, because the

frequency of valence vibrations of OH-groups depends on the binding strength inside of OH-ion, decreasing with the increase in the hydrogen bond strength.

According to Eliot's data [226], 3545 cm^- band appears starting from the fluorine content of 0.2% per cell unit. This absorption band was found in a tooth enamel spectrum. These results indicate that getting into apatite's structure, fluorine ions prefer the presence of hydroxyl ions as the nearest neighborhood, because otherwise no appreciable "perturbation" of hydroxyl groups could be observed by low fluorine content.

It is not excluded that the absence of hydrogen bond along the hexagonal axis in carbonate-containing apatite minerals is one of the causes of their microcrystallity. Sintering of such samples leads to a OH....F bond formation and enlargement of separate crystallites is always observed.

Reling on the OH....F bond existence it seems possible to explain the mechanism fluorine activity against caries, the most widespread disease of tooth enamel.

The possibility of ion diffusion along the hexagonal axis of apatite's crystal with the preservation of its structure was experimentally proved: in such a way a chlorapatite's monocrystal can be transformed into a hydroxyapatite monocrystal [226]. The presence of fluorine ions, «strengthens/reinforces» hexagonal axis by hydrogen bond with hydroxyl groups, prevents mobility of hydroxyl groups, inhibits ion exchange and reduces apatite solubility. By dispersion of impurity fluorine along crystal axis for essential decrease of apatite solubility very small.

In most of spectra presented on fig. 4.3 long-wave absorption band near 570 cm^- demonstrates clear splitting into two components. This indicates that symmetry of elements of tetrahedral sublattice in real crystalline phosphateapatites is lowered to C_{3v} symmetry, i.e. only three of four bonds are equivalent in PO_4^{3-} anion.

Splitting of a vibration band near 1030 cm^- into two components and occurrence of two new bands in the IR-spectrum near 970 cm^- and ~358 cm^- [221, 226-212]. Thus, the wide band near 1030 cm^- should consist of three components, as is observed in spectra of some crystals, for example, in $Sr_5(PO_4)_3F$ spectra. In certain cases, however, it is not possible to divide absorption in this field into separate components owing to considerable broadening of bands, like for example, in the case of $Ca_5(PO_4)_3Cl$. However the observed broadening is impossible to explain with the simple intensity redistribution of absorption components, as far as both short-wave ν_3 absorption component, and long-wave ν_4 component. The nature of this additional band broadening is not clear. Apparently, it is associated with a size variation and/or with the shape of PO_4^{3-} anion in tetrahedr on sublattice of apatite.

Substitution of OH^- group in crystal phosphate apatite for F^- ion really leads to the reduction of lattice parameter *a* from 9.422 Å to 9.364 Å, leaving parameter *c* almost unchanged. Chlorapatite has a somewhat smaller *c* parameter value (6.783 Å) and larger *a* parameter value (9.634 Å) [226]. Such changes in lattice parameters should influence the distortion of PO_4^{3-} anion. Hence, Cl^- ion in calcium apatite and OH^- ion in strontium apatite show the most intensive distorting action on tetrahedral sublattice.

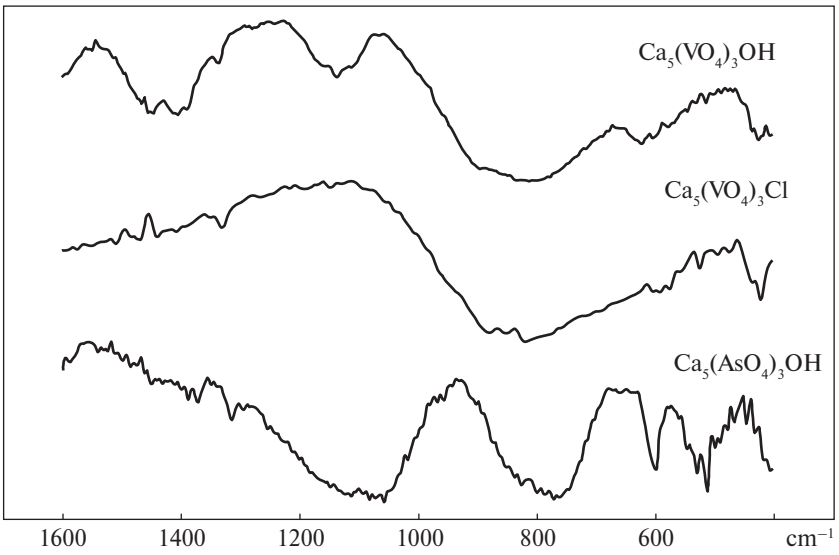

Fig. 4.4. IR-absorption spectra of apatites

Another possible mechanism of broadening of free oscillations of PO_4^{3-} anion is connected with the possibility of change of a tetrahedron volume as a whole ("respiratory" modes) in the crystal field of a lattice. Essentially, the presence of "respiratory" modes is equivalent to the thermal effect in absorption spectra. The more "respiration" degree is, the higher its effective temperature and, hence, the larger its absorption bands broadening. By-turn, volume change of tetrahedrons is limited with the crystal field of a lattice that can explain the influence of anion substitutions on the values of half-width of absorption vibration bands.

Thus, the influence of anion substitution in apatite structure on the spectra of IR-absorption, apparently, adds up to a change of the amplitude of vibrations of tetrahedrons as a whole that makes the contribution to the change of absorption band half-width.

$Ca_5(PO_4)_3Cl$ and $Sr_5(PO_4)_3Cl$ have almost identical spectrum structure, with the difference that bands in $Ca_5(PO_4)_3Cl$ spectrum are a little more widened, than in $Sr_5(PO_4)_3Cl$ spectrum possibly meaning that $Ca_5(PO_4)_3Cl$ structure is more "loose". In addition, spectra similarity means that frequency range of $1600 \div 400$ cm^- does not include the bands related to Ca^{2+} and Sr^{2+} ion oscillations. As might be expected, the bands related to these heavy ions, should be in more long-wave area, below 400 cm^-.

There is a sharply distinctive feature of $Ca_5(VO_4)_3OH$ spectrum (fig. 4.4), namely 1400 cm^- band, which is virtually absent in spectra of calcium hydroxoarsenate and chlorovanadate. As it was mentioned above, this band is connected with vibrations of OH-groups by overlapping of hydrogen bonds. Valence vibrations of these groups are observed in the form of absorption tail in the short-wave spectral range of $3000 \div 3400$ cm^-. $Ca_5(VO_4)_3OH$ spectrum has its own features distinguishing it

from the spectra of calcium hydroxyapatites [227]. First, the specified1400 см$^{-}$ band is strongly widened, and can be obviously presented in the form of superposition of several bands. Secondly, the basic absorption observed in Ca-HAP in a range of 1100 ÷ 1000 cm^{-}, shifted to 800 cm^{-} for $Ca_5(VO_4)_3OH$ and also splits to several bands. This result confirms that absorption in the range of 1100—1000 cm^{-} is related to vibrations of PO_4-groups, and substitution of P atoms for V atoms results in changes of the lattice structure (reduction of the lattice symmetry). When proceeding to $Ca_5(VO_4)_3Cl$ there is a limited effect on the spectrum, abstracting from the absence of the band connected with OH-group vibrations (~1400 cm^{-}).

Thus, the symmetry of XO_4^{3-} anion oscillations in the crystal lattice of apatite depends not only on the symmetry of its local environment, but also in a great measure on the nature of X-O chemical bonds within the anion. The effect of X-anion (OH, F, Cl) substitution along the *c* axis in an apatite structure on IR-absorption spectra adds up to the amplitude change of collective vibrations of tetrahedrons that contributes to the change of absorption band half-width. Cl^- ion has the greatest effect on tetrahedral sublattice in calcium apatite, and OH^- ion in strontium apatite, respectively. Tetrahedrons symmetry in strontium fluorapatite is higher in comparison with hydroxy- and chlorapatite.

4.2. Electronic structure of apatites

The electronic structure of apatites was investigated by X-ray spectroscopy, X-ray emission spectroscopy and quantum-mechanical calculations.

4.2.1. Hydroxyapatites of calcium and strontium

An advantage of X-ray emission spectroscopy is the possibility of getting the information about energy states across a valence band width. In addition, the accounting of rules of selection allows analyzing the energy distribution of electrons with different symmetry in a valence band, and thereby to judge the character of a chemical bond in solid bodies.

The features of electronic structure of calcium and strontium hydroxyapatite are considered on the basis of the analysis of X-ray spectra matched in a unified energy scale using the standard technique [228—230]. X-ray photoelectron spectra of a valence band for the given compounds are not analyzed in view of their low informativity because of low photoionization cross-section. Superposition was carried out taking into account the binding energy of spanning levels (table 4.3).

Spatial orientation of PO_4-groups causes more complex form of valence bands of calcium in Ca-HAP when compared with $CaCO_3$, where CO_3-group has planar orientation [231]. The form of calcium *K*-spectra (see fig. 4.5), in oxide and carbonate, is basically determined by two features. The main *A* maximum, which is formed by *d*- and

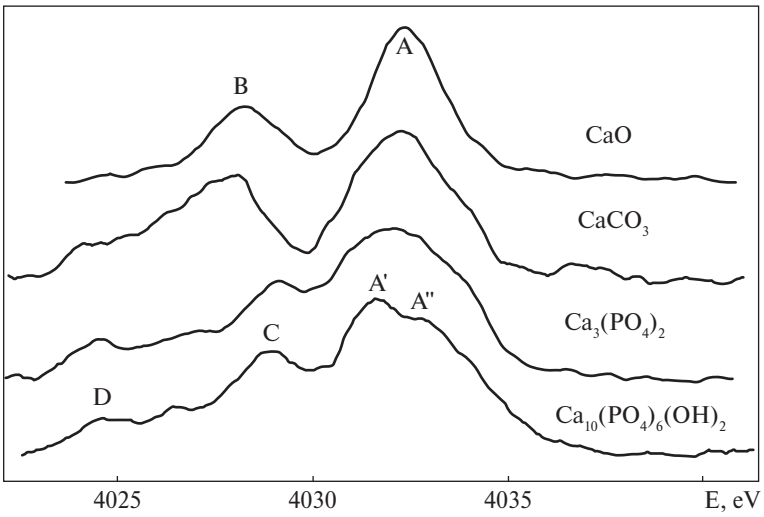

Fig. 4.5. Ca K_{β}-bands in the compounds

p-states of calcium and low-energy B maximum, connected with *p*-states of oxygen and carbon. Changing to the compounds containing phosphate groups, leads to reorganization of electronic *K*-spectrum of calcium, caused, basically, by different spatial orientation of CO_3^{2} and PO_4^{3-}-groups, though, in both cases calcium keeps an oxygen environment.

It is known (chapter 1), that in apatite structure there are two nonequivalent crystallographic points for calcium, namely — $Ca_{(1)}$ (Ca in a column) at z=0 and z=1/2, and $Ca_{(2)}$ (calcium screw axis) at z=1/4 and z=¾ exist. Each $Ca_{(1)}$ ion is surrounded with 9 oxygen atoms of $6PO_4$-groups and together with its environment forms coordination CaO_9 complexes, and $Ca_{(2)}$ ion is surrounded with 7 oxygen atoms of $5PO_4$-groups and 1 oxygen atom of OH group, and forms $CaO_6(OH)$ complex.

Proceeding from the fact that the form of calcium $K_{\beta 5}$-spectra for TCP and Ca-HAP (fig. 4.5) has minor differences, it is possible to conclude that oxygen of hydroxyl groups poorly influences the form of calcium $K_{\beta 5}$-band in Ca-HAP. The observable splitting (*A* ` and *A* ` `) of the main maximum of calcium *K*-band in hydroxyapatites in comparison with tricalcium phosphate (fig. 4.5) seem to be connected with the existence of two various structural positions of calcium, different by ligand environment.

Calcium *K*-spectra for the given compounds show their basic difference and at the same time calcium L_{α}-bands keep considerable similarity among investigated substances (fig. 4.19; 4.16) that possibly indicates that calcium 3*d*-shell has spanning character and almost poorly participates in a chemical bond [231].

Considering the absence of *d*-shell in calcium atom in unexcited condition, it may be assumed that *s*-states having considerable extension in space that can provide metal-metal (M-M) interaction play a significant part in the formation of calcium L_{α}-spectrum [232]. Just because of promotion of electrons into *d*-shell calcium possesses

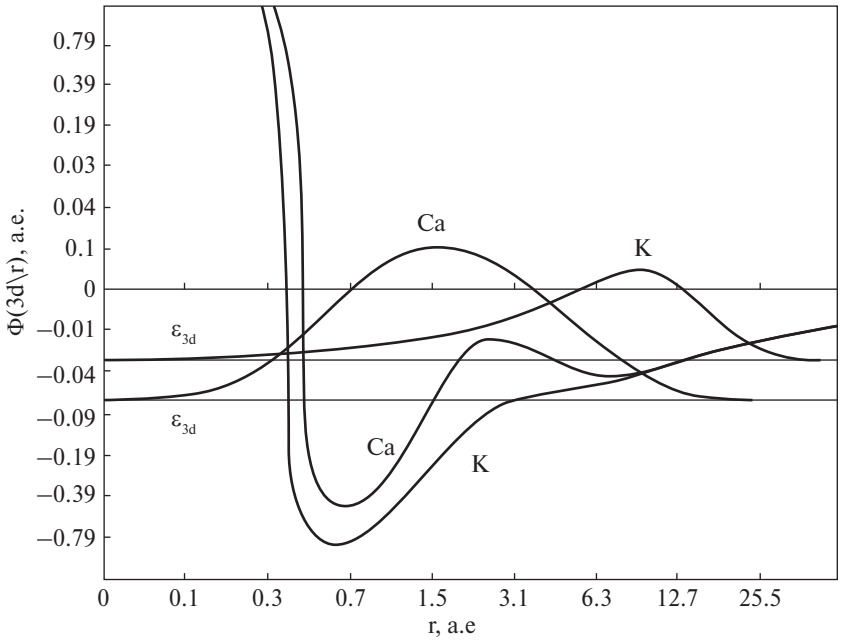

Fig. 4.6. Ca $L_{2,3}$-spectra of a quantum efficiency/yield of photoemission

metal properties whereas magnesium which belongs to the same group can also be in a gaseous state under normal conditions [233].

Spanning character of d-shell of calcium was the object of investigation in works [234, 235] and could be explained with centrifugal potential within the atomic sphere of calcium. In the case of its filling, 3*d*-electron can be localized both in an internal part of atom, and in an external valley of effective potential. Atomic and solid-state effects in absorption spectra of calcium for metal calcium and simple compounds are discussed in work [236].

Insufficient systematization of the data on the phenomenon of electrons wave function collapse in atoms is one of the reasons why it is still a lack of information and is not always taken into consideration by studying of X-ray spectra of atoms. Though this phenomenon takes place only in the case of some elements when the atom configuration contains excited electron with $l \geq 2$ or for the rather narrow interval of near-threshold energies, however in these cases it can lead to considerable effects and influence on various characteristics of atoms.

It is known [235] that the collapse of electron occurs in the case of an element which in a periodic table precedes an element containing this electron in a normal configuration of atom. Calcium, preceding scandium which has *d*-electron in a normal configuration, is an element with a possible collapse of *d*-electron in the crystal lattice.

For *d*-electron of calcium (fig. 4.7) the minimum of an external well of effective potential is nearby 6 a.u., and the collapse of its wave function leads to small changes of average distance and electron binding energy.

By the collapse of *d*-electron overlapping of radial wave function of 3*d* electron with the function of 3*p*-electron. This leads to the increase of electrostatic interaction between these electron shells. Hence, the collapse of *d*-electron in the isoelectronic sequence $3p^5$ 3*d* leads to the increase of the role of an electrostatic interaction in comparison with a spin-orbital one.

The comparison of L_α-spectra of calcium in compounds (fig. 4.19) and of $L_{2,3}$-spectra of quantum efficiency/yield of photoemission (fig. 4.6), that has shown their small change allows to assume that nuclear effects play an important role in the formation of L_α-spectra of calcium and, hence, participation of *d*-states of calcium in the bond is leveled by their considerable localization most likely, in the internal valley of effective potential.

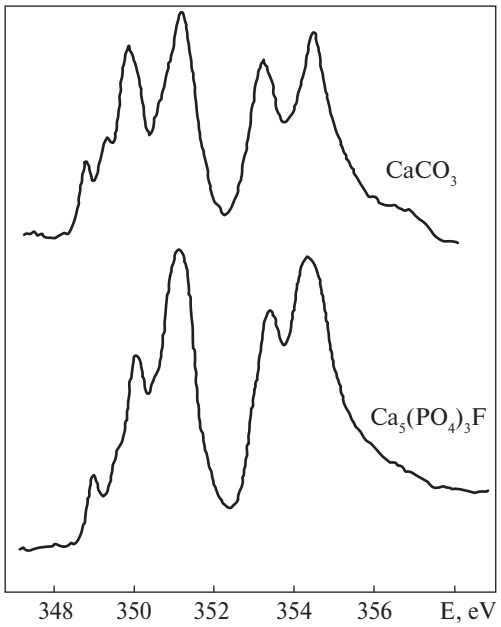

Fig. 4.7. Collapse of 3*d*-electron wave function [235]. Solid line — effective potential, dashed line — radial wave function.

The general mechanism of valence band formation of calcium hydroxyapatite can be clearly seen on fig. 4.8, 4.9. The shape of the main maximum of calcium *K*-spectra is determined, in general, by two features. The *D* feature, formed by *d*- and *p*-states of calcium and the short-wave maximum *F* generally related to the occurrence of *p*-states of oxygen and *d*-states of calcium. p-states of oxygen also contribute to the *D* feature of DOS. The *E* feature is formed mainly by hybridization of *p*- and *d*- states of calcium and *p*-states of phosphorus and oxygen. The main F maximum in the DOS is generated by *p*-states of oxygen and valence states of calcium.

The G feature in L_α X-ray absorption spectrum of calcium corresponds to the position of the main maxima of *K*- and *L*- spectra in the metal [236] and, hence, reflects metal-metal interaction that have mainly *s-s* character in Ca-HAP as proved by the absence of this feature in *K* X-ray absorption spectrum of calcium. The average metal-metal distance in apatite corresponds to the spatial position of the external valley of effective potential for *d*-electrons of calcium (fig. 4.7), confirming possibility of such steady interaction.

Since direct interaction between calcium atoms in apatite structure is ruled out by the atomic structure. Such interaction is partially mediated with oxygen atoms (Ca-O-Ca). As it can be seen from fig. 4.9, the features on partial curves of state densities that correspond to *G* peak in the DOS are observed on curves of calcium for both

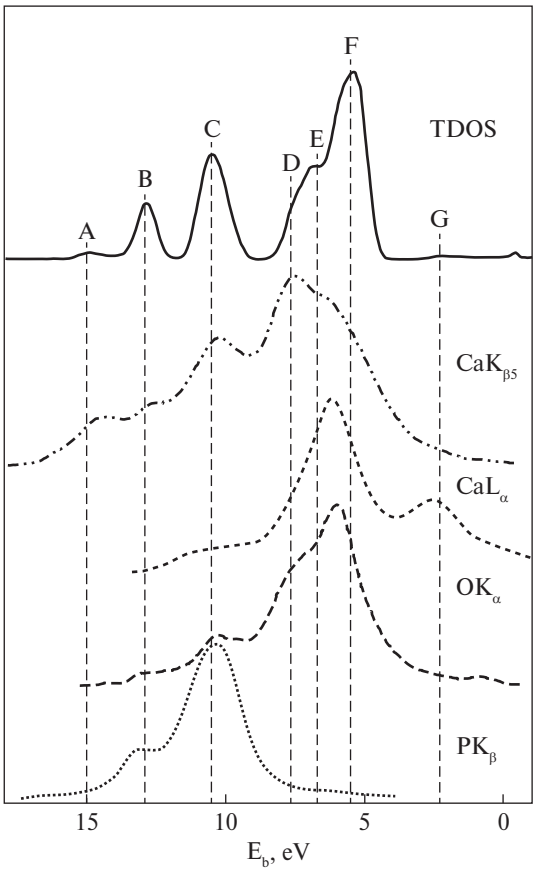

Fig. 4.8. Superposed in a single energy scale X-ray spectra and DOS of HAP (band calculation)

crystallographic positions of calcium ($Ca_{(1)}$(*s*), $Ca_{(2)}$(*s*, *p*, *d*), of oxygen of hydroxyl group (for $O_{(4)}$(*s*) and for $O_{(3)}$(*p*) of the phosphate group. Thus features in $Ca_{(1)}$(*s*) and $O_{(3)}$(*p*) have considerably lower intensity in comparison with $Ca_{(2)}$(*s*, *p*, *d*) and $O_{(4)}$(*s*), may indicate much greater participation of $Ca_{(2)}$ atoms in the bond. Metal-metal interaction with calcium atoms in $Ca_{(1)}$ position, judging by the feature in $O_{(3)}$(*p*), occurs with participation of *p*-density of oxygen of PO_4-group, as opposed to participation of $Ca_{(2)}$ atoms, realized with *s*-density.

Most likely, the interaction between calcium atoms in $Ca_{(1)}$-position is poorly expressed. The presence of the feature on curve of hydrogen *s*-density of in the considered area may indicate that indirect metal-metal interaction occurs with a participation of hydrogen *s*-density. Thus, it is possible to conclude from the above that interaction in the metal sublattice occurs mainly between atoms in $Ca_{(2)}$ positions with a participation of oxygen atoms of hydroxyl group, and at the same time the channel of $Ca_{(2)}$-$O_{(3)}$-$Ca_{(1)}$ interaction through oxygen atoms of PO_4-groups is less pronounced.

$K_{\beta1}$-emission band of phosphorus reflects 3*p*-states of PO_4^{3-}ion. Phosphorus is through one double (saturated) and three single (nonsaturated) bonds with oxygen ions that corresponds to valence 5. Direct P-Ca bond in hydroxyapatite is not present in apatite and binding with calcium ions can be only mediated through oxygen (P-O-Ca). The general feature C (fig. 4.8), observed in Ca K_{β}-, O K_{α}- and P K_{β}-spectra may be evidence of such bond.

Maximums *A* and *B* in the DOS in the range of 12 ÷ 15 eV completely coincide with long-wave features of calcium *K*-bands and are formed with that part of 2*p* electron density of oxygen which takes part in the chemical bond with phosphorus. Two peaks at the bottom of valence band in the range of 20 ÷ 25 eV are formed basically by oxygen *s*- states (fig. 4.9 a).

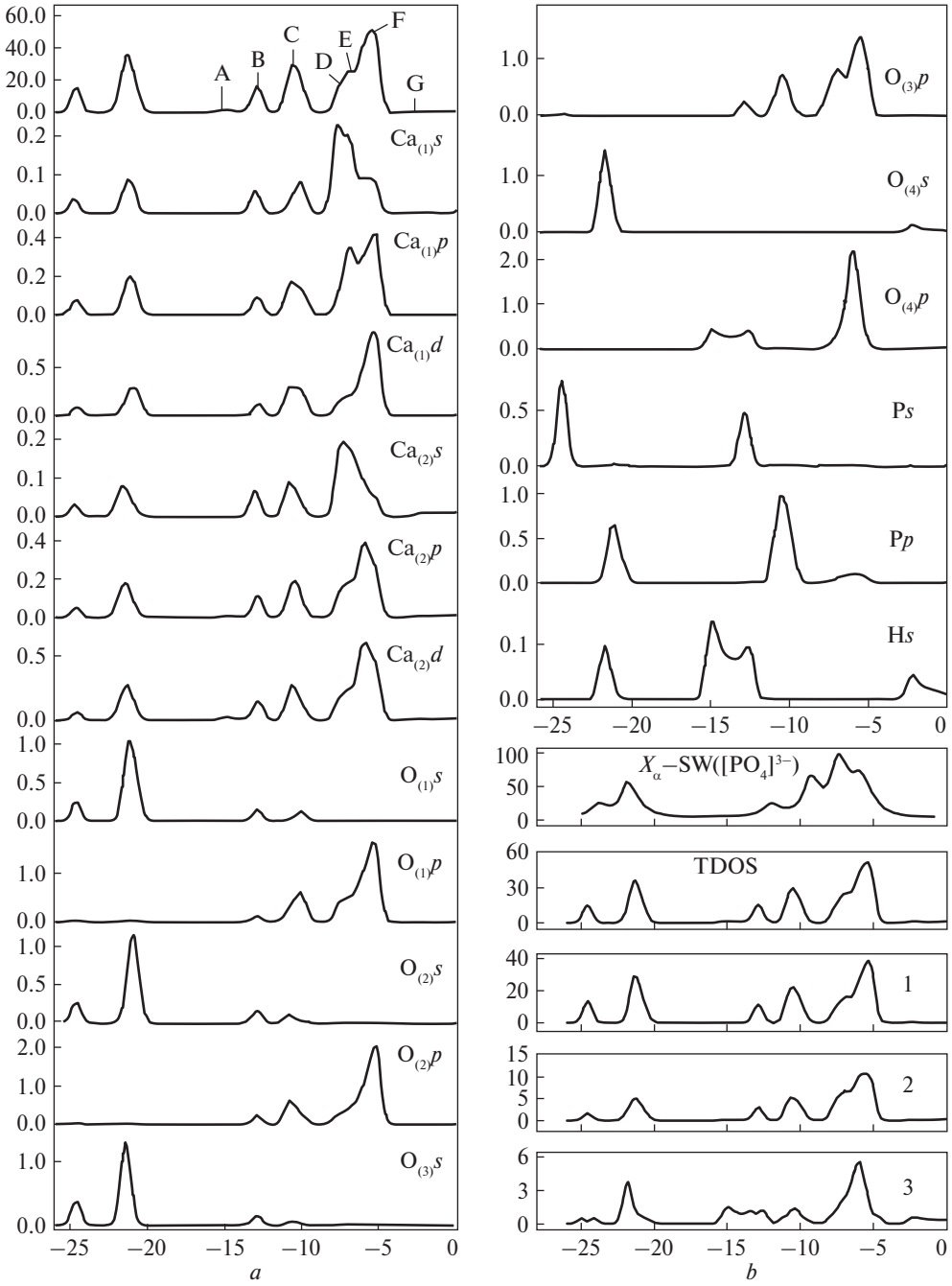

Fig. 4.9. Total and partial density of $Ca_{10}(PO_4)_6(OH)_2$ states(*a*) and density of states of $[PO_4]^{3-}$ cluster and HAP cell (band calculation) (*b*): 1 — the contribution of PO_4-tetrahedrons in the DOS of a crystal; 2 — the contribution of the metal sublattice in the DOS of a crystal; 3 — the contribution hydroxyl groups in the DOS.

Since in experimental spectra of tetrahedron systems it is usually possible to extract the contributions connected with XO_4^{3-} anions (X=V, P), metal atoms and their nearest environment, and hence, the most successful choice of clusters for quantum-chemical calculations in cluster approach are XO_4^{3-} groupings. Oxygen ions are common for metal polyhedra and groupings XO_4^{3-} that enables us to investigate interrelation of their electronic structure using inner states of ligands as an original reference. Thus the structure of the filled conditions of vanadate – and phosphate-ions is well-enough reproduced, however the value of band gap between filled and vacant orbital, as a rule, is considerably larger, than in experiment.

According to the crystallographic data, PO_4^{3-} and VO_4^{3-} ions in the apatite structure differ from the ideal tetrahedrons and at the same time our calculations were applied for undeformed tetrahedrons with T_d symmetry. The influence of structural distortions on the electronic structure of PO_4^{3-} and VO_4^{3-} ions was investigated on three types of XO_4^{3-} clusters with T_d, D_{2d} and C_1 symmetries in works [237, 238].

XO_4^{3-} distortions mainly influence only on spatially delocalized states that allows to use the results of calculations of ideal tetrahedron groupings for apatite-like structures.

Comparative investigation of the calculation data for the filled part of a valence band of $[PO_4]^{3-}$ cluster — X_α-SW cluster calculation and DOS of Ca-HAP cell – band LMTO calculation have revealed general tendencies in the formation of structure of a valence band. There are observed almost identical mechanisms of formation of features of a valence band of cluster and crystal, both in the field of a bottom of a valence band and in its middle part (fig. 4.9 b). The identical quantity of the basic features on the curves of DOS for cluster and crystal, except the feature at 15 eV, determined with the presence of hydroxyl group was also observed. The insignificant differences of energy positions of features of a valence band of cluster and crystal near valence band top may be connected with peculiarities of cluster calculation method. Hence, the sublattice of oxygen tetrahedrons determines the form defining in formation of the shape and the main features of full density of electron states of calcium and strontium apatites.

Whereas the energy position of hybridized *s*- and *p*-states of OH^- (hydroxyl) cannot be uniquely determined with X-ray emission spectra data, contributions in DOS of sublattices of PO_4, calcium and hydroxyl groups have been estimated. As it can be seen from fig. 4.9 b, partial densities of states of tetrahedral matrix ofoxygen make the largest contribution in DOS.

When comparing the obtained data to the results of work [231], where a variety of features was found in low-energy range of O K_α-, P K_β- and Ca K_β- bands for ultra-dispersed samples, it is possible to conclude that it was structure changes connected with position of OH-groups that determined those features.

Calcium substitution for strontium in calcium hydroxyapatite essentially changes the form of DOS of a crystal (fig. 4.10, 4.11). There is splitting of peaks both at

the valence band bottom, and at the valence band top observed that as it has already been shown, possibly is connected with symmetry reduction of tetrahedrons, because of increase in the size of metal atoms and change of lattice parameters.

On fig. 4.10 the X-ray spectra of strontium hydroxyapatite and DOS-zonal calculation superposed in the single energy scale are shown. The *B* feature corresponding to the main maximum/peak in the DOS curve is formed basically by valence states of oxygen and strontium, without participation of valence states of phosphorus, as it can be see from the calculation data (fig. 4.11). The *D* feature is formed by that part of 2*p* electronic density of oxygen which takes part in a chemical bond with phosphorus and mainly reflects phosphorus *p*-states. The *C* feature is connected with a decaying long-wave part of O K_α spectrum and short-wave part of P K_β spectrum.

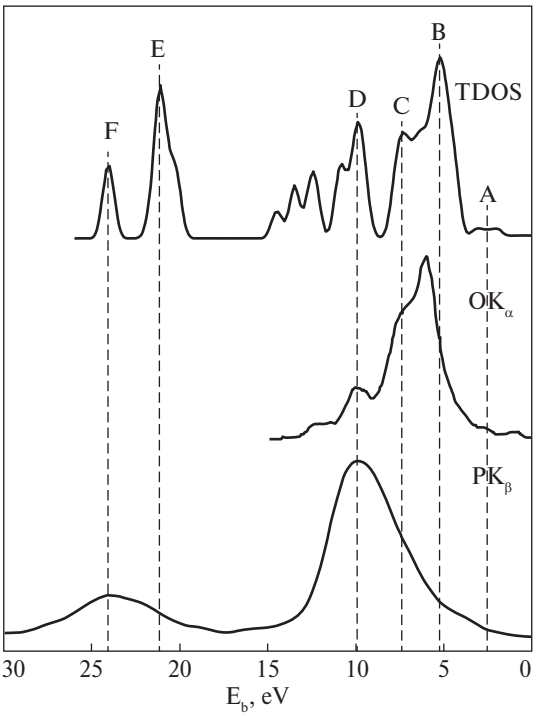

Fig. 4.10. Superposed in a single energy scale X-ray spectra of strontium hydroxyapatite

The emission K_α-band of oxygen consists of three basic parts: long-wave (features *D* and *C*) and the main peak (feature *B*). As the data of X-ray spectral analysis of oxygen-containing organic compounds and alakalis indicates all these structures reflect various orbitals of oxygen of *sp*- or *p*- origin.

Low-intensity *A* feature in the DOS curve reflects the bond of hydroxyl ion with metal atoms (fig. 4.11). The feature in the DOS curve near 2.5 eV is observed only for $O_{(4)}$ *s*, $O_{(4)}$ *p* and H *s* partial densities of electronic conditions. The absence of noticeable features in partial density curves of metals may indicate that indirect metal-metal interaction in Sr-HAP is practically absent [239, 240].

The presence of such interaction in calcium hydroxyapatite is probably determined by the incipient *d*-shell with a characteristic dependence of effective potential on distance. From the analysis of characteristics of both X-ray spectra and calculation data of calcium and strontium hydroxyapatite it is possible to conclude that in Sr-HAP the partial contribution of H *s*-states in DOS considerably increases. At the same time the main maximum of H *s*-density in Ca-HAP is near 15 eV, whereas in Sr-HAP near 22 eV. Band splitting at 15 eV in Ca-HAP may indicate a difficult

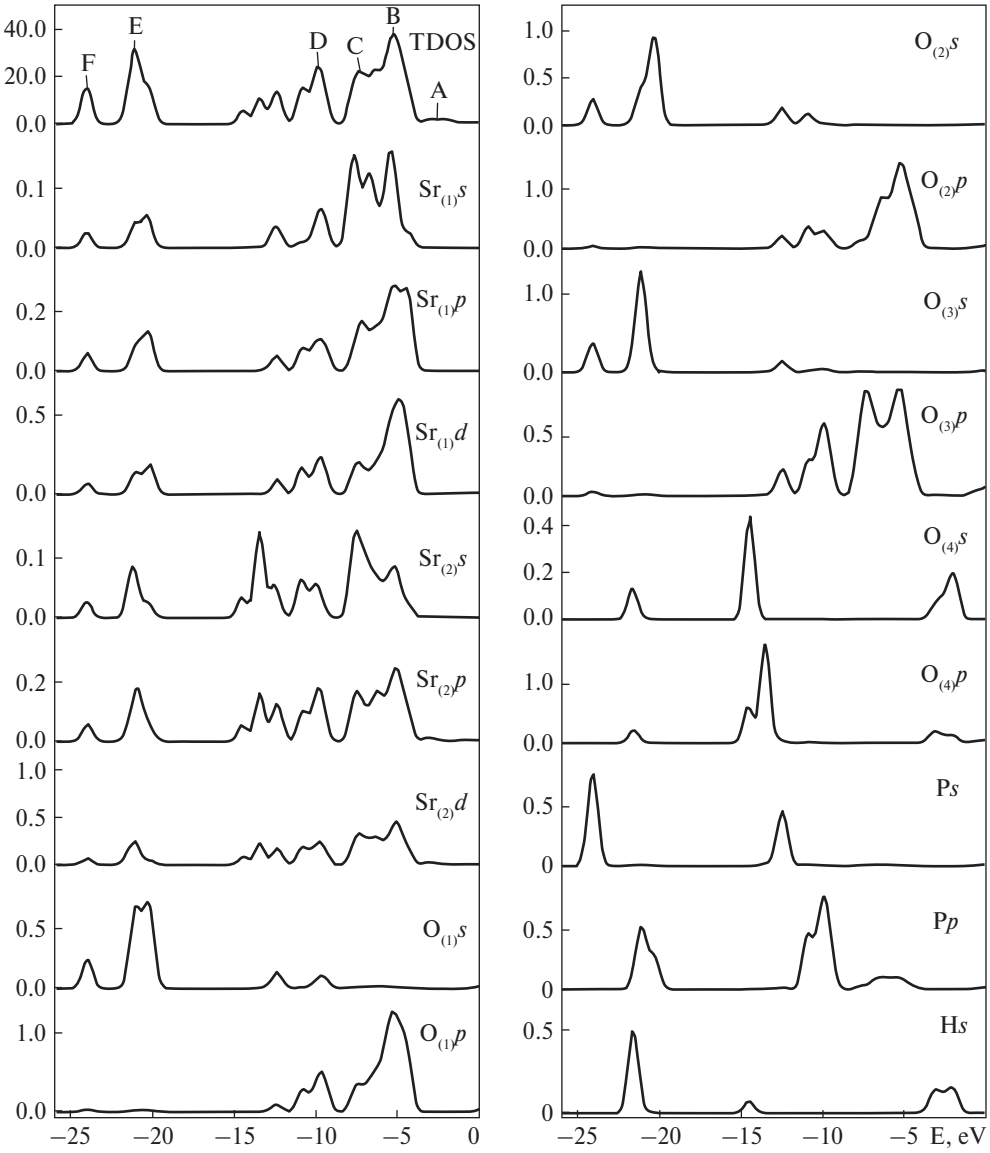

Fig. 4.11. Total and partial density of states of $Sr_{10}(PO_4)_6(OH)_2$

mechanism of hydrogen *s*-density hybridization with c $Ca_{(2)}$ *p* and $Ca_{(2)}$ *d* densities through $O_{(4)}$ *p* conditions. There is one peak of Sr-HAP with intensity lower than for Ca-HAP in this range of H *s* density. The feature near 2.5 eV in the curve of hydrogen *s*-density has more difficult structure for Sr-HAP consisting of two peaks generated, as it was mentioned above, by electronic density of atoms of hydroxyl $O_{(4)}$ (*s*, *p*)-conditions.

Most likely, the presence of greater spanning electronic density of strontium atoms in a free state in comparison with calcium atoms leads to initiation of *d*-shell of strontium in a crystal is accompanied with larger bond energy, than for calcium (for metal strontium bond energy of *d*-electrons is near 15 eV whereas for calcium is near 5 eV) and, hence, indirect metal-metal interaction in triangles of metal atoms is less expressed for strontium apatite.

The conducted diffused electron scattering spectra investigation of crystalline Ca-HAP, $Ca_5(PO_4)_3F$ and $Ca_5(VO_4)_3OH$ apatites have shown that these spectra almost completely coincide with the etalon reflexion in the area with no material absorption. There was a sharp increase in the absorption of Ca-HAP and $Ca_5(VO_4)_3OH$ samples in the range of 45000 cm^- and 32000 cm^-, respectively. Such character of absorption is apparently caused with zone-zone electron transition. Thus, zone bandwidth is ≈5.59 eV for HAP sample Ca-, and ≈4.05 eV for $Ca_5(VO_4)_3OH$. $Ca_5(PO_4)_3F$ sample absorption in the investigated measurement range is not detected, so, apparently, its band absorption is in more far ultraviolet. Thus, it may concluded that the investigated compounds show dielectric properties.

4.2.2. Other apatites of calcium and strontium

There are given of core electron binding energies of atoms of metal strontium, strontium oxide, hydroxy-, fluorine-, and chlorapatites of strontium (tab. 4.2). As it can be seen, by isomorphic substitutions in Sr-HAP binding energies of all levels are changed while linewidth is almost unchanged. OH-group substitution for halogens (F and Cl) leads to the increase of electron binding energies of all atoms. At the same time charge is shifted towards halogen atoms. OH-group substitution for Cl leads to the increases core electron binding energy of strontium for 0.6 eV that is 0.2 eV more than of fluorine apatite. Binding energy of O 1*s* electron increases by 0.3 eV. Binding energy of P 2*s* electrons increases approximately by the same value. The binding energy of Sr 4*p* electrons increases by 0.2 eV. The transition from Sr-HAP to Sr-FAP and Sr-CAP leads to increase in binding energy of O 1*s* level. The change in line half-width of P 2*s* electrons in the investigated compounds correlates with the reduction of symmetry of tetrahedrons in the series fluorapatite→chlorapatite→hydroxyapatite.

Density of electronic states curve of fluorapatite atoms in comparison with hydroxyapatite are characterised with bigger splitting that can be explained with higher symmetry of tetrahedrons for fluorapatite in comparison with hydroxyapatite as it has been noted above. For strontium hydroxyapatite in comparison with fluorapatite the significant IR-band broadening is observed characterising symmetry of tetrahedrons vibrations (fig. 4.3).

The calculated P *s* densities of states practically coincide for both compounds. Splitting of P 2*p* peak for hydroxyapatite occurs because of decrease of symmetry of tetrahedrons that follows from calculation of PO_4^{3-} clusters with different symmetry [237].

The relative increase of partial contribution of F 2*p*-states in comparison with contribution of $O_{(4)}$ *p* states into full density of states for Sr-FAP in comparison with Sr-HAP, may lead to the increase of metal and fluorine atoms bonding and, hence, to the crystal lattice hardening along *c* axis. An evidence of this can be relative increase of contribution of Sr *p*-states to fluorapatite DOS. It is confirmed with mineral composition of tooth enamel that is about 97% fluorapatite [1].

Relative prevalence of the contribution of $O_{(3)}$ *p* states to the full density of states in fluorapatite in comparison with hydroxyapatite may indicate that $Me_{(2)}$ position

Table 4.2. **Electron binding energy E_b (eV), linewidth (Γ) (eV) (measured at half height) of core levels of atoms.**

Compound	O 1*s*	P 2*s*	P 2*p*	F 1*s*	Ca 2*s*	Ca $2p_{3/2}$	Ca $2p_{1/2}$
$Ca_5(PO_4)_3OH$	532.4	190.7	133.3	—	439.2	347.5	351.2
$Ca_5(PO_4)_3Cl$	531.7	191.0	133.5	—	439.2	347.6	351.2
$Ca_5(PO_4)_3F$	531.5	191.1	133.6	685.2	439.2	347.5	351.1

Compound	O 1*s*	Sr 3*s*	Sr 3*p*	Sr 4*p*	P 2*s*	Sr $3p_{3/2}$	Sr $3p_{1/2}$	F 1*s*
Sr (metal) [241]	—	356.8 (4.1)	267.7 (2.2)	18.2	—	—	—	—
SrO [241]	528.2 (1.3)	357.2 (3.8)	268.1 (2.5)	18.6	—	—	—	—
$SrCO_3$ [241]	531.5 (1.5)	358.0 (4.2)	269.0 (2.5)	19.5	—	—	—	—
$Sr_5(PO_4)_3OH$	531.1 (2.3)	357.7 (4.0)	269.1 (3.0)	19.5	190.6 (3.0)	269.2	279.4	—
$Sr_5(PO_4)_5F$	531.5 (2.1)	358.1 (4.5)	269.5 (2.8)	19.7	190.9 (3.2)	269.5	280.0	685.3
$Sr_5(PO_4)_3Cl$	531.5 (2.2)	358.3 (4.4)	269.7 (3.0)	19.7	190.8 (3.3)	269.1	280.1	—

Compound	O 1*s*	Ca 2*s*	Ca $2p_{3/2}$	Ca$2p_{1/2}$	V 2*p*	As $3p_{1/2}$	As $3p_{3/2}$
$Ca_5(VO_4)_3OH$	530.4	438.7	346.8	350.5	517.3		
$Ca_5(VO_4)_3Cl$	530.1	438.8	347.0	350.5	517.2		
$Ca_3(VO_4)_2$	529.7	438.6	346.7	350.2	516.9		
$Ca_5(AsO_4)_3OH$	531.0	439.0	347.1	350.8		148.7	143.8

E_b values are given relative to E_b (C1*s*)=285.0 eV.

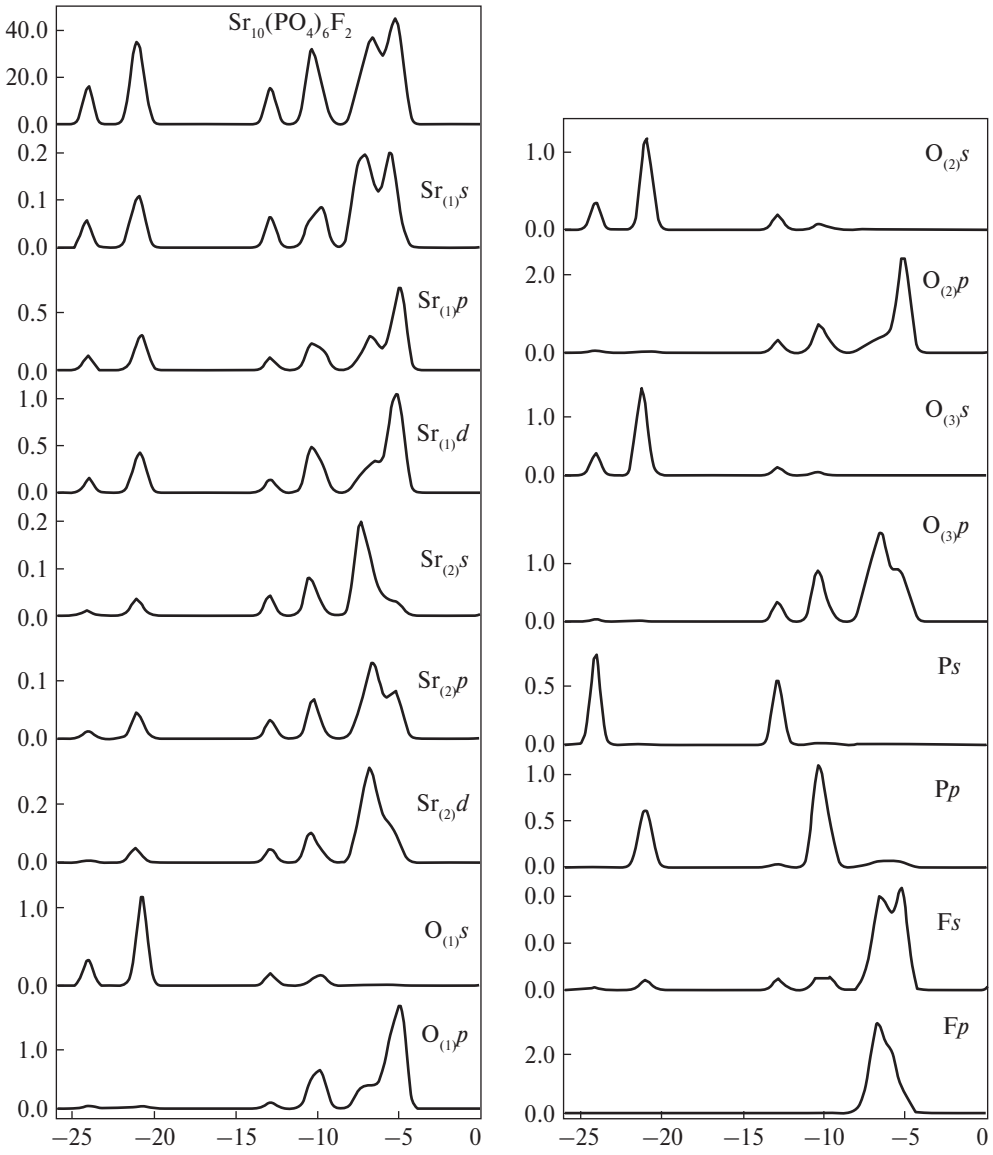

Fig. 4.12. Total and partial DOS of $Sr_{10}(PO_4)_6F_2$

for fluorapatite is more preferred at isomorphic substitution in comparison with hydroxyapatite.

The obtained Sr $L_{\beta 3,4}$-spectra (fig. 4.13) have shown that the degree of charge transfer from strontium decreases in the series Sr-FAP, Sr-HAP, SrO. Both interdoublet distance, and position of maximums change. XPS analysis of the given HAP samples with isomorphic substitution of OH anions for F and Cl anions has shown

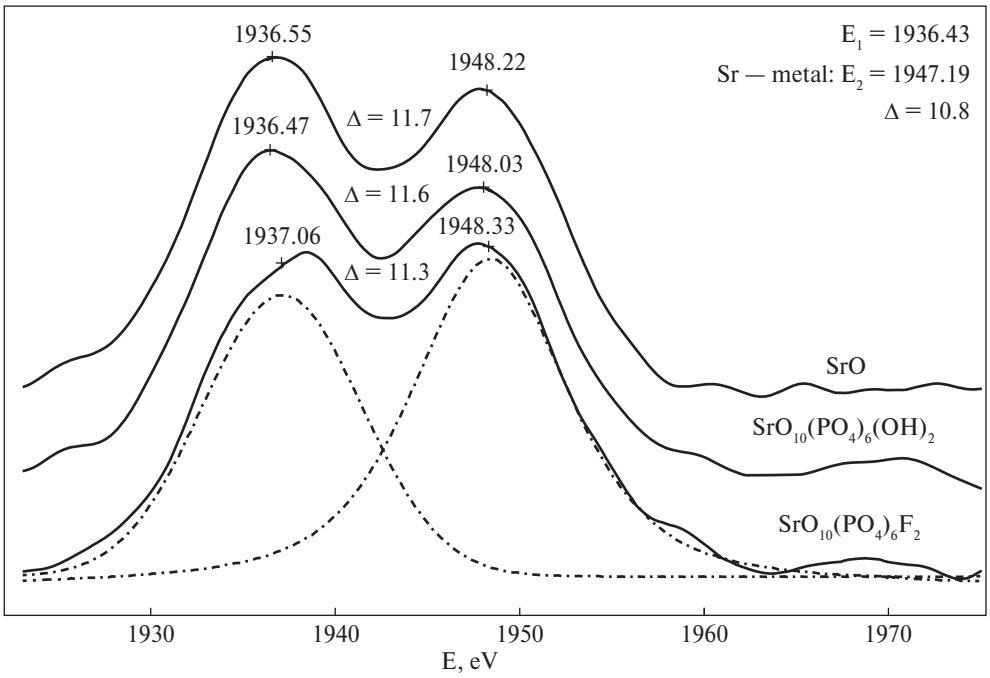

Fig. 4.13. Strontium $L_{\beta 3,4}$-lines

that such substitution leads to appreciable changes in the oxygen environment of strontium and phosphorus atoms. It appears in the binding energy increase of 1*s* electrons of oxygen atoms by 0.3 eV and in the binding energy increase of 2*s* and 2*p* strontium electrons. It has been established that the binding energy of $2p_{3/2}$ electrons of strontium atoms in Sr-HAP is close to the binding energy of Sr $2p_{3/2}$ electrons in $SrCO_3$, by different binding energies of O 1*s* electrons.

The obtained O K_α-spectra in apatites (fig. 4.14) are notable for almost full coincidence of shape of the spectra, confirming their independence on the symmetry of tetrahedrons and the anion type on *c* axis. There is observed a shift of their centres of gravity which is within the experimental error (fig. 4.14) indicating the electron density redistribution while preserving the nature of the chemical bond. It should be noted that significant changes in the topology of tetrahedrons observed in the IR-experiment, do not influence the position of core lines of elements that indicates the charging condition of ions practically remains.

The analysis of positions of the centres of gravity of O K_α—spectra in Ca-HAP, Ca-FAP and Ca-ClAP (fig. 4.15) — has shown its monotonous reduction in the investigated series that indicates the increase of effective charge of oxygen atoms. It is interesting that the change of energy position of the centres of gravity of O K_α-line and 1*s* level for calcium apatites correlates with the change of IR-absorption bandwidth characterising PO_4 tetrahedrons. Thus, taking into account

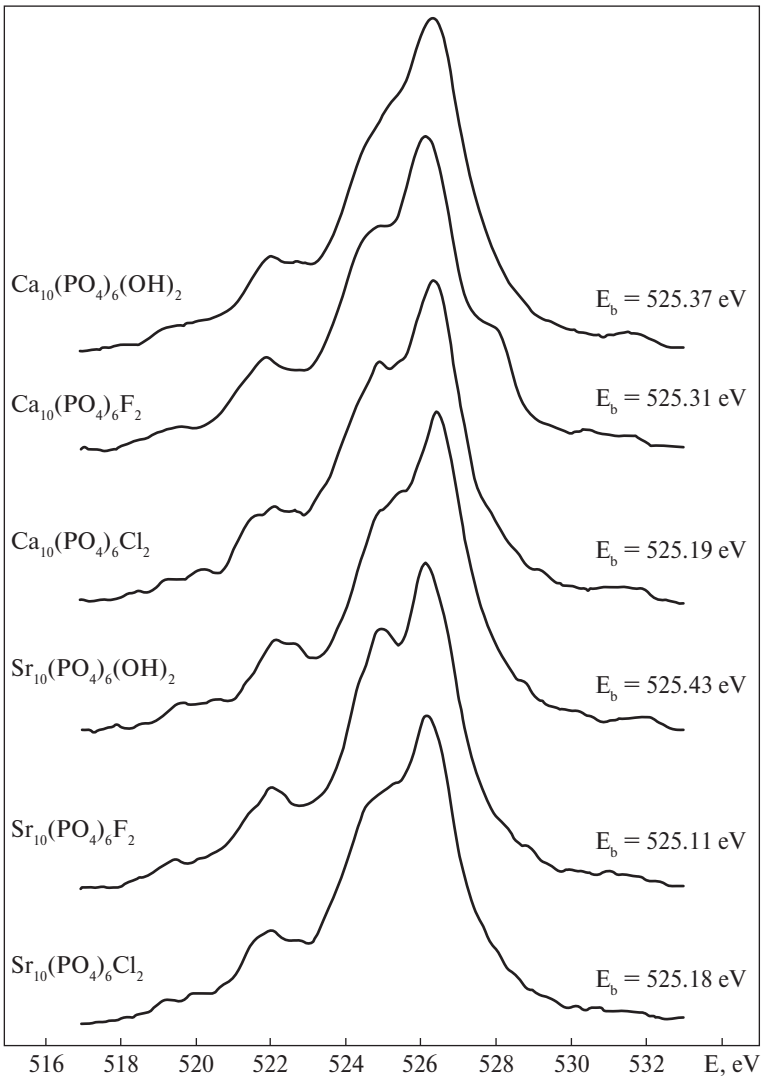

Fig. 4.14. Oxygen O K_α- X-ray spectra in the apatites

XPS data it is possible to assume that the increase of symmetry of oxygen tetrahedrons is accompanied with the reduction of electron density on oxygen atoms in the investigated series.

The comparison of XPS data on the change of binding energy of O 1*s* level among calcium apatites with changes in the binding energy of P 2*s* and P 2*p* levels allows to conclude that there is a charge redistribution between oxygen and phosphorus atoms (tab. 4.2). The obtained data correlates with IR bandwidth of tetrahedrons and taking into account that metal levels (Ca 2*s*, Ca 2*p* — tab. 4.2) in the given series practi-

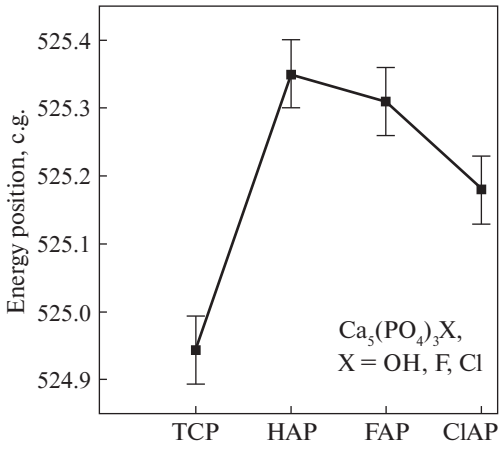

Fig. 4.15. Energy position of the centres of gravity of O K_α-spectra

cally do not changes, it is possible to conclude that charge redistribution by OH ion substitution for F and Cl ions occurs mainly within the limits of tetrahedral lattice, accompanied with simultaneous crystal lattice volume increase in the series F→OH→Cl.

The investigation of a similar series of strontium apatites for O 1*s*-level shows slightly different dependences, namely, by transition from Sr-HAP to Sr-FAP and Sr-ClAP the increase in binding energy of 1*s* oxygen core level is observed. The interesting fact is that unlike the calcium apatites for the strontium apatites the monotonous increase of bonding strength of strontium core levels in the series Sr-HAP, Sr-ClAP, Sr-FAP is characteristic. Such changes testify indicate that in strontic apatites the participation of metal atoms into redistribution of electron density is observed. XPS data on the investigated series of strontium apatites coordinate with the results of IR-study which have shown the increase of symmetry of tetrahedrons in the series F→Cl→OH for strontium apatites, and X-ray emission and absorption spectroscopy which indicate the monotonous energy decrement of *K*-edge of strontium absorption in investigated series (tab. 4.3) that indicates the electron density increase on strontium atoms.

The comparison of quantum mechanical calculations Ca-HAP, Ca-ClAP, Ca-FAP and Sr-HAP, Sr-ClAP, Sr-FAP (pic. 4.16) reveals small changes of the shape of DOS curve.

The transition from Ca-HAP to Ca-ClAP does not influence states near valence zone bottom. The changes occurring in the valence band top are insignificant excepting the main maximum with the additional feature occurring in the high-energy part. Transition to Ca-FAP increases splitting of the main maximum, the splitting of a *D* feature near the valence zone bottom is also observed. However, as it can be seen from fig. 4.16, all main/general features of curves completely remain.

Table 4.3. **Strontium K-edge absorption energies in compounds.**

Sample	E_{edge}, eV	Shift, eV
SrO	16143.9	0.00
$Sr_5(PO_4)_3F$	16143.5	–0.40
$Sr_5(PO_4)_3Cl$	16143.5	–0.40
$Sr_5(PO_4)_3OH$	16141.8	–2.10

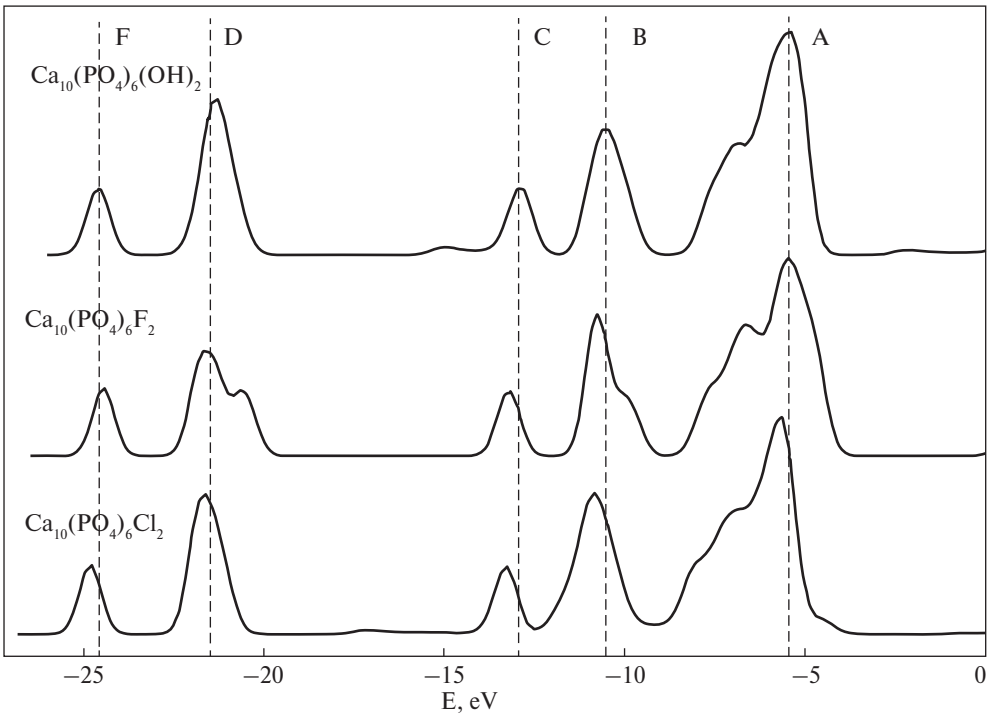

Fig. 4.16. DOS of compounds

Thus, it is possible to assert that the electronic structure of apatite is insensitive to the anion type on *c* axis until their removal that appears in the structure liability concerning this position.

The observed changes are connected, mainly, with the change of Ca *s* and $O_{(3)}$ *p* density and, apparently, are connected with the topology of PO_4 tetrahedrons, as it has been shown before .

The conducted quantum-mechanical calculations in zon approximation of crystal cells of calcium apatites (Ca-HAP, Ca-ClAP and Ca-FAP) without OH^-, F^-, Cl^- ions in their crystallographic positions also have shown small changes in the electron structure of crystals that also confirms small sensitivity of an electron structure of apatite to the type of anion in the *c* axis.

For a more complete description of the electron state of oxygen atoms of tetrahedrons we applied a procedure of decomposition of O 1*s*-level curves to components. It is known that there are three ordinary and one double bond of oxygen with phosphorus in tetrahedron. Considering this the experimental O 1*s* level curve was decomposed into two components with the intensity ratio of 1:3.

As can be seen from fig. 4.17 by transition from Ca-HAP to Ca-FAP the position of components within the limits of error does not change; there is only a minor

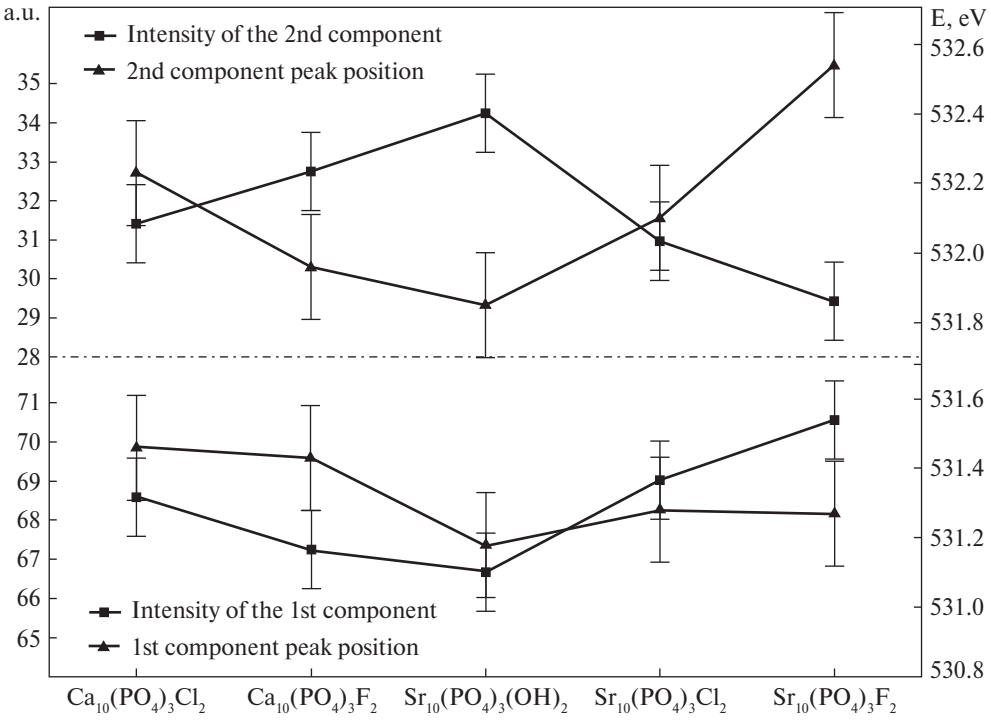

Fig. 4.17. The data on O 1s spectrum decomposition into components

changing of their intensity. Hence, the change of tetrahedron symmetry by transition from Ca-FAP to Ca-ClAP does not disturb the energy balance of the oxygen tetrahedron.

As it is seen from the given figure the intensity redistribution between components and their position in the strontium apatites undergo more essential changes. A monotonous reduction of the second component intensity with the increase of the first component intensity in the series hydroxo-, chloro-, fluorapatite is observed. At the same time energy position of the second component monotonously increases the position of the first component remains within the limits of error.

Hence, the increase in the tetrahedron symmetry which is observed in IR-spectra of strontium fluorapatite is accompanied with a reduction of a part of multiple bond in the tetrahedron by simultaneous increase of bond energy of oxygen 1*s* level of double bond.

The comparison of F K_α-spectra in CaF_2, Ca-FAP and Sr-FAP (fig. 4.18) shows the absence of the short-wave feature in F K_α-spectrum of Sr-FAP that indicates probably much weaker chemical bond between metal and fluorine atoms. This conclusion is confirmed by comparing of band LMTO-calculations of calcium and strontium fluorapatites (fig. 4.12). It is evident that the relative partial contribution of F *p*-conditions

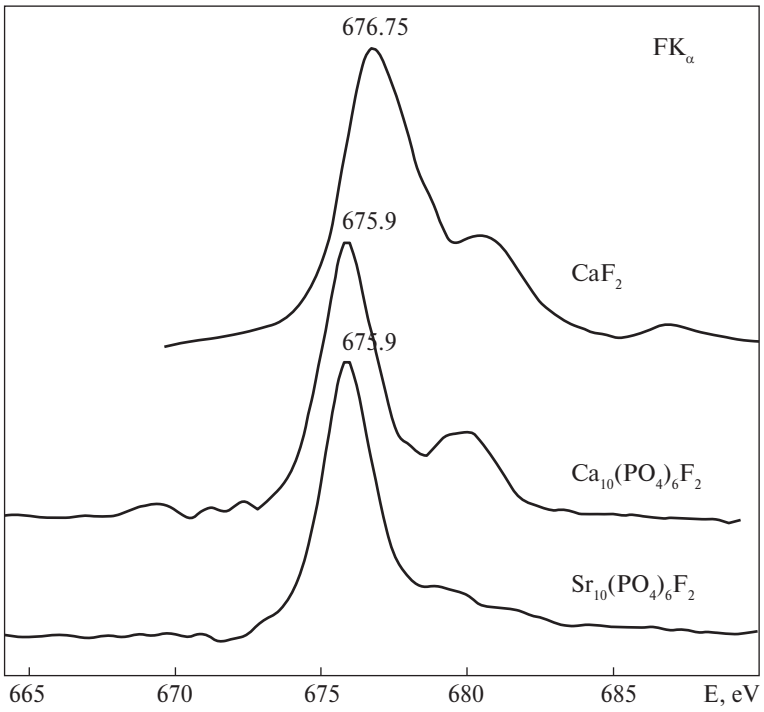

Fig. 4.18. F K$_\alpha$ X-ray spectra in compounds

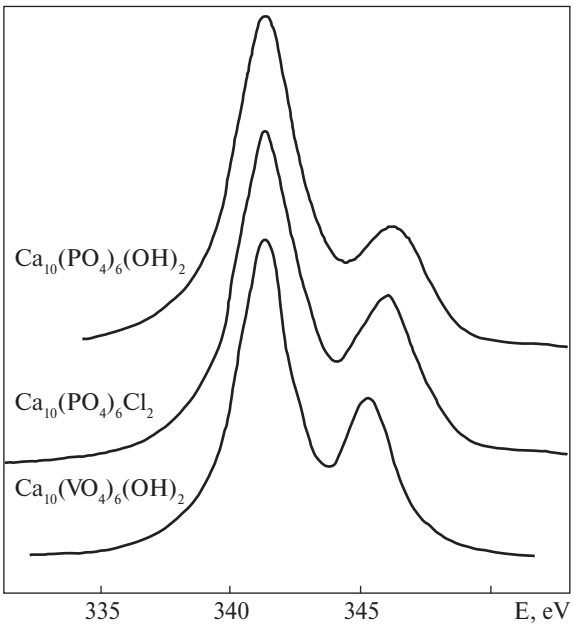

Fig. 4.19. Ca L$_\alpha$-bands

in DOS is approximately 2 times larger in Ca-FAP when compared with Sr-FAP. Herewith a considerable reduction of energy of F *p*-conditions for Sr-FAP (from ~5 eV up to 7 eV) is observed. The observed divergence in a character of the chemical bond should be confirmed with the behaviour of chemical compounds. Thus according to [226] the solubility of Sr-FAP is considerably higher than of Ca-FAP.

Simultaneous study of Ca Lα-spectra (fig. 4.19) of Ca-HAP, Ca-ClAP and $Ca_{10}(VO_4)_6(OH)_2$ shows their almost full coincidence except insignificant reduction of width at half-height for vanadate apatite that according to [242] is possibly connected with the increase of parameters of a the crystal lattice of vanadate apatite.

Quantum mechanical calculations of electron structure have shown that in comparison with Ca-HAP there are two more clearly defined parts in the valence band of calcium hydroxyvanadate. The valence band bottom (from ~17.5 up to ~22.5 eV) is formed by the features which are mainly determined with *s*-states of oxygen of tetrahedrons and vanadium *s*, *p*-states (fig. 4.20).

There are almost no features in the range from ~9.5 up to 17.5 eV in calcium hydroxyvanadate DOS curve. It is interesting that these features in Ca-HAP are observed in curves of $Ca_{(2)}$ *p*- and *d*-states. Thus, it is possible to assume that in hydroxyvanadate the interaction of $Ca_{(2)}$ ions with hydroxyl ions is less expressed. There are observed two separate peaks in the range from 0 up to 9.5 eV for hydroxyvanadate. The peak near 8 eV is formed mainly by *d*-conditions vanadium. The main peak of hydroxyvanadate DOS curve is determined with *s, p, d*-states of Ca and *s, p*-states of vanadium.

The absence of peaks in calcium hydroxyvanadate DOS curve in the range from 9.5 eV up to ~15 eV and their presence in Ca-HAP curve (fig. 4.9) is determined with the occurrence of *d*-electrons in vanadium atoms which have smaller binding energy and thus lead to higher density of states at the valence band top. For Ca-HAP these features are defined by phosphorus *p*-conditions.

The transition from calcium hydroxyvanadate to calcium hydroxyarsenate (fig. 4.22) almost restores the shape of DOS curve typical for Ca-HAP, except some peak splitting and displacement.

As it was mentioned above, a significant symmetry reduction of tetrahedrons is observed for calcium hydroxyarsenate. Such situation should affect a character of a chemical bond and lead to a change of the character of the chemical bond in a tetrahedron. From XPS data it is evident (tab. 4.3) that changing of the charge state of calcium atoms indicates weakening of the bond in the metal sublattice.

Bond energy of O 1*s*-levels and core levels essentially decreases by transition from Ca-HAP to calcium hydroxyvanadate that indicates the increase of electron density for oxygen and calcium atoms. In comparison with Ca-HAP the energy of O 1*s* and Ca core levels in calcium hydroxyarsenate also decreases, however, much less than in hydroxyvanadate.

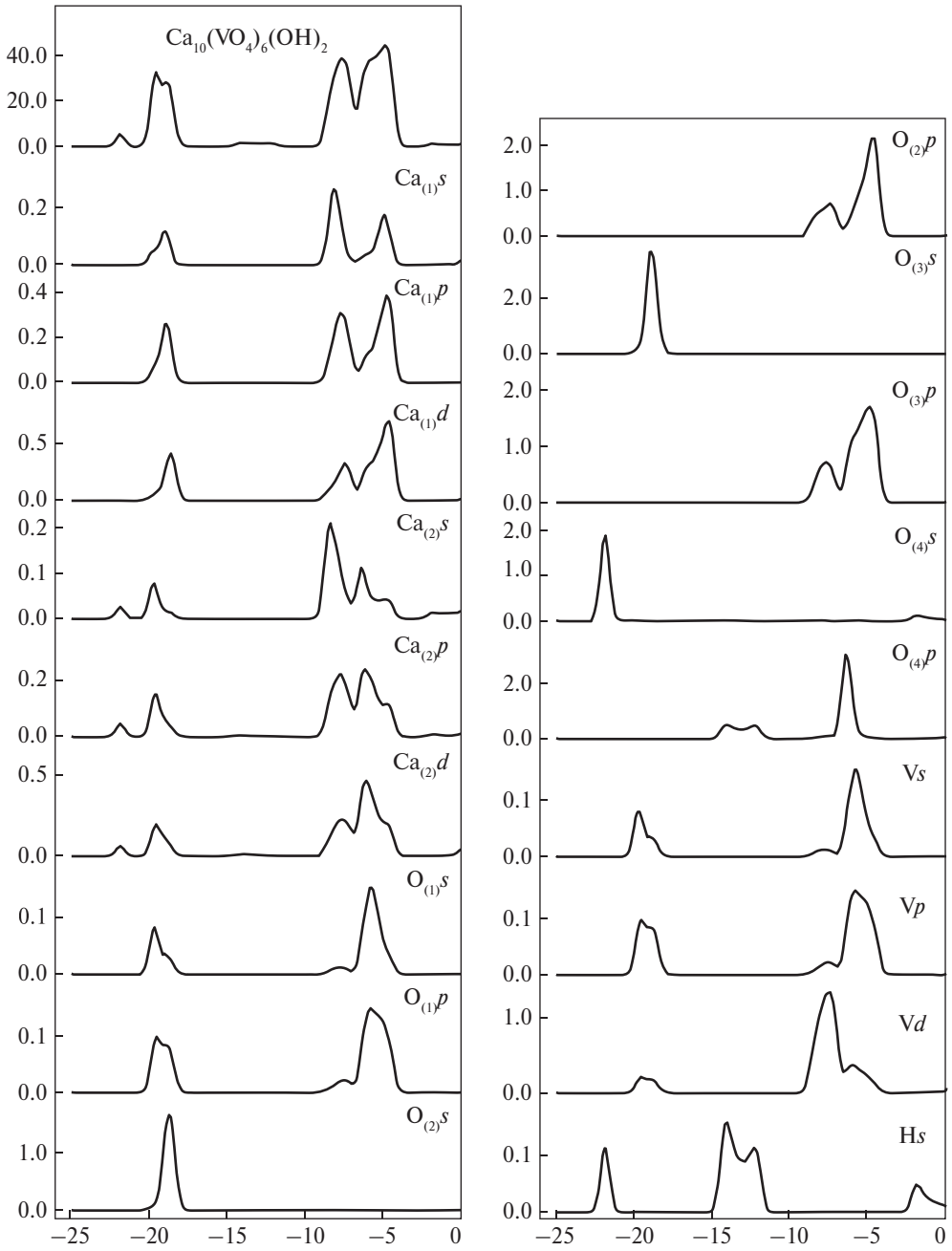

Fig. 4.20. Total and partial densities of states of $Ca_{10}(VO_4)_6(OH)_2$

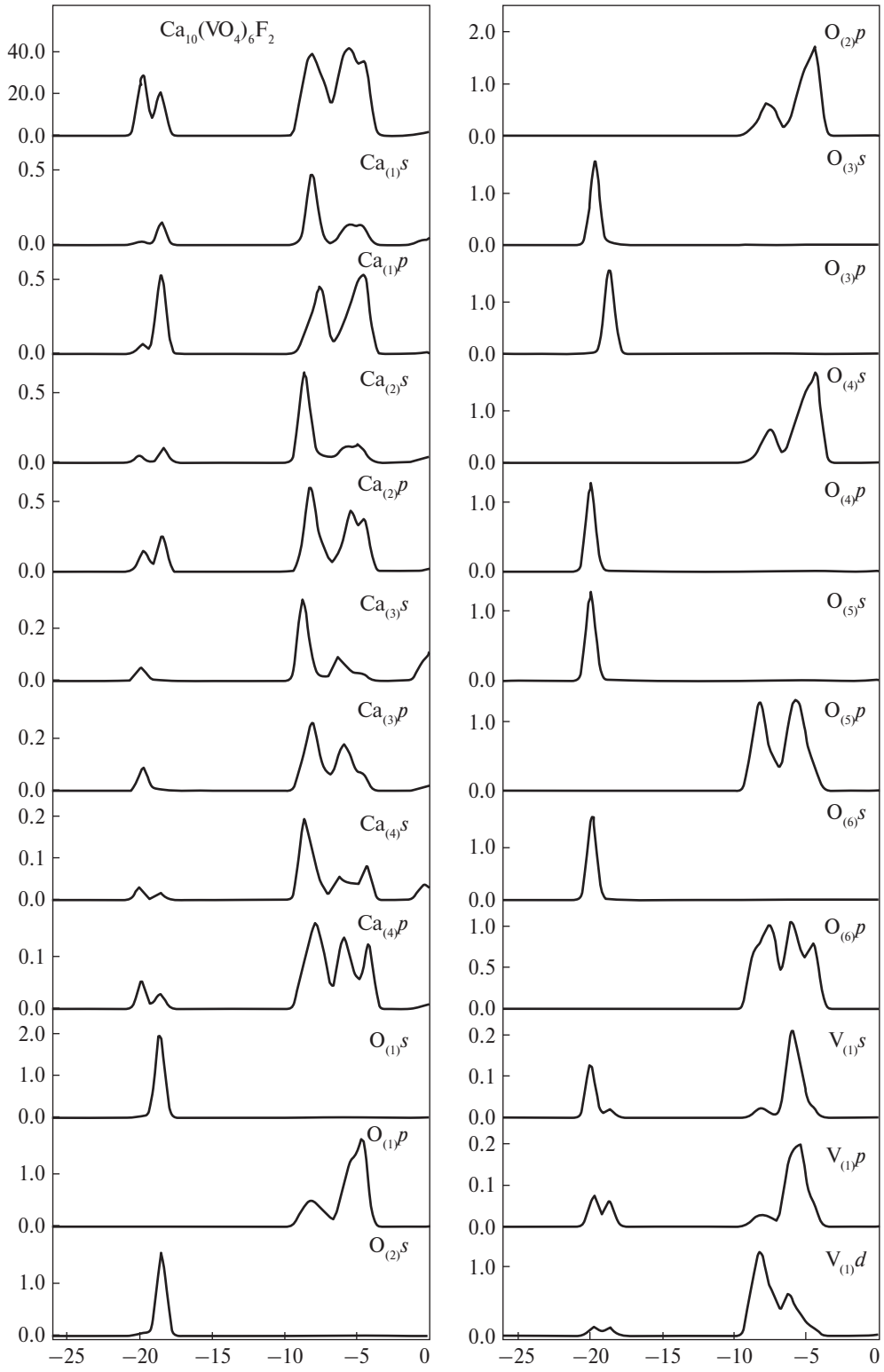
Ca10(VO4)6F2
Ca(1)s
Ca(1)p
Ca(2)s
Ca(2)p
Ca(3)s
Ca(3)p
Ca(4)s
Ca(4)p
O(1)s
O(1)p
O(2)s
O(2)p
O(3)s
O(3)p
O(4)s
O(4)p
O(5)s
O(5)p
O(6)s
O(6)p
V(1)s
V(1)p
V(1)d
−25
−20
−15
−10
−5
0

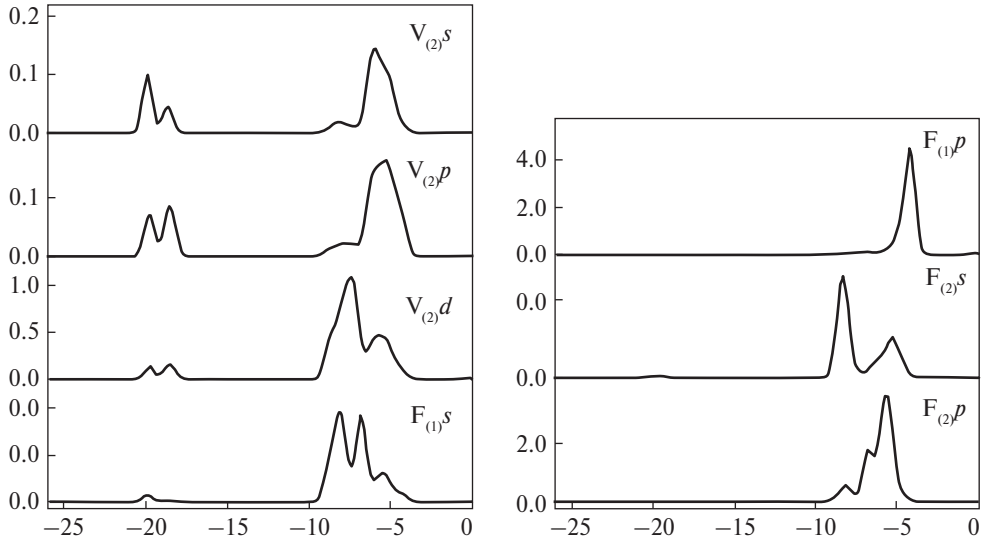

Fig. 4.21. Total and partial densities of states of $Ca_{10}(VO_4)_6F_2$

The comparison of vanadium $K_{\beta 2,5}$-bands in hydroxy- and calcium chlorovanadate (fig. 4.23) shows that both the form and the positions of peaks for all compounds practically coincide. Shift of the main maximum in hydroxy- and chlorovanadates into low-energy area (~0.5 eV) is connected with vanadium oxidation by tetrahedron formation. Energies of calculated O 2*s*, 2*p*-bands of VO_4^{3-} cluster, having some impurities of V 4*p*-states go with the position of corresponding peaks in V K_β emission spectra.

The pulling of low-energy tails of emission bands is observed due to many-particle effects in X-ray emission spectra and is a consequence of Auger processes in a valence band.

As it can be seen from fig. 4.24 O K_α-spectrum undergoes significant changes by changing of a tetrahedron type in calcium apatites in the series $PO_4^{3-} \rightarrow VO_4^{3-} \rightarrow AsO_4^{3-}$. In short-wave drop-down region in O K_α-spectrum of calcium hydroxyvanadate there is a feature that is determined with overlapping of *s*, *d*-wave functions of metal and arsenic as it is resulted from the calculation data. Reduction of symmetry of tetrahedrons leads to broadening of oxygen valence band in hydroxyvanadate. The shape of O K_α-band of calcium hydroxyarsenite in some features is similar to O K_α-band of Ca-HAP. However, the width at half-height is much less-for hydroxyarsenate.

The comparison of the calculation data on the electron structure of calcium hydroxy- and fluorovanadates (fig. 4.20, 4.21) shows considerable similarity except the deviations of the shape of DOS curve in the valence band top caused by the contribution of fluorine *p*-states.

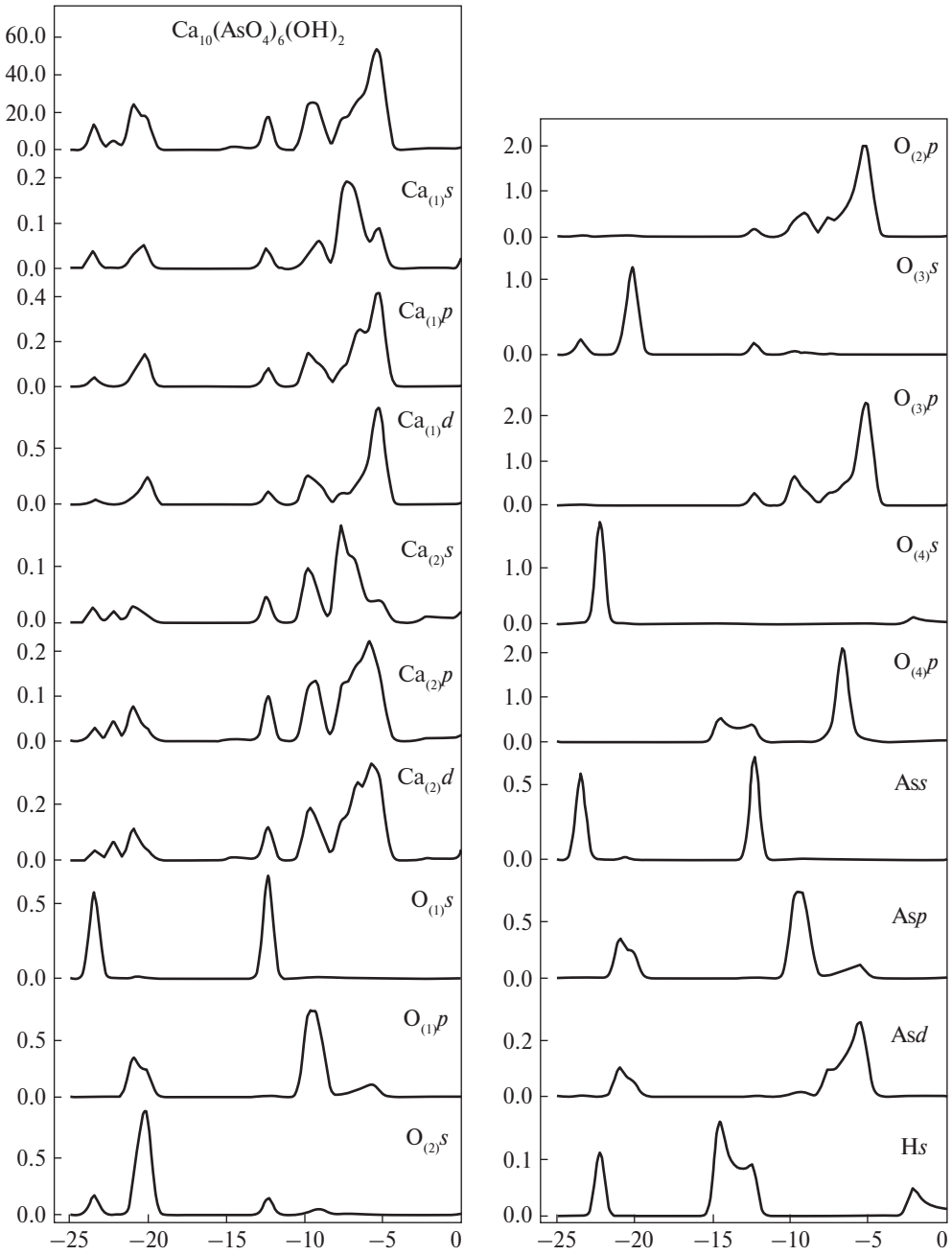

Fig. 4.22. Total and partial densities of states of $Ca_{10}(AsO_4)_6(OH)_2$

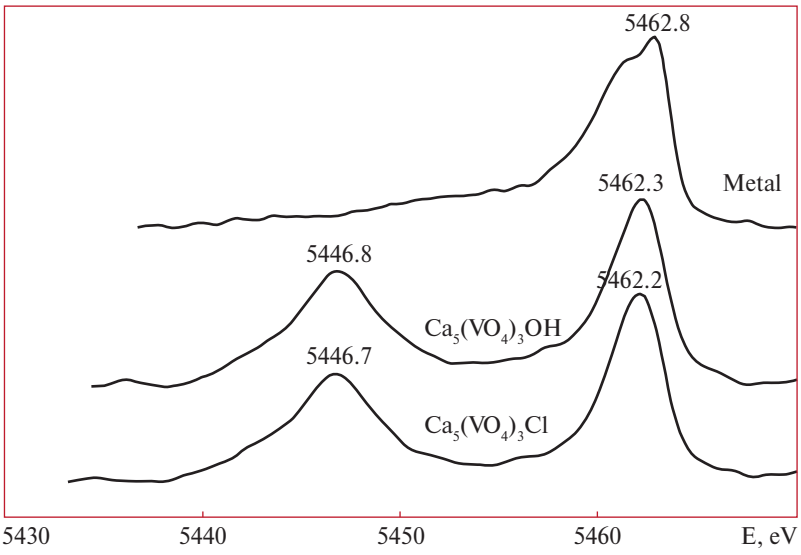

Fig. 4.23. Vanadium $K\beta_5$-bands in metal and compounds

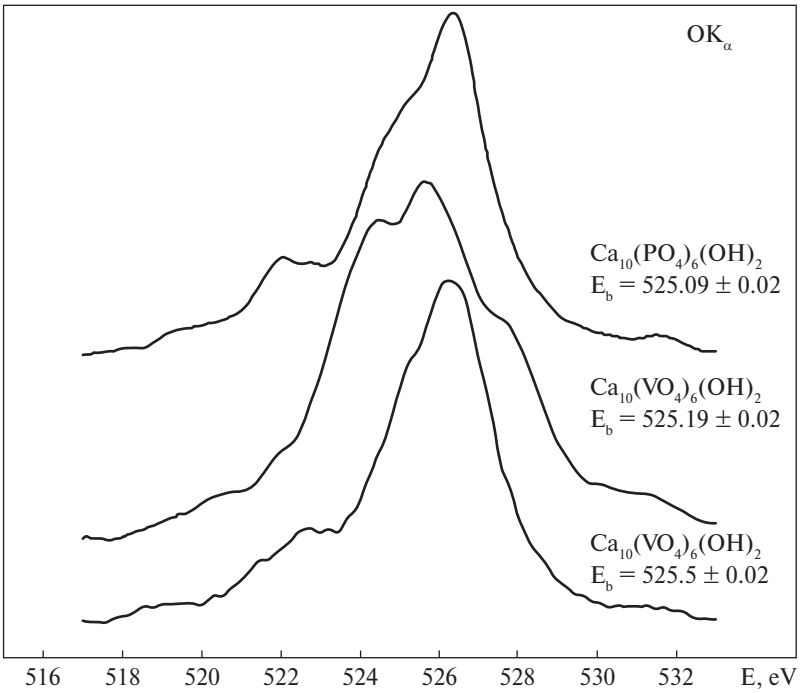

Fig. 4.24. X-ray K_α-spectra of oxygen

Hence, the structure of the occupied part of valence band of the investigated apatites has marked zone character with a different length of separate subbands. Two structural areas resolved by energy are revealed (subvalent states) namely the top and the bottom part of a valence band. The structure of the middle part of a valence band (area of valence states with energy from ~ 14 up to 19 eV) is poorly expressed, in particular for the compounds containing VO_4 tetrahedrons. Hybridized *s*-, *p*- and partially *d*-electron states of metal and phosphorus ions make the main contribution to the formation of the main features of the top part of a valence band of apatites and apatite-like compounds of calcium and strontium. Structure of the subvalence states is determined with *s*-states of oxygen and phosphorus.

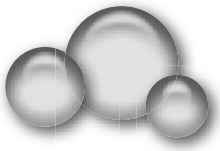

CHAPTER 5

ELECTRONIC STRUCTURE OF CALCIUM AND STRONTIUM APATITES ISOMORPHICALLY — MODIFIED IN CATION SUBLATTICE

The determinative influence of short-range order effects on solid body properties clearly appers in different properties of crystals of the same group having the same structural motive, but subjected to various isomorphic replacements. Studying of such family of crystals gives the information on the character of forces available in a crystal, distribution and localisation of impurities and, finally, about the mechanism of influence of individual structural changes on various properties of a crystal. It is known that isomorphic substitution in the case when the radius of the substituent atom differs little from the atom that is substituted, can be reduced to cellular disorder [243] that allows to conduct calculations of physical and chemical properties of such materials using traditional solid-state approaches.

This chapter includes the results of influence of calcium ion substitution for Fe, Ni, Cu, Mg ions and heterovalent isomorphic substitutions in the cation sublattice on electronic structure of apatites. There was investigated the influence of Ca^{2+} and Sr^{2+} ion substitution for lantanoids and alkaline elements in lattices of phosphate- and vanadateapatite (under the scheme $2Me^{2+}=Ln^{3+}+A^{+}$, Ln=La, Nd, Sm, Gd, Ho; A=Li, Na, K, Rb, Cs) on formation mechanisms of electron structure of crystals. There is described participation of valent and subvalent atomic shells in the formation of chemical bonds and the data about participation of 4*f* — electrons of rare-earth elements in the formation of X-ray electron spectra structure and chemical bonds with atoms of the environment are analyzed. There were also investigated changes of electron structure of calcium apatite isomorphically substituted with uranium.

The experimental data have been obtained using methods of high-vacuum X-ray photoelectron spectroscopy and X-ray emission spectroscopy.

For the theoretical description quantum-mechanical calculations of an electronic structure of the investigated systems by LMTO method using the data on atom positions in an elementary cell were used. The self-consistent calculation of the electronic structure, full and partial densities of states was conducted using linear method of MT-orbitals (LMTO), taking into account the combined corrections [244—246]. The self-consistency procedure included charge density of core states. Bart-Hedin approximation [247] was used for exchange-correlation part of potential. The detailed description of the calculation procedure is described, for example, in [248, 249]. *s*, *p* and *d* harmonics were taken into consideration by wave function decomposition both for metals, and for non-metals. Brillouin zone integration was carried out using an improved method of tetrahedrons [249] on a grid corresponding to 3375 reference points.

5.1. Calcium ion substitution for Fe, Ni, Cu and Mg ions in apatite structure

Investigation of 3*d*-metal ions entry into apatite matrix is interesting from the point of view of difficulty of their detection in natural apatite minerals, and also of physico-medical interest to their accumulation in apatite-containing human and animal bone skeleton. Research on clearing changes in the structure of calcium apatite valence band apatite has been conducted by isomorphic substitutions of calcium ions for 3*d*-metal ions, and also for magnesium ions — the element with a serial number 12 which is located in the Periodic system of elements in the same group with calcium and, hence, has a similar valence electron shell nS^2.

There are presented X-ray emissional $K_{\beta 2,5}$-spectra of calcium in stoichiometrical hydroxyapatite and in nickel-substituted apatite with a different degree of substitution in fig. 5.1. It can be seen that the shape of $K_{\beta 2,5}$-band of calcium in nickel-substituted HAP (Ca (Ni)-HAP) as a whole repeats the form of $K_{\beta 2,5}$-band in HAP, indicating a small influence of Ni on the redistribution of electronic density on calcium ions.

There is observed a shift of the main maximum of the band which reflects *d* and *p* calcium states, into short-wave area that is connected with an influence of *d*- states of nickel having smaller energy localization. Introduction of 1 at. % Ni into the structure of apatite ($Ca_{9.6}Ni_{0.4}(PO_4)_6(OH)_2$) causes a shift of the main maximum $K_{\beta 2,5}$ of calcium band of ~ 0.1 eV. When the nickel content increases to 2 at. % ($Ca_{9.2}Ni_{0.8}(PO_4)_6(OH)_2$) this shift increases to ~0.2 eV. Such behavior is connected with the increase in hybridization of *d*-states of calcium and nickel.

Significant changes in $K_{\beta 2,5}$- bands of doped samples are observed in long-wave area of the spectrum. So in unsubstituted HAP the absence of the feature near 4022 eV, caused by *s*-states of oxygen in isomorphically substituted samples is observed. It possibly indicates that by isomorphic substitution of calcium atoms for nickel atoms in HAP the bond of PO_4^{3-} oxygen matrix with metal atoms increases, thus weakening

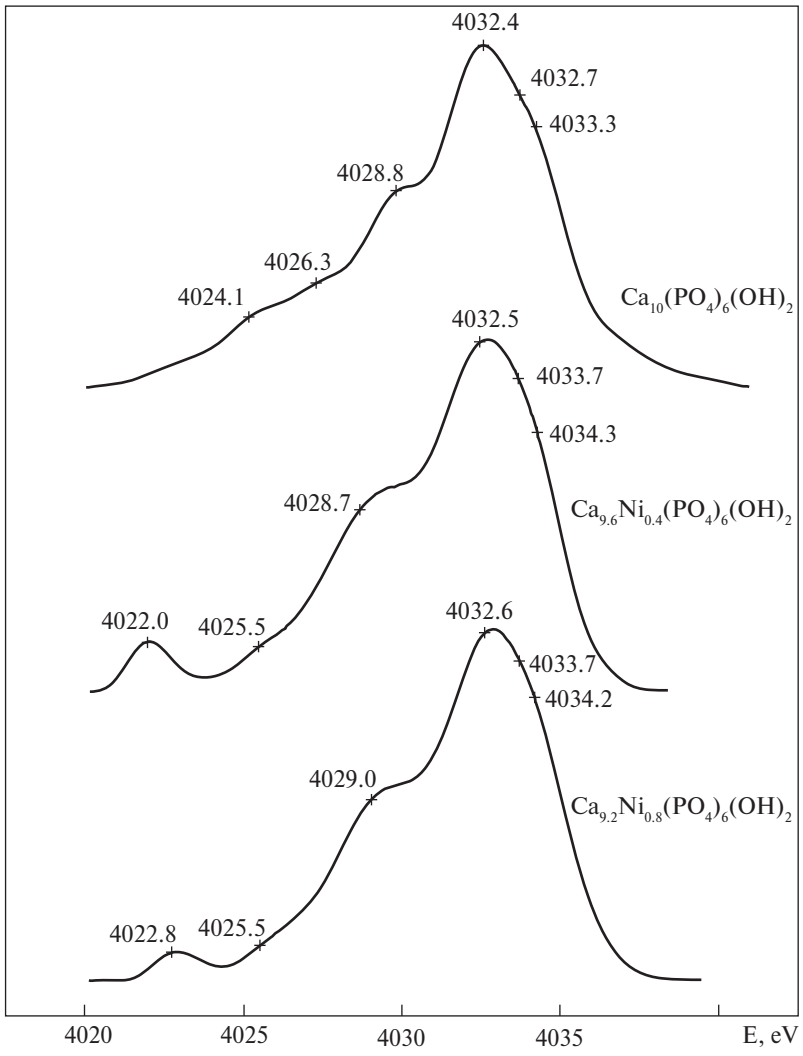

Fig. 5.1. $K_{\beta 2,5}$-spectra of calcium compounds

Ca(Ni)-O-Ca(Ni) bond along hexagonal axis. The essential redistribution of electronic density is confirmed with XPS data (tab. 5.1). It canbe seen that the value of binding energy of O 1*s* level in the isomorphically-substituted samples is higher than of stoichiometric HAP whereas in oxides this value is much less than a value of binding energy of O 1*s* of stoichiometric sample.

There is also an increase of Ca 2*p* level binding energy in isomorphically-substituted samples that indicates electronic density loss from calcium atoms and therefore an increase in of ionic component of chemical bond, confirming the conclusion about an increase in metal-oxygen bond [252].

On the assumption of simultaneus increase of binding energy of both calcium O 1*s* and core levels by isomorphic substitution of calcium ions for nickel ions, it is possible to conclude that in the general balance of chemical bond the essential role is played also by covalent component.

The features characterizing the main maximum of $K_{\beta 2,5}$-band are the result of the main maximum splitting because of existence of two different structural positions of calcium.

In table 5.1 there are given binding energies of core electrons of metal atoms (Ca, Ni, Cu, Fe, Mg) and of metal oxides. Core electron binding energies of oxides

Table 5.1. **Binding energy of core-level electrons (eV) of Ca and Ni atoms, Ca and Ni oxides, and also of the investigated compounds.**

Compound	O 1s	P 2s	P 2p	Ca $2p_{3/2}$	Ca $2p_{1/2}$	M=Cu, Fe, Mg, Ni 2p
Ca-metal [250]	—	—	—	345.9	—	—
CaO[251]	531.5	—	—	347.1	—	—
$CaCO_3$[250]	531.9	—	—	347.3	—	—
$Ca_{9.6}Ni_{0.4}(PO_4)_6(OH)_2$	531.3	190.8	133.3	—	—	859.3
$Ca_{9.2}Ni_{0.8}(PO_4)_6(OH)_2$	531.1	190.6	133.1	347.3	—	855.3
$Ca_{10}(PO_4)_6(OH)_2$	530.4	189.6	132.0	346.2	—	—
$Ca_{9.9}Cu_{0.1}(PO_4)_6(OH)_2$	531.9	190.6	133.3	347.5	351.1	933.7
$Ca_{9.9}Fe_{0.1}(PO_4)_6(OH)_2$	531.6	190.7	133.2	347.2	350.6	710.4
$Ca_{9.9}Mg_{0.1}(PO_4)_6(OH)_2$	531.9	190.8	133.5	347.5	350.9	51.9
$Ca_{9.8}Mg_{0.2}(PO_4)_6(OH)_2$	531.9	190.8	133.7	347.7	351.1	52.0
Ni-metal [250]	—	—	—	—	—	852.7
Cu-metal [250]	—	—	—	—	—	932.7
Fe-metal [250]	—	—	—	—	—	706.9
Mg-metal [250]	—	—	—	—	—	49.6
Ni_2O_3 [250]	—	—	—	—	—	856.0
NiO [250]	529.4	—	—	—	—	853.8
CuO [250]	—	—	—	—	—	933.8
FeO [250]	—	—	—	—	—	709.6
Fe_3O_4 [250]	—	—	—	—	—	710.8
Fe_2O_3 [250]	—	—	—	—	—	710.9
MgO [250]	529.8	—	—	—	—	51.5

Note: Values of electron binding energy are given relatively to C 1s electron binding energy (285.0 eV). Measurements inaccuracy is 0.1 eV.

are given for easy interpretation of experimental results. Binding energy of Ca $2p_{3/2}$ electrons of calcium atoms in isomorphically-substituted HAP coincides with binding energy of the same electrons in CaO that, apparently, is connected with similar ionization degree of calcium atoms in these compounds.

The significant increase of binding energy of Ca $2p_{3/2}$ electrons is thus observed by changing from HAP to isomorphically-substituted compound with simultaneous reduction of half-height linewidth that electronic density loss of calcium ions and possible normalization of calcium structural states.

By isomorphic substitution of calcium for nickel in HAP all atoms undergo changes of electron binding energy. O 1*s* line of oxygen increases binding energy by 0.9 (1 at. % Ni) and 0.7 eV (2 at. % Ni). Such considerable deviations of oxygen 1*s*-level positions may indicate considerable changes in the energy status of phosphate tetrahedrons. Ca $2p_{3/2}$ line of calcium core electrons shifts towards larger binding energies by 1.1 eV. P 2*s* line shifts towards larger binding energies by 1.2 eV (1 at. % Ni) and 1.0 eV (2 at. % Ni) relatively to stoichiometric HAP, thus remaining near one value for all substituted compounds. P 2*p* line shifts in this case is also shifted towards larger binding energies by 1.3 (1 at. % Ni) and 1.1 eV (2 at. % Ni). Hence, a larger shift is observed for the electronic levels located closer to valence band.

Thus, the analysis of XPS data on investigation of HAP samples with isomorphic substitution of calcium for nickel cation has shown that such substitution leads to appreciable changes in the oxygen environment of calcium, phosphorus and nickel atoms. It is shown in an increase of core electron binding energy of oxygen and phosphorus atoms and, apparently, leads to a change of local symmetry of tetrahedrons [252].

Similar changes of electronic structure are also observed by substitution of calcium for Fe, Cu and Mg ions. It can be seen (tab. 5.1) that by isomorphic substitution of calcium for copper in HAP all atoms undergo changes of electron binding energy. O 1*s* line of oxygen increases binding energy by 1.5 eV and is close by value to $CaCO_3$. $2p_{3/2}$ line of calcium core electrons shifts towards larger binding energies by 1.3 eV. P 2*s*-line is shifted towards larger binding energies by 1.0 eV. In this case P 2*p*-line is also displaced towards larger binding energies by 1.3 eV.

In the case of substitution for iron, O 1*s* line of oxygen increases binding energy by 1.2 eV and its value is close to that of CaO. The $2p_{3/2}$ line of calcium core electrons shifts towards larger binding energies by 1.0 eV. The line of phosphorus 2*s*-electrons is shifted towards larger binding energies by 1.1 eV. P 2*p* line in this case is also shifted towards larger binding energies by 1.2 eV. Fe 2*p* line is close to that of FeO.

Quite interesting is the investigation of the influence of isomorphic substitution of calcium for magnesium which is in the same group of the Periodic table of elements with calcium, having an atomic number 12 and an $3s^2$ outer shell that allows it to be in a gaseous state under certain conditions. Similarity of chemical properties of these elements and smaller radius of Mg atom, most likely, allow Mg to occupy both calcium positions in apatite structure.

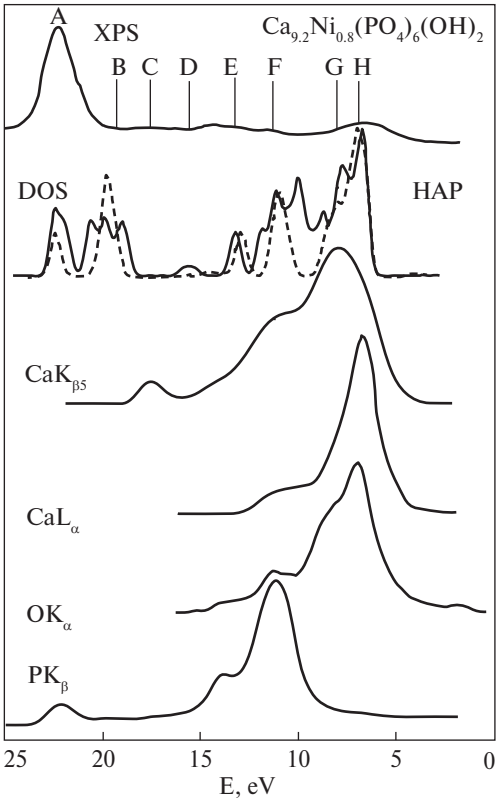

Fig. 5.2. The X-ray spectra of isomorphically-substituted HAP and total density of states (DOS) (band calculation) in a single energy scale

In the case of substitution for magnesium O 1*s* line of oxygen increases binding energy by 1.5 eV in $Ca_{9.9}Mg_{0.1}(PO_4)_6(OH)_2$ and $Ca_{9.8}Mg_{0.2}(PO_4)_6(OH)_2$. Ca $2p_{3/2}$ line of calcium core electrons shifts towards larger binding energies by 1.3 eV in $Ca_{9.9}Mg_{0.1}(PO_4)_6(OH)_2$ and by 1.5 эВ in $Ca_{9.8}Mg_{0.2}(PO_4)_6(OH)_2$. P 2*s* line is shifted towards larger binding energies by 1.2 eV both for $Ca_{9.9}Mg_{0.1}(PO_4)_6(OH)_2$ and for $Ca_{9.8}Mg_{0.2}(PO_4)_6(OH)_2$. In this case P 2*p* line is also shifted towards larger binding energies by 1.5 eV in $Ca_{9.9}Mg_{0.1}(PO_4)_6(OH)_2$ and by 1.7 eV in $Ca_{9.8}Mg_{0.2}(PO_4)_6(OH)_2$. Mg 2*p* line is close to that of MgO.

Thus, as follows from table 5.1, with an increase of atomic number of 3*d*-metal and by changing to magnesium there is a monotonous increase of binding energy of Ca $2p_{3/2}$ and O 1*s* electrons that indicates the reduction of electronic density of calcium and oxygen atoms.

Energy and charge equilibration almost does not affect P 2*s* levels though at the same time there is a significant change in the position of P 2*p* levels.

The analysis of combination of X-ray photoelectron spectra, X-ray emission spectra and theoretical calculations, for a case of nickel occupying the second position of apatite structure, has shown their significant correlation (fig. 5.2, 5.3).

The shape of the main maximum of calcium *K*-spectra is, generally determined by two features, namely *G* feature, formed by calcium *d*- and *r*-states and the short-wave *H* maximum mainly connected with the display of oxygen *p*-states and calcium *d*-states. *F* feature is formed mainly by hybridization of calcium *s*- *p*-, *d*-states and *p*-states of phosphorus and oxygen.

E and *D* maximums of DOS in a range of 13 ÷ 16 eV completely coincide with long-wave features of calcium *K*-bands and are generated by that part of oxygen 2*p* electronic density which takes part in a chemical bond with phosphorus. Two peaks near valence band bottom in a range of 20 ÷ 25 eV are formed basically by oxygen *s*-states. In a low-energy part of a valence band there is *A* feature, generated mainly by oxygen 2*s* states, which are hybridized with P 3*s* and P 3*p* states. This result of calculation is confirmed with P K_{β}-spectrum.

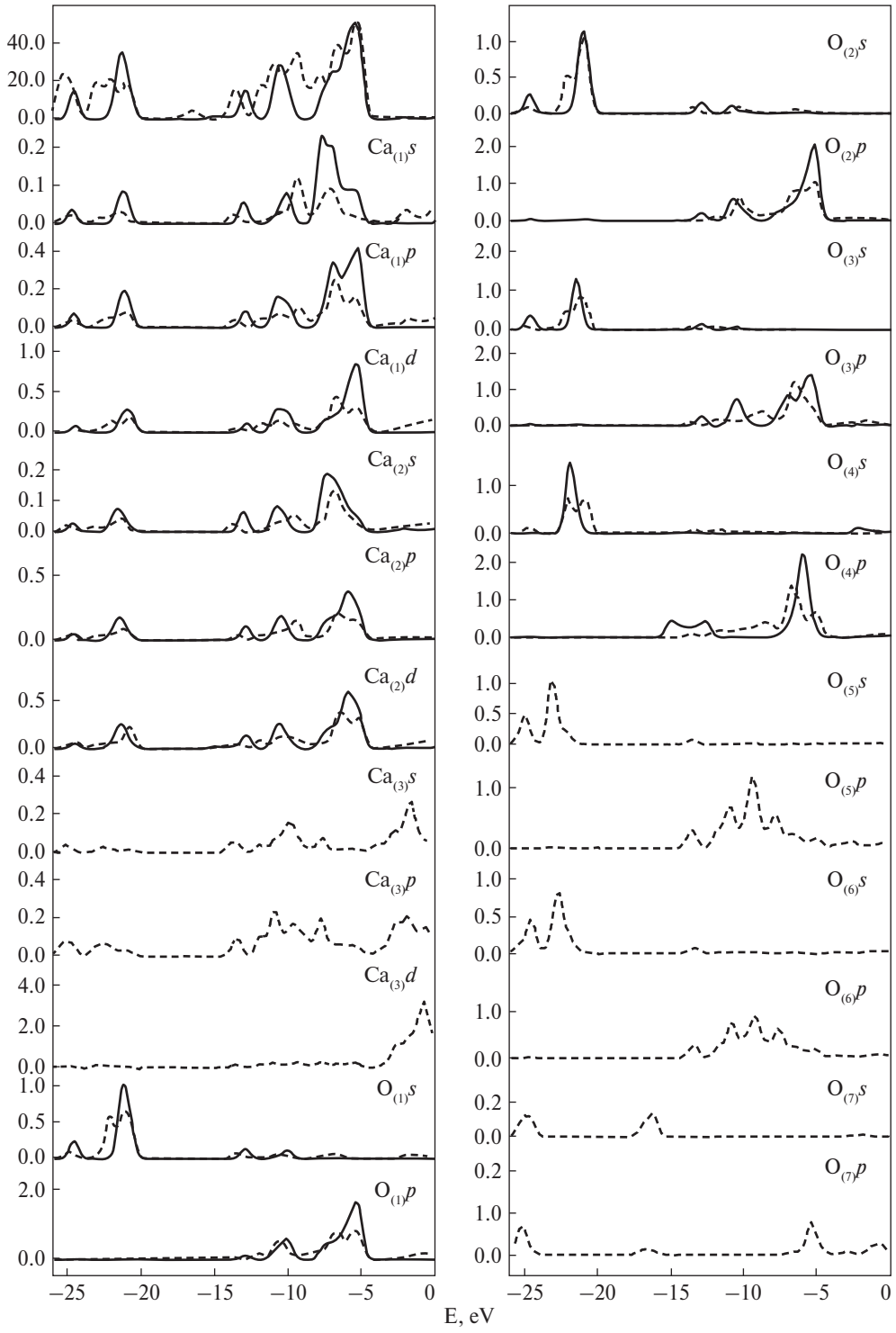
Ca(1)s
Ca(1)p
Ca(1)d
Ca(2)s
Ca(2)p
Ca(2)d
Ca(3)s
Ca(3)p
Ca(3)d
O(1)s
O(1)p
O(2)s
O(2)p
O(3)s
O(3)p
O(4)s
O(4)p
O(5)s
O(5)p
O(6)s
O(6)p
O(7)s
O(7)p
E, eV

Figure 5.3.

Continuation of figure 5.3

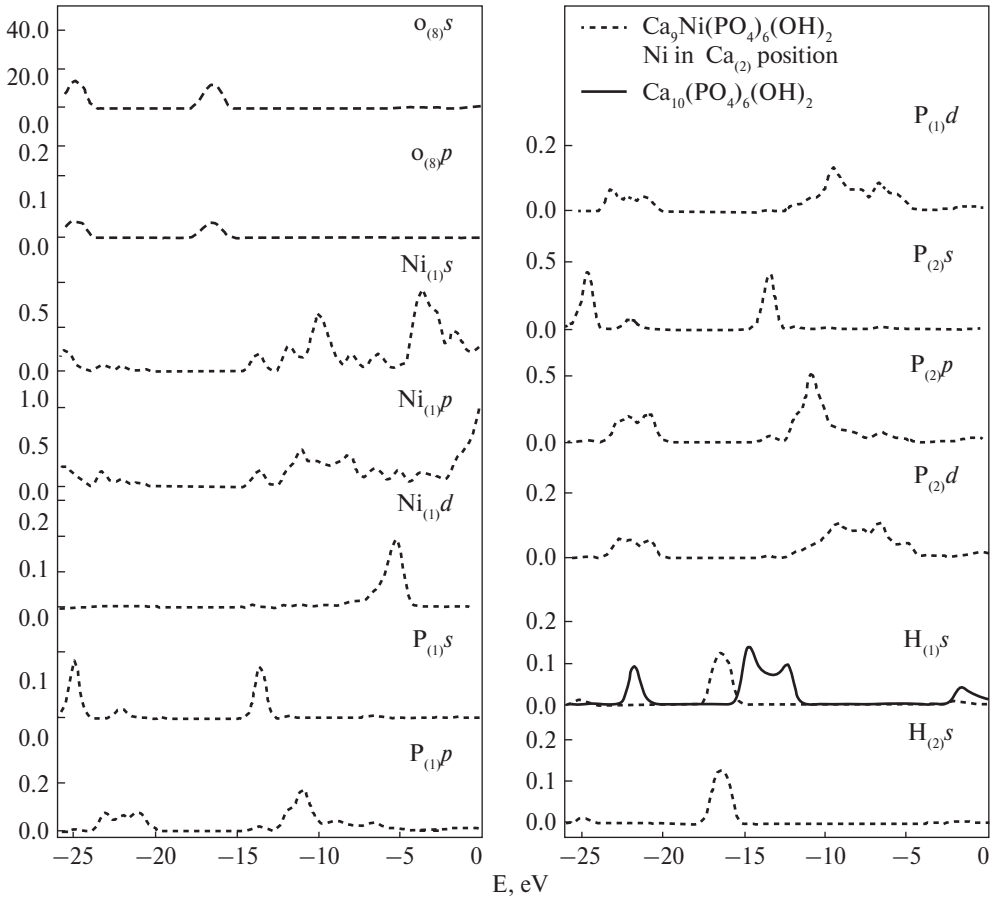

Fig. 5.3. Total and partial density of states of compounds

C feature near 18 eV, is hypothetically caused by oxygen *s*-states and displays Ca-O interaction.

Decrease in electronic density of calcium atoms leads to the increase of binding energy not only core levels, but also of valence electronic densities of atoms. As it can be seen from fig. 5.3, oxygen atoms of PO_4 tetrahedra play the considerable role in preservation of the overall charge balance. So by isomorphic substitution Ca → Ni and introduction of Ni atoms in $Ca_{(2)}$-positions, the shape of $O_{(1)}s$, *p*, $O_{(2)}s$, *p* curves is almost uchanged. There is only observed a small shift towards larger binding energies. Only the shape of curves of $O_{(3)}s$, *p* — densities is changed because of neighbourhood with $Ca_{(2)}$ positions.

Thus, the correlation of calculation and experimental data indicates the preferable occurrence of Ni atoms in $Ca_{(2)}$ position of apatite structure.

5.2. Substitution of calcium ions for strontium ions

Recently besides other applications calcium hydroxyapatite is considered as a matrix for a burial radioactive wastes and environmentally dangerous compounds of heavy metals. Large specific surface area (several hundred square meters per one gram of substance determines high reactivity of nanodisperce calcium hydroxyapatite.

There are cited results of investigation of changes of calcium apatite electronic structure, initiated by substitution of calcium atoms for strontium atoms here. Research was conducted using X-ray photoelectron spectroscopy, as the most direct research method of electronic structure of chemical compounds with application of LMTO quantum mechanical modeling.

Table 5.2 contains binding energies of core electrons of metal calcium atoms, calcium and strontium oxides and of the investigated compounds. Binding energy of Ca $2p_{3/2}$ electrons of calcium atoms in substituted HAP is close to binding energy

Table 5.2. **Binding energy of electrons (eV), half-width (eV) of core levels of Ca and Sr atoms, their oxides, and also of investigated compounds.**

Compound	O 1s	P 2s	P 2p	Ca $2p_{3/2}$	Ca $2p_{1/2}$	Sr 3s	Sr $3p_{3/2}$	Sr $3p_{1/2}$	Sr 4p
Ca-metal	—	—	—	344.7 (1.7)	—	—	—	—	—
CaO	528.9 (1.4)	—	—	346.0 (1.7)	—	—	—	—	—
$Ca(OH)_2$	531.2	—	—	—	—	—	—	—	—
$CaCO_3$	531.6 (1.6)	—	—	347.3 (1.7)	—	—	—	—	—
$Ca_{10}(PO_4)_6(OH)_2$	530.4 (2.6)	189.6 (3.6)	132.0 (2.5)	346.2 (2.3)	351.2	—	—	—	—
$Ca_5Sr_5(PO_4)_6(OH)_2$	531.1 (2.1)	190.3 (2.9)	133.5 (2.8)	347.2 (1.9)	350.8 (2.7)	—	269.0 (3.0)	279.3 (4.0)	—
$Sr_{10}(PO_4)_6(OH)_2$	531.1 (2.3)	190.6 (3.0)	—	—	—	357.7 (4.0)	269.2	279.4	—
Sr-metal	—	—	—	—	—	356.8 (4.1)	—	—	18.2
SrO	528.2 (1.3)	—	—	—	—	357.2 (3.8)	268.1 (2.5)	—	18.6
$SrCO_3$	531.5 (1.5)	—	—	—	—	358.0 (4.2)	269.0 (2.5)	—	19.5

Note: Values of electron binding energy are given relatively to the binding energy of C 1s electrons (285.0 eV). Measurement inaccuracy is 0.1 eV.

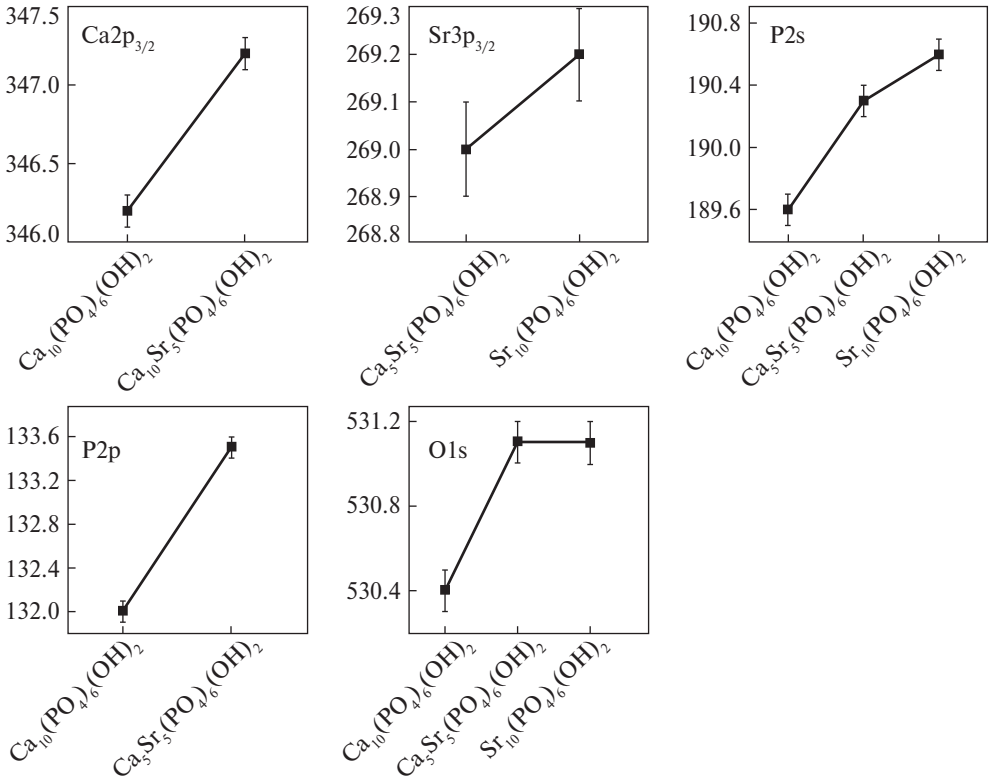

Fig. 5.4. Energy position of binding energy of electrons (eV) of atomic core levels of investigated compounds

of the same electrons in $CaCO_3$ that, apparently, is connected with close degree of ionization of calcium atoms in these compounds.

By changing from $Ca_{10}(PO_4)_6(OH)_2$ to $Ca_5Sr_5(PO_4)_6(OH)_2$ electron binding energy is changed in all atoms (tab. 5.2, fig. 5.4). O 1*s* line binding energy is increased by 0.7 eV. Lines of calcium core electrons shift towards larger binding energies, so for Ca $2p_{3/2}$ level the shift is 1.0 eV, and for the line of Ca $2p_{1/2}$ electrons it shifts towards lower energies — by 0.4 eV. In this case P 2*s* line is also shifted towards higher binding energies by 0.7 eV, and P 2*p* line by 1.5 eV. Hence, by HAP modification with strontium there are appreciable changes in the electronic structure of HAP components, and, larger shift is observed for electron levels located closer to valence band.

The width of O 1*s*, P 2*s*, P 2*p* and Ca 2*p* lines in the mixed apatite is less, than in stoichiometric HAP. Thus the significant increase in binding energy of the corresponding lines is observed indicating electronic density loss of calcium, oxygen and phosphorus atoms. Hence, metal sublattice in a mixed HAP, is more "loosened". Most likely, indirect interaction between atoms of metal weakens that affectts thr width of core lines. It also indicates the increase of covalent component in the general balance of chemical bond.

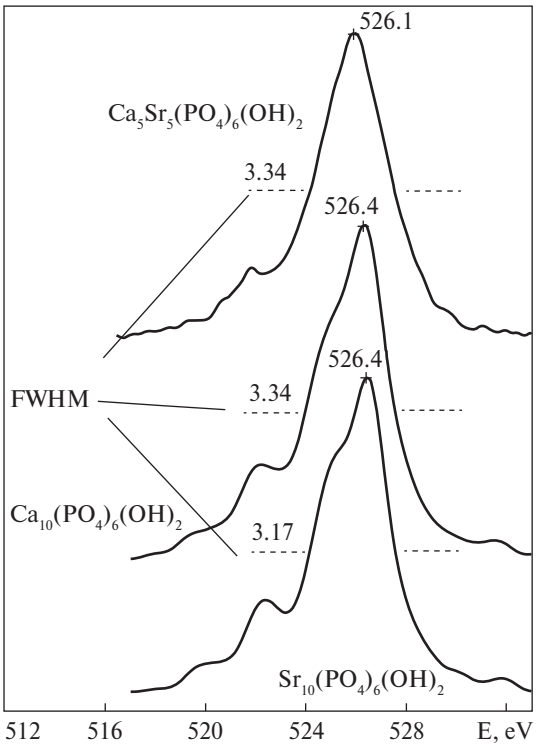

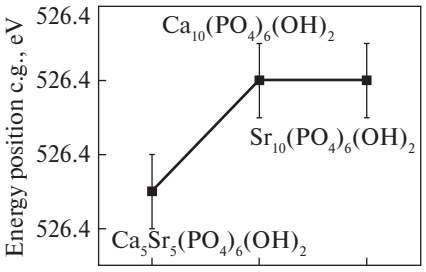

Fig. 5.6. Energy position of centers of gravity of O K_α-spectra of the investigated compounds

Fig. 5.5. O K_α-spectra of the investigated compounds

In strontium hydroxyapatite there is no shift of O 1*s* line, P 2*s* line shifted towards higher binding energies by 0.3 eV. Sr $3p_{3/2}$ line is shifted by 0.2 eV, and Sr $3p_{1/2}$ line is shifted by 0.1 eV towards higher binding energies. Binding energy of Sr $3p_{3/2}$ and Sr 3*s* electrons of strontium atoms in substituted HAP and Sr-HAP is close to the binding energy of the same electrons in $SrCO_3$ that, apparently, is connected with close degree of ionization of strontium atoms in these compounds.

The obtained results conform well to X-ray spectral investigation of oxygen state (fig. 5.5, 5.6).

Calcium substitution for strontium in calcium hydroxyapatite significantly changes the shape of full density of states of a crystal (fig. 5.7). The *B* feature corresponding to the main maximum in DOS curve is generated basically by valence states of oxygen and strontium, without participation of valence states of phosphorus, as evident in the calculation data (fig. 5.7). The *D* feature is generated by that part of 2*p* electron density of oxygen which takes part in a chemical bond with phosphorus and reflects, basically, phosphorus *p*-states.

Low-intensity *A* feature in DOS curve reflects the bond between hydroxyl ion metal atoms. The feature in DOS curve near 2.5 eV is observed only for $O_{(4)}$ *s*, $O_{(4)}$ *p* and H *s* partial densities of electronic states. The absence of appreciable features in

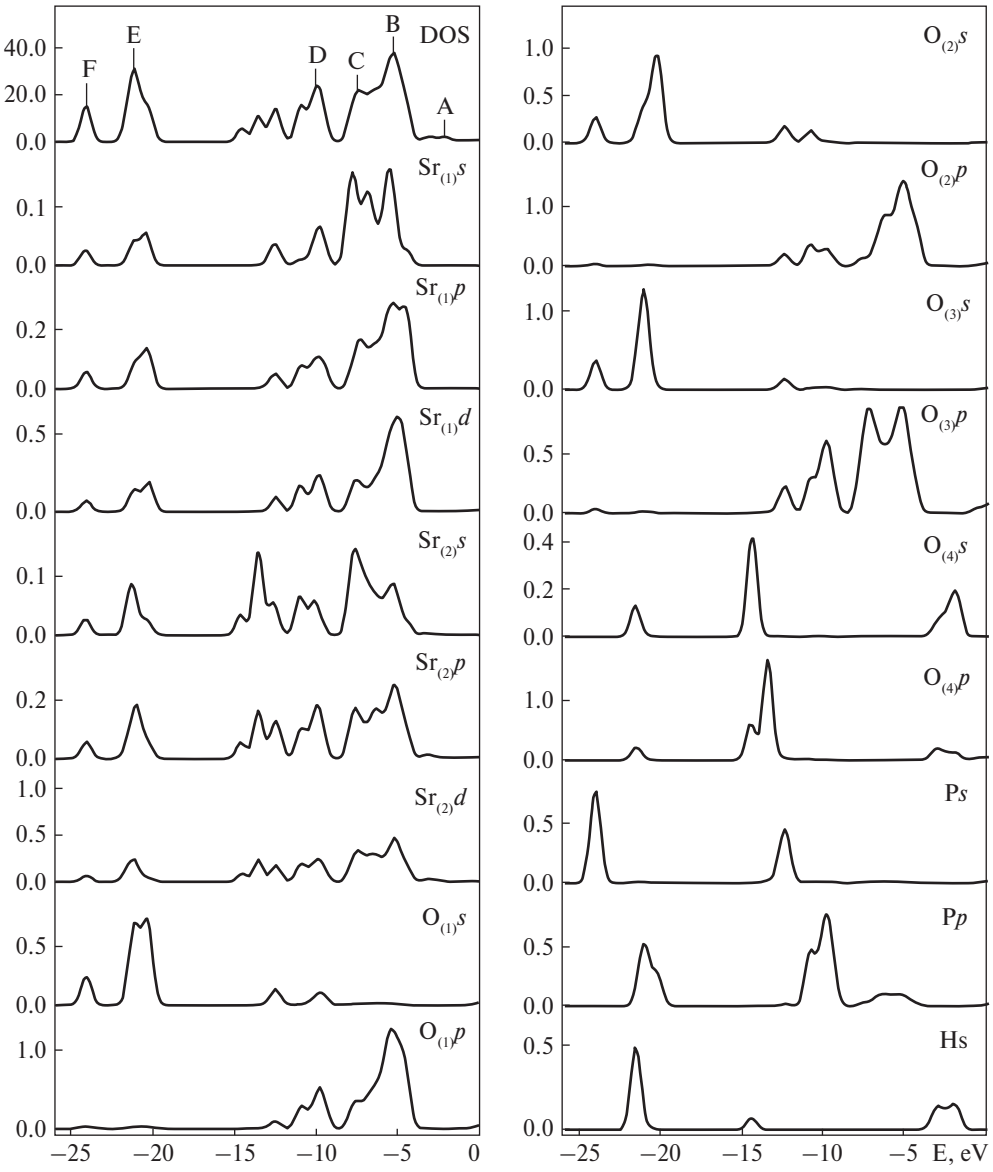

Fig. 5.7. Total and partial densities of $Sr_{10}(PO_4)_6(OH)_2$ states

the curves of partial densities of metal in this energy range may indicate that indirect metal-metal interaction in Sr-HAP is virtually absent.

The presence of such interaction in calcium hydroxyapatite, probably, is determined with the emerging *d*-cover having characteristic dependence of effective potential on distance. Based on the analysis of characteristics of X-ray spectra and calculation data of calcium and strontium hydroxyapatite it is possible to conclude

that in Sr-HAP the partial contribution of H *s*-states into FDS considerably increases. Thus, the main maximum of H *s*-density in HAP is near 15 eV, whereas in Sr HAP it is near 22 eV. Band splitting near 15 eV in HAP may indicate the complex mechanism of hybridization of hydrogen *s*-density with $Ca_{(2)}$ *p* and $Ca_{(2)}$ *d* densities through $O_{(4)}$ *p* states. There is one Sr-HAP H *s*-density peak in this range with intensity lower than of Ca-HAP. The feature near 2.5 eV in H *s*-density curve of Sr-HAP has more complex structure consisting of two peaks generated as it was mentioned above, by electronic densities of hydroxyl atoms of $O_{(4)}$ (*s*, *p*)-states.

Most likely, high core electron density of strontium atoms in a free state in comparison with calcium atoms leads to the fact that strontium *d*-cover nucleation in a crystal is accompanied with its higher binding energy, than for calcium (for metal strontium binding energy of *d*-electrons is near 15 eV whereas for calcium it is near 5 eV) and, hence, indirect metal-metal interaction for strontium apatite in triangles of metal atoms is less expressed.

5.3. Heterovalent isomorphic substitutions in apatite structure

Isomorphic substitution of apatite-like compounds leads to significant changes of physical and chemical properties, in particular, of X-ray spectra.

Rare-earth metals are located between lanthanum and hafnium in the Periodical system of elements. The configuration of valence electrons of both lanthanum and lutetium is $5d^16s^2$. However while lanthanum 4f-shell is empty lutetium shell is completely filled with 14 electrons. 4*f*-shell filling occurs in atoms of the elements that are between these metals. 6*s* – and 5*d*-levels are located rather close to each other. In comparison with 6*s*- and 5*d*-electrons (~5 eV) 4*f*-electrons have much bigger binding energy (~22 eV). Proceeding from such atomic structure, it is possible to expect that the valence zone will be formed by 6*s*- and 5*d*-electrons irrespective of 4*f*-electrons. As appears from fig. 5.8, at characteristic internuclear distances, the density of 5*d*-electrons is considerable, and maximal for 6*s*-electrons. It indicates that wave functions of 5*d*- and 6*s*-electrons, located in different lattice points, will overlap to a large extent and consequently, form a wide valence band. Such picture is typical for the transition metals located in the beginning of the periods in the Periodical System. At the same time 4*f* electrons are more strongly bound in atom and thereof form very narrow band.

Considering a high sensitivity of *f*-levels to a kind of potential very exact experiments are necessary for determining of their position in a spectrum characterizing the basic state of substance. On this account, and also because of the small content of REM elements in investigated compounds complete description of an electronic state of dopants was problematic.

As more than half of atoms of crystal belong to oxygen atoms of tetrahedrons, the investigation of valence levels of oxygen atoms have been undertaken. In fig. 5.9

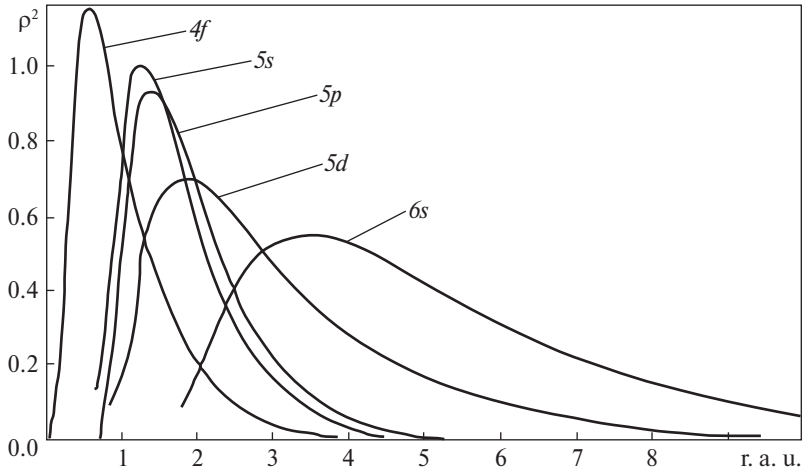

Fig. 5.8. Radial distribution of electronic density in Gd atom [253]

there are presented O K_α-spectra of isomorphically substituted calcium hydroxyapatite. Starting from the fact that the main changes in O K_α-spectrum occur in the long-wave part of spectrum where hydroxyl *s*, *p*-conditions make a considerable contribution, it is possible to conclude that calcium substitution occurs mainly in $Ca_{(2)}$-positions, coordinated by oxygen of OH. The charge redistribution determined with a change of the energy centre of gravity of O K_α-lines (fig. 5.10) is observed. The observed feature in the behaviour of position of the centre of gravity of O K_α-line for potassium-containing compounds (x=0.5 and x=1.0) most likely is connected either with a formation of the second phase during the experiment, or with an increase of priority of calcium atoms substitution in one of crystallographic positions. It is obvious that isomorphic doping of Ca-HAP with lanthanum and alkaline-earth elements monotonously lowers the position of the centre of gravity of O K_α-line in the series Li→K→Rb that is explained with an increase of electronic density on oxygen atoms.

Transition to strontium-containing compounds also shows the reduction of energy position of O K_α-band by doping with alkaline and rare-earth metals (table 5.3).

On fig. 5.11 there are given O K_α-spectra of isomorphically substituted calcium hydroxyvanadate. Proceeding from the fact that the form of all given spectra practically coincides, it is possible to conclude that in all samples calcium substitution

Table 5.3. **Energy position of the centre of gravity of O K_α-band in compounds.**

Compound	Position of the centre of gravity, eV
$Sr_{10}(PO_4)_6(OH)_2$	525.4
$Sr_{10-2x}Na_xLa_x(PO_4)_6(OH)_2$, x=0.6	525.3

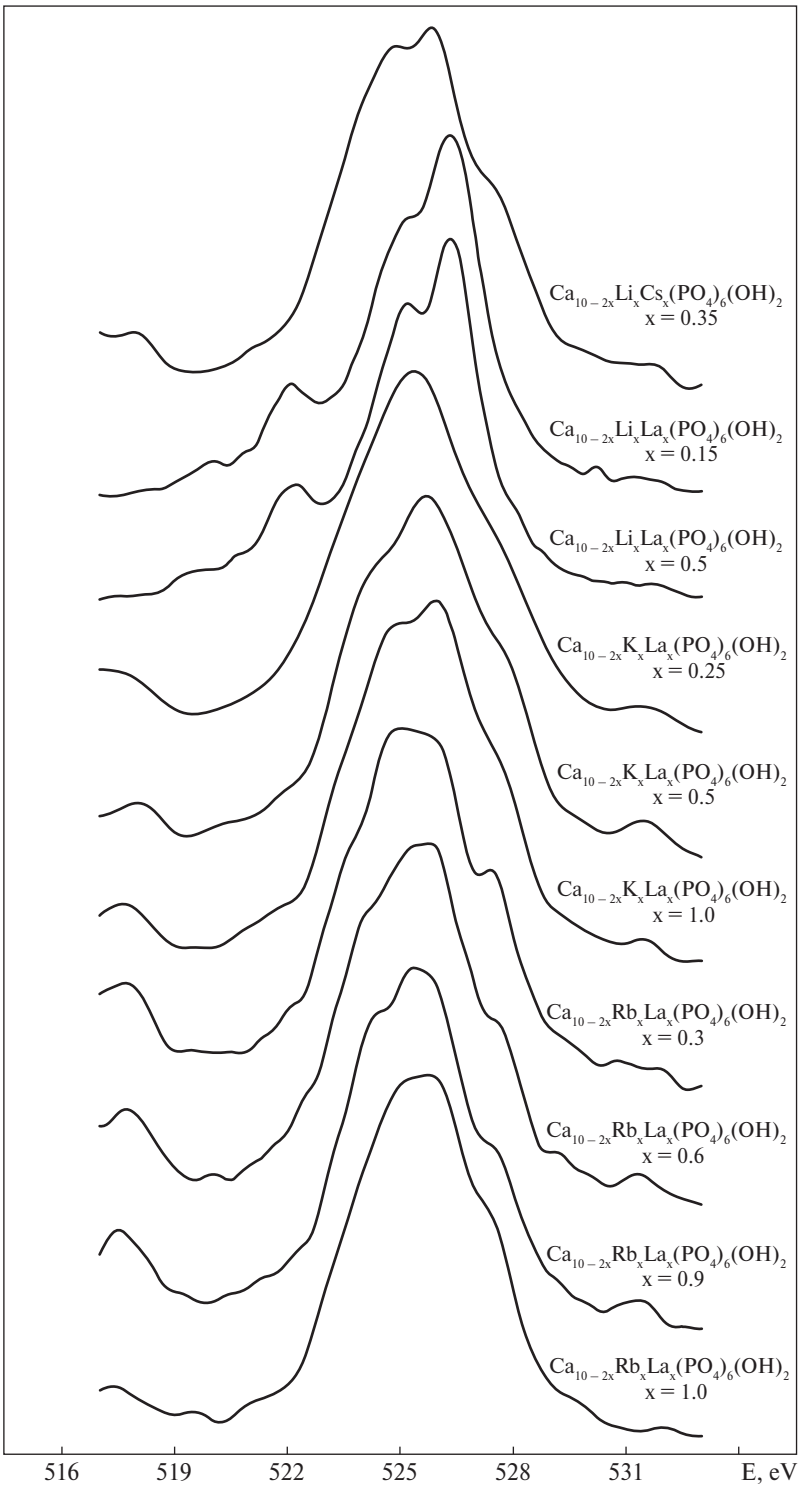

Fig. 5.9. X-ray O K_α-spectra of isomorphically substituted apatites

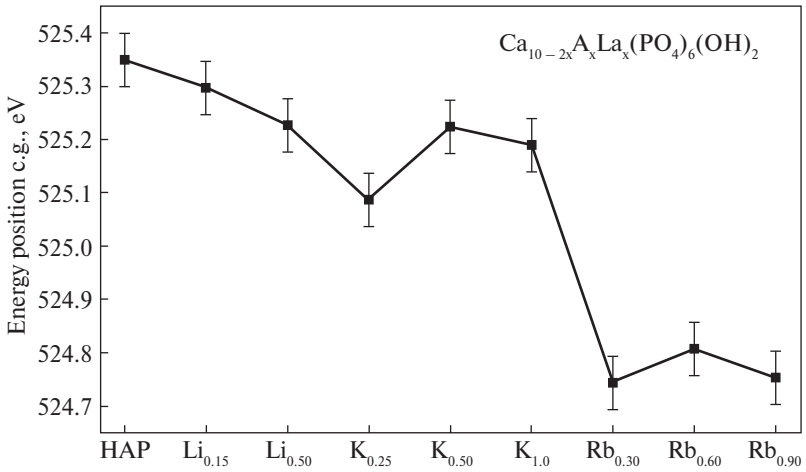

Fig. 5.10. Position of the centre of gravity of O K_α-line in isomorphically substituted hydroxyapatites of calcium

occurs both in $Ca_{(1)}$ and $Ca_{(2)}$ positions and arrangement of curves has symbasical character. There is no essential changes observed of position of the centre of gravity of O K_α-band by isomorphic modification with lanthanum and alkaline-earth elements for vanadium-containing apatites (fig. 5.11, 5.12). The exception is compound containing lithium and caesium. In this case there are observed differences in the position of the centres of gravity of O K_α-spectra, going beyond the limits of experimental error. There is observed considerable charge redistribution by modification with sodium and neodymium, and also with sodium and samarium described with a change of the energy centre of gravity of O K_α-lines (fig. 5.13).

Most likely, it is connected with chemical properties of elements (Sm and Nd) which unlike La and Ho may have valence, typical for atom that is replaced (2+) and, thus occupy easier both crystallographic positions of calcium. It is necessary to notice also that the important factor is thus the size of atom — ionic radiuses change for La — 1.30 Å, Nd — 1.25 Å, Sm — 1.22 Å.

The differences depending on position of the centres of gravity of O K_α-lines in phosphorus - and vanadium-containing apatites by isomorphic modifying with alkaline metals and lanthanum, most likely, are defined by different internal organization of tetrahedrons leading to smaller sensitivity of tetrahedral oxygen skeleton to cation substitutions in the case of vanadium hydroxyapatite that is probably connected with smaller spatial extent of *d*-states of vanadium, in comparison with valence *p*-states of phosphorus.

The constancy of O K_α-band position in compounds with lanthanum $Ca_{5-x}A_xLa_x(VO_4)_3OH$ by change of alkaline metal in the series Li→Na→K→Rb→Cs and the observed significant changes of the position of the centre of gravity of O K_α-line for sodium-containing compounds $Ca_{5-2x}Ln_xNa_x(VO_4)_3OH$ in the series La→Nd→Sm→Ho

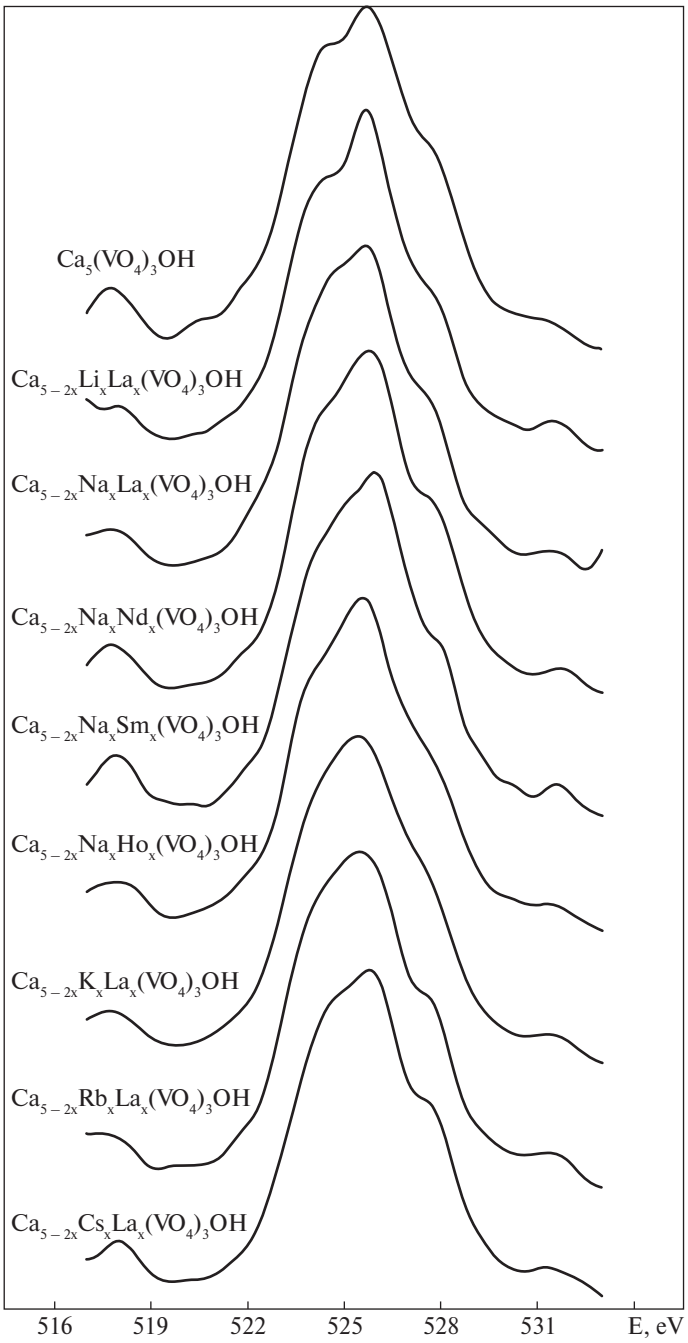

Fig. 5.11. X-ray O K_α-spectra of isomorphically substituted vanadates with apatite structure (x=0.05)

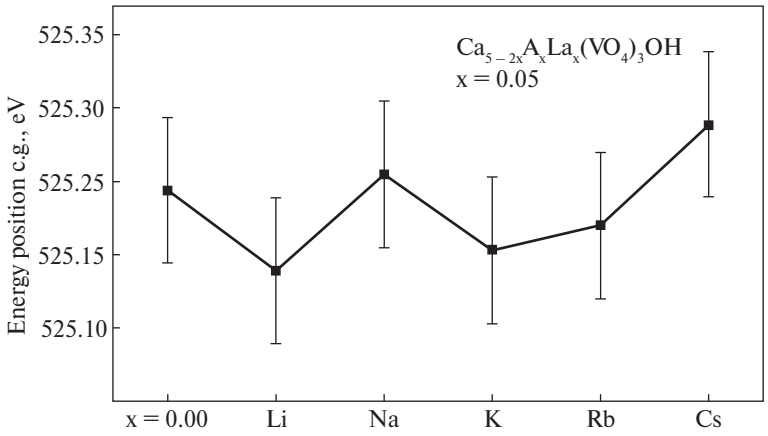

Fig. 5.12. Position of the centre of gravity of O K_α-spectra in isomorphically substituted calcium hydroxyvanadates

indicates the preferable calcium substitution for alkaline metals and rare-earth elements accordingly in $Ca_{(1)}$- and $Ca_{(2)}$-positions of apatite's structure. This is conformed with the change of *c* parameter of the apatite lattice in the case of apatites modified with REM. The change of *c* parameter in the investigated series of compounds almost completely correlates with a change of ionic radius of REM (fig. 5.14).

XPS studies have shown that modification of Sr-HAP with sodium and lanthanum leads to monotonous increase of binding energy of core levels of oxygen and strontium, and also to reduction of binding energy of P 2*s* level that indicates a loss of electronic density of oxygen and strontium and its increase in phosphorus atoms that in line with X-ray emission (tab. 5.4) studies. Levels of lanthanum and sodium by transition from $Sr_{10-2x}Na_xLa_x(PO_4)_6(OH)_2$ (x=0.5) to $Sr_{10-2x}Na_xLa_x(PO_4)_6(OH)_2$ (x=1.0) are shifted into area of larger binding energies that indicates electronic density transfer from lanthanum and sodium atoms to atoms of matrix.

By isomorphic substitutions in Sr-HAP binding energies of all levels undergo changes while linewidths remain unchanged. It must be noticed that using of P 2*p* line is complicated owing to superposition of Sr 3*d* line.

Partial isomorphic substitution of Sr for Na and La in strontium apatite depending on Na and La amounts leads to a reduction of binding energy of strontium core and valence electrons (tab. 5.5). Binding energy of P 2*s* electrons decreases by 0.2 eV,

Table 5.4. **Strontium *K*-edge absorbtion energy in compounds.**

Sample	E_{edge}, eV	Energy shift, eV
SrO	16143.9	0.00
$Sr_8NaLa(PO_4)_6(OH)_2$	16142.5	-1.41

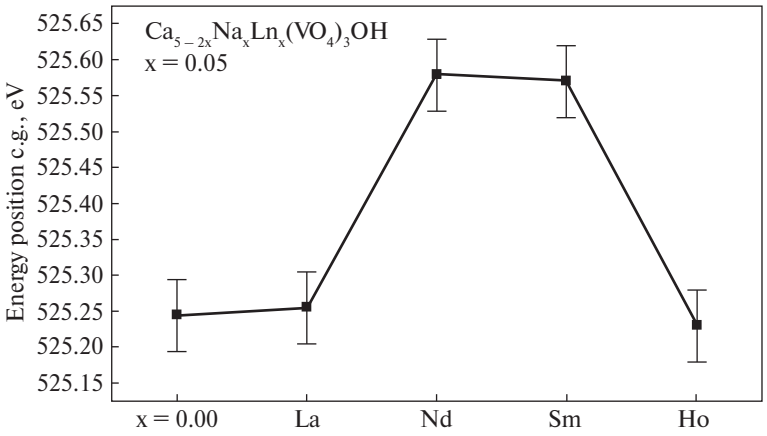

Fig. 5.13. Energy position of the centre of gravity of O K_α-band in compounds

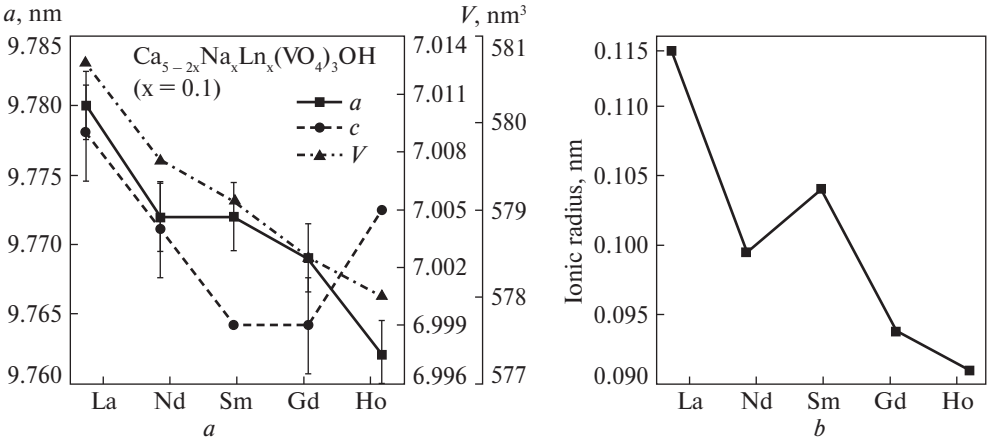

Fig. 5.14. The change of crystallographic parameters of Ca-HAP isomorphically modified with Na and REM (*a*), change of ionic radiuses of REM elements (*b*)

and binding energy of O 1*s* electrons remains unchanged. There is observed a small weakening of bonds of oxygen atoms with strontium and phosphorus.

In $Sr_8NaLa(PO_4)_6(OH)_2$ sample strontium core electrons increase binding energy by 0.1 eV whereas Sr 4*p* binding energy decreases by 0.3 eV. It indicates appreciable changes in the valence zone of this crystal. Lanthanum $3d_{5/2}$ line in this case is shifted towards larger binding energies by 0.5 eV in comparison with $Sr_9Na_{0.5}La_{0.5}(PO_4)_6(OH)_2$, and O 1*s* line moves by 0.2 eV that may indicate small weakening of Sr-O bond and strengthening of La-O and P-O bonds.

Hence, small amounts of sodium and lanthanum do not change the position of O 1*s* level, however by *x*=1 the displacement of O 1*s* level into area of larger binding energies

is observed. By transition from compound with x=0.5 to compound with x=1.0 lanthanum and sodium levels are shifted into area of larger binding energies that indicates a transfer of electronic density from lanthanum and sodium atoms to atoms of matrix.

Consideration of X-ray electron data of calcium-containing compounds (tab. 5.6) shows a decrease of binding energies of core electrons of oxygen and calcium by isomorphic modifying with lanthanum and potassium. It can be seen, that there is no monotonous dependence of change of binding energies of core electrons on concentration of dopants observed. Thus for $Ca_{10-2x}K_xLa_x(PO_4)_6(OH)_2$ (x=0.8) sample binding energies of Ca 2*s* and La 3*d*-levels were higher, and of O 1*s*-level lower, than for samples with x=0.5 and x=1.0. This fact may be attributed to violation of substitution priority of calcium in one of two crystallographic calcium positions. Larger shift for Ca 2*s*-level in comparison with Ca $2p_{1/2}$-level and an constancy for Ca $2p_{3/2}$—level indicates that general only *s*-density participates in redistribution that agrees with the calculation data (fig. 5.15). It can be seen that by modifying of Ca-HAP with potassium and lanthanum the contribution of *s*-density of calcium in full DOS increases, with simultaneous reduction of the contribution of *d*-states.

Table 5.5. **Electron binding energy E_b (eV), linewidth (Γ) (eV) (measured at half-height) of core levels of Sr atoms, oxides of Sr, Na, La and investigated compounds.**

Sample	O 1*s*	Sr 3*s*	Sr 3*p*	Sr 4*p*	P 2*s*	Na 1*s*	La 3*d*
$Sr_{10}(PO_4)_6(OH)_2$	531.1	357.7	269.2		190.5		
$Sr_{10-2x}Na_xLa_x(PO_4)_6(OH)_2$ x=0.5	531.1 (2.2)	357.6 (4.1)	269.0 (2.9)	19.4	190.4 (2.9)	1072.4 (2.1)	835.6
$Sr_{10-2x}Na_xLa_x(PO_4)_6(OH)_2$ x=1.0	531.3 (2.3)	357.9 (4.7)	269.2 (2.8)	19.2	190.5 (2.8)	1072.7 (1.6)	836.1
$La(OH)_3$ [228]	531.1	—	—	—	—	—	835.0
La_2O_3 [228]	529.0	—	—	—	—	—	834.9
LaF_3 [228]	—	—	—	—	—	—	836.0

E_b values are given relatively to E_b (C1s) =285.0 eV; — an error ±0.1 eV.

Table 5.6. **Electron binding energy E_b (eV) of compounds.**

Compound	O 1*s*	Ca 2*s*	Ca $2p_{3/2}$	Ca $2p_{1/2}$	La $3d_{5/2}$
$Ca_{10}(PO_4)_6(OH)_2$	532.4	439.2	347.5	351.2	—
$Ca_{10-2x}K_xLa_x(PO_4)_6(OH)_2$ x = 0.5	531.0	438.7	347.1	350.7	835.3
$Ca_{10-2x}K_xLa_x(PO_4)_6(OH)_2$ x = 0.8	530.7	438.9	347.1	350.6	835.6
$Ca_{10-2x}K_xLa_x(PO_4)_6(OH)_2$ x = 1.0	531.0	438.7	347.0	350.7	835.4

Proceeding from the assumption that these changes are less expressed in the case of doping with potassium in comparison with lanthanum (fig. 5.15) it can be concluded, that namely modifying with lanthanum leads to the significant redistribution in electronic states of atoms of a crystal. There is also a correlation between calculation and experimental data on the displacement of *s* - and *p*-density maxima of calcium towards smaller binding energies by doping. The participation of H *s*-density in chemical bond by transition to potassium- and lanthanum-containing compounds increases significantly. The behaviour of oxygen *s*- and *p*- densities of hydroxyl group is similar.

Hence, there are reasons to believe that calcium substitution in $Ca_{(2)}$ position under the scheme $2Ca^{2+}=La^{3+}+K^{+}$ leads to an increase of chemical bond of hydroxyl group directed along *c* axis of a crystal.

It is also interesting that by substitution with lanthanum the main feature in $O_{(7)}$ *s*-density curve nearby 22 eV disappears, with simultaneous increase in electronic density on lanthanum. The main maximum of $O_{(7)}$ *p*-density is also considerably displaced towards larger binding energies. Considering topological position of $O_{(7)}$ it is possible to conclude that doping with lanthanum leads to the significant change of symmetry of the tetrahedrons, that appears according to experimental data in its increase.

From examination of DOS of compounds it can be een that modifying of Ca-HAP with potassium practically does not change the curve shape with the exception of increase in intensity of feature nearby 14 eV while calcium substitution for lanthanum significantly changes the DOS curve shape on all its length. The observed changes of the shape of DOS curve of compound of $Ca_8KLa(PO_4)_6(OH)_2$ composition basically are determined with the influence of valence states of lanthanum.

Unlike phosphorus-containing compounds in vanadate-containing compounds there is no such considerable change of the shape of DOS curve (fig. 5.16).

To all appearances it is connected with the properties of tetrahedral ions. Unlike PO_4^{3-} VO_4^{3-} possess large size and, as a consequence, the vanadate compounds possess large size of elementary cell (tab. 5.7) and taking into account small topological extent of vanadium *d*-states in comparison with phosphorus *p*-states it is possible to expect less expressed changes in electronic structure by doping.

So doping with lanthanum and lithium leads to the displacement of the main maximum of DOS curve to the area of larger binding energies (~1 eV) and to occurrence of an additional maximum nearby ~3eV which as it can be seen from fig. 5.16 is generated basically, as well as all features of DOS curve in the area of 3 ÷ 8 eV with *s*-, *p*-, *d*-states of calcium, *p*-states of oxygen from the environment of lanthanum and *p*-, *d*-, *f*-states of lanthanum. There is also observed a significant contribution of *p*-states of vanadium to this feature. And a small feature nearby ~16 eV, formed by valence states of lithium, lanthanum and oxygen from their environment ($O_{(7)}$, $O_{(8)}$) (fig. 5.16). The transition to sodium-containing compound almost does not change the form of DOS curve except that it becomes smoother. The feature nearby 16 eV is shifted towards smaller binding energies by ~1 eV.

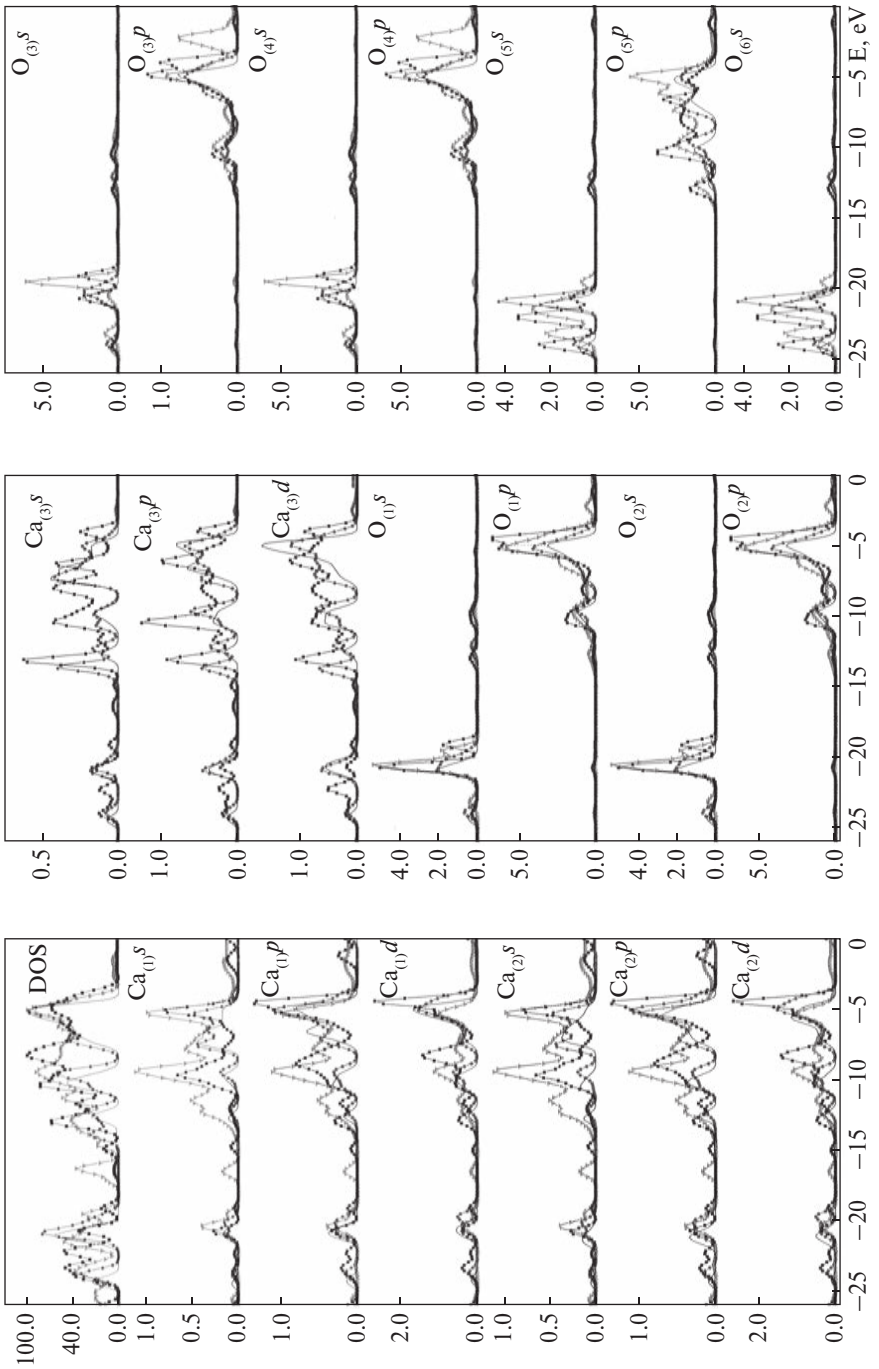
DOS
Ca(1)s
Ca(1)p
Ca(1)d
Ca(2)s
Ca(2)p
Ca(2)d
Ca(3)s
Ca(3)p
Ca(3)d
O(1)s
O(1)p
O(2)s
O(2)p
O(3)s
O(3)p
O(4)s
O(4)p
O(5)s
O(5)p
O(6)s
E, eV

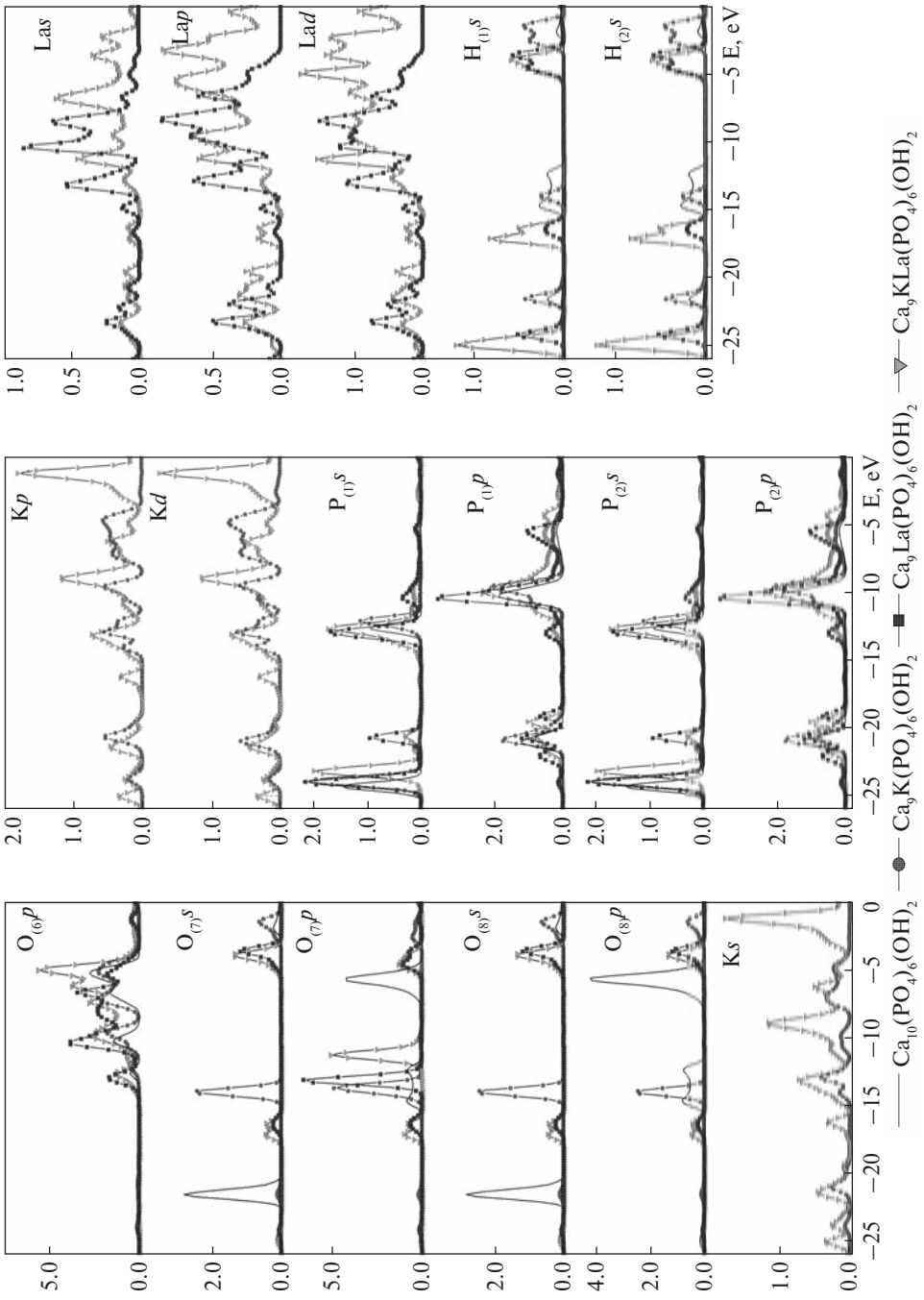

Fig. 5.15. Total and partial densities of states of compounds

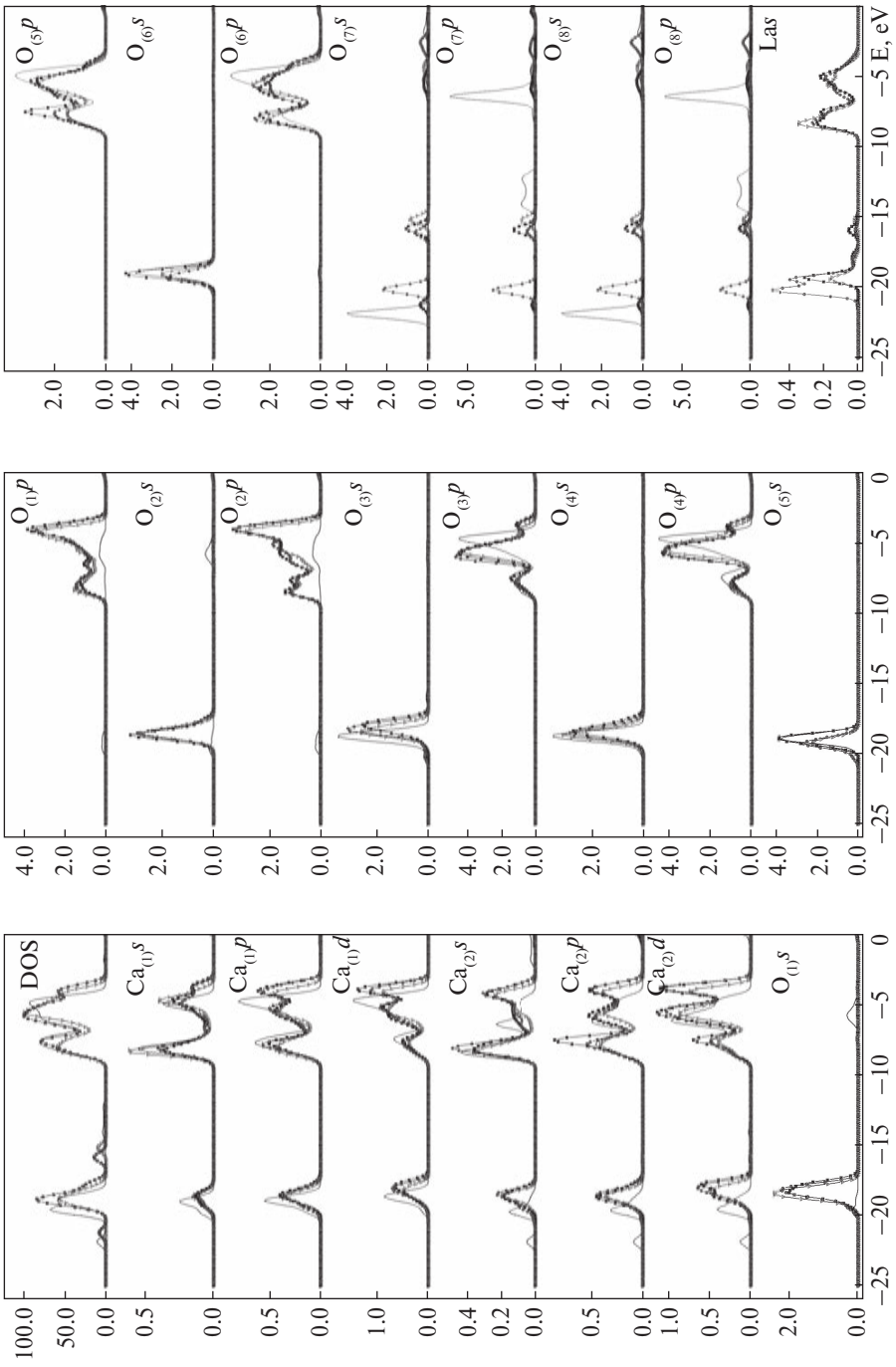
DOS
Ca(1)s
Ca(1)p
Ca(1)d
Ca(2)s
Ca(2)p
Ca(2)d
O(1)s
O(1)p
O(2)s
O(2)p
O(3)s
O(3)p
O(4)s
O(4)p
O(5)s
O(5)p
O(6)s
O(6)p
O(7)s
O(7)p
O(8)s
O(8)p
Las
E, eV

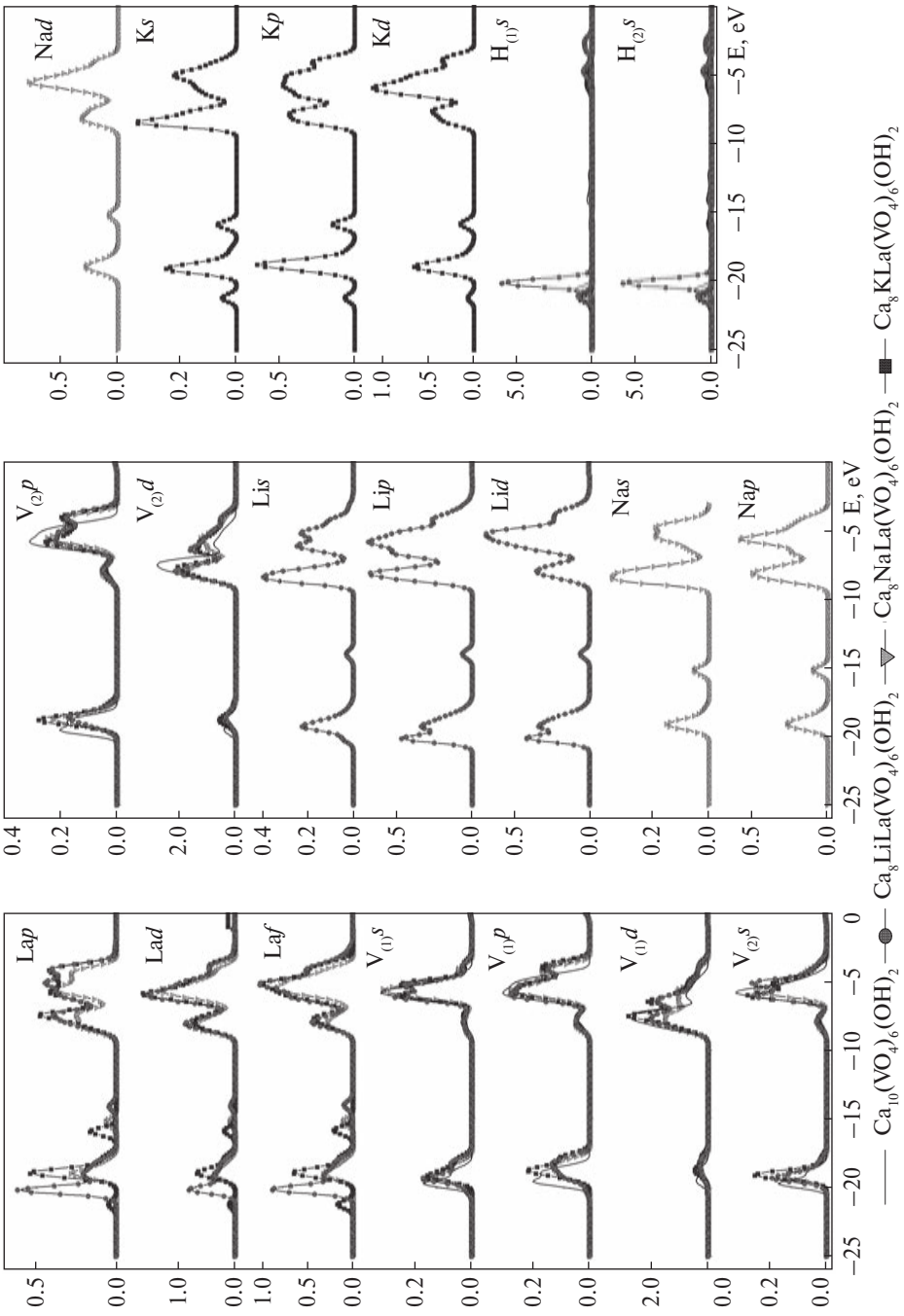

Fig. 5.16. Total and partial densities of states of compounds

DOS curves for lithium- and potassium-containing compounds practically coincide. However, transition alkaline metals with larger atomic number changes the form and position of features. For rubidium compound the feature in the middle of a valency band nearby ~15 eV disappears. A contribution to full electronic density of states at the bottom of a valence zone becomes relatively more expressed. It can be seen that the peak nearby ~18 eV becomes broader and more intensive. The

Table 5.7.**Change of crystallographic parameters by isomorphic substitution*.**

Composition	a	c	V
$Ca_{5-2x}M_x^{+}M_x^{3+}(VO_4)_3OH$ (x=0.1)			
$Ca_5(VO_4)_3OH$	9.768	7.003	578.60
$Ca_{5-2x}Li_xLa_x(VO_4)_3OH$	9.774	7.006	579.60
$Ca_{5-2x}Na_xLa_x(VO_4)_3OH$	9.780	7.009	580.70
$Ca_{5-2x}K_xLa_x(VO_4)_3OH$	9.781	7.006	580.55
$Ca_{5-2x}Rb_xLa_x(VO_4)_3OH$	9.778	7.009	581.52
$Ca_{5-2x}Cs_xLa_x(VO_4)_3OH$	9.781	7.010	580.86
$Ca_{5-2x}Na_xNd_x(VO_4)_3OH$	9.772	7.004	579.57
$Ca_{5-2x}Na_xSm_x(VO_4)_3OH$	9.772	6.999	579.10
$Ca_{5-2x}Na_xGd_x(VO_4)_3OH$	9.769	6.999	578.46
$Ca_{5-2x}Na_xHo_x(VO_4)_3OH$	9.762	7.005	578.00
$Ca_{5-2x}M_x^{+}M_x^{3+}(PO_4)_3OH$			
$Ca_5(PO_4)_3OH$	9.433	6.897	
$Ca_{5-2x}Li_xLa_x(PO_4)_3OH$ (x=0.1)	9.430	6.886	
$Ca_{5-2x}Li_xLa_x(PO_4)_3OH$ (x=0.5)	9.453	6.917	
$Ca_{5-2x}Li_xLa_x(PO_4)_3OH$ (x=1.0)	9.467	6.946	
$Ca_{5-2x}Na_xLa_x(PO_4)_3OH$ (x=0.1)	9.410	6.900	
$Ca_{5-2x}Na_xLa_x(PO_4)_3OH$ (x=0.6)	9.440	6.930	
$Ca_{5-2x}Na_xLa_x(PO_4)_3OH$ (x=1.0)	9.457	6.963	
$Ca_{5-2x}K_xLa_x(PO_4)_3OH$ (x=0.1)	9.447	6.901	
$Ca_{5-2x}K_xLa_x(PO_4)_3OH$ (x=0.6)	9.478	6.943	
$Ca_{5-2x}K_xLa_x(PO_4)_3OH$ (x=1.0)	9.521	7.016	
$Ca_{5-2x}Cs_xLa_x(PO_4)_3OH$ (x=0.1)	9.446	6.899	
$Ca_{5-2x}Cs_xLa_x(PO_4)_3OH$ (x=0.5)	9.461	6.932	

** — the data are given by Inorganic Chemistry Department of Donetskiy State University. - An error is 0.005 Å.*

transition to caesium-containing compound shows the increase of intensity of this feature with simultaneous tailing of peaks at the top of a valence zone. The feature in the middle of the valence band, connected with electronic states of dopants is observed again. For partial densities of lanthanum there are typical changes observed — however, topologically, atoms of dopes are located wide apart that eliminates their interaction and therefore it is expected that partial valence densities of states of lanthanum should show an invariance in the investigated series of substitutions Li→Na→K→Rb→Cs. Essential changes occur in curves of La *s*-, *p*-, *d*- and *f*-states mainly nearby 20 eV. Only caesium-containing compound is characterized with a significant increase in intensity of peak of lanthanum *p*-density in the range of small binding energies ~4 eV (fig. 5.17).

The observed changes in curves of partial densities of lanthanum *f*-states in the investigated series of substitutions Li→Na→K→Rb→Cs can be referred to interaction in the metal sublattice (fig. 5.18). These changes are small and do not exercise a significant influence on DOS shape.

Consideration of given sodium-containing compounds in the series La→Nd→Sm→Gd→Ho shows more significant changes in the curves of *f*-states. Thus, for samarium-containing compound there is observed an increase of the contribution of *f*-states to DOS, in comparison with La, Nd, Gd and Ho-containing compounds. This can be explained with the fact that among REM only samarium except oxidation level of +3 has oxidation level of +2.

Change of REM in the series La→Nd→Sm→Gd→Ho while preserving sodium in the series of alkaline metals shows a displacement of two basic groups of valence band features — at the valence band top (~2.5 ÷ 9.5 eV) and at the valence band bottom (~17.5 ÷ 22.5 eV) which is rather opposite to doping with different alkaline metals while preserving the same REM. Thus for lanthanum-containing vanadates the change of metal in the series Li→Na→K→Rb→Cs leads to the increase of fine structure of group of features at the valence band top and to its broadening by 1 eV. The features at the valence band bottom possess the same behaviour in the investigated series with a some increase of peak intensity.

For compounds with a change of REM in the series La→Nd→Sm→Gd→Ho the effect of "subsidence" is observed. As it can be seen from fig. 5.19, all features of a valence band increase binding energy. There is observed a displacement nearby 2 eV for end compounds in the series.

Unlike phosphorus-containing compounds vanadium-containing ones show in the investigated series an invariance of the middle part of the valence band located between two groups of features. As it was mentioned above, it is determined with the nature of tetrahedral ions and their hybridized valence orbitals (fig. 5.19).

Partial vanadium *s*- and *p*-densities undergo small changes. The contribution of vanadium *d*-states to DOS in the investigated series against the increase of the contribution of sodium *s*-states nearby 20 eV decreases essentially.

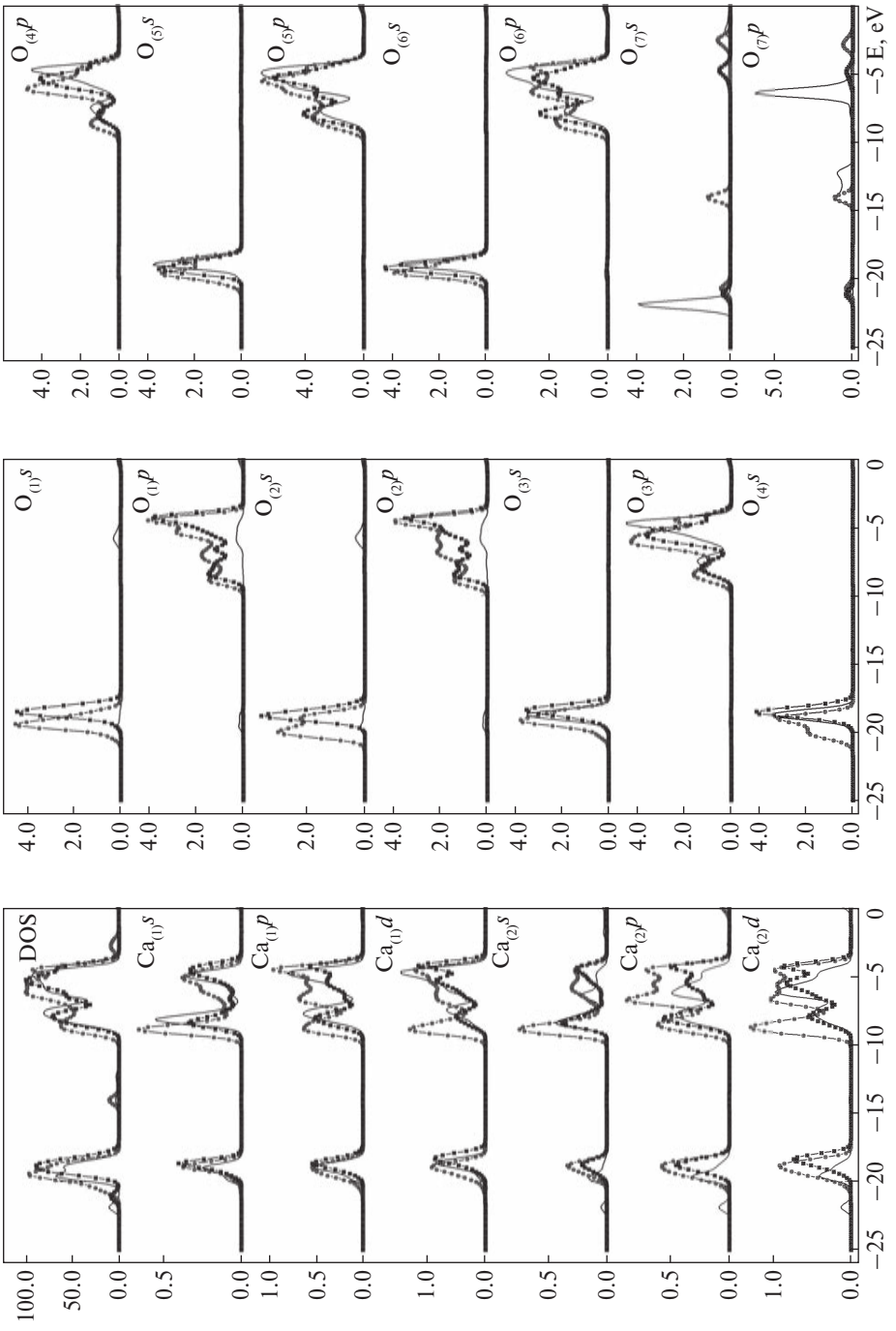
DOS
Ca(1)s
Ca(1)p
Ca(1)d
Ca(2)s
Ca(2)p
Ca(2)d
O(1)s
O(1)p
O(2)s
O(2)p
O(3)s
O(3)p
O(4)s
O(4)p
O(5)s
O(5)p
O(6)s
O(6)p
O(7)s
O(7)p
E, eV

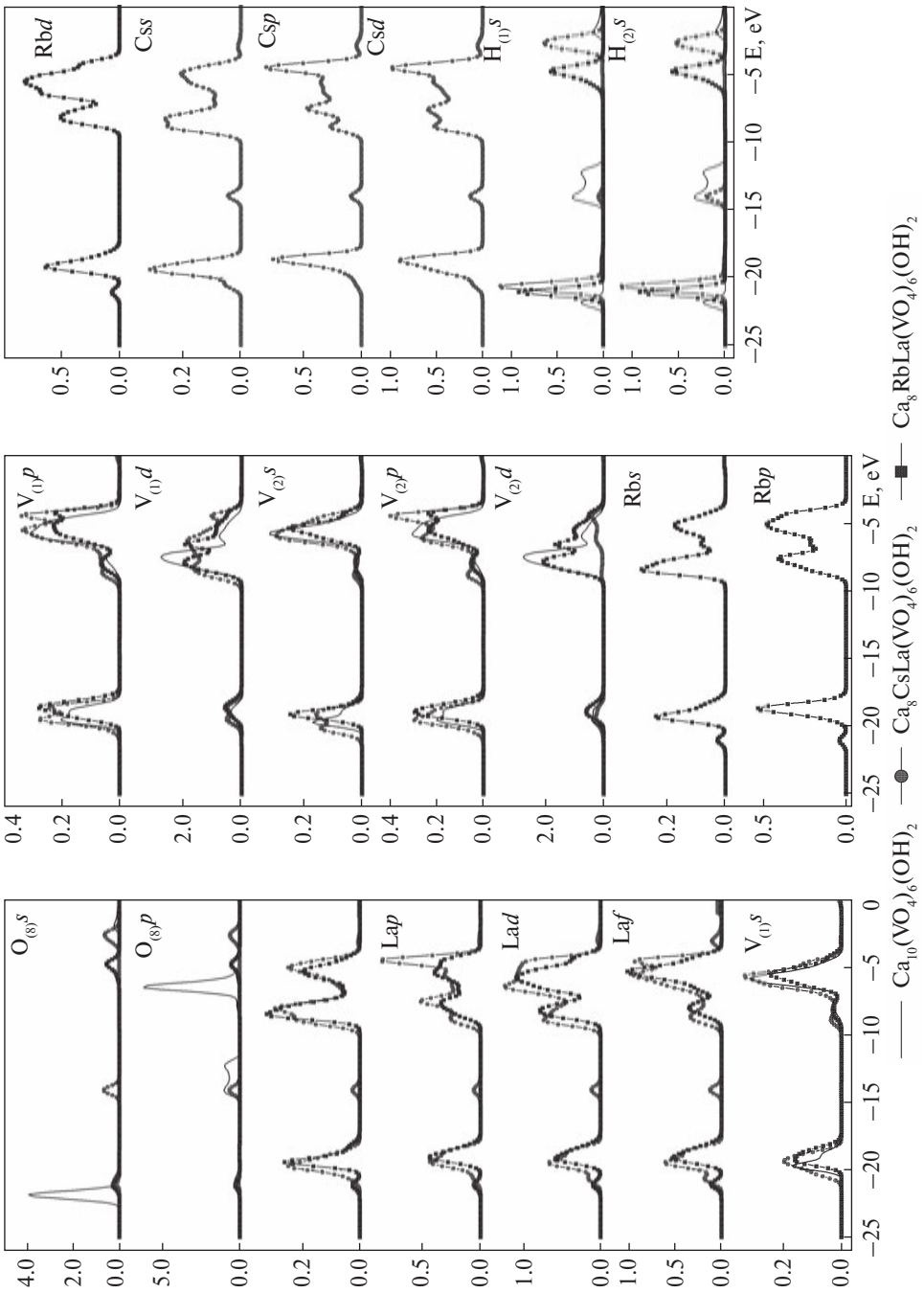

Fig. 5.17. Total and partial densities of states of compounds

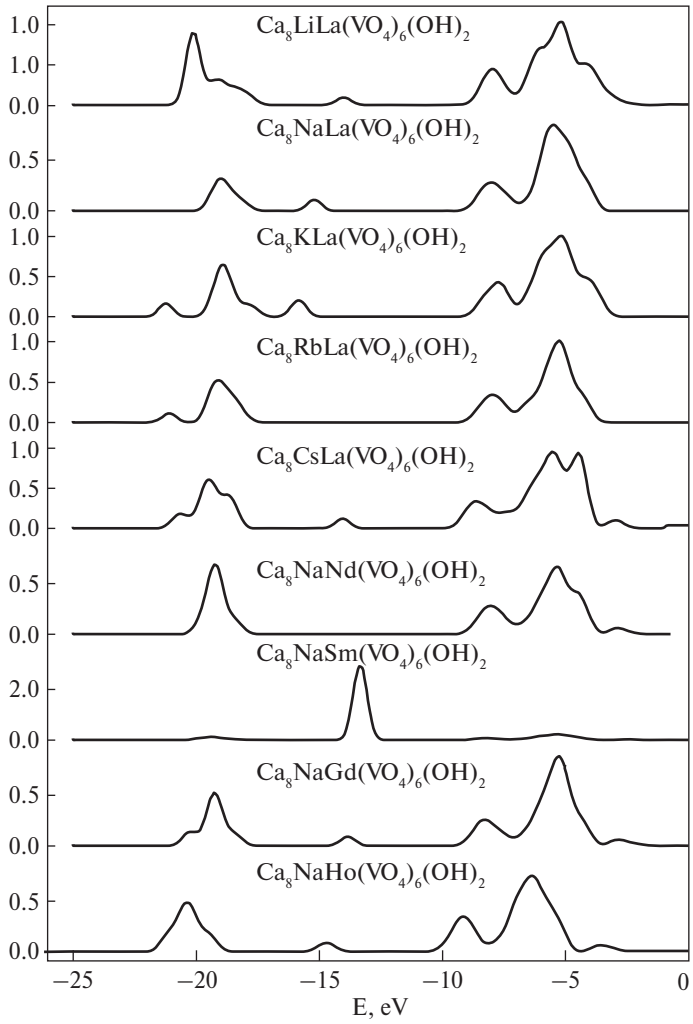

Fig. 5.18. Partial densities of *f*-states of REM in compounds

There is observed an increase of the contribution of hydrogen *s*-states nearby 20 eV by preservation of alkaline metal in the series La→Nd→Sm→Gd→Ho with a considerable reduction of the contribution of *s*- and *p*-states of hydroxyl oxygen (fig. 5.20, 5.21).

Hence, isomorphic modifying of calcium hydroxyvanadate with sodium and REM little changes the structure of peaks in DOS curve in the series La→Nd→Sm→Gd→Ho, leading only to the overall displacement of all groups of peaks towards larger binding energies.

Consideration of change of crystal total energy by isomorphic substitutions, obtained from quantum mechanical calculations in LMTO-approach (fig. 5.22),

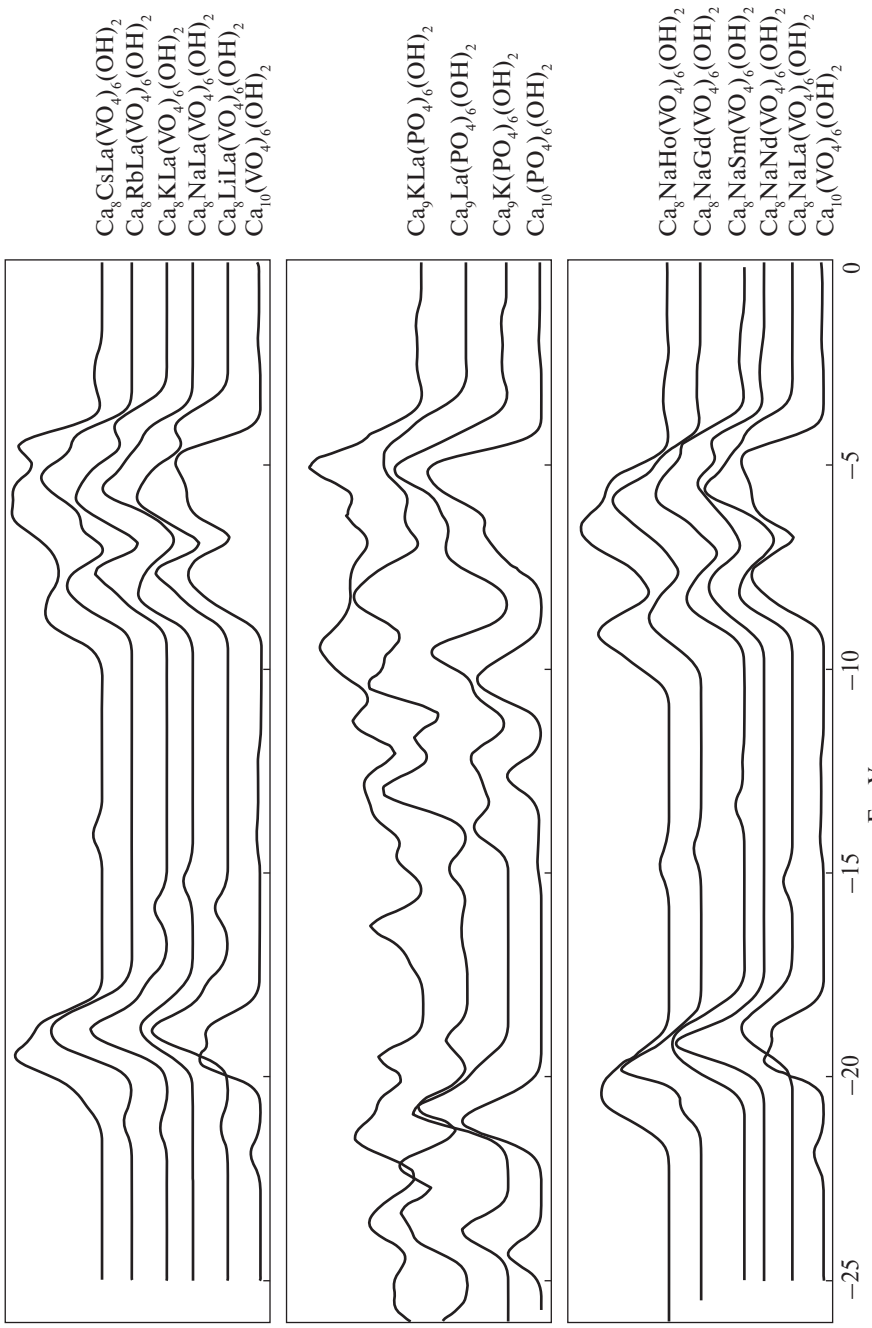

Fig. 5.19. Total densities of states of compounds

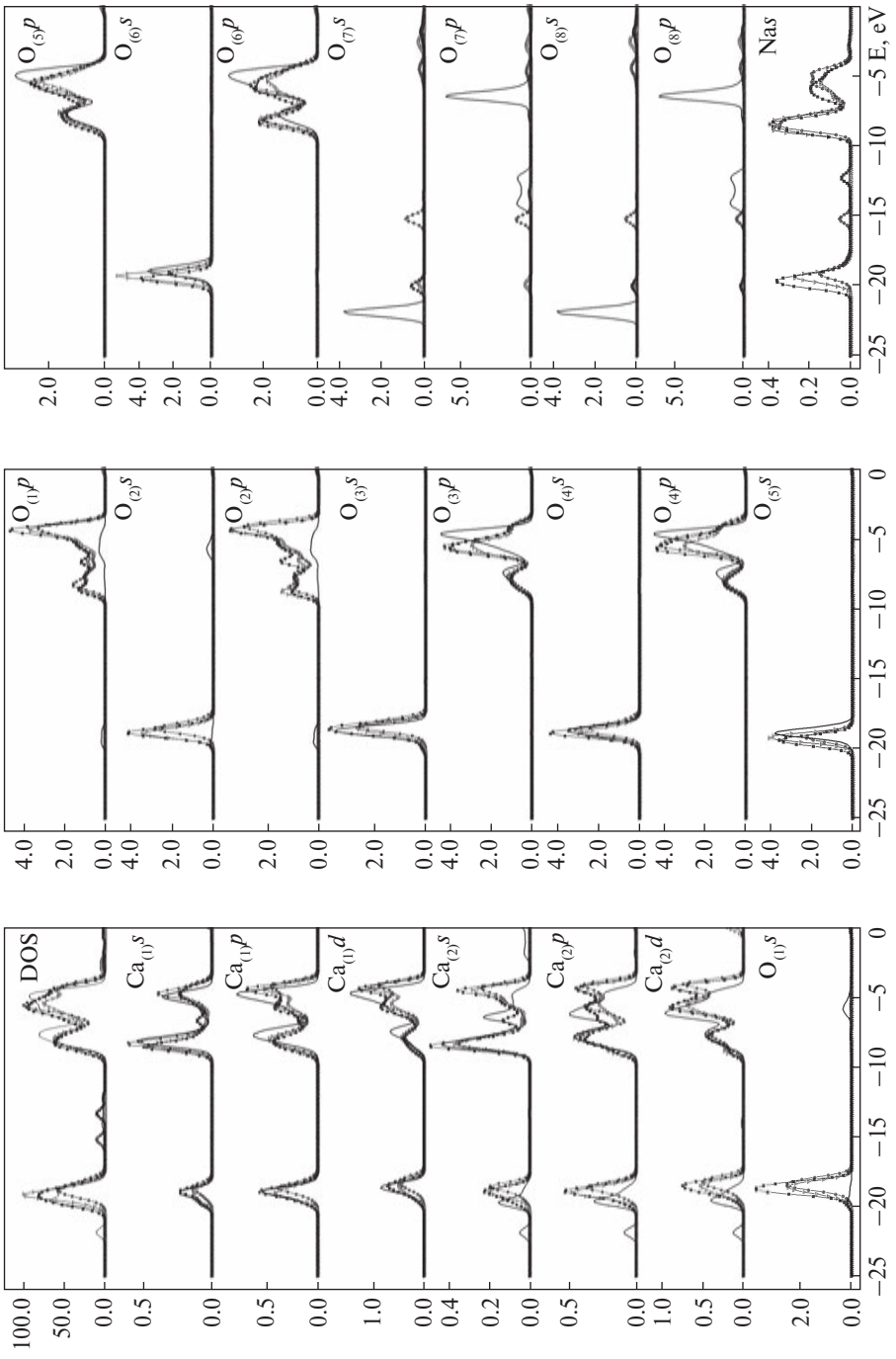
DOS
Ca(1)s
Ca(1)p
Ca(1)d
Ca(2)s
Ca(2)p
Ca(2)d
O(1)s
O(1)p
O(2)s
O(2)p
O(3)s
O(3)p
O(4)s
O(4)p
O(5)s
O(5)p
O(6)s
O(6)p
O(7)s
O(7)p
O(8)s
O(8)p
Nas
E, eV

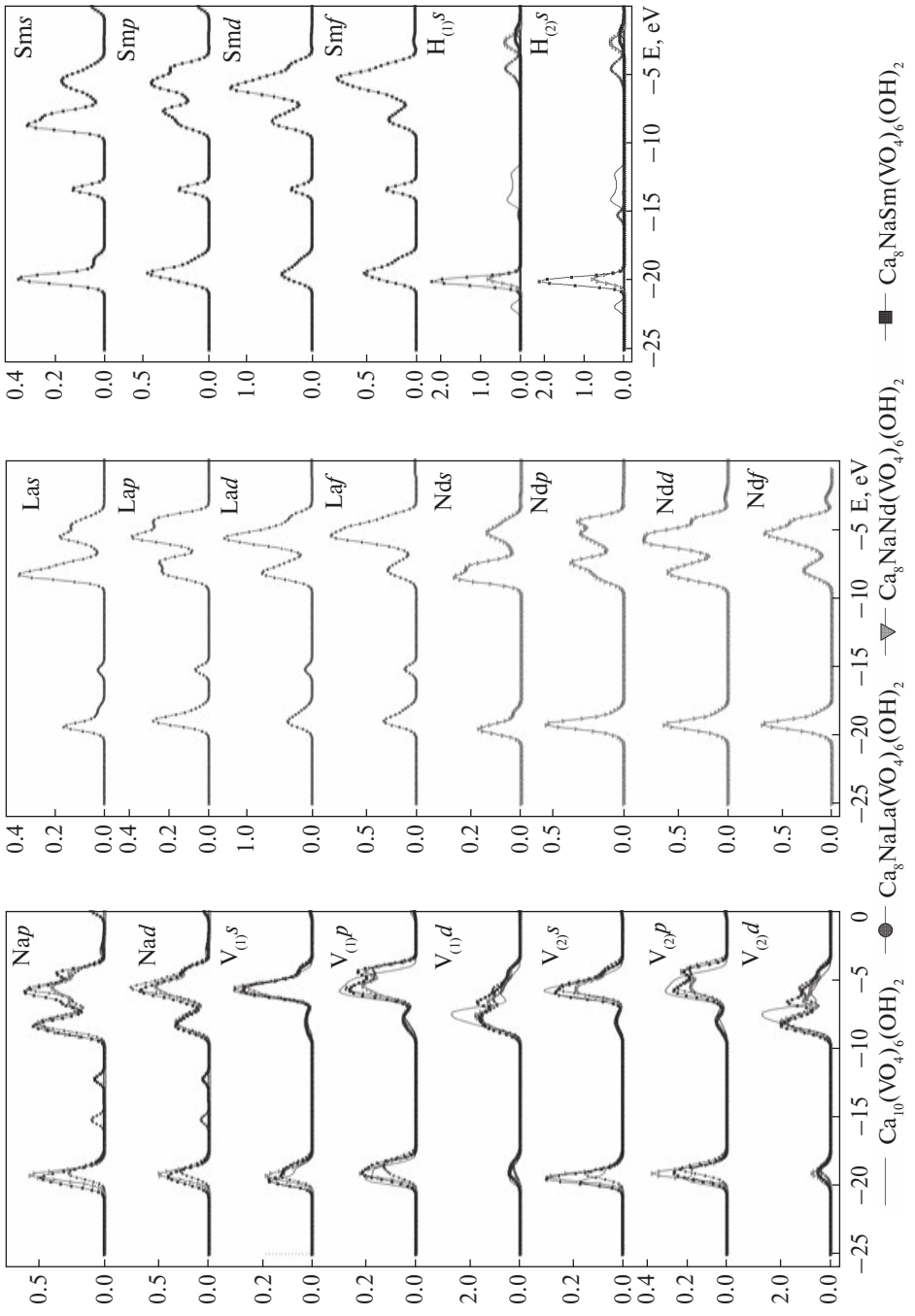

Fig. 5.20. Total and partial densities of states of compounds

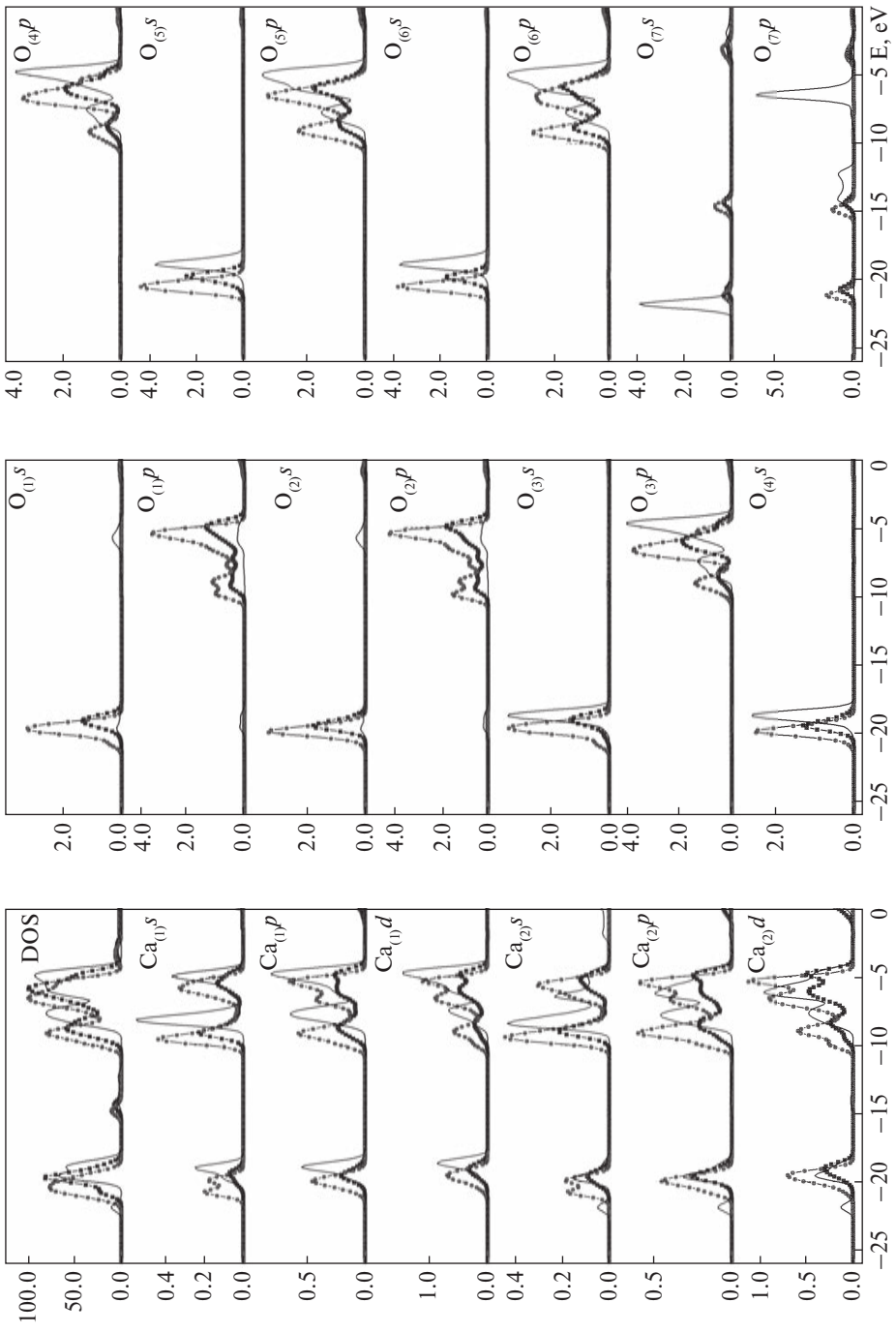
DOS
Ca(1)s
Ca(1)p
Ca(1)d
Ca(2)s
Ca(2)p
Ca(2)d
O(1)s
O(1)p
O(2)s
O(2)p
O(3)s
O(3)p
O(4)s
O(4)p
O(5)s
O(5)p
O(6)s
O(6)p
O(7)s
O(7)p
E, eV

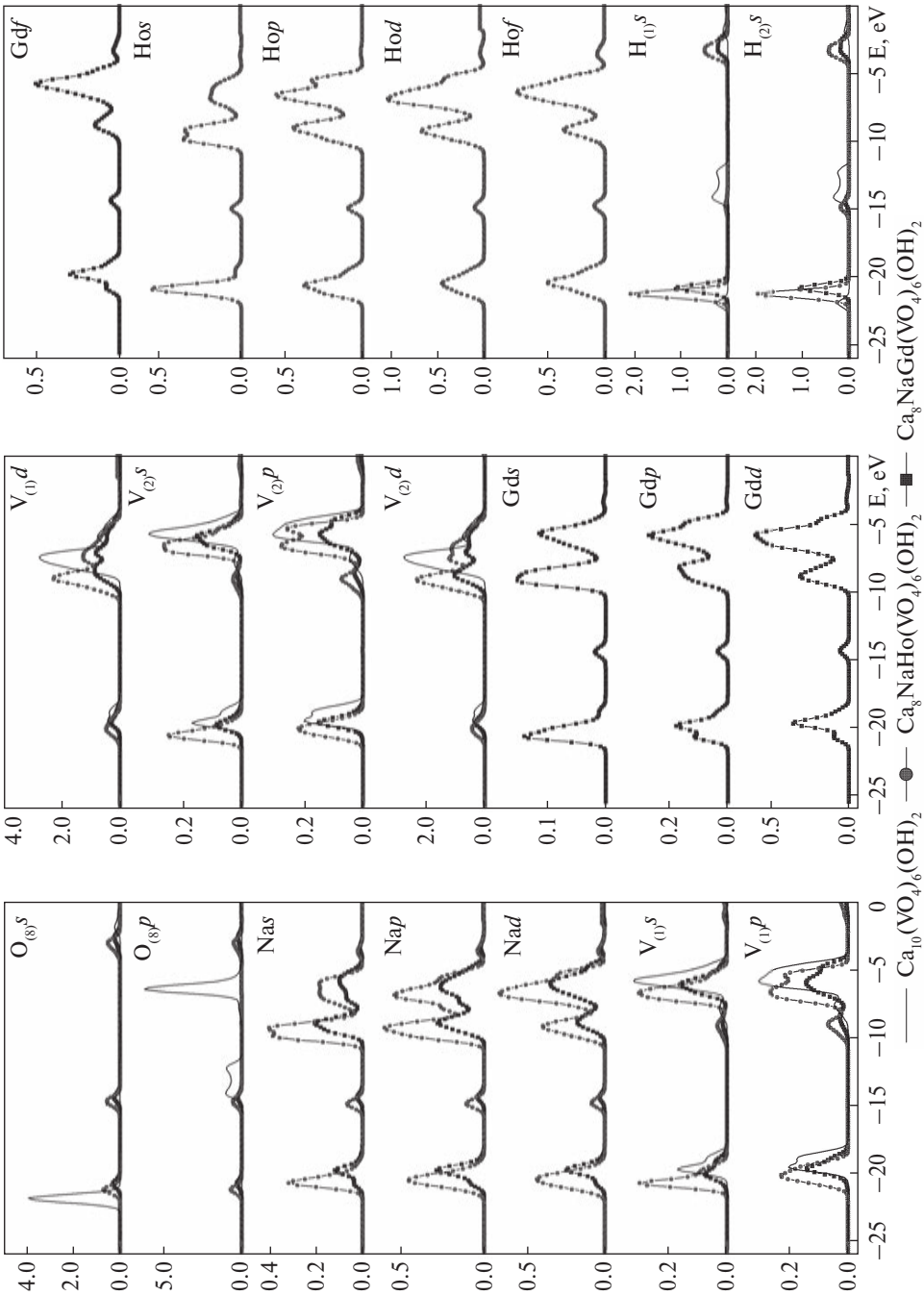

Fig. 5.21. Total and partial densities of states of compounds

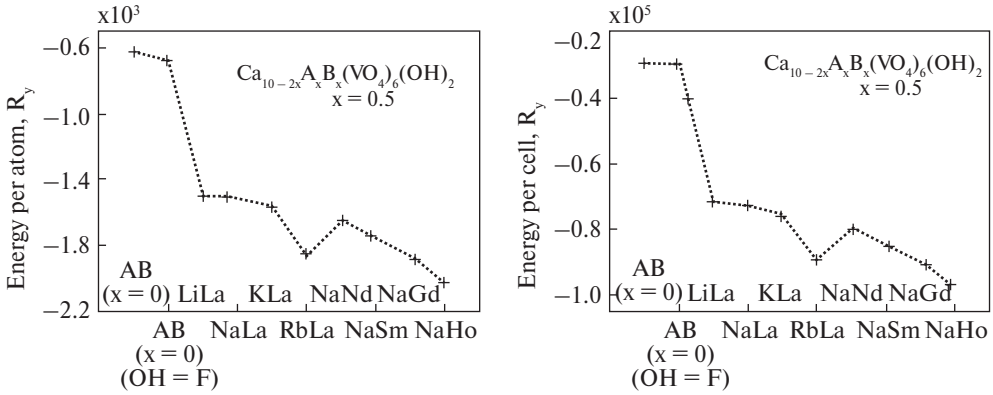

Fig. 5.22. Change of energy of calcium hydroxyvanadate crystal by calcium substitution for REM and alkaline metals

shows its reduction in the investigated series. There is observed a monotonous reduction of crystal energy with an increase of atomic nubmer of alkaline metal and REM. This fact agrees well with the data about a difficulty of obtaining of monocrystals of apatites, and also with the absence of apatites without impurities in the nature.

5.4. Isomorphic modification of calcium apatite by uranium

The inherent part of wastes of modern technogenesis along with heavy metals (Pb, Sn etc.) are metals of actinoid series that determines the scientific interest in the research of ways of their migration and accumulation [254 - 261]. One of the most used elements of actinoid number in industry is uranium which in the nature exists in two valence states — U^{4+} and U^{6+}. Ionic radiuses of actinoid oxides decrease with the increase of atomic number from Ac^{3+} (1.11 Å) to Cf^{3+} (0.94 Å) - "actinoid compression". Though there is an exception for uranium and plutonium. Owing to similarity of ionic radiuses of U^{4+} (0.93 Å) and Ca^{2+} (0.94 Å) various isomorphic substitutions are possible in apatite structure. In uraniferous minerals of calcium uranium is not an isomorphic impurity, and forms a mineral phase. However, it is possible to synthesise calcium hydroxyapatite isomorphically modified with uranium.

There have been desribed researches of metal substitution in apatite structure for uni- and bivalent metals before. Substitutions for elements in high valency states were practically not studied. It may be expected that such modifying will expand the possibility to influence directionally on the structure of apatite for the purpose of obtaining of practically significant properties. Recently, besides other applications calcium hydroxyapatite is also investigated as a matrix for a burial of radioactive waste and a storage of ecologically dangerous compounds of heavy metals. The high

specific surface of hundreds of square meters per one gramme of substance determines high reactivity of nanodispersed calcium hydroxyapatite.

In this paragraph the changes of electronic structure of calcium apatite, initiated with isomorphic modification by uranium are investigated. The researche was carried out using the method of X-ray photoelectron spectroscopy, as the most direct method of investigation of electronic structure of chemical compounds with using of quantum mechanical modeling using LMTO approach.

The key question in understanding of the electronic structure of actinoid-based compounds is the role of 5*f*-electrons. Namely do 5*f*-electrons remain localized as it happens with 4*f*-electrons in REM, or their conditions have zonal character. It was considered that the electronic structure of actinoids is similar to REM, i.e. it was assumed that the 5*f*-shell is strongly localized and the corresponding *f*-electrons do not take part in a chemical bond. However, such picture has appeared not absolutely true [253]. The degree of delocalization of 5*f*-electrons in actinoids is even higher, than of 3*d*-electrons of the elements of the first transitional period (fig. 5.23).

The configuration of neutral uranium atom is [radon] $5f^3 6d^1 7s^2$. Among REM neodymium has similar configuration. However unlike the latter, uranium atoms don't have localized magnetic moment connected with 5*f*-electrons. The intersection of 5*f*-level with 6*d*- and 7*s*-levels leads to formation of 6*d*-transitive period including thorium, protactinium, uranium and neptunium.

As it is described above, calcium hydroxyapatite valence band ranges from 0 up to 25 eV. It is caused with a formation of external and internal valence molecular orbitals in this crystal, generally connected with interaction of Ca $3p^6 4s^2$, P $3s^2 3p^3$ and O $2s^2 2p^4$ shell electrons of the adjacent atoms.

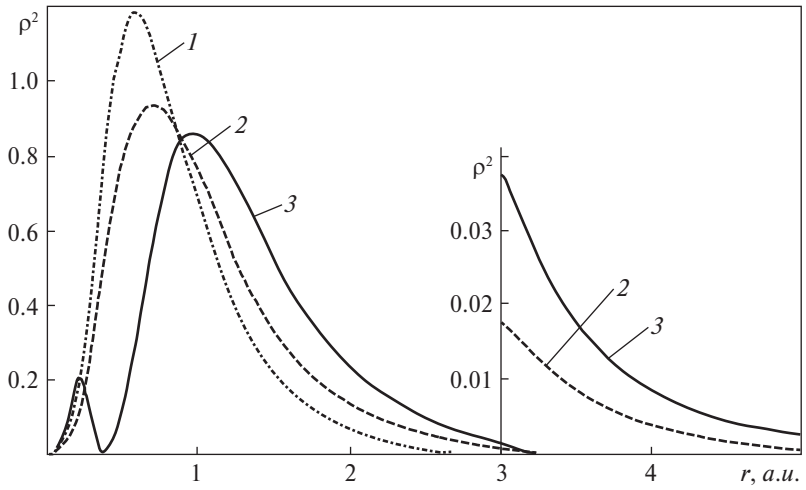

Fig. 5.23. A comparison of radial distribution of electrons: 1 — 3*d*-electrons in Fe; 2 — 4*f*-electrons in Sm; 3 — 5*f* -electrons in Pu [253]

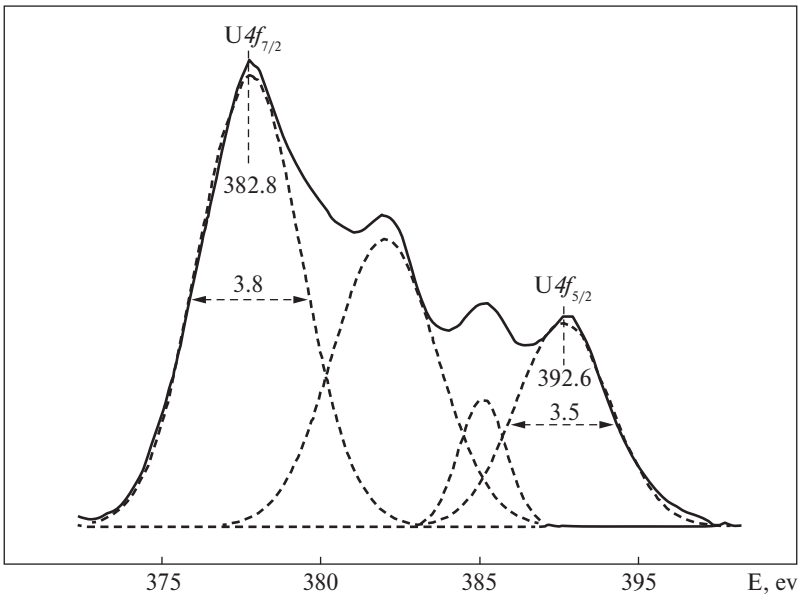

Fig. 5.24. U 4*f* X-ray spectrum in apatite

By isomorphic substitution of calcium atoms for uranium atoms in calcium apatite according to XPS there was determined an insignificant quantity of CO_3^{2-}-groups.

X-ray photoelectron spectrum of U 4*f*-electrons consists of two basic lines, caused with spin-orbital splitting nearby 10.2 eV, and shake-up satellites observed in the range of larger binding energies (fig. 5.24). Such structure of satellites is characteristic for uranium having oxidation state of 6+.

The most successful methods for determining the structural position of uranium in hydroxyapatite can be analysis of uranium XANES and EXAFS spectra. $O=U=O^{2+}$ orientation can be determinate from U L_3 and L_1 spectra of absorption edge [262]. $O=U=O^{2+}$ are structurally long rods (1.8 Å in length). The most intensive peak in Fourier transformant of L_3 edge of EXAFS spectrum depends on an angle of dispersion. The comparison of spectra of apatite samples with uranyl sorption between base planes of apatite as a function of angle of dispersion, allows to determine orientation of cations [263].

We have made an attempt to determine location of uranium ions in apatite's structure using X-ray spectroscopy and quantum-mechanical calculations.

Table 5.8 contains values of bonding energy of core electrons of metal Ca atoms, calcium and uranium oxides and of the investigated compounds. By isomorphic substitution of calcium for uranium in Ca-HAP all atoms undergo changes in electron binding energy. Oxygen O 1*s* line increases binding energy by 1.0 eV with preservation of linewidth. Lines of calcium core electrons move towards larger binding energies, so for Ca 2*s*-level the shift is 1.1 eV; for Ca 2*p* lines - 1.0 eV, respectively. The line of P 2*p*-electrons in this case is displaced towards larger binding energies by 1.0 eV too. Hence,

by isomorphic modification of Ca-HAP with uranium there are appreciable changes in electronic structure of Ca-HAP components, and, larger shift is observed for the electronic levels located closer to the upper edge of a valence zone [264].

Binding energy of uranium 4*f*-electrons atoms is close to that in UO_3 compound [266] that indicates the maximum valence of uranium atoms. However, in uraniferous apatite shift of binding energy of 4*f*-electrons is considerably larger, than for UO_3, at thus symbasic change of spectrum linewidth is observed, i.e. the effect of small quantity of substance or "cluster" effect takes place.

According to quantum-mechanical calculations (fig. 5.25) energy states of oxygen determine the form of $Ca_9U(PO_4)_6(OH)_2$ DOS curve, as well as in the case of Ca-HAP [267]. By transition to uraniferous apatite there is observed a displacement of all peaks of density of $O_{(1)}$ *s*, $O_{(1)}$ *p* and $P_{(1)}$ *s*, $P_{(1)}$ *p* electronic states towards low energies that may indicate an increase of P-O bond energy in a tetrahedron. Binding energy of $O_{(2)}$ *s* and $P_{(2)}$ *p* electrons increases a little by simultaneous reduction of $O_{(2)}$ *p* and $P_{(2)}$ *s* binding energies that indicates a redistribution of electronic density for the case of sp_3-hybridization. For $O_{(3)}$ *p* and $O_{(4)}$ *p* peaks in DOS curves nearby 7—8 eV become more expressive. All this indicates the decrease of local symmetry of PO_4 tetrahedron.

It is necessary to notice that for all electronic densities of calcium there is a shift of peak nearby 10 eV by 0.7 eV towards low binding energies. Considering that $P_{(1)}$ *p*,

Table 5.8. **Electron binding energy E_b (eV), halfwidth (eV) of core levels of calcium, calcium and uranium oxides, and also of investigated compounds.**

Compounds	O 1*s*	Ca $2p_{3/2}$	P 2*s*	P 2*p*	Ca 3*p*	U $4f_{7/2}$
Ca-metal [265]	—	344.7 (1.7)	—	—	—	—
CaO [265]	528.9 (1.4)	346.0 (1.7)	—	—	—	—
$Ca(OH)_2$ [265]	531.2	—	—	—	—	—
$CaCO_3$ [265]	531.6 (1.6)	347.3 (1.7)	—	—	—	—
$Ca_{10}(PO_4)_6(OH)_2$	530.4 (2.6)	346.2 (2.3)	189.6 (3.6)	132.0 (2.5)	25.4	—
$Ca_9U(PO_4)_6(OH)_2$	531.4 (2.6)	347.2 (2.3)	190.6 (3.6)	133.0 (2.5)	25.1	381.7 (3.3)
UO_3 [266]	530.7 (1.8)	—	—	—	—	380.6 (2.3)
UO_2 [266]	—	—	—	—	—	379.6
U [266]	—	—	—	—	—	376.7

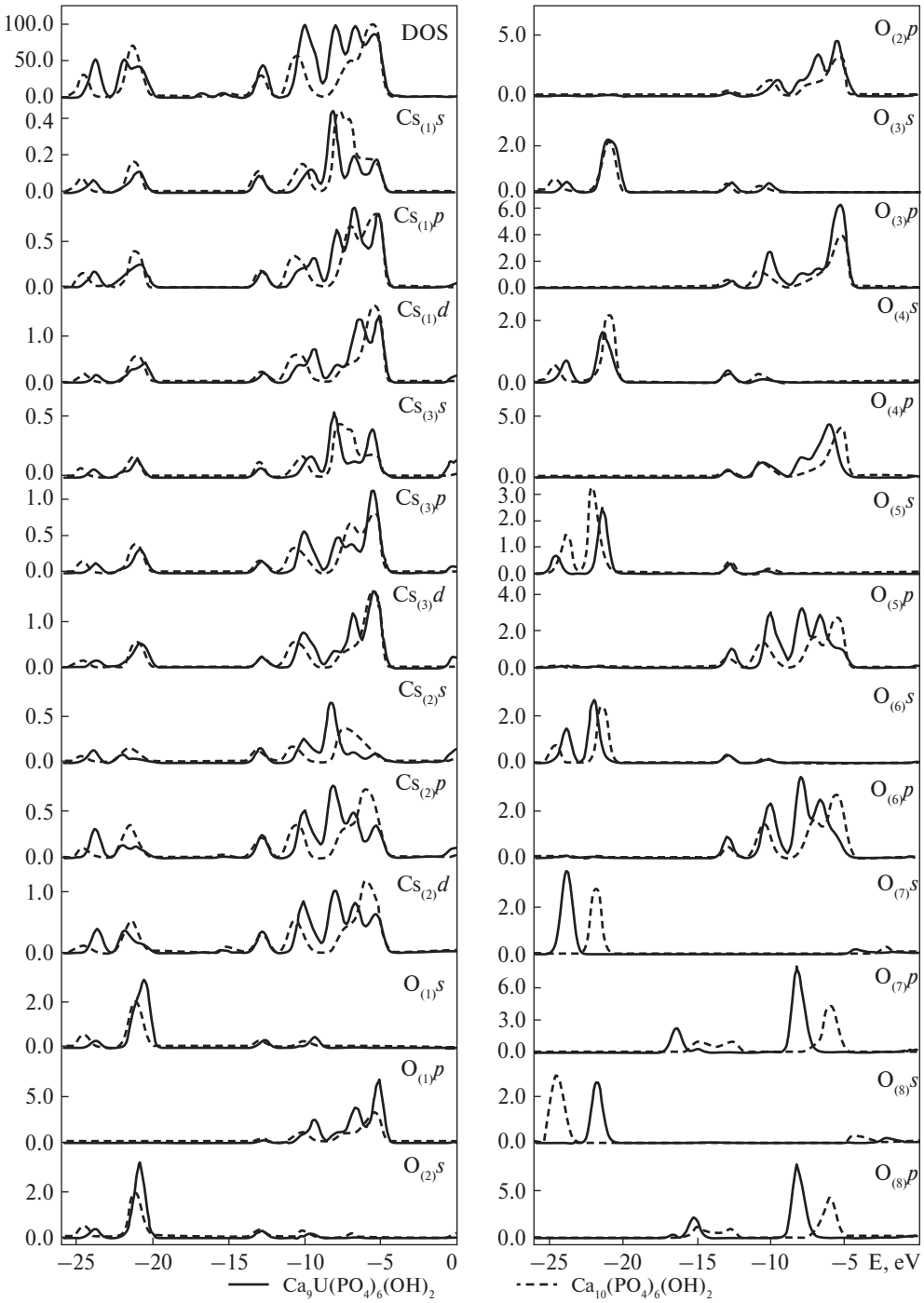

Fig. 5.25. Total and partial densities of states of $Ca_9U(PO_4)_6(OH)_2$ (continuous line) and $Ca_{10}(PO_4)_6(OH)_2$ (dashed line)

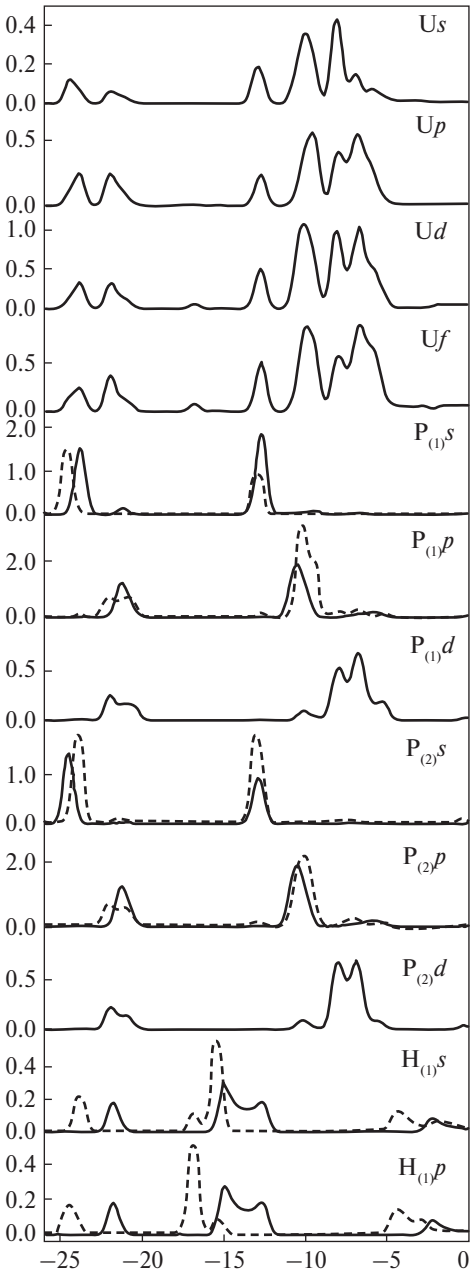

$P_{(2)}$ *p* and $O_{(1)}$ *s*, $O_{(1)}$ *p*, $O_{(2)}$ *s*, $O_{(2)}$ *p*, $O_{(3)}$ *s*, $O_{(3)}$ *p* are shifted by a similar value, it is possible to talk about some weakening of Ca-O-P bond.

The isomorphic uranium impurity significantly influences the shape of DOS curve of stoichiometric Ca-HAP. Since uranium entering into Ca-HAP lattice lowers symmetry of tetrahedrons because of mismatch of calcium and uranium atomic radiuses there is a splitting, and also a shift of available and occurrence of new peaks. Thus for $Ca_{(1)}$ *s*, $Ca_{(1)}$ *p*, $Ca_{(1)}$ *d* and $Ca_{(3)}$ *d*- electronic densities the peak nearby 5-8 eV is splitted into 3, and $Ca_{(3)}$ *s*, $Ca_{(3)}$ into 2 new peaks. In $Ca_{(1)}$ *p* and $Ca_{(3)}$ *p* curves there is a new peak nearby 8 eV. For $Ca_{(2)}$ *s*-density the main peak is shifted by 1.5 eV, and also become narrower. Thus its intensity increases a little. The form of the given peak correlates with the shape of the corresponding peak in U *s*-density curve. For $Ca_{(3)}$ *s* and $Ca_{(3)}$ *d*-densities there is also a peak at 8 eV and splitting of the peak nearby 6 eV into 2 components occurs. Significant changes in the density of electronic states is observed for $O_{(5)}$ *p* and $O_{(6)}$ *p* densitites. A peak at 7 eV appears. Intensity of the peak nearby 10 eV raises. 2 peaks nearby 20-25 eV become more expressed that can be a result of interaction of oxygen of hydroxyl groups with uranium. There is observed a shift of peaks into an area of high binding energies by 2 eV for $O_{(7)}$ *s*, $O_{(7)}$ *p* and $O_{(8)}$ *s*, $O_{(8)}$ *p* DOS. Similar displacements are observed for $H_{(1)}$ *s* and $H_{(2)}$ *s* too. The shape of peaks for hydrogen H 1*s* density nearby 15-17 eV is similar to the shape of the corresponding peaks for $O_{(7)}$ *p* and $O_{(8)}$ *p* DOS, that corresponds to

Table 5.9. **M/P ratio in the investigated samples of Ca-HAP, calculated according to X-ray diffraction measurements.**

Sample	Ca/P, Pb/P
$Ca_{10}(PO_4)_6(OH)_2$	1.66
$Ca_{10-x}U_x(PO_4)_6(OH)_2$	1.64
$Pb_{10}(PO_4)_6(OH)_2$ [268]	1.54

O-H bond. The correlation between shifts of positions of X-ray electron lines and the calculation data (uranium atom is located in $Ca_{(2)}$-position) indicate the preferable uranium position in $Ca_{(2)}$-position.

Many authors use X-ray diffraction spectral data to characterize powder phases of calcium phosphates thus detrmining Ca/P ratio [268-272]. It is especially important for analysis of film coatings and adsorbed phases when such methods as X-ray diffraction are non-applicable. Calcium enrichment of Ca-HAP surface was determined from measurement of Ca/P ratio. Moreover, there was revealed the increase in this ratio with time that indicates migration of calcium atoms to the surface at a room temperature [273].

Hydroxyapatites with isomorphic substitution of calcium for strontium, vanadium, barium and lead have already been investigated by X-ray diffraction spectroscopy [274]. In these cases cations were bivalent, but as many researchers note, it is extremely difficult to obtain stoichiometric metal/phosphorus ratio. Usually this ratio for calcium is in a range of 1.43-1.72 [226] while stoichiometric ratio is 1.67.

The measured Ca/P ratios for the investigated samples are given in table 5.9. For unsubstituted Ca-HAP sample, volume value of Ca/P ratio is 1.67. Quantitative analysis of X-ray diffraction spectra gives the Ca/P ratio equal to 1.66. For the sample with partial cation substitution the Ca/P ratio is 1.64, i.e. deficiency of Ca atoms is observed.

It can be seen from table 5.9 that calcium substitution for heavier cation in hydroxyapatite reduces metal/phosphorus ratio on the sample surface. It can be supposed that interaction between apatite and metal ions in a solution is controlled with apatite dissolution leading to formation of metallo-phosphates. New phosphates are nucleated on the HAP surface which play the role of catalyst.

CONCLUSIONS

Isomorphic substitution of calcium ions for ions of 3*d*-metals, magnesium, strontium and uranium in calcium hydroxyapatite little changes the structure of the occupied part of a valence band which keeps expressed zonal character with various extent of separate subbands - the top part of a valence band and the bottom part of a valence band. The main contribution to the formation of the main

features of the top part of a valence band is made by hybridized *s*-, *p*- and partially *d*- electronic states of metal and phosphorus ions. The structure of subvalence states is determined with *s*-states of oxygen and phosphorus. As well as in stoichiometric apatite sublattice of oxygen tetrahedrons is determinative in formation of shape and the main features in full density of electronic states curve of isomorphically substituted calcium apatites. The preferable position of 3*d*-metals, magnesium, strontium and uranium ions in calcium hydroxyapatite is $Ca_{(2)}$-position.

Isomorphic substitution of calcium atoms for 3*d*-metal, magnesium, strontium and uranium atoms in apatite structure for all dopants concentration leads to a decrease of electronic density of calcium and oxygen atoms.

High core electron density of strontium atoms in comparison with calcium atoms leads to higher binding energy of strontium *d*-shell by its nucleation, than for calcium in crystal (for metal strontium binding energy of *d*-electrons is ~15 eV whereas for calcium it is ~5 eV) and, hence, indirect metal-metal interaction in triangles of metal atoms is less expressed for strontium apatite.

Isomorphic modifying of calcium apatite matrix with alkaline metals and REM leads to significant redistribution of electronic density of crystal and as a consequence to a change of the shape of the curve characterising the valence band. Unlike phosphate apatites in vanadate analogs by substitution there is no considerable change of the shape of DOS curve.

Isomorphic modifying of calcium hydroxyvanadate with sodium and REM little changes the structure of peaks in DOS curve in the series La→Nd→Sm→Gd→Ho, leading only to the overall displacement of all groups of features towards larger binding energies. At the same time there is observed an increase of the contribution of hydrogen *s*-states nearby 20 eV associated with a considerable reduction of contribution of oxygen *s*- and *p*-states of hydroxyl group.

Isomorphic doping of Ca-HAP with lanthanum and alkaline-earth elements monotonously lowers the position of the centre of gravity of O K_α-line in the series Li→K→Rb that is associated with an increase of electronic density on oxygen atoms. The transition to strontium-containing compounds also shows the reduction of O K_α-band energy position by doping with alkaline and rare-earth metals. The differences in dependence of position of the centres of gravity of O K_α-lines in phosphorus- and vanadium-containing apatites by isomorphic modifying with alkaline metals and lanthanum, most likely, are determined with various internal organisation of tetrahedrons leading to smaller sensitivity of tetrahedral oxygen skeleton to cation substitutions in the case of vanadium hydroxyapatite that is probably connected with smaller spatial extent of vanadium *d*-state, in comparison with valence *p*-states of phosphorus.

The constancy of position of O K_α -band centre of gravity in lanthanum-containing compounds with composition $Ca_{5-2x}A_xLa_x(VO_4)_3OH$ by change of alkaline metal in the series Li→Na→K→Rb→Cs and significant changes in position of the centre of gravity of O K_α-line for sodium-containing compounds with composition Ca_{52-}

$_x$Ln$_x$Na$_x$(VO$_4$)$_3$OH in the series La→Nd→Sm→Ho, and also significant changes of *c* parameter of apatite lattice by modifying with REM indicates the preferable substitution of calcium for rare-earth elements in $Ca_{(2)}$-position of apatite structure.

Strontium phosphateapatite modification with sodium and lanthanum on approaching the limiting degree of substitution monotonously increases the energy of oxygen and strontium core levels, and also leads to decrease of P 2*s* level energy that may indicate a considerable redistribution of electronic density characterised with a decrease of electronic density of phosphorus and its increase on oxygen and strontium atoms. Small concentrations of sodium and lanthanum do not change the position of O 1*s* level. By an of atomic concentration of dopant ions from 0.5 to 1.0 energy levels of lanthanum and sodium atom shells shift to an area of higher binding energies that causes electronic density transfer from atoms of matrix to lanthanum and sodium atoms. The insignificant increase of energy gap width of vanadate apatites from 3.97 up to 4.07 eV in the series of substitutins Li→Na→K→Rb→Cs is accompanied with normalization of the occupied valence levels.

f-state curves of sodium-containing compounds in the series La→Nd→Sm→Gd→Ho changed more substantially. Thus for samarium-containing compound the increase of the contribution of *f*-states into DOS, in comparison with La, Nd, Gd and Ho-containing compounds is observed. It is because in the whole REM series only samarium besides oxidation state of +2 may have oxidation state of +3.

The established reduction of energy of apatite crystal by isomorphic modifying in the series of alkaline metals and REM with increasing atomic number agrees with the data on difficulty of obtaining of apatite monocrystals, and also with absence of undoped structures of apatites in the nature.

It is established that isomorphic modifying of Ca-HAP with uranium leads to a reduction of metal/phosphorus ratio on the surface of samples that by interaction between apatite and ions of metals in a solution can lead to formation of metallo-phosphates. New phosphates are nucleated on Ca-HAP surface which acts as a catalyst of this reaction. The entering of uranium atoms into $Ca_{(2)}$- positions of apatite opens up the possibility of using apatites as matrices for long-term burial of radioactive waste.

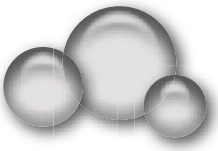

CHAPTER 6

ELECTRONIC STRUCTURE OF APATITES WITH ISOMORPHIC SUBSTITUTIONS IN TETRAHEDRAL POSITIONS

The perspective of application apatite-based materials cannot be understood enough without elucidation of correlation between isomorphic substitutions in an apatite structure and properties of such substances. Structural modification by isomorphic substitutions in tetrahedral sublattice leads to significant changes of physical properties of apatites. To date this problem is not studied enough that indicates absence of the directed synthesis of isostructural compounds with a planned design of properties.

This section contains the data on the influence of anion isomorphic substitutions in apatite-like calcium structures on the electron structure of compounds of composition $Ca_{10}(PO_4)_{6-x}(VO_4)_x(OH)_2$ (x=0, 1, 3, 5, 6) [275].

As it is known, tetrahedral $(XO_4)^{3-}$ anion is a structural element of many crystalline compounds and, as a rule, physical and chemical properties of compounds that have gotten their practical application, are determined to a large extent with sublattice of tetrahedrons [232].

Table 6.1 contains core electron binding energies of atoms of metal Ca, calcium and vanadium oxides, and of the investigated compounds obtained with X-ray photoelectronic spectroscopy. The data on calcium and vanadium oxides are cited for ease of interpretation of results.

The maximum in O 1*s* curve, by substitution of one anion group (PO_4 for VO_4), does not change binding energy, however its width increases on 0.1 eV. The maximum in Ca $2p_{3/2}$ curve electrons also does not change position, and the linewidth decreases by 0.2 eV. Ca 3*p* line is shifted towards lower binding energies by 0.1 eV. In this case P 2*p* linewidth decreases by 0.3 eV and is shifted towards higher binding energies 0.1 by eV. Thus, such substitution leads to a small shift of binding energy of electron levels of calcium and phosphorus.

Substitution of three anion groups in $Ca_{10}(PO_4)_6(OH)_2$ leads to even greater changes in electronic structure. O 1*s* binding energy shifts by 0.2 eV towards lower energies, and O 1*s* linewidth increases by 0.4 eV that indicates formation of a new energy state of oxygen. All calcium electron lines shift towards lower binding energies: Ca 2*s* line shifts by 0.2 eV, Ca $2p_{3/2}$ and Ca 3*p* by 0.1 eV. P 2*p* line shifts by 0.1 eV towards lower binding energies too, whereas in the first case the shift occurred towards higher binding energies. V 2*p* lines shift towards lower binding energies.

By substitution of five anion groups there are much more considerable changes in electronic structure of the apatite. O 1*s* line shifts by 1.0 eV, Ca $2p_{3/2}$ and P 2*p* shift by 0.5 eV. All values of electron binding energy are shifted towards lower binding energies. V $2p_{3/2}$ line is shifted towards lower binding energies by 0.6 eV too. In this case O 1*s* line is similar in binding energy to O 1*s* line of vanadium oxides (tab. 6.1).

Table 6.1. **Electron binding energy E_b (eV), linewidth (Γ) (eV) (measured at half-height) of core levels of Ca atoms, Ca and V oxides, and investigated compounds.**

Sample	O 1*s*	Ca 2*s*	Ca $2p_{3/2}$	Ca 3*p*	P 2*p*	V $2p_{3/2}$
Metal Ca [241]	—	—	344.7 (1.7)	—	—	—
CaO [241]	528.9 (1.4)	—	346.0 (1.7)	—	—	—
$Ca(OH)_2$ [241]	531.2	—	—	—	—	—
$CaCO_3$ [241]	531.6 (1.6)	—	347.3 (1.7)	—	—	—
$Ca_{10}(PO_4)_6(OH)_2$	531.2 (2.0)	439.2	347.3 (2.0)	25.4	133.3 (2.4)	—
$Ca_{10}(PO_4)_5(VO_4)(OH)_2$	531.2 (2.1)	439.2	347.3 (1.8)	25.3	133.4 (2.1)	517.6 (2.3)
$Ca_{10}(PO_4)_3(VO_4)_3(OH)_2$	531.0 (2.4)	439.0	347.2 (1.9)	25.2	133.2 (2.3)	517.4 (1.7)
$Ca_{10}(PO_4)(VO_4)_5(OH)_2$	530.2 (2.5)	438.8	346.8 (1.9)	25.0	132.8 (2.2)	517.0 (1.7)
$Ca_{10}(VO_4)_6(OH)_2$	530.1 (2.8)	438.7	346.8 (2.1)	24.8	—	517.0 (1.8)
V_2O_5 [276]	529.8 (1.55)	—	—	—	—	517.0 (1.3)
V_6O_{13} [276]	530.0 (2.2)	—	—	—	—	516.5 (3.4)
V_2O_3 [276]	530.0 (2.0)	—	—	—	—	515.15 (4.8)

E_b values are given relative to E_b (C 1s) =285.0 eV. An error is 0.1 eV.

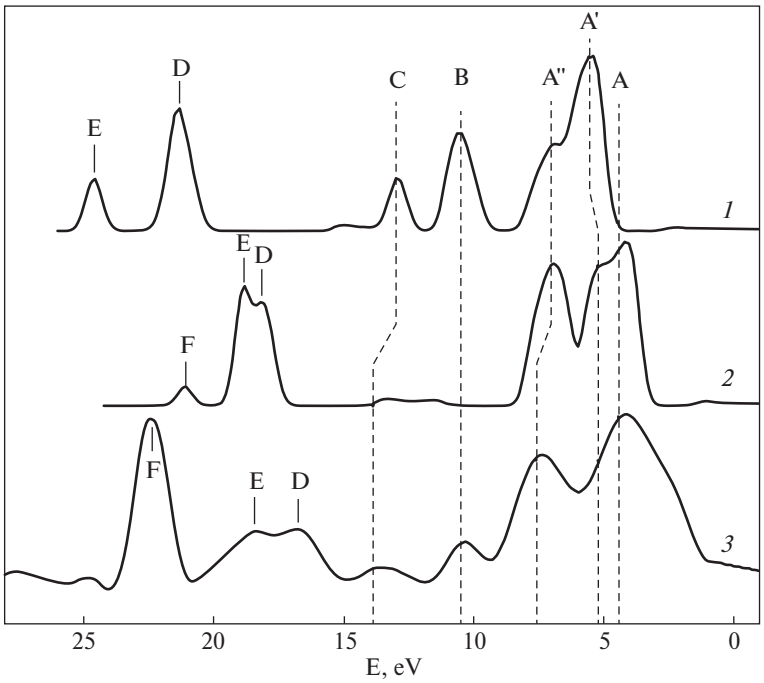

Fig. 6.1. Total density of states: $Ca_{10}(PO_4)_{6-x}(VO_4)_x(OH)_2$: 1 — x =0; 2 — x =6; 3 — x =3

Substitution of six anion groups leads to further reduction of electrons binding energy of oxygen and calcium. O 1*s* line widens by 0.8 eV that indicates the occurrence of new positions for oxygen atoms. O 1*s* binding energy decreases by 1.1 eV. Hence, new oxygen states have considerably higher negative charge on atoms that indicates the considerable changes in an oxygen environment of calcium and vanadium atoms in the crystal lattice of a compound. In this case V $2p_{3/2}$ binding energy is close to that of V_2O_5.

From the calculation data on the electronic structure of $Ca_{10}(PO_4)_6(OH)_2$ (fig. 6.2) obtained using LMTO method and taking into account the quantity of atoms of the given type in an elementary cell it can be seen that $O_{(3)}$ *s* and $O_{(3)}$ *p* oxygen electronic states make the greatest contribution to DOS. Summation of curves for $O_{(3)}$ *s* and $O_{(3)}$ *p* states generally determines of the shape of DOS curve. Thus $O_{(4)}$ *p* states also make a significant contribution to A` and A`` features of DOS of $Ca_{10}(PO_4)_6(OH)_2$ (fig. 6.1). Thereby oxygen states of tetrahedral lattice determine the main features of DOS curve .

As it is noted in [232] it is very easy to extract the contributions connected with $(XO_4)^{3-}$. *B, C* and *D*, *E* features are generated mainly by $O_{(3)}$ *p*, $O_{(1)}$ *p*, $O_{(1)}$ *s*, P *s* and P *p* states and thus reflect sp_3-hybridization in a tetrahedron. The considerable energy interval between these features makes it possible to use this fact for the analysis of states of oxygen atoms in a tetrahedron and therefore to judge the change of local symmetry of a tetrahedron.

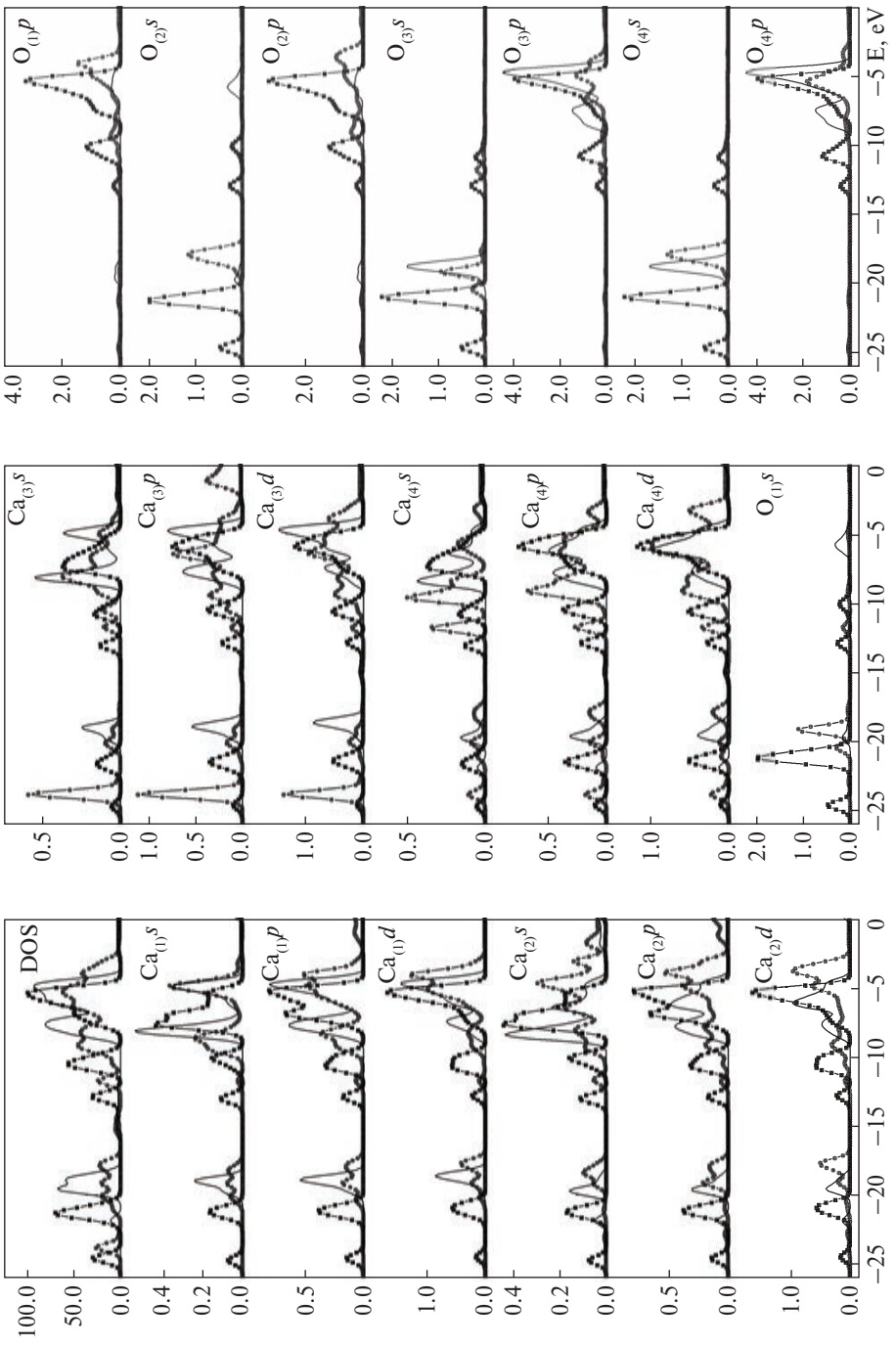
DOS
Ca(1)s
Ca(1)p
Ca(1)d
Ca(2)s
Ca(2)p
Ca(2)d
Ca(3)s
Ca(3)p
Ca(3)d
Ca(4)s
Ca(4)p
Ca(4)d
O(1)s
O(1)p
O(2)s
O(2)p
O(3)s
O(3)p
O(4)s
O(4)p
−25 −20 −15 −10 −5 0
−25 −20 −15 −10 −5 E, eV

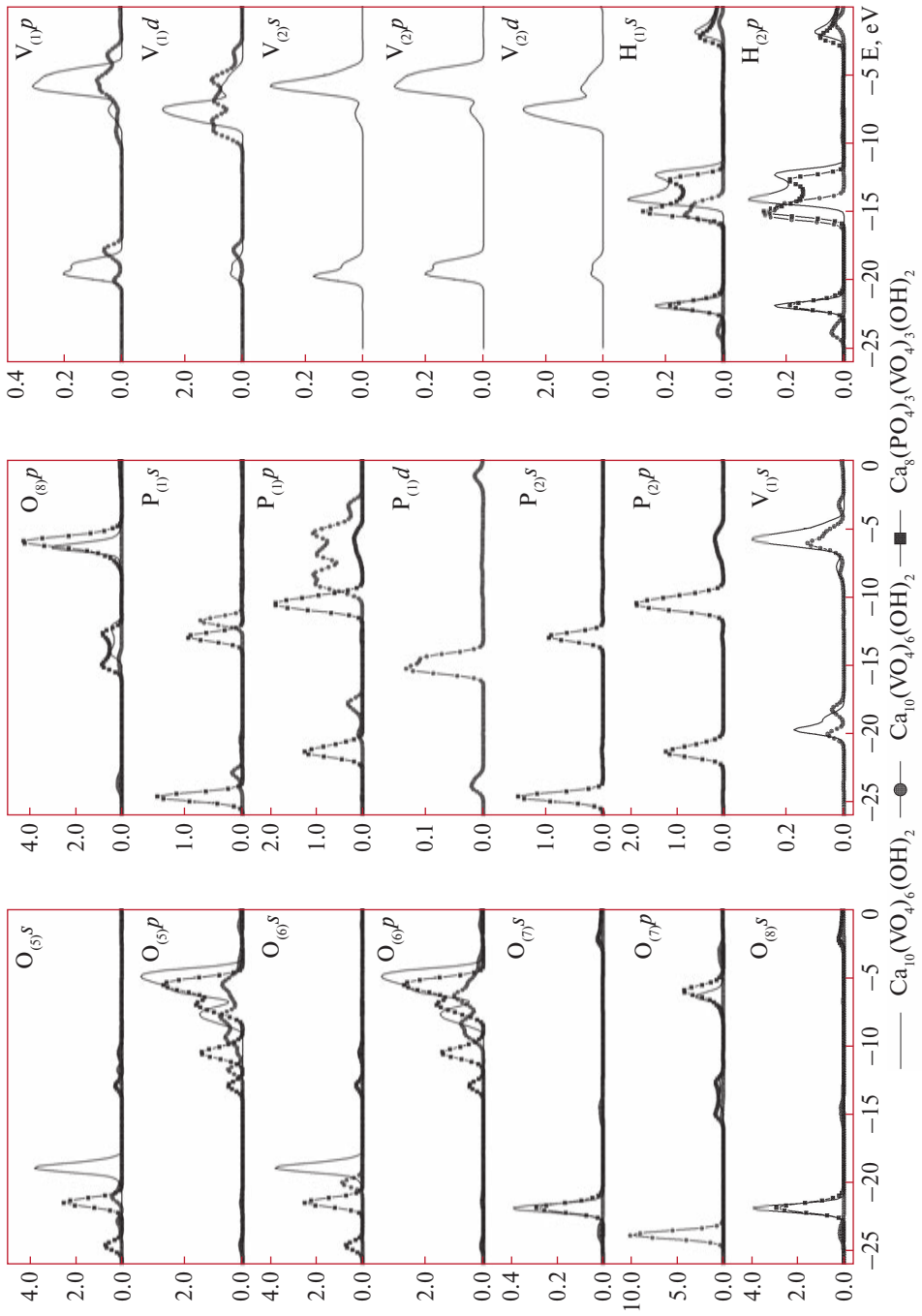

Fig. 6.2. Total and partial densities of electronic states of compounds

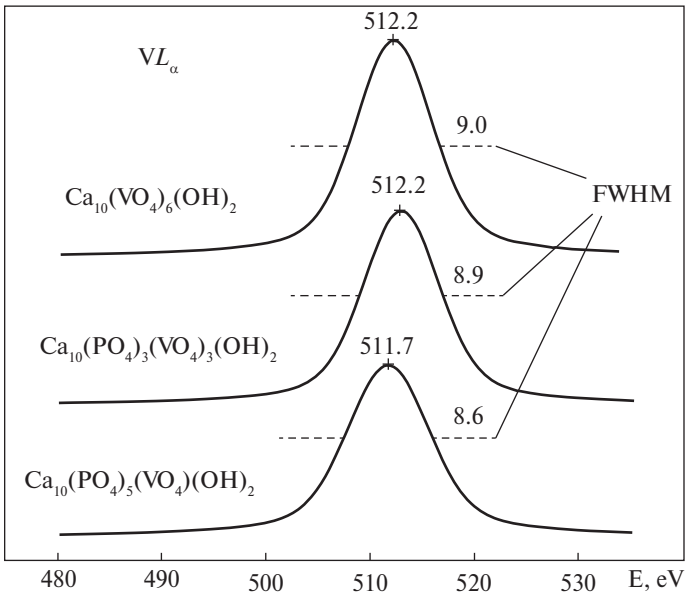

Fig. 6.3. X-ray spectra of vanadium

Substitution of a fraction of anions in a lattice essentially influences both the position and intensity of these features (fig. 6.1). For hydroxyvanadate *C* and *D* features are not observed , and *E* and *D* features undergo significant changes that indicates changes in a character of a chemical bond. Taking into account topological position of $O_{(3)}$ state in a lattice it is possible to assert that the reduction of intensity of *E* and *D* features in isomorphically substituted apatite may indicate an increase of P-$O_{(3)}$ distance, that is confirmed with IR-studies and, consequently, a larger growth of lattice parameter *a* than of parameter *c* that agrees with the structural data. Hence, the offered approach can be used for the description of dependence of topological arrangement of oxygen atoms on the output parameters of the calculation data.

Intensity and the shape of hydrogen *s*-density curve for hydroxyapatite and hydroxyvanadate coincide and a some change of the curve shape is observed in isomorphically substituted compound (fig. 6.2). Hence PO_4 substitution for VO_4 influences little the state of hydrogen *s*-density in the investigated compounds, and thereby the state of *c* axis of a crystal.

The partial contribution of vanadium *d*-density is reduced in calcium hydroxyvanadate in comparison with the substituted compounds that indicates a possible mechanism of atomization of *d*-electron wave functions. V L_α-band (fig. 6.3), generally reflecting 3*d*-states of the metal in investigated series, shows the reduction of at half-height width along with a reduction of concentration of vanadate ions. There is also observed a large shift of the main maximum to low-energy area (~0.5 eV) and a reduction of width and low-energy shift of V 2*p* levels that confirms a conclusion about increase of

atomization of vanadium *d*-electrons wave functions too. The latter, most likely, plays an essential role in suppression of anharmonicity in mixed tetrahedral structures.

As it is noted in [231, 236] atomic effects play a significant role in the formation of calcium *L*α-spectra of apatite-like compounds. Hence participation of calcium *d*-states in bond is levelled by its considerable localization. The greatest contribution of vanadium *d*-states in DOS of hydroxyvanadate is observed in the range from 6 up to 9 eV, whereas in isomorphically substituted vanadate — from 2 up to 6 eV. It can be directly connected with an expansion of atomic levels, connected *d*-states to the zone of Bloch functions as integrals of cation-anion overlapping are very small outside of atomic spheres, and the width of *d*-zones is explained with a dependence on the distance between such atoms as R^{-5} [242] that is coordinated with structural parameters (tab. 6.2).

The contribution of vanadium *p*-density is proportional to its atomic concentration in hydroxyvanadate and isomorphically substituted compound, however energy intervals of the main contribution are different (from 4 up to 6 eV for hydroxyvanadate and one from 1 up to 4 eV for isomorphically substituted compound).

The contribution of V *s*-density for $Ca_{10}(PO_4)_3(VO_4)_3(OH)_2$ is larger in comparison with hydroxyvanadate. The contribution of phosphorus *d*-states is proportional to its atomic content in compounds. Energy interval of the contribution of *d*-states is from 6 to 8 eV for hydroxyapatite, and from 1 to 5 eV for isomorphically substituted compound.

Proceeding from the relation of intensity maxima of density of states curves it follows that phosphorus *p*-density is proportional to its atomic concentration (fig. 6.2). The maximum in the curve of phosphorus density of states of hydroxyapatite is at 10 eV and for $Ca_{10}(PO_4)_3(VO_4)_3(OH)_2$ at 6 eV. The contribution of phosphorus *s*-density is not proportional to its atomic concentration. The contribution for $Ca_{10}(PO_4)_3(VO_4)_3(OH)_2$ is larger and the maximum of density of states is at 8.5 eV, whereas for hydroxyapatite it is at 12.5 eV.

For hydroxyapatite and hydroxyvanadate contributions of $O_{(4)}$ *p* and $O_{(4)}$ *s* states are almost identical and coincide in form and intensity. The given fact is a natural

Table 6.2. **Structural data of compounds.**

	Compound	*a*, Å	*c*, Å
1.	$Ca_{10}(PO_4)_6(OH)_2$	9.424	6.879
2.	$Ca_{10}(PO_4)_5(VO_4)(OH)_2$	9.492	6.903
3.	$Ca_{10}(PO_4)_3(VO_4)_3(OH)_2$	9.619	6.924
4.	$Ca_{10}(PO_4)(VO_4)_5(OH)_2$	9.730	6.984
5.	$Ca_{10}(VO_4)_6(OH)_2$	9.768	7.003

— Error is 0.005 Å.

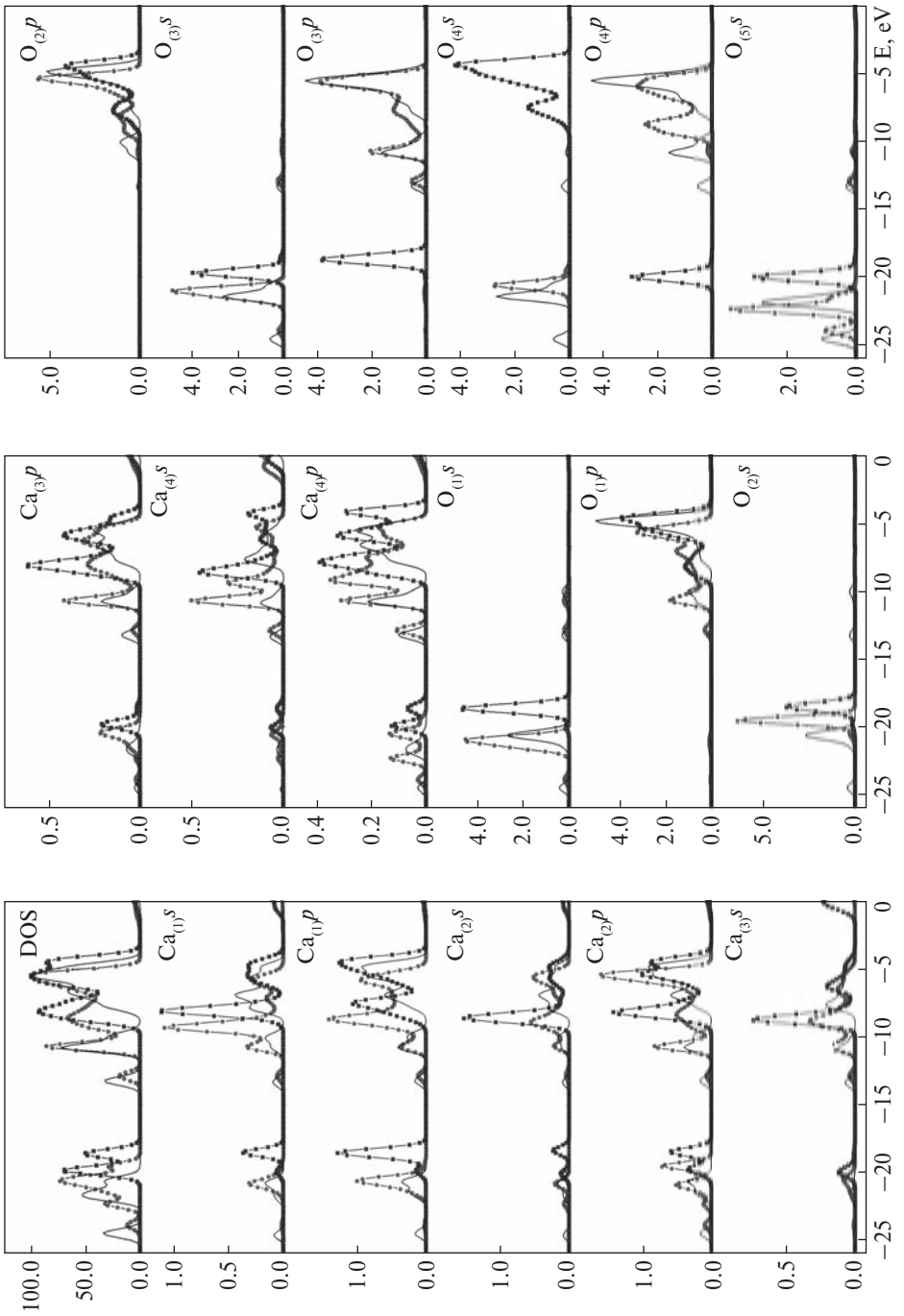
DOS
Ca(1)s
Ca(1)p
Ca(2)s
Ca(2)p
Ca(3)s
Ca(3)p
Ca(4)s
Ca(4)p
O(1)s
O(1)p
O(2)s
O(2)p
O(3)s
O(3)p
O(4)s
O(4)p
O(5)s
E, eV

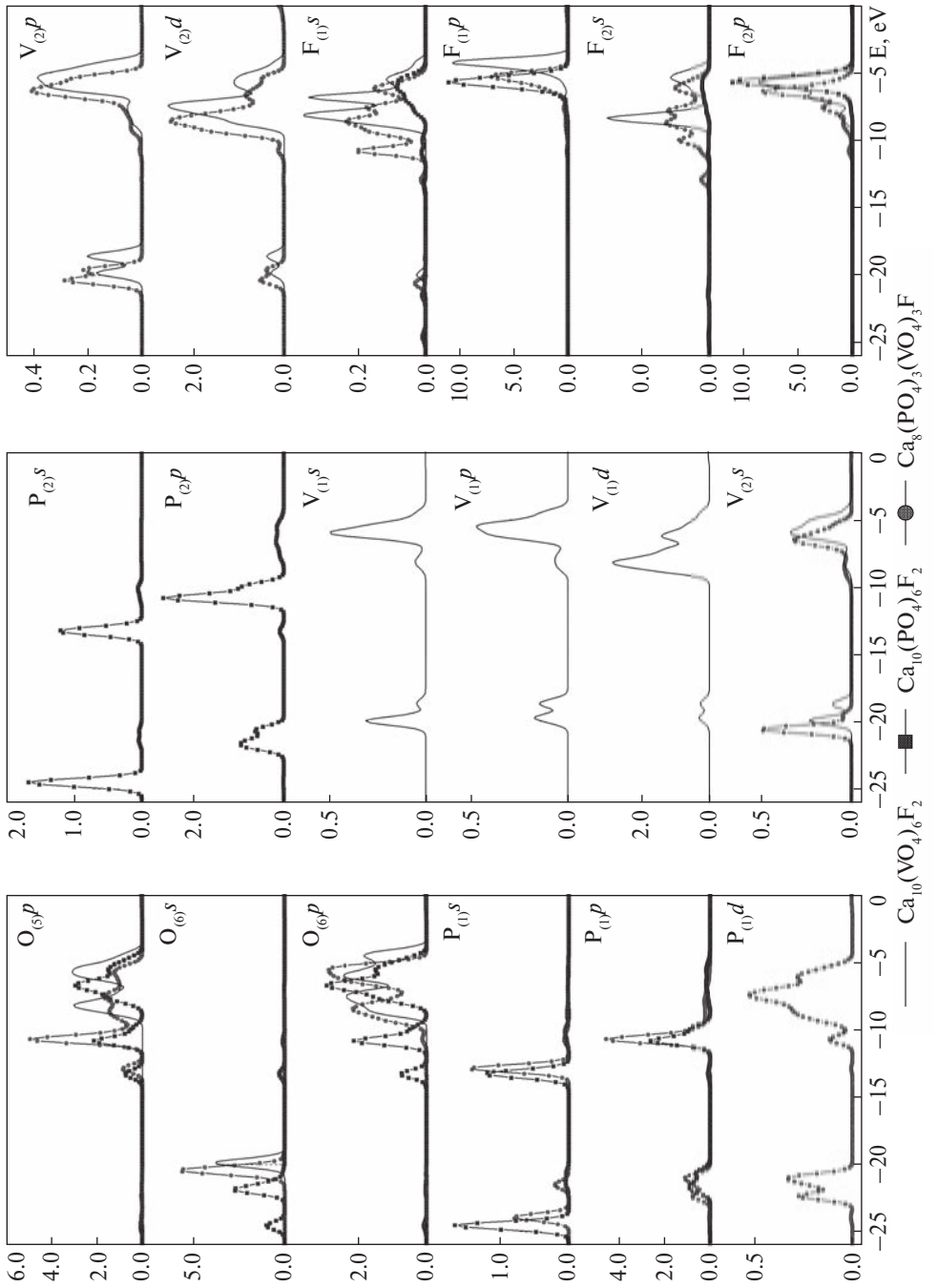

Fig. 6.4. Total and partial densities of states of compounds

consequence of isostructurality and weak differences of interatomic distances for the given compounds.

There is observed a considerable contribution of $O_{(2)}$ *p* in the range from 4.5 up to 9 eV for hydroxyvanadate and the total lack of such peak for hydroxyapatite, thus contribution of the feature at 20 eV decreases twofold. There is one peak for hydroxyvanadate and two peaks for hydroxyapatite in $O_{(2)}$ *s*—density curve nearby 20 eV.

The analysis of the calculation data on calcium compounds (fig. 6.2) revealed that the greatest differences are observed in $O_{(1)}$ energy state. The contribution of $O_{(1)}$ *p* in hydroxyvanadate is extremely small in comparison with the contribution of p-state of $O_{(1)}$ in hydroxyapatite (~8 fold lower). DOS maximum is nearby 10 eV. The contribution of $O_{(1)}$ *s* in hydroxyvanadate is small in comparison with hydroxyapatite too. There is observed almost identical contribution of $Ca_{(2)}$*d*-density for hydroxyapatite and hydroxyvanadate. The shape of $Ca_{(2)}$ *p*-density curve for $Ca_{10}(PO_4)_6(OH)_2$ and hydroxyvanadate almost repeats the shape of DOS curve.

Shapes of $Ca_{(2)}$ *p*- and $Ca_{(2)}$ *s*-density curves for $Ca_{10}(PO_4)_6(OH)_2$ are almost identical, whereas for hydroxyvanadate they are different. $Ca_{(1)}$ *d*-density curves for hydroxyapatite and hydroxyvanadate almost coincide. $Ca_{(1)}$ *s*-density curve repeats the shape of a valence band both for hydroxyapatite and hydroxyvanadate. However finer structure of calcium partial density curves for hydroxyapatite indicates a greater nonequilibrium of contributions chemical bond components.

Energy-gap width between filled and vacant states decreases from hydroxyphosphate to hydroxyvanadate from 5.6 to 4.8 eV. Use of the self-consistent calculation leads to the decrease of the forbidden band approximately by 1.5 eV in comparison with experimentally measured forbidden gap.

The consideration of the calculation data of mixed hydroxyapatite $Ca_{10}(PO_4)_3(VO_4)_3(OH)_2$ shows a contribution of vanadium partial electronic states which is disproportionate to the reduction of structure (fig. 6.2) that can be connected with a character of *d*-density. The relative contribution of oxygen states decreases too.

Table 6.3. **Ca/P, Ca/(P+V) and Ca/V ratios in the investigated samples, calculated according to XPS data.**

Sample	Ca/P, Ca/(P+V), Ca/V
$Ca_{10}(PO_4)_6(OH)_2$	1.66
$Ca_{10}(PO_4)_5(VO_4)(OH)_2$	1.52
$Ca_{10}(PO_4)_3(VO_4)_3(OH)_2$	1.57
$Ca_{10}(PO_4)(VO_4)_5(OH)_2$	1.76
$Ca_{10}(VO_4)_6(OH)_2$	1.81

The transition to fluor-containing compounds shows the scheme of contributions of partial densities of states into DOS which is more proportional to concentration (fig. 6.4).

Ca/P ratios measured by us with the specified technique for the investigated $Ca_{10}(PO_4)_6(OH)_2$ samples are resulted in table 6.3.

For unsubstituted $Ca_{10}(PO_4)_6(OH)_2$ Ca/P ratio was 1.66. Quantitative analysis of XPS spectra indicate that Ca/P ratio is equal to 1.63. For samples with substitution for one and three anion groups Ca/(P+V) ratio is 1.52 and 1.57 respectively , i.e. a deficiency calcium atoms is observed.

For samples with five and six vanadate groups ratio Ca/(P+V) makes 1.76 and 1.81 accordingly. In these cases an excess of Ca atoms is observed that also determines features of electronic structure of these compounds [267].

CONCLUSIONS

The shape of DOS curve of $Ca_{10}(PO_4)_{6-x}(VO_4)_x(OH)_2$ (x=0, 1, 3, 5, 6) compounds is determined with an energy state of oxygen of tetrahedrons. Isomorphic substitution of PO_4^{3-} for VO_4^{3-} anions among investigated compounds leads to significant changes in an oxygen environment of calcium, phosphorus and vanadium atoms, which appear in a reduction of 1*s* electrons binding energy of oxygen atoms by 1.1 eV, and in O 1*s* line broadening by 0.8 eV that indicates an occurrence of new oxygen positions in the apatite crystal lattice.

Among investigated compounds a reduction of extent of vanadium *d*-band with vanadate ions concentration decrease is observed. There was detected a shift of the main maximum of V L_α-band into low-energy area (~0.5 eV) that is explained with possible increase of "atomization" of *d*-electron wave functions. The last fact correlates with the observed suppression of anharmonicity of lattice vibrations in mixed tetrahedral structures and decrease of thermal stability of compounds.

The calculated differences in electronic structure of isostructural compounds correlate with existing differences in experimental spectra. The analytical model, allowing to ascribe topological distortions of a tetrahedron with parameters of quantum mechanical calculations, is offered.

There had been conducted an estimation of the surface composition stoichiometry of investigated powder samples which showed the least calcium content for $Ca_{10}(PO_4)_5(VO_4)(OH)_2$.

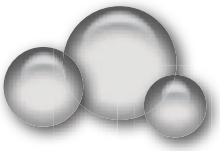

CHAPTER 7

OPTICAL, VIBRATIONAL SPECTRA AND THERMAL PROPERTIES OF ISOMORPHICALLY SUBSTITUTED CALCIUM APATITES

7.1. Optical spectra of calcium apatites, isomorphically-modificated with alkaline elements and lanthanides

One of the most intriguing questions concerning apatite-like systems is a problem of influence of dopes on electronic properties of a base material as the relation of quantities and type of atoms substantially changes various properties [226], in particular, doping with REM significantly changes optical properties.

High crystal lattice "porosity" of apatites causes a weak field of ligands and allows to replace ions in a wide range of elemental ratios without significant distortion of structure. This feature stimulates their investigation as laser mediums and fluorescent materials by crystal activation with corresponding cations [277, 278]. On the other hand, ion substitution in an apatite lattice can be useful in studying of electronic structure of the crystal.

On fig. 7.1 there are given $Ca_{10}(PO_4)_6(OH)_2$ and $Ca_{10}(VO_4)_6(OH)_2$ luminescence spectra, obtained using the same excitation level. As it can be seen vanadate luminescence maximum is shifted into far long-wave region (approximately by 0.27 eV), and the quantum yield of luminescence is 10 times less than for phosphate. It can be explained with more intensive $Ca_{10}(VO_4)_6(OH)_2$ vibration spectrum – the band is more broadened because of the presence of a set of peaks which apparently reflect vibration modes. Most likely energy dissipation on vanadate-ions can occur both by high-energy absorption of a photon with VO_4^{3-} matrix and radiationless dissipation on crystal lattice deffects. The shape of luminescence band does not vary by synchronisation pulse delay time meaning that all constituent radiating transitions have close values constant of transition time constant (7×10^{-7} s). It should also be considered that the absorption edge for phosphate is in a region of shorter wavelengths so that the line of excitation of 337 nm is out of absorption area.

Diffuse reflexion spectra reveal a sharp increase the material absorption near 3 eV. The absorption edge (fig. 7.2) approximately coincides for all samples, however broadening in a short-wave region is various and increases with an increase in ionic radius of a substituent in the series Li^+ (0.475 Å), Na^+ (0.875 Å), K^+ (1.185 Å), Rb^+ (1.320 Å), Cs^+ (1.455 Å).

It is possible to observe phonon repeats at the absorption edge with an interval of about 800 cm^{-1}, which corresponds to vibration modes in VO_4 tetrahedral sublattice.

There was revealed a broad emission band with a maximum, lying in the range of 500 ÷ 550 nm in photoluminescence spectra of the samples with isomorphic substitutions (fig. 7.3). The emission band contains structural features separated with an interval of 800 cm^{-1}, which indicates participation of vibrational levels in the emission. At a room temperature there was observed a change of luminescence spectra in comparison with spectra obtained at a temperature of liquid nitrogen. The centre of gravity of emission band shifted into short-wave area (fig. 7.3). Besides, there was observed a consecutive shift of the centre of gravity of emission band into short-wave area by an increase in radius of the substituent introduced into apatite lattice (fig. 7.4).

As it is known, crystal phosphate apatite has a forbidden zone with a width of about 5.5 eV [279]. Activating impurities or substituents can cause considerable shift of an absorption edge into long-wave region. Dot defects in the crystal structure, that are formed, for example, as a result of a deviation from stoichiometry of structure [280, 281] also can be a source of additional levels in the forbidden zone. As it has been shown previously [282-284], a radiation band of apatites of composition $Ca_5(PO_4)_3X$ (X=F,Cl,OH) with a maximum nearby 400 nm is caused with electronic transitions in tetrahedral sublattice. Thus calcium substitution is observed mainly in Me_{II}-positions which are in close proximity to tetrahedral sublattice and lead to its distortion [1].

$Ca_5(VO_4)_3OH$ crystal emission, observed in area 500 ÷ 550 nm, can be attributed to electronic transitions in $(VO_4)^{3-}$ sublattice. Long-wave shift of this emission band in comparison with a band emitted by phosphate-apatites can be caused with a change of lattice parameters (increase of an elementary cell volume by ~50 $Å^3$).

The shape of emission band is determined with superposition of electronic transitions with participation of vibronic levels of the excited and ground electronic state. As it can be seen from luminescence spectra (fig. 7.3), at low temperature

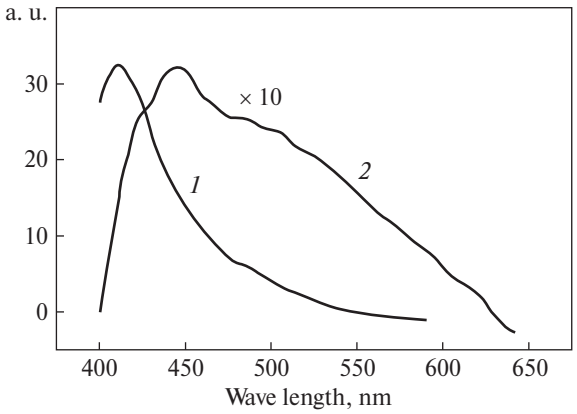

Fig. 7.1. $Ca_{10}(PO_4)_6(OH)_2$ and $Ca_{10}(VO_4)_6(OH)_2$ luminescence spectra

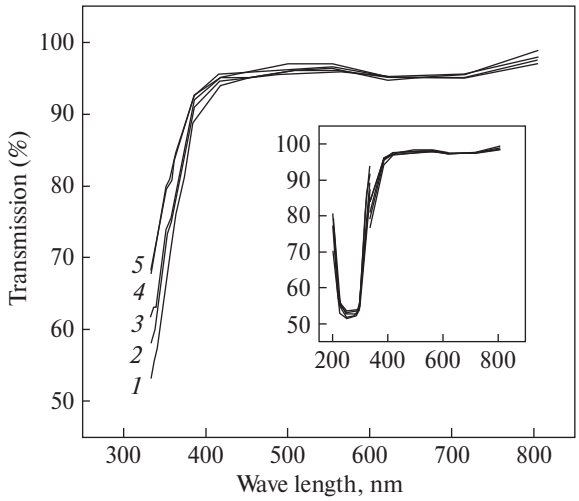

Fig. 7.2. Diffuse reflexions spectra of $Ca_{5-2x}La_xMe_x(VO_4)_3OH$ ($x = 0.05$), where Me=Li (1); Na (2); K (3); Rb (4); Cs (5). The absorption edge is zoomed in; in the inset the full spectrum is shown. Spectrum discontinuity at 330 nm is connected with change of a source and monochromator of spectrophotometer.

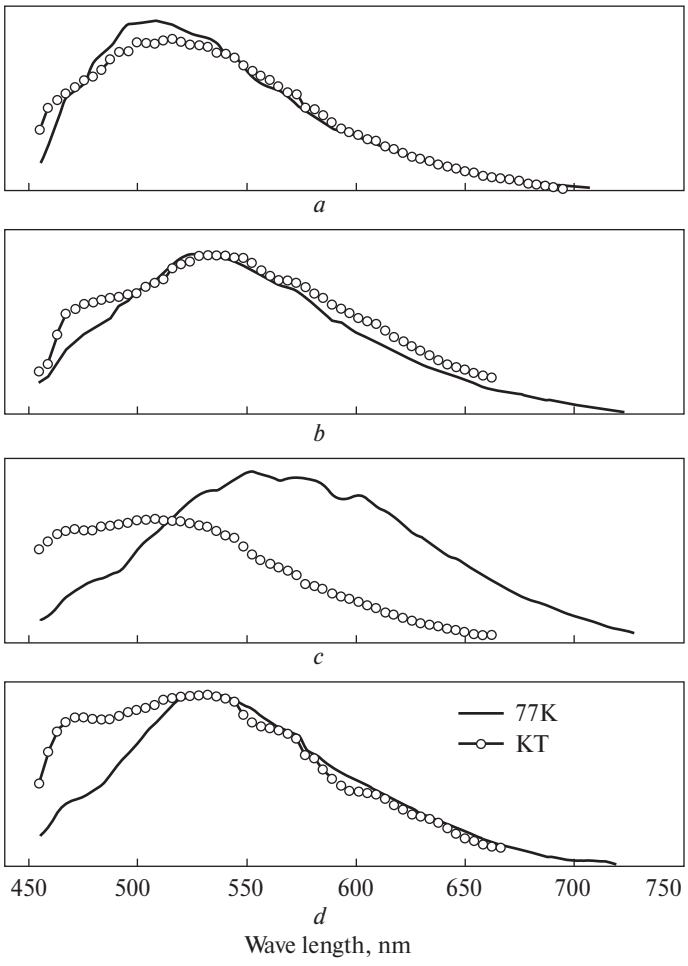

Fig. 7.3. Luminescence spectra at a temperature of liquid nitrogen (77 K) and at a room temperature (RT) (x=0.05): 1 — $Ca_{5-2x}La_xNa_x(VO_4)_3OH$, 2 — $Ca_{5-2x}La_xK_x(VO_4)_3OH$, 3 — $Ca_{5-2x}La_xRb_x(VO_4)_3OH$, 4 — $Ca_{5-2x}La_xCs_x(VO_4)_3OH$

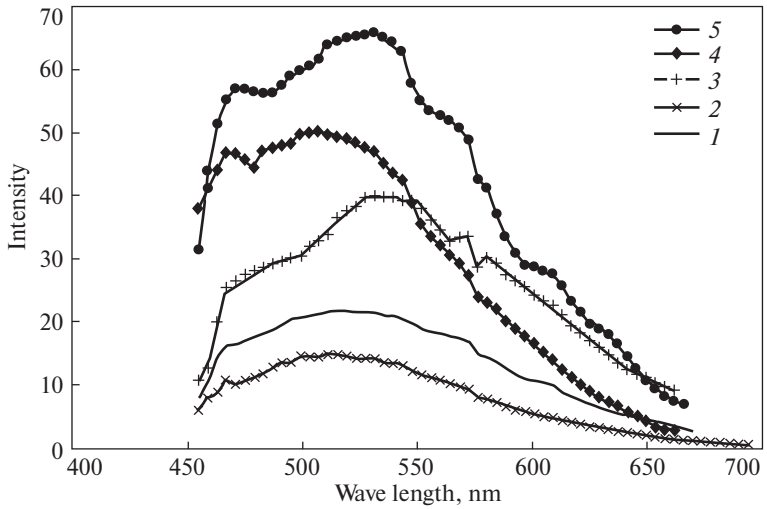

Fig. 7.4. Comparison of $Ca_{5-2x}La_xMe_x(VO_4)_3OH$ luminescence spectra, where Me = Li(1); Na(2); K(3); Rb (4); Cs(5), obtained at a room temperature (x=0.05)

there is a considerable Stokes shift (~120-130 nm) of emission band maximum relatively to absorption edge. It means that by emission transitions to higher vibronic levels of the ground state prevail over transitions to lower level. This result can be explained with a shift of configuration coordinate by electronic excitation of a lattice (fig. 7.5 a).

When temperature rises lattice parameters increase, and this thermal expansion, apparently, promotes electronic transitions to lower vibronic levels of the ground state that corresponds to the configuration diagram represented on fig. 7.5 b. Similar changes of the configuration diagram should occur by introduction of the assistant. Namely, by introduction of substituent with bigger ionic radius there should be a shift from the state represented on fig. 7.5 a to the state, represented on fig. 7.5 b. It should be noted that the physical reason of spectral changes remains the same — increase of the size of unit cell of a crystal. On fig. 7.6 the change of unit cell volume depending on the size of an substituent ion by identical levels of doping is shown.

Considering this it is possible to conclude that widening of absorption band edge and the change of the form of a emission band by introduction of alkaline-earth elements into $Ca_{5-2x}La_xMe_x(VO_4)_3OH$ structure can be explained with various probability of electronic transitions by participation of vibronic levels that is schematically represented on fig. 7.5.

Investigation results of show that crystalline $Ca_5(VO_4)_3OH$ has the lowest excited electronic state with energy ~3 eV. Change of apatite lattice parameter by introduction of substituent or temperature rise causes redistribution of density of electronic states in the lowest excited state according to the scheme represented on fig. 7.5.

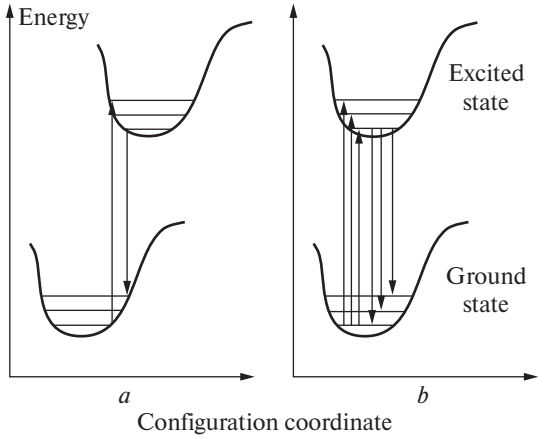

Fig. 7.5. The configuration diagram, explaining possible electronic transitions in $Ca_{5-2x}La_xMe_x(VO_4)_3OH$

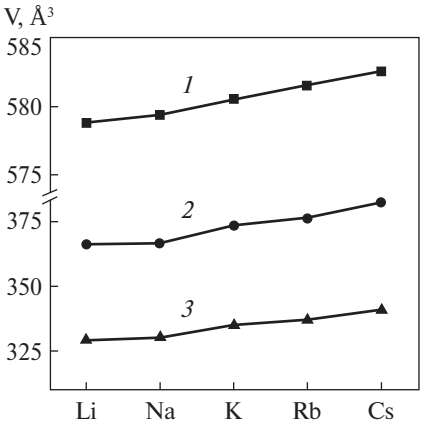

Fig. 7.6. Change of the size of unit cell of $Ca_{5-2x}La_xMe_x(VO_4)_3OH$ crystal by Ca^{2+} substitution for Me = Li, Na, K, Rb, Cs. The volume of atoms of the unit cell is given for demonstration of the lattice "friability"

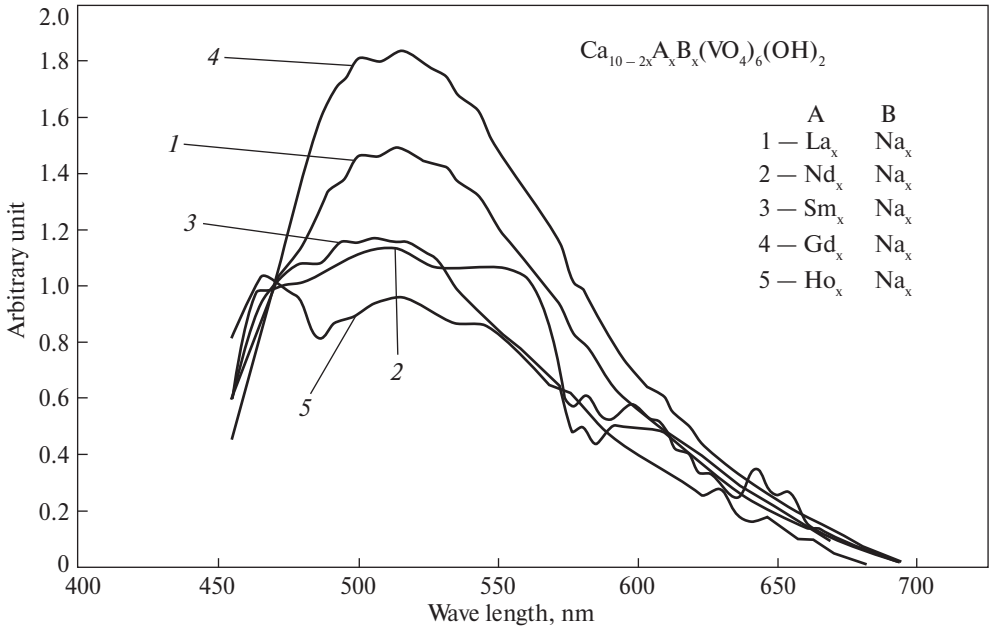

Fig. 7.7. Luminescence spectra of hydroxyvanadates (x=0.05), normalised to an intensity of zero-phonon maximum

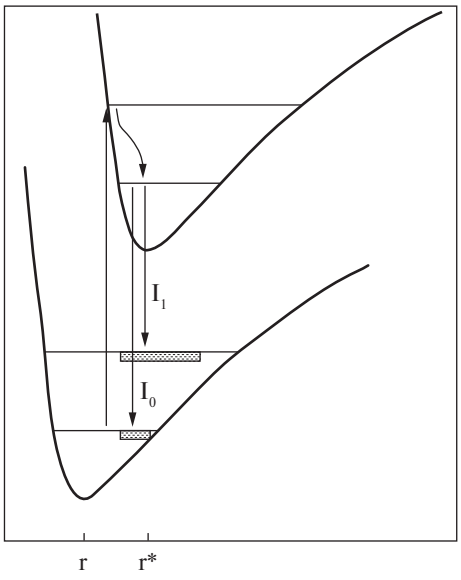

Fig. 7.8. The diagram of coordination curves of the ground and excited states and corresponding values of r and r* equilibrium position for the ground and excited states. The shaded rectangles represent the values of overlapping integrals. By increase of r* (Stokes shift) the value of overlap integral of I_0 transition sharply decreases

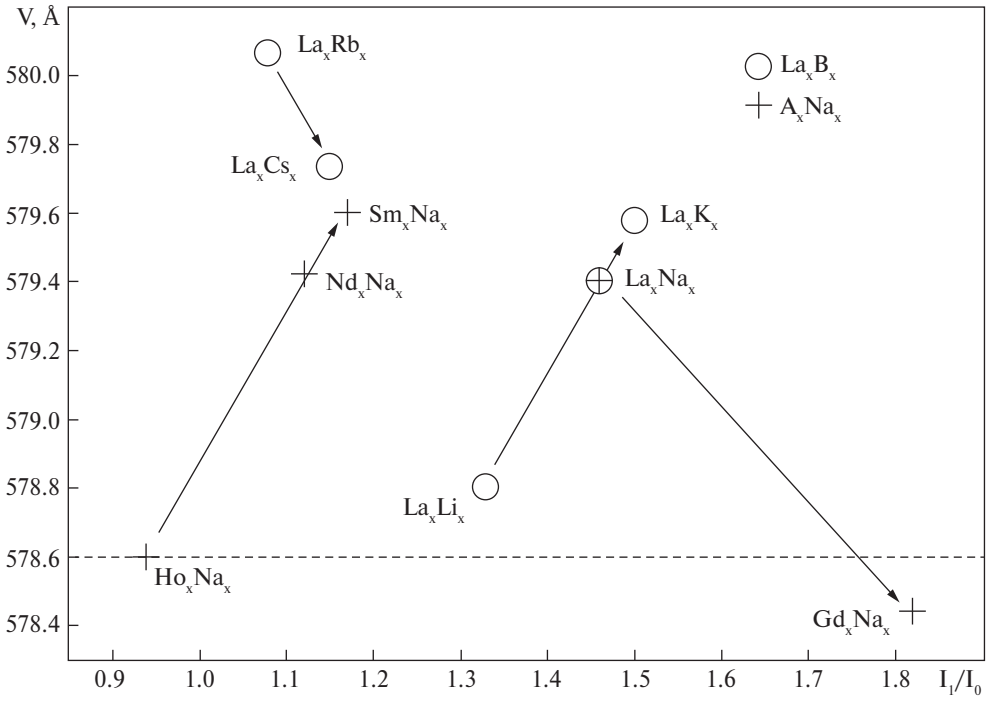

Fig. 7.9. Correlation between the band shape (the relation of the first phonon maximum to zero-phonon maximum) and the volume of a crystal lattice. The value of lattice volume of unsubstituted hydroxyapatite is indicated by a dotted line

As it can be seen from fig. 7.7, the intensities of zero-phonon band are lower than the intensity of the first phonon repeat (the exception is a spectrum for the case of Ho substitution). In the case of substitution for potassium, the maximum shift into long-wave area is observed. Probably, such behaviour is connected with the fact that among all substituents atomic radius of potassium is very close to atomic radius of calcium which is substituted.

It is possible to represent luminescence band intensity as product of transition probability (W_{if}) and integral of overlapping of wave functions of (M_{if}). If stokes shift is big enough it is possible that the probability of transition to a lower level becomes less than to a vibrational level though the probability of a transition to a lower level can be higher. It occurs because of reduction of overlapping integral (fig. 7.8). In such situation the ratio of intensities of the first phonon repeat and zero-phonon band can be an indicator of a shift of spatial equilibrium position of the excited r*-r state.

Let's analyze the obtained spectral dependences, having compared the ratio of intensities I_1/I_0 with the volume of unit cell (fig. 7.9). As it can be seen (fig. 7.9) for both alkaline and rare-earth substituents there is a monotonous dependence only for those elements which have not *d*-orbitals on outer and filled shells or on the top shells after the external. These are sequences from replacing atoms Li, Na, K and Ho, Nd, Sm — as it can be seen from the figure, just these points are within one line indicating that the larger is the cell volume, the larger is the spatial shift of equilibrium position of the excited state relatively to the ground state. For hydroxyapatites with calcium substituted for alkaline metals Cs and Rb, having *d*-orbital in one of outer shells lower ratio of intensities I_1/I_0 corresponds to larger volume of an unit cell. The shape of band changes similarly by calcium substitution for lanthanoids, containing *d*-orbitals in the outer shell (La and Gd).

7.2. IR- and UV-spectra of isomorphically-substituted calcium and strontium apatites

It is possible to realize a wide range of anion and cations substitutions outside of tetrahedral sublattice. Thus tetrahedrons themselves can distort depending on the ratio of dimensions of substituent ions and tetrahedrons that correspond to their steady configuration. An important task is determining of influence of ion substitutions in phosphate-apatite lattice on the structure of vibrational absorption bands of tetrahedral sublattice. As vibrational spectra of tetrahedral sublattice are sensitive to local environment symmetry it is possible to make a conclusion about variation of its local symmetry based on changes in IR-spectra.

By introduction of rare-earth and alkaline-earth elements into $Sr_5(PO_4)_3OH$ lattice, the reduction of half-width of absorption bands (tab. 7.1) was observed.

IR-spectra of isomorphically modified calcium hydroxyvanadate show monotonous reduction of bandwidth in the series Li→Na→Rb (fig. 7.10) indicating suppres-

sion of anharmonicity of fluctuations of tetrahedral sublattice, by doping with lanthanum and alkaline earth metals.

As the atomic number of alkaline metal oscillations corresponding to ~800 cm^- and 620 cm^- become separated. From fig. 7.10 we can see that for $Ca_{5-2x}Rb_xLa_x(VO_4)_3OH$ sample the bands corresponding to oscillations near 800 cm^- and 620 cm^- practically do not overlap.

Thus, isomorphic doping of calcium hydroxyvanadate with lanthanum and alkaline earth elements increases symmetry of oscillations of tetrahedrons in the series Li→Na→Rb. At the same time, as it can be seen from table 7.2, there is an insignificant increase of width of the forbidden zone from 3.97 up to 4.07 eV that may be a consequence of normalization of the occupied valence levels.

The last conclusion is proved by consideration of calculation data on electronic structure of compounds. Thus the comparison of theoretical DOS curves of $Ca_8NaLa(VO_4)_6(OH)_2$ and $Ca_8KLa(VO_4)_6(OH)_2$ shows (chapter 5) an increase of DOS curve intensity in the region of subvalence states (~20 eV) and a shift of the main peak of DOS curve into a region of higher binding energies for potassium-containing compounds.

All isomorphically substituted compounds have shown absorption in UV area at frequency of radiation over 30 000 cm^- (tab. 7.2). The width of the zone of all samples is approximately identical and almost coincides with the width of the zone of unsubstituted $Ca_{10}(VO_4)_6(OH)_2$ (~4.05 eV). It indicates that substitution of calcium ions for ions of alkaline-earth and rare-earth elements in the given proportions doesn't significantly influences the electronic (zonal) crystal structure. Introduction of alkaline elements (Cs (E_g=4.07 eV) and Li (E_g=3.97 eV), and also rare-earth element Sm (E_g=4.00 eV) leads to.

In the visible region of only spectra of two samples ($Ca_{10-4x}Na_{2x}Nd_{2x}(VO_4)_6(OH)_2$ and $Ca_{10-4x}Na_{2x}Ho_{2x}(VO_4)_6(OH)_2$) have shown narrow absorption lines, characteristic for ions of the rare-earth elements. As a whole, the presence of absorption lines in the visible region of spectra of $Ca_{10-4x}Na_{2x}Nd_{2x}(VO_4)_6(OH)_2$ and $Ca_{10-4x}Na_{2x}Ho_{2x}(VO_4)_6(OH)_2$ samples is characteristic for Nd^{3+} и Ho^{3+} ions. Gd^{3+} ions have no absorption lines in the visible region.

Suppression of anharmonicity of vibration in a crystal lattice of apatite with a mixed composition. It is known that widening of vibrational bands in absorption spectra of a crystal lattice is mainly connected with anharmonicity of its vibrational

Table 7.1. **Half-width of absorption band at 1030 cm^{-1} depending on the structure of phosphate-apatite.**

Compound	Band half-width, cm^{-1}
$Sr_5(PO_4)_3OH$	430
$Sr_3NaLa(PO_4)_3OH$	330

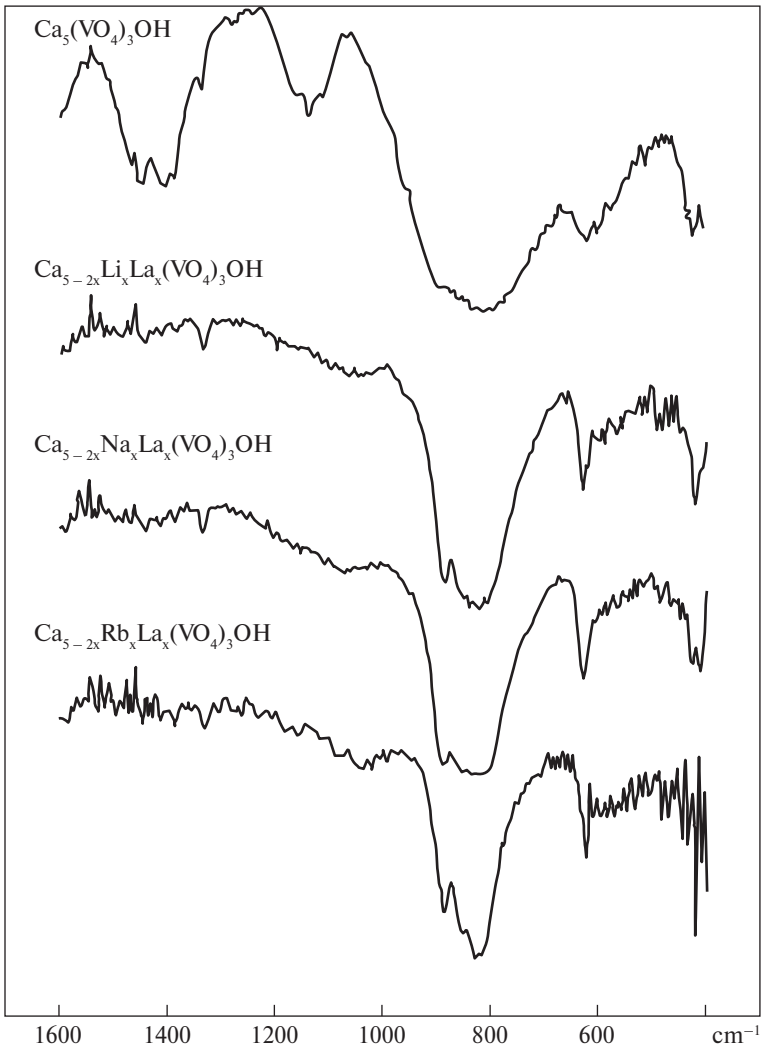

Fig. 7.10. IR-spectra of compounds (x=0.05)

modes [285-287]. The necessary condition for harmonic vibrations is independence of oscillators. By interaction of oscillators an anharmonic component of their fluctuations appears, leading to widening of vibrational modes.

Real observation of the contribution of anharmonicity into widening of vibrational bands in spectra often is complicated by the influence of other factors, for example, such as decrease of local environment symmetry of oscillators [288], leading to spitting of symmetry of vibrations and splitting of absorption lines. The contribution of anharmonic component into the widening of vibrational bands, however, can be traced by an example of the crystals, allowing ion substitution without distortion

of crystal structure of a lattice. Apatites belong to such crystals. The crystal structure of hydroxyapatite belongs to spatial group $P6_3/m$, and includes tetrahedral sublattice which allows phosphorus substitution for vanadium or arsenic [1]. In the apatites with mixed composition synthesized by us, PO_4 and VO_4 tetrahedrons alternate in tetrahedral sublattice. The ratio of these elements can be randomly set that is allowed by full isomorphic substitution.

On fig. 7.11 there are shown transmission spectra of samples of investigated apatites. The spectra of initial phosphate and vanadium apatites are characterised with two intensive groups of bands near 1030 cm^{-1} and 550 cm^{-1} for phosphate apatite, 850 cm^{-1} and 450 cm^{-1} for vanadate apatite which correspond to ν_3 and ν_4 vibrations of tetrahedral groups [221]. The half-width of the given absorption bands is determined, in particular, with splitting of vibrational modes of a free tetrahedron owing to decrease of local symmetry of an environment as it has been shown in [289]. In spectra of samples with mixed composition there is observed a simple superposition of the bands indicated above and belonging to different tetrahedral groups, however, with a change of relative intensity of bands. The change of intensity of bands is proportional to a change of the P/V ratio in apatite structure. There wasn't observed new bands or widening of bands, corresponding to initial crystal structures in spectra, indicating that symmetry of a lattice in the samples with mixed composition practically does not differ from the symmetry of initial forms. It is confirmed with X-ray diffractions study showing gradual change of the lattice parameters by substitution of elements in tetrahedral sublattice [275, 290].

Virational modes ν_3 for phosphate and vanadate apatite are significantly spaced and do not overlap. From absorption spectra (fig. 7.11) it can be seen that by change of ratio of phosphate and vanadate tetrahedrons, there is a reduction of half-width of absorption band of corresponding tetrahedrons by reduction of their concentration in

Table 7.2. **Energy extent of the forbidden zone of compounds (x=0.05).**

	Compound	Bandwidth, E_g, eV
1.	$Ca_{5-2x}Li_xLa_x(VO_4)_3OH$	3.97
2.	$Ca_{5-2x}Na_xLa_x(VO_4)_3OH$	4.03
3.	$Ca_{5-2x}K_xLa_x(VO_4)_3OH$	4.05
4.	$Ca_{5-2x}Rb_xLa_x(VO_4)_3OH$	4.05
5.	$Ca_{5-2x}Cs_xLa_x(VO_4)_3OH$	4.07
6.	$Ca_{5-2x}Na_xNd_x(VO_4)_3OH$	4.05
7.	$Ca_{5-2x}Na_xSm_x(VO_4)_3OH$	4.00
8.	$Ca_{5-2x}Na_xGd_x(VO_4)_3OH$	4.05
9.	$Ca_{5-2x}Na_xHo_x(VO_4)_3OH$	4.05

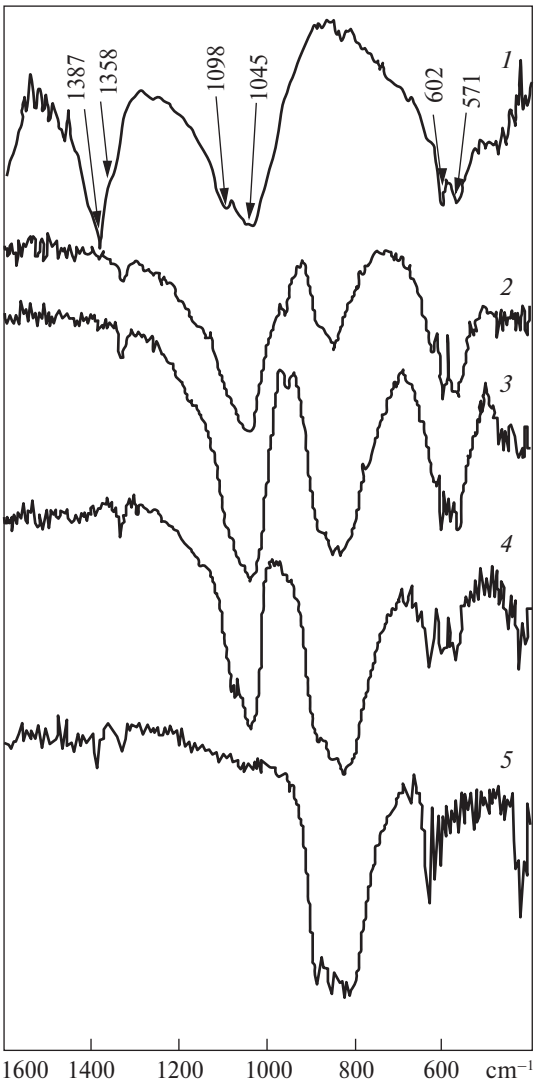

Fig. 7.11. IR — absorption spectra of $Ca_{10}(PO_4)_x \times (VO_4)_{6-x}(OH)_2$ apatites: (1) $x=6$, (2) $x=5$, (3) $x=3$, (4) $x=1$, (5) $x=0$

apatite sublattice (tab. 7.3). It is significant that half-width of bands for phosphate and vanadium tetrahedrons correlates with each other for the same P:V and V:P ratios [291].

When the ratio of one type of tetrahedrons to another decreases to 1:5 the concentration of the first type of tetrahedrons becomes small enough, so they are isolated from each other and it is possible to consider that there is no interaction of their characteristic vibrational modes between. Thus the half-width of absorption line decreases 2-fold comparing to the initial "undiluted" form. This reduction of half-width of absorption band is connected with the reduction of interaction and, as a consequence, with suppression of anharmonicity of oscillations of quasi-free tetrahedrons.

The residual widening of absorption bands is connected, apparently, with interaction with the surrounding tetrahedrons having other frequency of oscillations, and with internal factors in the tetrahedron (for example, a decrease of local symmetry etc.).

Comparison of contributions into half-width of absorption band of internal factors and anharmonicity of lattices shows that the latter factor determines the half-width of absorption band. Hence, anharmonicity of oscillations in an apatite lattice may be changed depending on the concentration of oscillators of one type in a crystal structure. These changes are local and it is possible to create the necessary spatial distribution of anharmonic component in a crystal using various substitutions that opens a prospect of controllable change of heat conductivity, coefficient of temperature expansion and other parameters in a crystal which depend on anharmonicity of lattice oscilations.

7.3. Thermal properties

Investigation of thermal properties is important for evaluation of not only thermal stability, but also for realization of processes of anharmonicity in mixed tetrahedral structures.

There was conducted thermogravimetric investigation of samples with composition: $Ca_{10}(PO_4)_6(OH)_2$, $Ca_{10}(PO_4)_3(VO_4)_3(OH)_2$, $Ca_{10}(PO_4)_1(VO_4)_5(OH)_2$ [292]. Samples of identical weight (~0.3 g) were heated up in platinum tigls to different temperatures at various heat rate, in air, in the limited space in the conditions of free convecting exchange (fig. 7.12).

From the analysis of the obtained time dependences $T = f(\tau)$ - temperature, $T = (DTA) = f(\tau)$ — temperatures difference between a sample and the standard, $\Delta M(TG) = f(\tau)$ — changes of weight and $\frac{\Delta M}{\Delta t}(DTG) = f(\tau)$ — speed of change of weight, it follows that the process of change of weight and enthalpy (heat content) has complex and multistage character with different kinetic and thermodynamic parameters for each stage.

First three low-temperature effects — two endothermal (315—473—715 K) and one exothermal effects (527—608 K) — are considerable in magnitude and correspond to a great reduction of weight (15—17% by weight) with the general weight losses making 22—27%. The next 5 thermal effects with starting temperatures of 715, 1013, 1623, 1733 K correspond to phase processes, the last three of which do not change the law of change of weight of investigated probe determined up to this period. It must be noted that in this experiment the reversibility of the last phase transition was determined. This transition corresponds to 1773 K in the heating curve, and in the cooling curve it appears at 1767 K while the maximum heating temperature is 1776 K.

On the basis of DTA-curves it follows that the processes progressing in the range of temperatures up to 800 K, generally are endothermic, however, starting approximately from 850 K, endothermacy of the process decreases and DTA curve tend to the initial zero position.

Table 7.3. **Half-width of ν_3 absorption band in phosphate-vanadate apatites.**

Compound	Half-width of absorption band of PO_4^{3-} subblatice, cm^{-1}	Half-width of absorption band of VO_4^{3-} sublattice, cm^{-1}
$Ca_5(PO_4)_3OH$	210	—
$Ca_{10}(PO_4)_5(VO_4)(OH)_2$	150	90
$Ca_{10}(PO_4)_3(VO_4)_3(OH)_2$	130	135
$Ca_{10}(PO_4)(VO_4)_5(OH)_2$	95	140
$Ca_5(VO_4)_3OH$	—	190

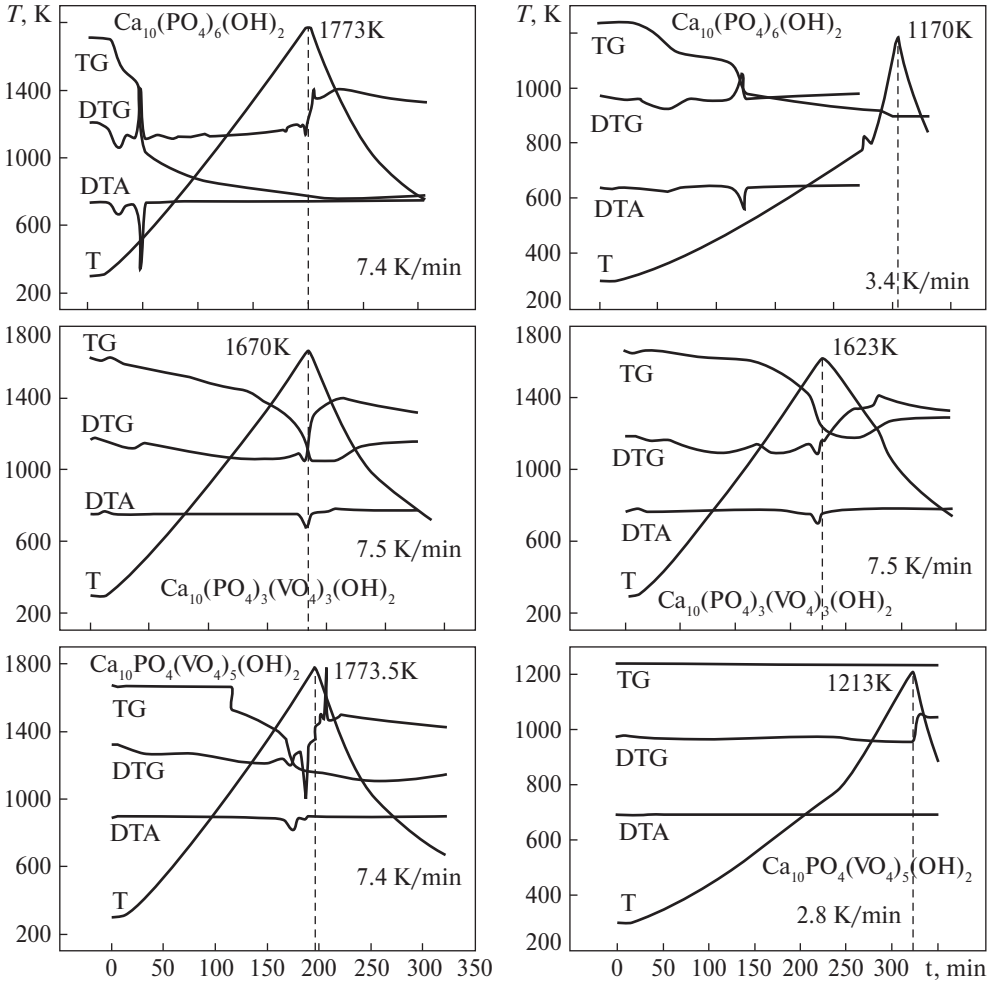

Fig. 7.12. DTA curves of compounds

When comparing parameters of kinetics of processes occurring in $Ca_{10}(PO_4)_6(OH)_2$ during heating at various speeds (~8÷2.5K/min) it is found that at low heating rates temperature intervals of the first 2 stages are shifted towards lower temperatures. There are 2 stages of weight reduction process in TG and DTA curves in the temperature interval 570÷850 K and at the heating rate of 8 K/min and in the curve obtained at the heating rate of 2 K/min there is only the third stage in this temperature interval.

It must be noted that character of TG, DTA, DTG curves by heating obviously depends on the technology of the material preparation.

By substitution of a part of PO_4 ions for VO_4 ions in apatite $Ca_{10}(PO_4)_6(OH)_2$ the general character of a curve of weight change by heating does not vary and can be described with the same mathematical model.

By heating of $Ca_{10}(PO_4)_3(VO_4)_3(OH)_2$ to 1673 K multistage character of the process is clearly found in the TG-curve. At the same time on the DTA-curve, unlike Ca-HAP, there are only two indistinct minima and the general increasing endothermic deviation which tends to decrease at temperatures above 1305 K. Against this reduction of endothermic deviation in the temperatures interval from ~1600 up to 1675 K there is clearly found an endothermic effect corresponding to the highest rate of weight loss. In this interval the weight decreases by 0.9% while the general losses make ~2.7%. The revealed endo-effect is partly reversible as there were found two small subsequent exo-splashes in the temperature interval from 1485 to 1405 K by cooling. The maximum heating temperature was equal to 1675 K. From the temperature of this effect (1600 K) it follows that the majority of the absorbed heat is connected with the reduction of weight and rather small part – with the reversible phase transformation. Proceeding from the visual studying of heating products with the subsequent fast cooling the mentioned effect can be connected with a partial fusion of the product.

The most important feature of the transformations observed by heating of apatite $Ca_{10}(PO_4)_3(VO_4)_3(OH)_2$ is the absence of 2 low-temperature stages occurring in the temperature interval from 315 up to 715 K which are characteristic for apatite $Ca_{10}(PO_4)_6(OH)_2$ and are accompanied with a great reduction of weight and with the presence of one isolated endothermic effect and superposition of one endothermic and one exothermal effects on the DTA curve. The second feature of process of the mixed apatite is that the total losses of sample weight make only 2.7%, i.e. by an order of magnitude less than losses determined for Ca-HAP. It must be noted that total weight losses are lower than the content of hydroxyl group in the initial material.

And, finally, one more feature the mixed apatite is that the maximum losses and the rate of weight reduction are observed in the range of high temperatures (~2% by weight; $V_{max} \approx 1.80 \div 1.90$ g/g· s) while for Ca-HAP such large values of parameters of kinetics are observed in low-temperature regions ($5 \div 8$ (I stage) and 10-9 (II stage), V_{max}=9 (I stage) and 80 (II stage) g/g·s). After heating of apatite $Ca_{10}PO_4(VO_4)_5(OH)_2$ that had formed by PO_4 substitution for VO_4 the general character of processes didn't change greatly. The quantity of stages considerably decreases. There is no small fragmentation and there are only three stages found. Three stages are discernable also in the DTA-curve (to endothermic effect at 1528 K) which has smaller endothermic deviation than DTA-curve, obtained for apatite $Ca_{10}(PO_4)_3(VO_4)_3(OH)_2$ by heating in the same temperature interval. It is caused with a lower weight loss of apatite $Ca_{10}PO_4(VO_4)_5(OH)_2$ in this temperature interval and in the general process (2.11% in comparison with 2.7% by weight). Both the rise of desorption temperature and the shift of the endothermic effect into a region of low temperatures (1623→1528→1523 K) must be labeled as quantitative changes caused with an increase of VO_4 content.

From the analysis of temperature of endothermic effects and of temperature interval of fusion of apatite $Ca_{10}PO_4(VO_4)_5(OH)_2$ (1668-1733 K) it follows that with the increase of content of VO_4 component in apatite the fusion temperature decreases.

Besides shift of desorption processes into a region of higher temperatures by isomorphic introduction of VO_4 ions into apatite $Ca_{10}(PO_4)_6(OH)_2$ it is possible to assume that the physics of the phenomena occurring by heating changes too.

CONCLUSIONS

The comparison of luminescence spectra of calcium hydroxyapatite with PO_4 and VO_4 tetrahedral lattices shows that the luminescence of vanadates has by an order of magnitude lower quantum yield that is caused with the presence of intensive vibrational modes which are channels of radiationless recombination. Spectral luminescence maximum of vanadate is shifted by 0.27 eV into long-wave region. The energy value of the corresponding vibrational transitions in VO_4 sublattice is less, than in PO_4 sublattice.

The comparison of the shape of luminescence band (which was analyzed by value of the–ratio between the first phonon repeat and the intensity of zero- phonon maximum) with the lattice parameters shows correlation of these parameters, namely, by an increase of crystal cell volume as a result of calcium substitution for alkaline-earth and rare-earth metals (in equal concentrations) the I_1/I_0 ratio which is connected with an increase in Stocks-shift increases. The given dependence is broken by substitution for elements containing outer *d*-shells.

By introduction of REM ions into apatite lattice they begin intensively luminesce and are effective quenchers of intrinsic luminescence of VO_4^{3-} ions.

It was found that substitution $PO_4 \rightarrow VO_4$ in $Ca_{10}(PO_4)_6(OH)_2$ with the concentration increase leads to a shift of desorption into a region of higher temperatures and, presumably, to a change of mechanism of the phenomena occurring by heating. The melting temperature decreases with the increase ofcontent of tetrahedral component VO_4 .

The reduction of half-width of IR absorption band characterizing tetrahedrons is connected with a reduction of their interaction and, as a consequence, with the suppression of anharmonicity of oscillations of quasi-free tetrahedrons. It was also found that anharmonicity of oscillations in a crystal lattice of apatite may change depending on a concentration of tetrahedrons of the given type. Such changes are local and it is possible to generate the necessary spatial distribution of anharmonic component in a crystal that opens a perspective of controlled modification of heat conductivity, factor of temperature expansion and other parameters in a crystal which are determined with anharmonicity of lattice fluctuations. The comparison of contributions of internal factors and anharmonicity of lattice fluctuations to half-width of absorption band shows that the last factor determines half-width of absorption band.

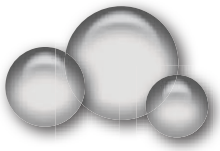

CHAPTER 8

NATURAL APATITE MINERALS

8.1. Geochemistry and geology of calcium phosphate formations in the nature

The exsolutional mechanism of mineral formation, as well as its consequences, remains one of the little-studied sections of mineralogy. At the same time underestimation of such phenomenon in investigation of mineral associations in various genetic structures may lead to serious errors. Especially, if it is considered that dissociation of solid solutions is rather widely spread and, apparently, is characteristic for many, if not for the majority of minerals. In work [293] the case of anomalous type of apatite disintegration which is known as rather steady phase, that is formed in a very wide range of physicochemical conditions and is notable for considerable variability of a chemical composition is considered. In this case by full preservation of a chemical composition of the initial system its phase structure has drastically changed: as a result of apatite disintegration the number of minerals in the neogenic exsolutional paragenesis has increased 6-fold that is interesting in different aspects.

At the decision of genetic questions of mineral formation it is essential to consider: crystallization pressure which in certain cases may reach 100 kg/cm^2 (especially for silica); the possible reason promoting the occurrence of unique concentrations of separate elements and their natural paragenesis in specific natural systems, etc.; the special geochemical role of elements with variable valence, and also of isotopes with magic numbers of protons and neutrons in their nuclei (only 5 from 284 stable isotopes, namely ^{16}O, ^{27}Al, ^{28}Si, ^{39}K, ^{40}Ca, make more than 87% of the Earth crust substance).

Therefore consideration of geochemistry and mineralogy of any chemical element or of its natural paragenesis should be begun with revealing and studying of the causes of specific geochemical properties of these elements. Potentially possessing

almost all possible geochemical properties, elements show each of these properties only in specific conditions of natural systems. In geochemistry and mineralogy actual data on quantitative distribution of elements (and their isotopes) and minerals in natural systems both in dispersed (clarkes) and in concentrated state. Thus the presence of each fact should be defined by the set of such scientifically-proved criteria of factology, as objectivity, imposing appearance, reliability, reproducibility, the importance (scientific, applied, etc.) and causality of its display and spatial localization.

Minerals and synthetic compounds with the general formula $A_{10}(TO_4)_6X_2$ (A=Ca, Sr, Ba, Pb, REE, Na, Mg, Cd, Fe, K, Li; T=P, Si, Ge, As, Cr, N, V, S; X=F, Cl, OH, O, Br, J, CO_3) and with apatite structure form a big family of compounds which is widely studied in connection with biological, technical and ecological aspects of their application. Thanks to wide structural compatibility of isomorphic substituents, the structure of many of these compounds is complex; nevertheless most of them are characterized with low degree of cation and anion ordering. The discovery of a new representative of this family of minerals is of interest for studying of structural ordering in apatite rich in isomorphic impurities.

The new mineral conventionally named "R-apatite" (R=Sr, Na, Ce), was found in ultra-apatite pegmatites of the Hibinsky alkaline massif (Kola Peninsula) and described in work [294]. It is represented with transparent pale yellow prismatic crystals up to 5 mm in size and their aggregations in epitaxial intergrowths with other apatite-like minerals – deloneite and belovite. The new mineral is optically negative, monoaxial, with n_e=1.637 and n_0=1.649.

The Chemical composition of a mineral determined using the microprobe analysis is:

$$(Ca_{6.31}Sr_{2.33}Na_{0.65})_{\Sigma 9.29} \times (Ce_{0.24}La_{0.19}Nd_{0.10}Pr_{0.02}Sm_{0.01})_{\Sigma 0.66} \times$$
$$\times (P_{5.93}Si_{0.11})_{\Sigma 6.04}O_{24}(F_{1.33}(OH)_{0.67})_{\Sigma 2.0}$$

Well studied structural type of apatite is characterized with a presence of A-polyhedra of two configurations (heptahedrons and nonahedrons) which merge into framework with shared vertexes, edges and facets. PO_4-tetrahedrons are located in cavities of framework, and extraradical X-anions are located on 6_3 axes. Symmetry of single-cation apatites, as a rule, belong to spatial group $P6_3/m$. Symmetry reduction may be caused with a shift of X-anions from individual positions on a symmetry plane *m* because of mismatch between dimensions of these anions and cations that are introduced. The plastic of apatite framework supposes various cation and anion isomorphism and can be deformed in *a* and *c* axes by change of composition, often with decrease of the general symmetry to monocline one. Thus in polycation apatites the main factor that lowers symmetry of the structure, apparently, is ordering of isomorphic impurities both in cation positions (including tetrahedral), and in positions of extra-radical anions.

Symmetry reduction to $P6_3$ of the structure of the studied R-apatite is caused with ordered distribution of Na, Sr and Ce impurities in polyhedrons located on tri-

ple axes. Displacement of extraradical (F, OH)-anion from a position in a plane *m* to a common position is also a factor that breaks the symmetry of the given apatite.

In Europe is one of the apatites' formations is territory of Italy. Characteristics of minerals of apatite group from some rocks of late Pleistocene in Italy were compared with apatites of other formations [295]. There have been identified three genetic groups of apatite. The group I includes apatite samples with high content of P, Sr, REM and F. Group II includes apatites from well-granulated samples with high content of C, Si, O, and low of S and with prevailing substitution of P for C and Si. Group III includes apatites from alkalic rocks with high content of S, F and low content of C and O and with prevailing substitution of P for S and Si. Considerable differences between geochemical characteristics of apatites from displaced and alkaline breeds may indicate magma stratification into silicate and carbonate liquid melts in corresponding conditions. Data on the occupation of crystallographic positions and length of the bonds determined in the course of refinement of the samples structure, show that for REE and Sr $Ca_{(2)}$ positions are preferable including cases when in the REE-enriched samples partial Ca substitution for REE in $Ca_{(l)}$ position [296] was observed.

Important changes in crystal chemistry of FAP from deposits of St. Marcel Praborn of Val d'Aosta mine (Italy) are studied in work [297]. Cathode luminescence along with electron probe analysis have revealed direct dependence between intensity of the luminescence spectrum and concentration of Mn^{2+} and As^{5+}. The increase in degree of P substitution for As or Ca substitution for Sr, connected with formation of cracks and filterability of minerals, was observed in apatite at the last stage of its formation. Arsenic effectively suppresses the luminescence caused with incorporation of REE, and only partially suppresses emission in samples with high concentration of Mn^{2+}. Substantial increase of As content (up to 10 weight. % As_2O_5) causes full suppression of a luminescence.

Evolutionary apatite, possibly, formed due to recrystallization of phosphate which was present during deposition of silica or in organic slime which is a product precipitated at the [298]. Isotope composition of the apatite indicates that Sm/Nd fractionation occurred within last 100 million years. The formation of Nd-isotope anomalies can be described as a process of diagenetic burial, including local enrichment of apatite with REE and additional exhaustion of surrounding rocks concerning REE. Though experimental of the apatite/melts distribution coefficients, defined by conditions of magmatic temperatures, predict much lower Sm/Nd fractionation, than it is really observed in the obtained samples, it is possible to make the assumption that the fractionation degree may increase considerably after cooling of the given samples. The presence of these anomalies does not reject a model of age profiling of Sm-Nd for sea sandstones. In the course of studying the special attention should be given to revealing of correlation between the age of Sm-Nd model and the Sm/Nd fractionation coefficients which may indicate a presence of abnormal effects. For such cases the isotope relation $^{143}Nd/^{144}Nd$ can give a reliable information about a source.

Apatite occurs throughout Ontario complex with mines including mainly norite, quartz gabbro and granophyr [299]. Apatite is found in the form of a postaccumulation and of a formed mineral in quartz gabbro. Despite textural signs of fast growth, apatite is homogeneous and contains F^-, Cl^- and OH^-. The content of Cl^- and O^{2-} is lowered. Concentration of REE reaches 2 weight.% of La_2O_3+Ce_2O_3+Nd_2O_3. The sedimentary complex was developing by fractional crystallisation of highly enriched basic magma. High initial values of $^{87}Sr/^{86}Sr$ ratio in the apatite indicate that relatively silicon-enriched basic magma corresponded in composition to the basic component of the Earth crust or probably completely consisted of the melted bark. Apatite from metamorphized parts of complex has much lower content of Cl^- and REE ions in comparison with the most ancient primary apatite.

Sr and REE in carbonatite deposits of Lyulekop (republic of South Africa) are investigated in work [300]. This field is known for complex copper sulfide, noble metal and phosphate ores. After detailed studying of sulphides in carbonatites there was revealed various mineralization of Sr-REE.

8.2. Lyulekop field

Lyulekop field forms the central part of the Palabor massif. It embraces an area of 675 × 360 m and is a vertical cylindrical body with concentrically-zonal structure. Carbonatites that interstratify with phoskorites are located closer to the center of deposit. Secant carbonatites are younger than interstratified. They make are the central part of a deposit and integrally form lenses and body secants. The age of the Palaborsky complex by the last estimates makes 2050-2012 million years.

Interstratified carbonatites refers to sevites. The main part of rock (nearby 70 w. %) makes medium-grained calcite. There are present dolomite bars in calcite that were generated due to decomposition of the primary firm carbonate solution. There are also larger grains of dolomite of 3-5 mm in diameter and their aggregates.

The most widespread accessories of Lyulekop carnonatites are magnetite, phlogopite, apatite and various sulphides. Magnetite of early generation forms isometric grains, 1-10 mm in size, and late generation magnetite forms borders around sulphide aggregates. Chalcopyrite, cubanite, pentlandite, bornite and chalcosine prevail among sulphides. Sulphides dissect calcite-dolomite aggregation in the form of lenses and veinlets, 2-3 mm thick. In the interstratified carbonatites rare isometric and idiomorphic grains of thorianite, brazilite, and also minerals of Sr and REE occur. Their dimensions, as a rule, do not exceed 200 microns.

Intersecting carbonatites are composed of fine- and medium-grained dolomite-calcite aggregates. In the studied samples of carbonatites dolomite makes about 70 w. %, 15 w. % falls at calcite. Calcite crystallised after dolomite and formed xenomorphic and lens-shaped isolations in the dolomite aggregate. Sulphides are present in these rocks in the form of lenses and veinlets up to 5 mm in thickness. The prevailing

sulphides are pirrotine and cubanite. Accessory minerals of intersecting carbonatites are magnetite, thetraferriphlogopite, and also carbonates of Sr and REE.

The character of distribution of REE in different minerals allows to assert that at the beginning of the process of carbonatite formation conditions for REE occurence in crystal lattices of the minerals were more favorable, and until near the end of this process a decrease of carbonatite formation was observed. Apparently, these facts are connected with dynamics of change of the environment acidity during the period of carbonatite formation.

The complete similarity of the character of distribution of the REE in all studied minerals allows to assume that during formation of carbonatite of Lyulekop field throughout the whole period of their evolution there was no losses or introduction of significant amounts of the rare earth elements from outside. Essentially it means the absence of any prospect of search for significant concentrations of rare-earth minerals in rocks that are directly adjacent to Lyulekop carbonatites.

The features of REE composition of the investigated minerals indicate the existence of, at least, two paragenetic associations of minerals in the interstratified carbonatites. They differ in physical and chemical conditions of formation. As a whole the results of the analysis of REE distribution and the values of indicator Nd/La and Ce/La ratios indicate the following scheme of the course of carbonatite formation processes. The beginning of crystallization of interstratified (it is essential, calcite ones) carbonatites occurred in the conditions of increased alkalinity that promoted the occurrence of cations in a crystal lattice of minerals, characterized with large ionic radiuses. Among such elements Sr^{2+} is, and in early paragenesis of minerals (carbonatites) there is really observed increased content of strontium minerals – strontianite, celestine and high-strontium apatite. The later stage of formation of interstratified carbonatites was characterized with a significant decrease of alkalinity, favouring the incorporation of light REE cations into carbonates and phosphates. Thereof in late associations of interstratified carbonatites the maximum content and variety of rare-earth minerals is observed. The latest intersected carbonatites of Lyulekop field formed in the conditions of increased alkalinity of environment of mineral formation that is observed in an increase of content of strontium minerals (ancylite and strontianite) and in the general decrease of rare-earth minerals content in these rocks.

Sr- and REE-containing minerals are genetically inseparably linked with a crystallization of the main rockforming minerals, namely calcite, dolomite and apatite. Both carbonate, and apatite stages of carbonatites formation began with the formation of these main minerals, and came to the end with a crystallization of REE carbonates and phosphates. And most likely, Sr and REE originally dissipated in rockforming minerals, and the main part of rare-earth minerals in carbonatites of Lyulekop field was formed during hydrothermal transformation of primary protocarbonates and protophosphates. The sulphide mineralization occurred after rare-earth one that is confirmed with structurally-morphological relations of carbonatites minerals.

8.3. Features of carbonate apatites of Dunkeldyksky massif (Eastern Pamir)

Thermometric investigation of some carbonatites has shown the presence of multiphase crystalfluid, crystalgas and carbonate inclusions, containing up to 6-8 solid phases. Their homogenization occurs in a range of temperatures of 870-860 (garnet), 830-810 (apatite), 700-610 (fluorite), 620-600 °C (celestine) [301].

As a result of change of physical and chemical conditions primarily because of temperature decrease (Dunkeldyk carbonatites crystallized at 600-800 °C and above), the solid solution with complex composition becomes unstable and decomposes into two or several separate phases (mainly calcite and strontianite). The decomposition which is a consequence of decrease of solubility of one component in another occurs in the solid state and, probably, is accompanied with an increase of sulphur content. In addition, the activity of sulphate-ions may intensify strontium transition from the isomorphic to own mineral form.

There can be assumed sulphate incorporation into calcite crystal lattice in consideration of existence of $CaCO_3$-$CaSO_4$ solid solution that is quite possible at high temperatures. By protocarbonate decomposition with the formation of sterile calcite there is a release of sulphate-anion and dopant cations (Sr, Ba, Fe, Cu, Pb, Zn, etc.) and formation of exsolutional phases in the form of sulphates (celestine, barite) and sulphides.

Among carbonatites fluorite plays even more important role, than celestine which content fluctuates between 5-7 and 30-35 weight %. Fluorite forms various regular accretions with calcite: fluorite forms dendritic, branch-like and latticed joints with rhomboid cells. Therefore can be assumed that fluorite in carbonatites is a product of decomposition of primary fluorine carbonate, containing Sr and Ba, an also Mg, Fe, REE, etc. Thus exsolutional phases should differ from a matrix only in anion structure. In the described carbonatites calcite ($CaCO_3$) and fluorite (CaF_2) are generated by protocarbonate decoposition. It is interesting that exsolutional fluorite is characterized with sharply increased content of rare-earth elements (0.47-0.78%), and first of all of lanthanides, that are impurities in primary calcite of carbonatites.

Carbonatites often possess striation which is caused with alternation of more intensive calcite and thin celestin streaks. The streaky habit of carbonatites is also due to parallel layers and lenses of both fluorite and fluorine carbonates of REE in mosaic calcite. The front of the noted isolations of celestine, fluorite and fluorine carbonate of REE usually is parallel to a contact of carbonatite dykes with deads or coincides with their extension. Fluid texture of carbonatites can be observed under microscope in good enough expressed orientation of calcite grains which direction of lengthening coincides with a direction of current.

Carbonatite melt, isolated in alkaline rocks of Dunkeldyk rose to the earth surface, in the weakened zones, mainly filling ruptures and cracks (and at that the melt also penetrated into a system of the thinnest cracks) as evidenced by sharp, usually rectilin-

ear contacts of carbonatite bodies with deads. As the pressure decreased and the melt cooled pyroxene, potassium feldspar, phlogopite, apatite, garnet started to crystallize at about 1000 °C and then at a temperature near 700 °C calcium protocarbonate started to crystallize which decomposes with a formation of calcite, fluorite, celestine, strontianite and barite. Simultaneously with calcite and minerals that are connected with it a small amount of sulphides is generated. Thus, carbonatites are products of a magmatic stage of evolution of deeply differentiated complex of potassium alkaline rocks.

8.4. Definition of deposition age

FAP may be used as a radiochronometer and a potential matrix for storage of secondary actinides obtained after reprocessing of spent nuclear fuel [302]. In work [303] there were carried out thermo-experiments where FAP was used as the standard for the description of helium diffusion from apatite. At temperatures below 265 °C, helium diffusion from apatite is a simple thermal process and does not depend on the quantity of accumulated helium. The speed of helium diffusion is determined by inverse dependence on square of a grain radius. Measurement of the crystallographic-focused extended sections indicates that coefficient of helium diffusion in apatite is practically isotropic. The estimation of activation energy of helium diffusion from apatite has shown that E_a=33±0.5 kcal/mole, with $\log(D_0)$=1.5±0.6 cm^2/s. When the apatite temperature raises from 265 up to 400 °C, there is a progressive and irreversible change in diffusion behaviour of He and, thus, the activation energy decreases. Such change coincides with activation of annealing of radiation damages in Durango apatite, indicating that transformation of defects during annealing plays a role in helium mass transfer through the apatite.

Thus the true age of apatite is usually described by relation (U-Th)/He which depends on the temperature dynamics in a zone mineral deposition and other geological factors [304].

In work [305] there was suggested an empirical calibration method of (U-Th)/He thermochronometer. The age of the apatites extracted from white mountains according to (U-Th)/He ratio in the surface cortical levels makes approximately 50-55 million years and decreases to ~12 million years at 4.5 km paleodepth. The uncovered temperature-sensitive windows of measurement of U-Th)/He ratio and thermo chronometers of tracks well supplement each other and may be used for reconstruction of thermal history that was clearly shown for a temperature window of 40-110 °C.

The tracks apatite decomposition and analysis of dynamics U-Th/He ratio are used for determination of low-temperature thermal boundary of San Gabriel and San Bernardino mountains (SGM and SBM) (Southern California [306]. The age of 33 samples from SGM is within 3 to 64 million years. The helium age determined for 13 samples is within limits 3 ÷ 43 million years. According to TS (track splitting) it has appeared that 10 SBM samples are older and their age is within 45 to 90 million years.

TS and He-data indicate, at least, three periods of cooling for SGM and only two for SBM samples. The thermal history of SGM for the first 7 million years seems to be identical during the basic period of cooling 60 ÷ 40 million years to the present period starting at 23 million years and proceeding to 10 million years. In SBM based on the TS data, there were registered two periods of cooling: they correspond to the period from 65 to 55 million years ago, and from 18 million years till today. The choice of time of the second period is poorly limited and, hence, the information on the SBM source is absent. The last period of cooling, possibly, has begun in 7 million years in SGM after beginning of shrinking deformation. The accelerated period of cooling, probably, has begun in 3 million years. The investigation indicates that faster lifting of a zone of deposits in eastern and southern parts of the hump has caused the present physical geography. Despite a large average height, SBM is much less divided than SGM, and it also can be seen that the present period of cooling and lifting of deposits has begun in the last 3 million years, i.e. much later than the lifting of deposits in SGM.

In U-Pb-descriptions of apatite simple volume scattering, without secondary growth and recrystallization which can deform U-Pb-systematization [307] is usually ascertained. Though in the apatite U and Pb are lattice-bound and, thus, U-Pb-systematization is not controlled with micro inclusions that is observed in a case of other uranium-deficient minerals like garnet and staurolite. The temperature values estimated from experimental and empirical investigations, are within 425 °C to 500 °C for typical scattering radiuses and cooling speeds (2-100 °C/million years, respectively). This area can be used for restriction of cooling and history of maturing of both ignous and metamorphic rocks. Apatite is a widespread phase in many types of rocks, and U-Pb-apatite dating can be a reliable thermochronometer. U-Pb-dating accuracy of apatite may vary from ±1.2% to ±0.3% by dating of Archaean or Proterozoic eruptions. The main restriction of accuracy in apatite U-Pb-dating is a medium or low value of U/Pb ratio, and the corresponding dependence of co-ordinate scale on a choice of initial Pb of isotope structure. For Proterozoic samples $^{206}Pb/^{204}Pb=100$ and the area of geologically acceptable initial lead isotope compositions can shift calculated U-Pb age on 60 million years.

The thermochronological survey of splitting tracks of Corsican apatite was undertaken for decoding of Neozoic thermotectonic evolution [308]. The considerable difference of TS-age of geographical zones from the southwest (old) and the northwest (younger) is interpreted as a result of two big cooling stage 26-20 million years and 18-10 million years old, accordingly.

Owing to stability of isotope system of apatite in relation to endogenous processes, this mineral is an indicator for search of the magmatic source using $^{87}Sr/^{86}Sr$ ratio [309]. Hence, apatite can be used as a reliable reference for construction of Rb-Sr isochore. $^{87}Sr/^{86}Sr$ values for apatite have allowed to determine three groups of copper molybdenum-porphyry deposits: 0.70393-0.70436 (the Late Palaeozoic – early Mesosoic; Mongolia); 0.70427-0.70509 (the Middle Palaeozoic; Kuznetsk Alatau, Tuva); and 0.70495-0.70902 (the Late Mesosoic; East Transbaikaliya, Stanovaya

Ridge). Due to metasomatic transformations of granites there was generated apatite with increased $^{87}Sr/^{86}Sr$ ratio (owing to enrichment with radiogenic strontium inherited from stone-forming granite-like minerals.

The kinetics of HAP transformations by interaction with sea water was studied. Decrease of pH and concentration of fluoride and a carbonate in the sea water occurs in a certain interval of concentrations of the introduced lime, which initiates the transition of HAP to fluorine hydroxyapatite. Within five weeks after start of experiments the composition of the sea water approach the equilibrium. It was determined that equilibrium concentration of the dissolved phosphorus decreases with an increase of fluoride concentration and increases with an increase of carbonate alkalinity.

8.5. Research of Martian meteorites

Martian soil keeps chemical information which is contained in the rocks and which age exceeds the age of the earliest Archaean geological era in the Earth history (about 3800 million years [310]). Organisms which used phosphorus, carbon and caused fractionating of carbon isotopes have been existed on the Earth for 3800 million years or within 600 million years after the Earth formation. The emergence of life on the Earth supposes a potential possibility of comparatively early emergence of life on Mars. This hypothesis will be plausible if it is found out that conditions (liquid water, available energy) were optimal for the origin of life, and life had reached the level of complexity when it could be recognized by chemical and maybe morphological remnants. The information about biological origin of minerals, their features and traces of organic compound in Martian meteorite ALH84001 was partially obtained from extrapolation interpretation of the supposed "nano-fossils" and of the nature of mineral formations of volcanic origin. Research of mineral formations of Martian meteorites and the oldest geological formations of the Earth give the possibility of search for life on Mars. The decision is based on the use of a phase ratio of minerals; obtaining of analytical data about distribution of carbon isotopes; solving of a important problem of interpretation of morpho-fossils.

Spectral study of minerals of Martian meteorite ALH84001 is resulted in work [311]. There were obtained Raman spectra of carbonates, silica and amorphous plagioclase and also micro-Raman and reflection IR spectra of phosphates in ALH84001. The obtained data show that carbonates have complex compositional heterogeneity at submicron scale; phosphates and chlorapatite predominantly are anhydrous; amorphous silica and plagioclase experienced peak pressure of >32 GPa and >50 GPa, respectively; glassy plagioclase was hardened during shock-induced melting after release of peak pressure.

The observed general widening of Raman bands of the lattice and internal modes of carbonates in ALH84001 indicate complex microscopic composite heterogeneity and probably structural disorder. Any prospecting of biogenetic traces in ALH84001 should consider thermal history of a mineral.

Research of chlorapatite inclusions of Martian meteorite Nakhla was carried out in work [312]. It was revealed that minerals are connected in boundary regions with halite. There was made an assumption that halite and other minerals have Martian origin, since conditions of meteorite impact prevent contamination of the meteorite ; textures indicate that minerals of this group crystallized in the same way as some silicates and other oxide forms of minerals within a meteorite; C and O-isotope compositions do not correspond to terrestrial origin.

Siderite has a number of components: $CaCO_3$, 0.1—5.7; $MgCO_3$, 2.0—40.9; $FeCO_3$, 23.2—87.0; $MnCO_3$, 1.0—39.9 mole %. There are two composite groupings, that have high (±30 mole %) and low $MnCO_3$ content with high $FeCO_3$ content. Structures of groupings do not composite groups may have different origin. Structural proofs of this or that interpretation are not found. Determination of solubility limit demands conducting of investigation of Fe and Mn carbonates. The presence of microelements was determined using ionic microprobe analysis of three siderite grains and one anhydrite grain. Siderite contains light and heavier REE except Ce or Eu. They are not typical for hydrothermal signatures which usually do not have such accurate pictures of relative content of REE. The nature of a mineral combination indicate that evaporites were its rocky sources on Mars. They may be present in craters and floodplains of Martian southern mountain location. There were suggested two models for explanation of incorporation of evaporite material in Nakhla-meteorite. Possibly incorporation has occurred in the process of low-temperature (<200 °C) crystallization from a water solution that goes with available experimental data concerning siderite stability. Alternatively it was suggested that evaporite material, probably, had been incorporated in natural Nakhla rock during melting and crystallization at 800 °C. The last model may explain the abundance of microelements, and also the presence of siderite texture which mean coalescence with the rest of intermediate melt. Both high- and low-temperature model is co-ordinated with the presence of evaporite deposits on Mars.

8.6. Crystalochemical aspects of biominerals formation

It is known that the main mineral of a bone is hydroxyapatite $Ca_5(PO_4)_3OH$. This mineral forms not only body skeleton, but also take part in metabolic interaction with it. More than 35 weight. % of dry degreased native bone is an organic part whereas the main part is inorganic calcium phosphate. The great interest inorganic calcium phosphate is not surprising if considering that hydroxyapatite represents the main source of phosphorus and calcium in the Earth's crust. Thus, in rocks of volcanic and sedimentary origin calcium phosphate is a prevailing component. The understanding of structure of calcifyied tissue increases with broadening of the area of existence and apatite application in various practical aspects of life.

Now the important questions of research of phosphates are problems of a mineral phase formation and its interaction with an organic matrix.

Fig. 8.1 and 8.2 illustrate stages of origin and the main cycles of calcium phosphate transformation in sea water starting from rocks of a volcanic origin and on a way to vegetative and animal forms. Originally on the Earth all apatite was present only as a part of rocks. Throughout many geological epochs the saturation of these primary rocks with water has caused formation of biological calcium phosphate, in its turn, resulted in deposition of so-called sedimentary apatite stratums. Goldschmidt [313] has determined that since the Earth origin 600 g of substance of bedrock falls per each kilogram of sea water. As the present sea water contains less than 0.1 million share of phosphorus, hence, on the average 99.8% of the total content of calcium phosphate that is dissolved in it precipitates anyway.

Skeletons of many sea inhabitants contain calcium phosphate minerals. Skeletons of organisms that were not reabsorbed in cycles, a carnivorous life, precipitating after death of these organisms form deep-water deposits of mineral substances.

Dissolution and reprecipitation of apatite in the biosphere represents a problem which has benn occupating minds of the scientists working in area of apatite-conduction for a long time. Biological decomposition and release of calcium phosphate in waters of the sealeads to formation of apatites which properties depend on their specific surface. On the other hand, bedrocks of volcanic origin as hydrothermal changing bedrocks contain apatite crystals possessing large critical sizes. Researche of physical properties of apatite is carried out using large crystals owing to difficulties of obtaining of ultra disperse materials. According to these measurements it is possible to judge properties of biologically important apatite systems though as it will be shown further, useful results of measurement of properties were obtained in a case of mineralized tissues.

Apatite mineral in bones and teeth is a source of information concerning diet, climate and environment factors. Apatite is used in geochemical research for dating of geological events and construction of schemes of the general phosphate cycle [314]. Apatites integrate the biogeochemical information, geochemical events and features of environment. But they also are a source of information for medical diagnostics. It is known that the mechanism of origin of deceases both natural and caused anthropologically in a global scale may be tracked in apatite mineral depositions.

In human and animal bones approximately 70% of weight accounts for $Ca_5(PO_4)_3(OH)$. Now bone diseases are extremely widespread [315]. There are annually fixed 1.5 million fractures caused with osteoporosis, a reduction of density of a bone. Recently obtained data indicate that there is a need in analysis of stability of Ca-HAP in a man's bone depending on geochemical features of environment. Till now the traditional approach to explanation and treatment of many diseases of bones and teeth was limited to studying of features of a human body. Environment influence was studied only from the point of view of excessive amounts of Sr, Se, U,

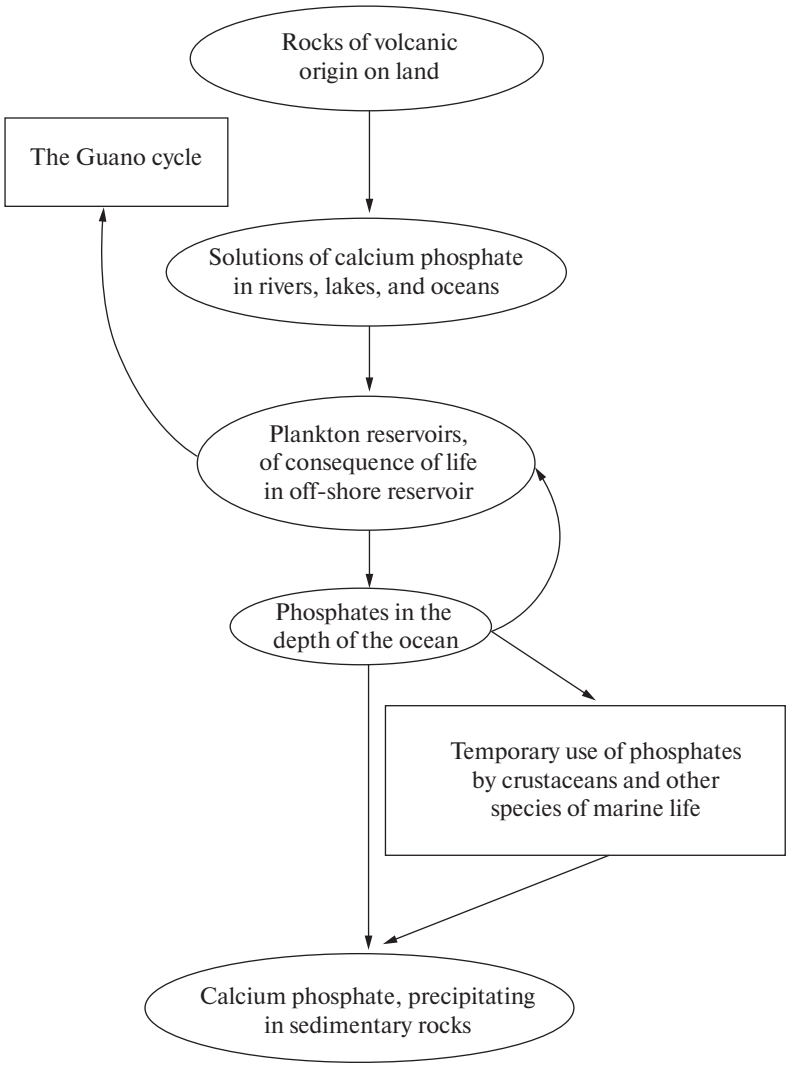

Fig. 8.1. The sea cycle of transformation of calcium phosphate [313]

Th and other micro components most of which isomorphically substitute calcium in apatite structure.

The structure of bones which is regenerated each 10 years is not always constant and is caused with a number of diseases. It is not excluded that the lack of calcium in blood can replenish for the account of hydroxyapatite, i.e. cause its washing away from bones, and the excessive calcium amount that is eliminated from blood can promote urolithiasis, deposition of salts and cause sclerosis and heart attack.

In a normal situation ratio between calcium and phosphorus in bones, approximately corresponds to stoichiometry of apatite (molecular ratio — 1.67, weight ra-

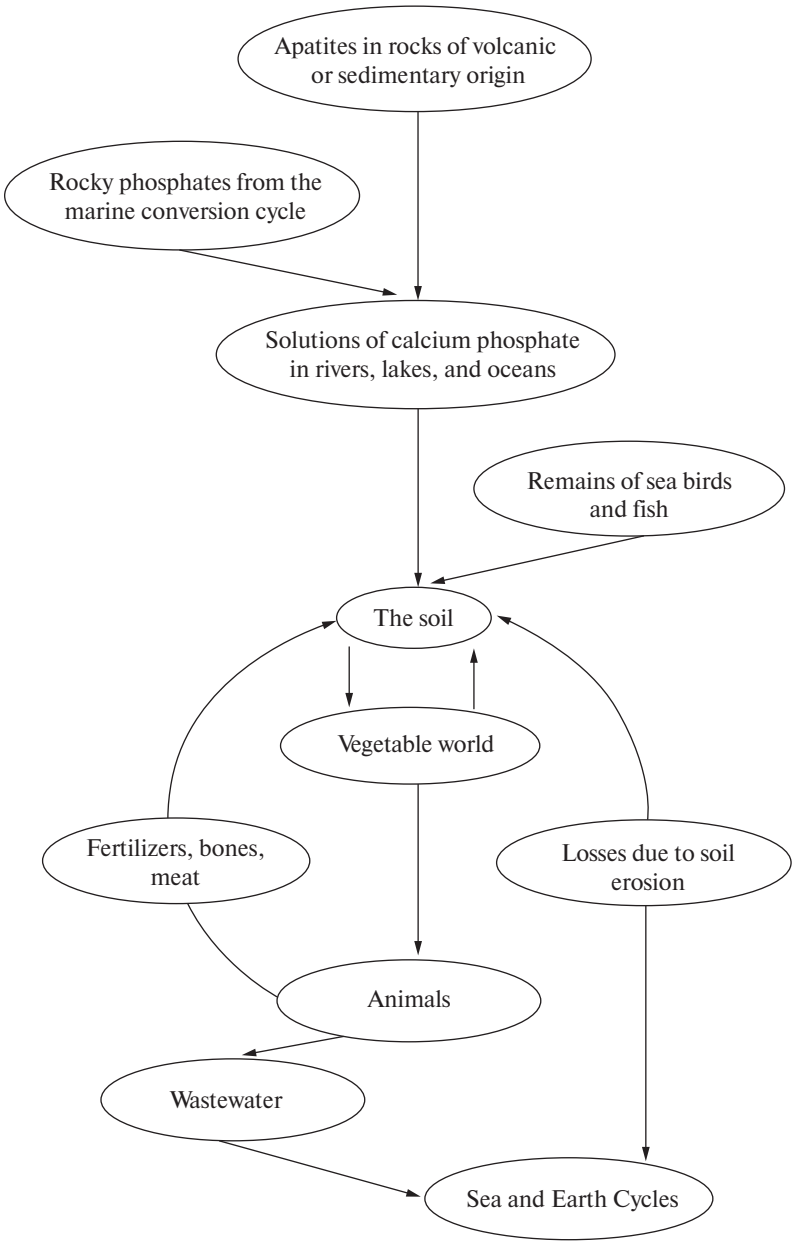

Fig. 8.2. The Earth cycle of transformation of calcium phosphate [313]

tio — 2.15). If with water and food there is coming relatively a large amount of phosphorus and not enough calcium into an organism, apatite will dissolve, despite efforts of an organism to protect it. Thus after inspection of the population of Kazakhstan, Western Siberia and Ivanovo city normal adaptable abilities based on homeostasis

are found out only in 8-25% of the population. The same situation is in the case when there is an excess of calcium, and not enough phosphorus. In both cases the main construction material of bones ceases to be initial apatite. It will transform to calcium phosphate either with a large content of phosphorus (calcium is washed away from bones), or with a large content of calcium (phosphorus is washed away).

That's why medics consider Ca-HAP to be not the most appropriate material for building of skeleton, and its fitness is not universal. Thus it is known that calcium is washed out from the bones of astronauts, thereof that apatite in skeleton is piezoelectric and is stable only in conditions of terrestrial gravity.

However, such estimation is a little bit rash. The problem is that scientists still have not properly understand and so have not learned sufficiently how to manage the process of phosphate-calcium exchange for ensuring of optimal conditions of organism functioning.

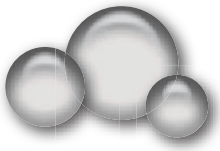

CHAPTER 9

BIOSPHERIC APATITES

Now the widest application in medical applications and for elimination of defects of bones and treatment of crises finds calcium hydroxoapatite. New medical elaborations demand huge capital investments and time, 15-20 million dollars and eight years minimum are needed usually for new developing to pass a way from the concept to the product approved for application, according to authors of work [316]. These requirements are so high that the majority of innovations in biomaterials are never realised on the industrial conveyor.

9.1. Features of formation of apatites in biosphere

9.1.1. Structure of apatite of a biological origin

Le Jong [317] was the first who observed similarity between X-ray diffractograms of powders of a bone and calcium hydroxoapatite. However, the first definition of a mutual spatial arrangement of ions of Ca^{+2}, PO_4^{-3} and OH^- in the structure of hydroxoapatite has been made on the basis of studying of a picture of X-ray diffractional reflexions from the artificially grown up crystals of apatite by Posner with employees [318]. Kay with collaborators have received these results, observing neutron diffraction in samples of apatite of a geological origin [319]. The elementary crystal cell of apatite which, repeating in space because of operations of symmetry, reproduces full crystal structure, represents a rectangular rhombic prism with a=9.432 Å and c=6.881 Å [318], the maintenance of atoms in which is set by the formula $Ca_{10}(PO_4)_6(OH)_2$. Hexagonal spatial symmetry does not manage to be defined precisely enough for smaller, than in the given formula, set of atoms and consequently the writing of this formula for hydroxoapatite instead of $Ca_5(PO_4)_3OH$ is often preferable.

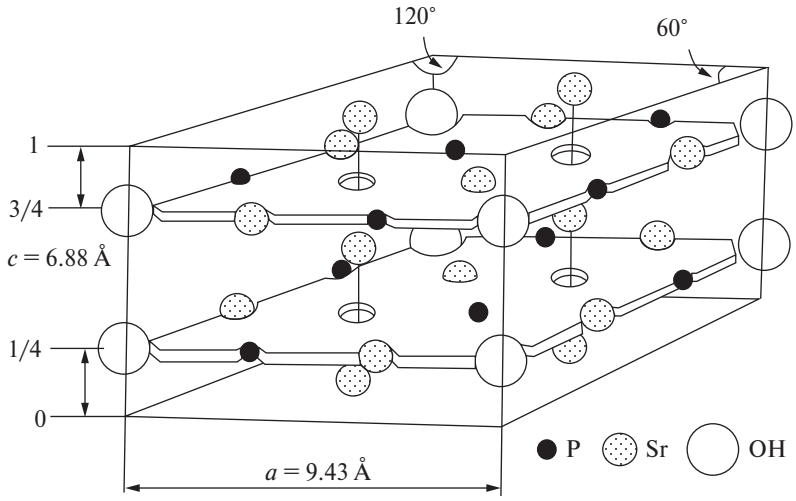

Fig. 9.1. Kind of an elementary cell of hydroxoapatite [1]

The analysis of the crystallographic the data of variety of apatites are resulted in chapter 1. The arrangement of atoms in an elementary cell of calcium apatite is resulted on fig. 9.1. Ions of hydroxyl are located in corners of the basis of an elementary cell and lie on identical distances from each other, forming the intervals equal to half of height of a cell (3.44 Å – along directions, perpendicular a base plane and parallel to an axis *c*).

Six of each ten ions of calcium in a cell are connected with hydroxyl groups on verticals (where form among themselves the equipotential triangles aligned concerning verticals and perpendicular planes to last, i.e. on what ions are located OH-). The flat triangles following one after another made of ions of calcium, are consistently turned on 60 ° (round an aforementioned axis), will defend from each other on the distances equal to half of value of parametre of an elementary cell (fig. 9.2).

Other four ions of calcium of an elementary cell are located along two verticals parallel to an axis *c*, at the heights equal to half of distance between bonded by hydroxyl ions and calcium triangles. Calcium ions are co-ordinated by phosphatic tetrahedrons.

Ions OH^- located around an axis of the sixth order, do not lie in the centres of planes of calcium triangles. Actually, the oxygen centre of each of hydroxyl ions will is apart on 0.3 Å from the centre of the nearest triangle from calcium ions. The ion OH^- is always focused perpendicularly the nearest plane from calcium ions in such a manner that the face-to-face ion of hydrogen of corresponding group O-H never crosses this plane. Contrary to it ions of fluorine in fluoric apatite (where according to chemical formula $Ca_{10}(PO_4)_6(OH)_2$ ions of fluorine replace ions of hydroxyl) are located in the centre of triatomic calcium planes (fig. 9.2). More dense arrangement

of ions of fluorine, in comparison with OH^--ions, concerning the nearest ions of calcium can be connected partly with increase of chemical stability fluorine-substituted hydroxoapatite [320] that is shown also in stability of a bone tissue to such pathology as caries of teeth.

Structure of $Ca_5(PO_4)_3Cl$ illustrates, how small changes in the spatial organization of a crystal of apatite can cause essential changes in their properties [321]. Calcium and phosphatic contributions to apatite structure are almost identical as in a case of fluorine apatite, and hydroxoapatite; however, chloride-ion, replacing an ion OH^- taking into account presence of an axis of rotation of the sixth order, gets into a plane from calcium ions "more deeply", than the ion OH^- (fig. 9.2).

As chlorine ions are not located equidistantly between the planes populated with ions of calcium, the structure loses elements of symmetry of a mirror plane, and, thus, symmetry goes down. Chlorine ions appear thus further from the nearest calcium triangle, than OH^- and not surprisingly therefore that chlorapatite appears less steady, than hydroxoapatite [320]. It explains why bioapatite does not contain the ions of chlorine replacing ions OH^-.

It is to be noticed also that there are only small distinctions in an arrangement of calcium ions and phosphatic ions in fluor-, hydroxo- and chlorapatite. These changes are shown in small, but quite measurable distinctions of thin structure of infra-red spectra of these three compounds [322]. Distinctions are connected with F-, Cl- and OH^--ions which are essentially responsible for observable change of properties. In view of this Yang and Elliot [320] have come out with the assumption that the axis passing through calcium triangles, is not an essential element of the basic structure.

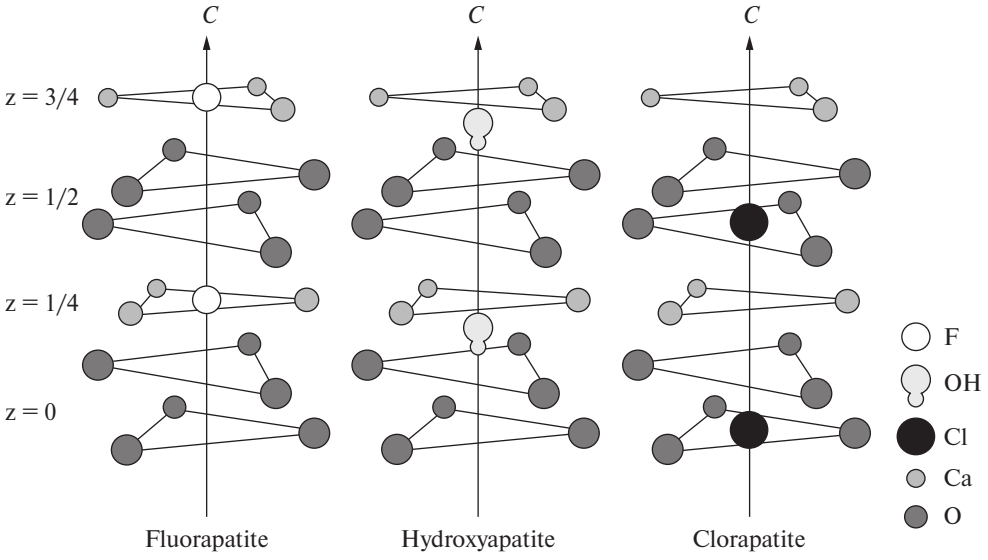

Fig. 9.2. Comparison of F^-, OH^- and Cl^-- knots in the apatite structure [1]

Removal of ions from this axis does not lead to structure destruction, so far as local distribution of a charge can remain invariable.

In apatite-like compounds $Pb_5(PO_4)_3SiO_2$ [323] and $Ba_{10}(PO_4)_{6-}(BO_4)_2$ [324] mentioned channels are not filled. As they are great and are supported by all other structure, they form low-barrier trajectories of diffusion of atoms. Thanks to it fluoride ions are capable to replace ions OH^- in fossils of bone apatites [325].

In the small, lacking in fluorine crystals of hydroxoapatite which have the same size, as in bone tissue (from 100 to 500 Å) presence of vacancies of ions OH^- is less probable. Thus, it is rather probable that the described vertical from ions OH^- represents the individual dipole stretched for all length of a crystal in a direction of an axis *c*. The question of orientation of such dipole at transition from one vertical to another stills. Quite probably that at formation of a crystal of apatite the orientation of one of the mentioned vertical sequences of OH^- ions can initiate identical orientation of adjoining columns, causing thereby formation of eccentrical symmetric crystal with all properties corresponding to it (for example, piezoelectricity display, ferromagnetism). This assumption coincides with the spatial mechanism of formation which has been postulated by Young [321] for the purpose of an explanation of effect of influence of focused column-like sequences of ions of chlorine in chlorapatite on orientation of screw axes of symmetry. Dielectric measurements on large crystals of hydroxoapatite allow assuming presence in them of domains in size to 1000 Å. This circumstance, apparently, supports the assumption that crystals of such sizes, or even less, possibly have the polar nature.

In work [326] it is confirmed that piezoelectric effects are inherent in a bone tissue. Shamos and Lavine [327] postulated that these effects are connected only with presence in native collagen bones whereas other researchers [326] came up with idea that bone apatite is partially responsible for these piezoelectric effects. Whatever is the explanation, the analysis of crystal structure of apatites represents a basis for modelling at check of the similar conclusions.

As a whole the structure of hydroxoapatite is subject to isomorphic substitutions. It is well-known, for example, that strontium, lead and sodium reversibly can replace calcium in its site. In the same way fluoride- and chlorides-ions can replace ions OH^-. In bone apatite the majority of substitutions, such, for example, as substitution by iron, copper, lead, manganese, tin, aluminium, strontium and a boron [328] is shown in the form of traces, except for substitution by ions of carbonates. The carbonate ion in general is the third under the account the most often meeting assistant of native ions of a bone mineral and consequently its role will be separately described.

The fluorine-apatite mineral francolite contains 3.3 wt.% of carbonates-ions CO_3^{2-} [329]. As the carbonate maintenance in a bone mineral is the size of the same order, that in francolite it is rather useful to consider a structural role of carbonate ions separately in good and in badly taken shape systems. Apparently, the most com-

prehensible is the judgement that the carbonate in apatites with the big size of crystals is present at a lattice as ions CO_3^{-2}, substituting somehow either ions of phosphatic residue PO_4^{-3} or ions OH^-. Legeros with employees [330] have shown for crystals of hydroxoapatite, allocated of a solution that the parametre *a* decreases, and *c* — increases as the maintenance of carbonate ions grows. This fact, along with IRS data, is the proof of substitution of ions PO_4^{-3} by ions CO_3^{-2}. It is rather interesting that influence on fluorine apatite by dry dioxide of carbon at 900 °C leads to substitution of phosphatic ions by carbonate ones [331]. Substitution by carbonates of hydroxyl groups occurs if process hydroxoapatite with dry dioxide of carbon at high temperatures [332]. Hence, it is possible to expect that in carbonate-containing hydroxoapatite there was a substitution of ions OH^- by ions CO_3^{2-}. Later on it is necessary to show more precisely a way of substitution and the mechanism of realization of an electroneutrality as a result of similar substitutions.

The problem looks absolutely different if it is a question of the maintenance of carbonate ions in nano-dispersed hydroxoapatite, which average size of particles is in area 100-500 Å, i.e. in the field of the sizes close to those for bone apatite. In this case a site of the surface fit on a crystal is abnormal and there is enough empty space for a concentration of bigger part of carbonate ions on a surface of crystals.

There is an opinion that the carbonate on a surface of bone crystals is a reserve source of alkali [333].

It seems quite obvious that occurrence of carbonate ion in crystal structure, especially in positions of phosphatic ions, causes distortions in a lattice. It is shown that with growth of maintenance of carbonate ions, degree of crystallity of hydroxoapatite decreases. Even in case of large carbonate-containing crystals of hydroxoapatite the picture of X-ray diffraction ascertains broadening of diffractional picture, possibly connected with the pressure and defects. Observed in infra-red area of a spectrum effect, confirms increase in intracrystal pressure as far as maintenance of carbonate ions in structure increases [330]. It is connected with that circumstance that the flat carbonate ion substitutes tetrahedral phosphate-ion, or in certain cases a polar hydroxy-ion that is crystallographic discordance and leads to occurrence of pressures.

9.1.2. Sizes and the form of crystals of apatite in biocomposites

As it was already mentioned, in 1926 on the basis of the analysis of insufficiently well resolved X-ray pictures was made the conclusion that the basic component of a mineral of a bone is the apatite which is in a kind of crystals of the small sizes [317]. In later work Carlstrom [334], using X-ray data, has counted up that the greatest parametre of bone crystals does not surpass 230±20 Å. Crystals of tooth enamel of the adult person as shown in work [335] have the approximate sizes

1400 × 800 × 800 Å. Long time bone crystals were considered to be either needle-shaped, or, on the contrary, plate-like on habitus.

Wolpers [336], tending to the needle-shaped form, has described these crystals, as having 400-1000 Å at length and 30-60 Å at width. The same way also Molnar [337], and after him Ascenzi and Bonucci [338] have shown that bone crystals have only 30-50 Å at thickness, but vary on length from 50 Å to 1000 Å. On the other hand, Fernandez-Moran and Engstrom [339] as well as Durning [340], have found length of crystals of bone apatite not surpassing 300 Å though the width by which they have measured, was in the good consent with the data of other researchers.

Contrary to this Robinson and Watson [341, 342], and then Johansen and Parks [343] observed plate-like crystals of bone apatite. The characteristic sizes of crystals, following these authors, were $400 \times (200 \div 350) \times (23 \div \div 50)$ Å.

Molnar [337], Ascenzi and Bonucci [338] have come out with the assumption that bone crystals consist of chains of the crystals soldered by the ends in block structures. By similar adhesive processes the disorder of values of length of the crystals, observed in the literature, and also the various form of resultants of crystallites can be caused. Results of X-ray Posner's researches with collaborators [344] according to which the greatest size of crystals possibly does not exceed 100 Å, is better coordinated with the affirmed point of view on the nature of bone apatite, as on three-dimensional mosaic structure from microcrystals.

Crystals of bone apatite are similar in the sizes to crystals of hydroxoapatite, prepared by a method of sedimentation from water solutions. It is the probable proof of presence of some physical and chemical restrictions of the sizes of crystals of bone apatite. Crystals of tooth enamel, in comparison with crystals of a bone mineral, differ in extraordinary large sizes which do not manage to be reproduced by a synthetic way, close to physiological conditions. Besides, crystals of tooth enamel differ in unusual parametres of growth. At research of development of tooth enamel of rats, Nylen with collaborators [345] has defined that in the beginning growth occurs along an axis with, and extremely wide thin plates are formed. These plates gradually are transformed, with the years, in hexagonal cores.

Supporting that biological factors define the sizes, the form and orientation of native crystals of a mineral of a bone, there are enough proofs. So, Engstrom and Zetterstrom [346] on X-ray researches of the stiffened sinews and muscles of birds have managed to show that the direction of an axis *c* in apatite of crystals always appears as parallel collagenic fibres. In the same way, by results of research of a bone by a method of X-ray dispersion under small corners, Finean and Engstrom [347] have shown that the axis *c* in apatite crystals always appears parallel to the most developed direction of growth of a crystal of a bone mineral and that this size, in turn, coincides in a direction with an axis of fibres of collagen. The similar information is received at the analysis of electronic diffractogramm, made for a parietal bone of the dairy mouse [348].

Electronic-microscopic researches specify also in some conformity between crystals and collagen threads in native bone. Robinson and Watson [342] have found out a small amount of the inorganic sedimentations genetically connected with interperiod band structure of collagen in the investigated bone.

The additional proof of existence of associate "crystal-collagen" can be found in results of biological researches of a bone fabric. Currey [349] on the basis of similar researches has made a conclusion that strengthening and elastic properties of a bone are rather close to that at fibrous glass. From observable so close functional analogies between a bone and fiber glass Currey has concluded that the mineral and a matrix of a bone do not give additional and independent contributions to mechanical properties of a bone.

He has paid attention that rheological features and behaviour of a bone allow an occasion to assume that there is very close and difficult affinity between collagen and crystals of a bone apatite. Confirming to it, research of a bone by EPR method [350] has found out that bone crystals are connected with collagen and covalent bindings.

Results of X-ray diffractional researches of the bones [344] directed on finding-out of a role of ions of fluorine as a part of apatite of a bone tissue of the person, confirm the concept that the collagenic matrix defines length of crystals of bone apatite and promotes achievement of parallelism of an arrangement of fibres of collagen and an axis *c* of apatite crystal. In this research it is shown that the increase in the maintenance of ions of fluorine was accompanied by increase of the sizes of a crystal bone mineral only in directions perpendicular to axes *c* whereas the prevailing direction of development of the crystal growth, parallel to this axis, remains invariable irrespective of the maintenance in a bone of ions of fluorine. As the axis *c* – a direction of growth of crystals of a bone, is parallel to a direction of orientation of fibres of collagen so the results of the analysis on fluorine allow to assume that the length of crystals in a direction of an axis *c* is limited by length of the basic period of a chain of collagen and can be defined by quantity of the centres of nucleation on length. In tooth enamels where there is a matrix of keratin [351], such restrictions in fluorine-induced growth along an axis *c* does not exist.

In an initial stage of the natural calcification of collagen matrix, primary sedimentation of a mineral are extremely small. Robinson and Watson [342] have informed that they observed in front of calcification of granule-like sedimentations in size 25-50 Å. Ascenzi and Bonucci [338] have described existence in the same area of dense stains, more than 19 Å in a diameter, having made the conclusion that initial initiation of mineral formation in the presence of a matrix occurs very quickly, but in the subsequent is accompanied by slow sedimentation of a mineral. Possibly, slower process is the combination of process of growth of initial grains with formation and growth of crystals of apatite, especially in intercollagenic intervals, in internal pores of a bone.

Change of the sizes of bone crystals is noticed with the years at X-ray structural researches of finely grained powders of bones of rats [352]. It is established that the average size of crystals increases with the years of an animal up to maturity achievement. Then (in 40 days of a life) occurs sudden change of growth rate, the size becomes rather constant and independent from age in the sequel.

Robinson [353] has underlined that circumstance that growth of crystals of a mineral of a bone is interfaced to increase in the expense of a liquid. Therefore, the parity "water/mineral" decreases with increase in degree of a mineralization of a bone. The specified decrease in the maintenance of water in process of bone formation can suspend maturing of crystals and, thus, brings the contribution to maintenance of a constancy of the sizes of crystals.

Rowland [354] on the basis of the analysis of the radio graphic data has made a conclusion that only 0.65% of calcium containing in person bones can be replaced, whereas other researchers of a bone mineral specify that, basically, ~27% of calcium are potentially replaced [355]. These results allow to come out with the assumption that in a live bone only recently mineralized sites which are near to a surface as, for example, lines of channels of Harvezian and other cavities, can easily exchange ions of a mineral origin. Probably, ejection of a fabric liquid by minerals in the course of their calcification [353] interfers the development of considerable chemical diffusion in internal cavities completely mineralized bone fabrics.

9.2. Amorphous phosphate of calcium in mineralized fabrics

By results of chemical, X-ray structural, electron microscopic researches the assumption has been made that inorganic component of a bone tissue is not completely crystallized calcium phosphate similar with hydroxoapatite on structure and composition. Such single-phase description of structure has caused objections and now the model is accepted when the bone consists, at least, of two types of calcium phosphate. Last of known results specify that except apatite phase, the bone mineral contains considerable quantity of APC (amorphous phosphate of calcium).

As the proof of that the amorphous phase is the main component of a bone mineral also served the results of X-ray structural researches described in works [356, 357]. This phase has been identified, when intensity of "a crystal part" in a picture of X-ray diffraction of a bone tissue has appeared insufficient for the statement that all substance of a mineral of a bone consists of only one apatite. On divergence size between observed and expected intensities of reflexions from apatite phase are made quantitative estimations of presence of an amorphous phase in a mineral of a bone [356]. This not crystal phase has appeared in regular intervals extended in samples of a bone fabric of many animals.

Harper and Posner [356] have found out that approximately 40% of a bone mineral of a femur of the adult person, cows and rats are in noncrystalline state. Termine

and Posner [357] have established that degree of amorphization of a bone tissue in organisms of rabbits of 65-day age practically does not depend on its anatomic origin. The resulted values fluctuated from 40% to 48% for a femur. The maintenance of amorphous substance in a bone in the obvious form varied depending on age of an animal. The maintenance of amorphous substance in a bone mineral of a femur of a rat decreased from 69% for 5-day, to 36% for 70-day animals. Similar character of reduction of amorphous substance is found out with the years in shinbone, perone and a cranium of a rat.

The amorphous material, most likely, dominates in young bones, however in due course is gradually replaced with crystal apatite. Similar dependence on age of an amorphous mineral of a bone has been shown by the quantitative infra-red spectrophotometric analysis [358].

According to electronic microscopy, X-ray structural and electron-diffractional researches the use of term "amorphous" for these objects is quite justified. The approximated form of particles of an amorphous phase, considerably differs from rectangular needle-shaped crystals of a bone apatite [348]. The picture from several wide and dim maxima which are visible on electron-diffractional pictures of this material is typical for amorphous substances. Contrary to it electronic diffractogram of a bone apatite finds out a few well resolved and diffractional maxima. Diffraction from APC carries fuzzy diffused character and this explains that circumstance that APC is not distinguishable on X-ray diffractogram of a bone.

In the described substances of amorphous type, unlike crystal ones, there is no distant order. It does not mean that in APC there is no local ordering of atoms. Presence of several wide diffractional maxima on electro-diffractional pictures specifies in certain degree of local ordering of atoms. It is possible to assume that phosphatic tetrahedrons in a crystal are focused under the relation to each other, however their mutual placing is not strictly periodical, as it takes place in crystal apatite.

Extreme degree of diffusiveness and absence of thin structure on X-ray- and electron-diffraction pattern the APC of a live bone does problematic successful use of the diffractional analysis for research of similar phases. We (chapter 3) conducted regular researches of a nuclear structure of amorphous phosphate of strontium. However, researches of biominerals last and spatial distribution of the ions forming amorphous substance in a bone mineral is still necessary to find out.

9.3. Synthetic amorphous phosphate of calcium

The resulted description of amorphous phosphate of calcium of a live bone illustrates degree of a level of study of properties of this substance. Now additional data on its properties can be taken at studying of synthetic analogues of phosphate of calcium.

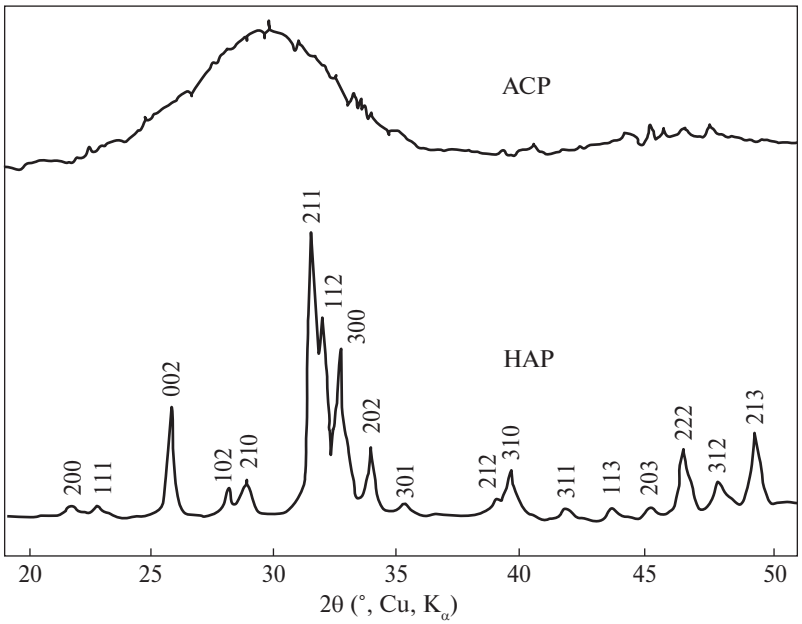

Fig. 9.3. Comparison of X-ray diffractogram ACP and crystallized HAP

That way Watson and Robinson [359] were the first ones who have described properties and structure of amorphous synthetic phosphate of calcium, as precursor of hydroxoapatite. At electro-microscopic studying this material has appeared consisting of nanosized particles. Amorphous material, contacting with preparative environment, passes in some intermediate condition and quickly turns to crystal apatite. Watson's and Robinson's examinations have been continued for the purpose of the description of thin details of a morphological structure, a chemical compound and behaviour in a solution of these transitive intermediate phases. Noncrystalline character of this substance has been established from X-ray structural researches [360]. Diffractogram find out only two weak diffuzed maxima, not coinciding with the characteristic main maximum of synthetic apatite (fig. 9.3). As appears from the electronic microphotos which have been taken in a mode on transit, amorphous particles of synthetic apatite have the same sizes and the same toroidal form, as that which were described by Molnar studying a cut of a live bone [361]. Application of additional "shadow" techniques of electronic microscopy has shown that particles have the spherical form.

Thus particles of synthetic APC are particles of the spherical form, surrounding transparent for electrons internal kernel.

Synthetic APC do not possess accurately certain chemical compound. The molar ratio Ca/PO_4 as it has appeared, depending on preparation conditions varies from 1.44 till 1.55 [362]. However, their structure changes less, than in case of the apatites

synthesized in the same conditions [363]. Despite lacking a constancy of structure of the amorphous phase, the transformed apatite has higher molar ratio Ca/PO_4 than its amorphous predecessor. Besides, the amorphous substance with molar ratio equals to 1.50 possesses the raised stability to reagent influence. Last observation is chemically justified by consideration of amorphous structures of noncrystal TCP or nanodispersed crystals of hydroxoapatite, deficient on calcium. Calculations of Bienenstock and Posner [364] have shown that X-ray structural reflexions of amorphous calcium phosphate do not occur from systems of nanodispersed crystals of hydroxoapatite. The further specifications have shown that nanodispersed, deficient on calcium hydroxoapatite, having molar ratio $Ca:PO_4$ of an order 1.5 do not give amorphous-like X-ray diffractogram. The opinion is expressed that synthetic amorphous substances represent species of TCP.

It is known that synthetic amorphous phosphates of calcium are unstable in the water environment. At contact with mother liquor these substances crystallize in apatite. In work [365] some mechanisms operating such transformation are established. Transformation of an amorphous phase into the crystal carries autocatalytic character, i.e. speed of this transformation is proportional to quantity of crystals of apatite which were already formed, and at all to quantity of the remained amorphous substance. Such behaviour is an example of secondary heterogeneous nucleation when the crystal phase grows for the account of new crystals on a surface of already developed crystals. There is a branch of again formed crystals from a parent matrix where both phases do not participate anymore in nucleation that leads to exponential increase of potential of transformation of all system. The phenomenon of secondary nucleation can occur only in solutions, oversaturated with ions of a crystallizable phase – in this case by ions of calcium, phosphate and hydroxyl. It allows to consider that solubility of ACP is greater than of crystal apatite. The fact that the secondary mechanism is a stage defining speed of transformation, allows to assume that the amorphous phase behaves passively, being the calcium and phosphate tank and providing steady conditions of oversaturation in the course of such transformation.

Isothermal instability of ACP in a matrix solution allows to assume that formation of this phase is faster kinetic, than the thermodynamic phenomenon.

Spontaneity of origin of calcium phosphate in a solution is the proof of formation of this phase in substance of a bone without participation of auxiliary substance. Similar homogeneous process of nucleation is realized only at the concentration much more exceeding necessary for initiation of heterogeneous nucleation. The fact that apatite crystals at so high concentration of a solution nevertheless are absent, though from the thermodynamic point of view their formation is more favorable than formation of amorphous parts, allows to assume that they can grow and develop only by rather slower heterogeneous mechanisms of nucleation. Presence of alien substances for process of formation of primary apatite crystals within the

limits of heterogeneous nucleation is absolutely necessary. These alien substances always are present at synthesis, however their rather low concentration along with low efficiency in quality of nucleation explains, why after occurrence of several crystals of apatite secondary nucleation becomes the dominating and operating factor in the course of transformation of ACP to a crystal apatite. Nevertheless, secondary nucleation cannot compete to process of initially homogeneous nucleation if degree of oversaturation is high enough to favour to the last, therefore the amorphous phase arises the first.

Thus, the bone represents a mix of amorphous and crystal phases, and both phases contact to a solution. It is reasonable to assume that the certain mechanism is necessary for stabilisation of an amorphous phase as in the conditions of optimum functioning of organism when contact to physiological solutions is carried out, there is a fast transformation into a crystal phase. The easiest way of stabilization of an amorphous phase is water removal in the process of lyophilization.

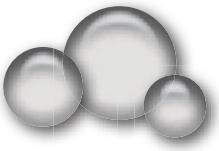

REFERENCES

1. *T. Kanazawa*. Inorganic phosphate materials. / Under Ed. A.P. Shpak and V.L. Karbivsky. — Kiev: Naukova Dumka, 1998. — 298 p.
2. *J. Y. Kim, R. R. Fenton, B. A. Hunter, B. J. Kennedy.* Powder diffraction studies of synthetic calcium and lead apatites. — Australian Journal of Chemistry, 2000, **53**, № 8, p. 679—686.
3. *K. Sato, Y. Suetsugu, J. Tanaka, S. Ina, H. Monma.* The surface structure of hydroxyapatite single crystal and the accumulation of arachidic acid. — Journal of Colloid and Interface Science, 2000, **224**, № 1, p. 23—27.
4. *T. Ikoma, A. Yamazaki, S. Nakamura, M. Akao*. Preparation and structure refinement of monoclinic hydroxyapatite. — Journal of Solid State Chemistry, 1999, **144**, 2, p. 272—276.
5. *A. Ito, S. Nakamura, H. Aoki, M. Akao, K. Teraoka, S. Tsutsumi, K. Onuma, T. Tateishi*. Hydrothermal growth of carbonate-containing hydroxyapatite single crystals. — Journal of Crystal Growth, 1996, **163**, № 3, p. 311—317.
6. *P. A. Henning, E. Adolfsson, J. Grins*. The chalcogenide phosphate apatites $Ca_{10}(PO_4)_6S_2$, $Sr_{10}(PO_4)_6S_2$, $Ba_{10}(PO_4)_6S_2$ and $Ca_{10}(PO_4)_6Se_2$. — Zeitschrift für Kristallographie, 2000, **215**, № 4, p. 226—230.
7. *S. Lazic*. Microcrystalline hydroxyapatite formation from alkaline solutions. — Journal of Crystal Growth, 1995, **147**, 1—2, p. 147—154.
8. *S. Muramatsu, C. Kato, K. Fujita, K. Matsuda*. Formation of strontium hydroxyapatite by homogeneous precipitation method. — Nippon Kagaku Kaishi, 1994, **6**, p. 531—537.
9. *D. Notzold, H. Wulff*. Determining the crystal structure of $Sr_5(PO_4)_3Br$, a new compound in the apatite series, by powder diffraction modeling. — Powder Diffraction, 1998, **13**, 2, p. 70—73.
10. *S. Lazic, J. Katanicpopovic, S. Zec, N. Miljevic*. Properties of hydroxyapatite crystallized from high temperature alkaline solutions. — Journal of Crystal Growth, 1996, **165**, № 1—2, p. 124—128.
11. *S. Nadir, A. Belainass, A. Irhzo, J. L. Lacout*. Neutralization synthesis of pure hydroxyapatite using orthophosphoric acid and calcite. — Source Phosphorus Sulfur and Silicon and the Related Elements, 1996, **112**, № 1—4, p. 33—40.
12. *H. Takahashi, M. Yashima, M. Kakihana, M. Yoshimura*. Synthesis of stoichiometric hydroxyapatite by a ''gel" route from the aqueous solution of citric and phosphonoacetic acids. — European Journal of Solid State and Inorganic Chemistry, 1995, **32**, № 7—8, p. 829—835.
13. *V. P. Orlovskii, N. A. Zakharov, V. A. Klyuev, Y. P. Toporov*. Exoelectronic emission of $Ca_{10}(PO_4)_6(OH)_2$ and native human bone. — Inorganic Materials, 1995, **31**, № 8, p. 1013—1015.

14. *S. Sugiyama, T. Nakanishi, T. Ishimura, T. Moriga, H. Hayashi, N. Shigemoto, J. B. Moffat*. Preparation, characterization, and thermal stability of lead hydroxyapatite. — Journal of Solid State Chemistry, 1999, **143**, № 2, p. 296—302.
15. *R. Fabian, I. Kotsis, P. Zimany, P. Halmos*. Preparation and chemical characterization of high purity fluorapatite. — Talanta, 1998, **46**, № 6, p. 1273—1277.
16. *S. Oishi, N. Michiba, N. Ishizawa, J. C. RendonAngeles, K. Yanagisawa*. Growth of barium chlorapatite crystals from a sodium chloride flux. — Bulletin of the Chemical Society of Japan, 1999, **72**, № 9, p. 2097—2101.
17. *A. Yasukawa, T. Matsuura, M. Nakajima, K. Kandori, T. Ishikawa*. Preparation of nonstoichiometric calcium hydroxyapatite using formamide. — Materials Research Bulletin, 1999, **34**, № 4, p. 589—601.
18. *A. Slosarczyk, C. Paluszkiewicz, M. Gawlicki, Z. Paszkiewicz*. The FTIR spectroscopy and QXRD studies of calcium-phosphate based materials produced from the powder precursors with different Ca/P ratios. — Ceramics International, 1997, **23**, 4, p. 297—304.
19. *W. Weng, J. L. Baptista*. A new synthesis of hydroxyapatite. — Journal of the European Ceramic Society, 1997, **17**, № 9, p. 1151—1156.
20. *P. A. Henning, M. Moustiakimov, S. Lidin*. Incommensurately modulated cadmium apatites. — Journal of Solid State Chemistry, 2000, **150**, № 1, p. 154—158.
21. *M. Kikuchi, A. Yamazaki, R. Otsuka, M. Akao, H. Aoki*. Crystal structure of Sr-substituted hydroxyapatite synthesized by hydrothermal method. — Journal of Solid State Chemistry, 1994, **113**, № 2, p. 373—378.
22. *A. Yasukawa, M. Kidokoro, K. Kandori, T. Ishikawa*. Preparation and characterization of barium-strontium hydroxyapatites. — Journal of Colloid and Interface Science, 1997, **191**, № 2, p. 407—415.
23. *I. Ntahomvukiye, I. Khattech, M. Jemal*. Synthesis and thermochemistry of calcium-lead fluorapatites. — Annales de Chimie — Science des Materiaux, 1997, **22**, № 7, p. 435—446.
24. *Y. Suetsugu, I. Shimoya, J. Tanaka*. Configuration of carbonate ions in apatite structure determined by polarized infrared spectroscopy. — Journal of the American Ceramic Society, 1998, **81**, № 3, p. 746—748.
25. *Y. Suetsugu, Y. Takahashi, F.P. Okamura, J. Tanaka*. Structure analysis of A-type carbonate apatite by a single-crystal X-ray diffraction method. — Journal of Solid State Chemistry, 2000, **155**, 2, p.292—297.
26. *B. Donazzon, G. Dechambre, J. L. Lacout*. Calcium-strontium hydroxyapatite: Hydrothermal preparation. — Annales de Chimie — Science des Materiaux, 1998, **23**, № 1—2, p. 53—56.
27. *E. A. P. Demaeyer, R. M. H. Verbeeck, D. E. Naessens*. Optimalization of the preparation of Na^+-containing and CO_3^{2-}-containing hydroxyapatite by the hydrolysis of monetite. — Journal of Crystal Growth, 1994, **135**, № 3—4, p. 539—547.
28. *E. A. P. Demaeyer, R. M. H. Verbeeck, D. E. Naessens*. Stoichiometry of Na^+- and CO_3^{2-}-containing apatites obtained by hydrolysis of monetite. — Inorganic Chemistry, 1993, **32**, № 25, p. 5709—5714.
29. *R. Ternane, M. Ferid, N. Kbir-Ariguib, M. Trabelsi-Ayedi*. The silver lead apatite $Pb_8Ag_2(PO_4)_6$: hydrothermal preparation. — Journal of Alloys and Compounds, 2000, **308**, №1—2, p. 83—86.
30. *G.V. Rodicheva, V.P. Orlovsky, N.M. Romanova*. Synthesis and physico-chemical study of glycine-containing calcium hydroxyapatite. — Journal of Inorganic Chemistry, 2000, **45**, No. 4, p. 648—651 (in Russian).
31. *A. Bigi, E. Foresti, M. Gandolfi, M. Gazzano, N. Roveri*. Inhibiting effect of zinc on hydroxylapatite crystallization. — Journal of Inorganic Biochemistry, 1995, **58,** № 1, p. 49—58.
32. *F. Apfelbaum, I. Mayer, C. Rey, A. Lebugle*. Magnesium in maturing synthetic apatite: A Fourier transform infrared analysis. — Journal of Crystal Growth, 1994, **144**, № 3—4, p. 304—310.

33. *N. Kanzaki, K. Onuma, G. Treboux, S. Tsutsumi, A. Ito*. Inhibitory effect of magnesium and zinc on crystallization kinetics of hydroxyapatite (0001) face. — Journal of Physical Chemistry B, 2000, **104**, № 17, p. 4189—4194.
34. *J. GuerraLopez, R. Gonzalez, A. Gomez, R. Pomes, G. Punte, C. O. DellaVedova*. Effects of nickel on calcium phosphate formation. — Journal of Solid State Chemistry, 2000, **151**, № 2, p. 163—169.
35. *H. Unuma, K. Ito, T. Ota, M. Takahashi*. Precipitation of hydroxyapatite under stearic acid monolayers. — Journal of the American Ceramic Society, 1996, **79**, № 9, p. 2474—2476.
36. *M. S. Tung, T. J. Ofarrell*. Effect of ethanol on the formation of calcium phosphates. — Colloids and Surfaces A — Physicochemical and Engineering Aspects, 1996, **110**, № 2, p. 191—198.
37. *S. Koutsopoulos, E. Dalas, N. Tzavellas, N. Klouras, P. Amoratis*. Effect of vanadocene dichlorides on the crystal growth of hydroxyapatite. — Journal of Crystal Growth, 1998, **183**, 1—2, p. 251—257.
38. *S. H. Rhee, J. Tanaka*. Effect of chondroitin sulfate on the crystal growth of hydroxyapatite. — Journal of the American Ceramic Society, 2000, **83**, № 8, p. 2100—2102.
39. *W. Paul, C. P. Sharma*. Infection resistant hydroxyapatite/alginate plastic composite. — Journal of Materials Science Letters, 1997, **16**, № 24, p. 2050—2051.
40. *W. O. S. Doherty, O. L. Crees, E. Senogles*. Polymeric additives: Effects on crystallization of hydroxyapatite scales. — Crystal Research and Technology 1996, **31**, № 3, p. 281—286.
41. *X. D. Sun, C. L. Ma, Y. Wang, H. D. Li*. Effects of polarization on crystallization of calcium phosphate. — Materials Letters, 2001, **47**, № 4—5, p. 267—270.
42. *S. Koutsopoulos, E. Dalas*. Hydroxyapatite crystallization on sodium cholate. — Journal of Crystal Growth, 2001, **222**, № 1—2, p. 279—286.
43. *D. T. Beruto, M. Giordani*. Influence of electromagnetic fields on the microstructure of precipitated calcium phosphate nanometric-grains. — Journal of the European Ceramic Society, 1999, **19**, № 9, p. 1731—1739.
44. *E. I. Suvorova, F. Christensson, H. E. L. Madsen, A. A. Chernov*. Terrestrial and space-grown HAP and OCP crystals: effect of growth conditions on perfection and morphology. — Journal of Crystal Growth, 1998, **186**, № 1—2, p. 262—274.
45. *H. E. L. Madsen, F. Christensson, L. E. Polyak, E. I. Suvorova, M. O. Kliya, A. A. Chernov*. Calcium phosphate crystallization under terrestrial and microgravity conditions. — Journal of Crystal Growth, 1995, **2**, № 3, p. 191—202.
46. *K. Onuma, A. Ito, T. Tateishi*. Investigation of a growth unit of hydroxyapatite crystal from the measurements of step kinetics. — Journal of Crystal Growth, 1996, **167**, № 3—4, p. 773—776.
47. *J. Christoffersen, J. Dohrup, M. R. Christoffersen*. The importance of formation of hydroxyl ions by dissociation of trapped water molecules for growth of calcium hydroxyapatite crystals. — Journal of Crystal Growth, 1998, **186**, № 1—2, p. 275—282.
48. *K. Onuma, A. Oyane, T. Kokubo, G. Treboux, N. Kanzaki, A. Ito*. Nucleation of calcium phosphate on 11-mercaptoundecanoic acid self-asSEMbled monolayer in a pseudophysiological solution. — Journal of Physical Chemistry B, 2000, **104**, № 50, p. 11950—11956.
49. *R. Rodriguez-Clemente, A. Lopez-Macipe, J. Gomez-Morales, J. Torrent-Burgues, V. M. Castano*. Hydroxyapatite precipitation: A case of nucleation-aggregation-agglomeration-growth mechanism. — Journal of the European Ceramic Society, 1998, **18**, № 9, p. 1351—1356.
50. *J. Christoffersen, M. R. Christoffersen, T. Johansen*. Kinetics of growth and dissolution of fluorapatite. — Journal of Crystal Growth, 1996, **163**, № 3, p. 295—303.
51. *V.A. Sinyaev, E.S. Shustikova, L.V. Levchenko, A.A. Sedunov*. Synthesis and behavior under heating conditions of amorphous calcium polyphosphate. — Inorganic Materials, 2001, **37**, No. 6, p. 735—738. (in Russian)
52. *M. Valletregi, M. T. Gutierrezrios, M. P. Alonso, M. I. Defrutos, S. Nicolopoulos*. Hydroxyapatite particles synthesized by pyrolysis of an aerosol. — Journal of Solid State Chemistry, 1994, **112**, № 1, p. 58—64.

53. *K. Kandori, A. Yasukawa, T. Ishikawa*. Preparation and characterization of spherical calcium hydroxyapatite. — Chemistry of Materials 1995, **7**, № 1, p. 26—32.
54. *M. Aizawa, T. Terado, F. S. Howell, K. Itatani*. Preparation of spherical apatite particles by the homogeneous precipitation method in the presence of magnesium ions and their ion-exchange properties. — Materials Research Bulletin, 1999, **34**, № 8, p. 1215—1225.
55. *M. Aizawa, T. Hanazawa, K. Itatani, F. S. Howell, A. Kishioka*. Characterization of hydroxyapatite powders prepared by ultrasonic spray-pyrolysis technique. — Journal of Materials Science, 1999, **34**, № 12, p. 2865—2873.
56. *A. Nakahira, M. Tamai, K. Sakamoto, S. Yamaguchi*. Sintering and microstructure of porous hydroxyapatite. — Journal of the Ceramic Society of Japan, 2000, **108**, № 1, p. 99—104.
57. *N. Asaoka, H. Suda, M. Yoshimura*. Preparation of hydroxyapatite whiskers by hydrothermal method. — Nippon Kagaku Kaishi, 1995, **1**, p. 25—29.
58. *E. Bouyer, F. Gitzhofer, M. I. Boulos.* Suspension plasma spraying for hydroxyapatite powder preparation by RF plasma. — IEEE Transactions on Plasma Science, 1997, **25**, № 5, p. 1066—1072.
59. *J. Torrent-Burgues, J. Gomez-Morales, A. Lopez-Macipe, R. Rodriguez-Clemente*. Continuous precipitation of hydroxyapatite from Ca/citrate/phosphate solutions using microwave heating. — Crystal Research and Technology, 1999, **34**, № 5—6, p. 757—762.
60. *I. Soten, G. A. Ozin.* Porous hydroxyapatite-dodecylphosphate composite film on titania-titanium substrate. — Journal of Materials Chemistry, 1999, **9**, Issue 3, p. 703—710.
61. *I. V. Melikhov, V. F. Komarov, A. V. Severin, V. E. Bozhevolnov, V. N. Rudin*. Two-dimensional crystalline hydroxyapatite. — Reports of the Academy of Sciences, 2000, **373**, No. 3, p. 355—358. (in Russian)
62. *M. V. Chaynikova*. Peculiarities of chemical interaction in multicomponent systems at the mechanochemical synthesis of phosphates and apatites. — Chemistry for Sustainable Development, 1998, **6**, p. 141—150. (in Russian)
63. *W. Kim, Q. W. Zhang, F. Saito*. Mechanochemical synthesis of hydroxyapatite from $Ca(OH)_2$-P_2O_5 and CaO-$Ca(OH)_2$-P_2O_5 mixtures. — Journal of Materials Science, 2000, **35**, № 21, p. 5401—5405.
64. *H. S. Liu, T. S. Chin, L. S. Lai, S. Y. Chiu, K. H. Chung, C. S. Chang, M. T. Lui*. Hydroxyapatite synthesized by a simplified hydrothermal method. — Ceramics International, 1997, **23**, № 1, p. 19—25.
65. *A. Slosarczyk, E. Stobierska, Z. Paszkiewicz, M. Gawlicki*. Calcium phosphate materials prepared from precipitates with various calcium: phosphorus molar ratios. — Journal of the American Ceramic Society, 1996, **79**, № 10, p. 2539—2544.
66. *X. H. Yang, Z. H. Wang*. Synthesis of biphasic ceramics of hydroxyapatite and beta-tricalcium phosphate with controlled phase content and porosity. — Journal of Materials Chemistry, 1998, **8**, № 10, p. 2233—2237.
67. *M. G. S. Murray, J. Wang, C. B. Ponton, P. M. Marquis*. An improvement in processing of hydroxyapatite ceramics. — Journal of Materials Science, 1995, **30**, № 12, p. 3061—3074.
68. *Y. Fang, D. K. Agrawal, D. M. Roy, R. Roy*. Fabrication of transparent hydroxyapatite ceramics by ambient pressure sintering. — Materials Letters, 1995, **23**, № 1—3, p. 147—151.
69. *A. J. Ruys, C. C. Sorrell, A. Brandwood, B. K. Milthorpe*. Hydroxyapatite sintering characteristics: Correlation with powder morphology by high-resolution microscopy. — Journal of Materials Science Letters, 1995, **14**, № 10, p. 744—747.
70. *M. K. Sinha, S. Chatterjee, D. Basu, M. K. Basu*. Synthesis, characterisation and fabrication of hydroxyapatite ceramics. — Journal of the Indian Chemical Society, 1995, **72**, № 10, p. 771—773.
71. *N. Senamaud, D. BernacheAssollant, E. Champion, M. Heughebaert, C. Rey*. Calcination and sintering of hydroxyfluorapatite powders. — Solid State Ionics, 1997, **101**, № 2, p. 1357—1362.
72. *Y. Ota, T. Kasuga, Y. Abe*. Preparation and compressive strength behavior of porous ceramics with beta-$Ca(PO_3)_2$ fiber skeletons. — Journal of the American Ceramic Society, 1997, **80**, № 1, p. 225—231.

73. *X. Zhang, G. H. M. Gubbels, R. A. Terpstra, R. M. Etselaar*. Toughening of calcium hydroxyapatite with silver particles. — Journal of Materials Science, 1997, **32**, № 1, p. 235—243.
74. *M. Milosevski, J. Bossert, R. Milosevska, M. Buucker.* Obtaining and properties of dense and porous biohydroxyapatite. — Sciense of Sintering, 1997, **29**, № 1, p. 33—44.
75. *T. Matsuno, K. Watanabe, K. Ono, M. Koishi*. Preparation and characterization of compositionally graded multilayered hydroxyapatite/zirconia ceramics. — Journal of the Ceramic Society of Japan, 1999, **107**, № 11, p. 1105—1110.
76. *J. Y. Kim, B. A. Hunter, R. R. Fenton, B. J. Kennedy*. Neutron powder diffraction study of lead hydroxyapatite. — Australian Journal of Chemistry, 1997, **50**, № 11, p. 1061—1065.
77. *S. Raynaud, E. Champion, D. Bernache-Assollant, J. P. Laval*. Determination of calcium/phosphorus atomic ratio of calcium phosphate apatites using X-ray diffractometry. — Journal of the American Ceramic Society, 2001, **84**, № 2, p. 359—366.
78. *M. G. Taylor, K. Simk, S. F. Parker, P. C. H. Mitchell*. Inelastic neutron scattering studies of synthetic calcium phosphates. — Physical chemistry chemical physics, 1999, **1**, № 13, p. 3141—3144.
79. *H. J. Kleebe, E. F. Bres, D. Bernache-Assolant, G. Ziegler*. High-resolution electron microscopy and convergent-beam electron diffraction of sintered undoped hydroxyapatite. — Journal of the American Ceramic Society, 1997, **80**, № 1, p. 37—44.
80. *A. Jillavenkatesa, D. T. Hoelzer, R. A. Condrate*. An electron microscopy study of the formation of hydroxyapatite through sol-gel processing. — Journal of Materials Science, 1999, **34**, №19, p. 4821—4830.
81. *N. Kanzaki, K. Onuma, A. Ito, K. Teraoka, T. Tateishi, S. Tsutsumi*. Direct growth rate measurement of hydroxyapatite single crystal by Moire phase shift interferometry. — Journal of Physical Chemistry B, 1998, **102**, № 34, p. 6471—6476.
82. *L. G. Gilinskaya, L. M. Krivoputskaya, L. N. Pospelova*. Problems of theoretical and genetic mineralogy. New complexes of paramagnetic oxygen in F → Cl natural series of apatite. — Novosibirsk: Science, 1999, — 140 p. (in Russian)
83. *P. Moens, F. Callens, S. Vandoorslaer, P. Matthys*. ENDOR study of an O-ion observed in X-ray-irradiated carbonated hydroxyapatite powders. — Physical Review B — Condensed Matter, 1996, **53**, № 9, p. 5190—5197.
84. *Y. Pan*. ^{31}P-^{19}F rotational-echo, double-resonance nuclear magnetic resonance experiment on fluoridated hydroxyapatite. — Solid State Nuclear Magnetic Resonance, 1995, **5**, №3, p. 263—268.
85. *Y. Pan*. The investigation of the spatial distribution of F- in fluoridated hydroxyapatite by ^{31}P-^{19}F rotational-echo double-resonance (REDOR) NMR. — Phosphorus Sulfur and Silicon and the Related Elements, 1999, **146**, p. 413—416.
86. *L. G. Gilinskaya*. EPR centers OH^--O-HO^- in natural apatites. — Journal of Structural Chemistry, 2001, **42**, No. 3, p. 446—453. (in Russian)
87. *L.G. Gilinskaya, Yu. N. Zanin*. Factors of stabilization of paramagnetic radicals CO_2^-, CO_3^- and CO_3^{3-} in natural carbonapatites. — Journal of Structural Chemistry, 1998, **39**, No. 5, p. 821—842. (in Russian)
88. *C. G. Kontoyannis, N. C. Bouropoulos, P. G. Koutsoukos*. Raman spectroscopy: A tool for the quantitative analysis of mineral components of solid mixtures. The case of calcium oxalate monohydrate and hydroxyapatite. — Vibrational Spectroscopy, 1997, **15**, № 1, p. 53—60.
89. *Y. Liu, P. Comodi, P. Sassi.* Vibrational spectroscopic investigation of phosphate tetrahedron in fluor-, hydroxy-, and chlorapatites. — Neues Jahrbuch für Mineralogie-Abhandlungen, 1998, **174**, № 2, p. 211—222.
90. *P. N. de Aza, F. Guitian, C. Santos, S. de Aza, R. Cusco, L. Artus.* Vibrational properties of calcium phosphate compounds. 2. Comparison between hydroxyapatite beta-tricalcium phosphate. — Chemistry of Materials, 1997, **9**, № 4 p. 916—922.
91. *R. Cusco, F. Guitian, S. de Aza, L. Artus*. Differentiation between hydroxyapatite and beta-tricalcium phosphate by means of mu-raman spectroscopy. — Journal of the European Ceramic Society, 1998, **18**, № 9, p. 1301—1305.

92. *E. E. Lawson, B. W. Barry, A. C. Williams, H. G. M. Edwards*. Biomedical applications of Raman spectroscopy. — Journal of Raman Spectroscopy, 1997, **28**, № 2—3, p. 111—117.
93. *A. M. Tudor*. The Analysis of biomedical hydroxyapatite powders and hydroxyapatite coatings on metallic medical implants by near-IR Fourier transform Raman spectroscopy. — Spectrochimica Acta Part A — Molecular Spectroscopy, 1994, **50**, № 11, p. 2035.
94. *G. Leroy, N. Leroy, G. Penel, C. Rey, P. Lafforgue, E. Bres*. Polarized micro-Raman study of fluorapatite single crystals. — Applied Spectroscopy, 2000, **54**, № 10, p. 1521—1527.
95. *T. Ishikawa, A. Teramachi, H. Tanaka, A. Yasukawa, K. Kandori*. Fourier transform infrared spectroscopy study of deuteration of calcium hydroxyapatite particles. — Langmuir, 2000, **16**, № 26, p. 10221—10226.
96. *P. Serra, J. Fernandez-Pradas, G. Sardin, J. L. Morenza*. Interaction effects of an excimer laser beam with hydroxyapatite targets. — Applied Surface Science, 1997, **110**, p. 384—388.
97. *P. Serra, J. L. Morenza*. Fluence dependence of hydroxyapatite laser ablation plumes. — Thin Solid Films, 1998, **335**, № 1—2, p. 43—48.
98. *P. Serra, J. M. FernandezPradas, J. Navarro, J. L. Morenza*. Study of the plume generated by Nd:YAG laser ablation of a hydroxyapatite target. — Applied Physics A — Materials Science & Processing, 1999, **69**, Suppl. S, p. S183—S186.
99. *M. Gaft, R. Reisfeld, G. Panczer, P. Blank, G. Boulon*. Laser-induced time-resolved luminescence of minerals. — Spectrochimica Acta Part A — Molecular and Biomolecular Spectroscopy, 1998, **54**, № 13, p. 2163—2175.
100. *A. Sery, A. Manceau, G. N. Greaves*. Chemical state of Cd in apatite phosphate ores as determined by EXAFS spectroscopy. — American Mineralogist, 1996, **81,** № 7—8, p. 864—873.
101. *N. Okude, M. Nagoshi, H. Noro, Y. Baba, H. Yamamoto, T. A. Sasaki*. P and SK-edge XANES of transition-metal phosphates and sulfates. — Journal of Electron Spectroscopy and Related Phenomena, 1999, **103**, sp. Iss. Si, p. 607—610.
102. *A. P. Shpak, V. L. Karbovsky, E. I. Kopylova*. Fourier analysis of EXAFS spectra of strontium in disordered phosphate systems — Metallofizika I Noveishie Tekhnologii, 2001, **23**, No. 8, p. 1117—1125. (in Russia)
103. *V. D. Dobrovolsky*. Electronic structure of transition metals and their alloys. — Kiev: ONTI IMP AS UkSSR, 1968. — p. 296. (in Russian)
104. *D. I. Kochubei, Yu. A. Babanov, K. I. Zamaraev et al*. X-ray methods for studying the structure of amorphous solids. EXAFS spectroscopy. — Novosibirsk: "Science", 1988. — 305 p. (in Russian)
105. *A. G. McKale*. Improved ab initio calculations of amplitude and functions for Extended X-Ray Absorption Fine Structure (EXAFS). — J. Amer. Chem. Soc., 1988, **110**, p. 3763—3783.
106. American Mineralogist Crystal Structure Database. — www.geo.arizona.edu.
107. *A. P. Shpak, V. L. Karbovskii, V. V. Trachevskii*. Peculiarities of electronic structure of ultra disperse of calcium hydroxyapatite. — J. Elec. Spec. and Related Phenomena, 1998, № 88—91, p. 973—976.
108. *A. A. Marakushev, T. A. Stolyarova*. Thermodynamics of minerals of the apatite group. — Geochemistry. Reports of the Academy of Sciences, 2000, **372**, No. 3, p. 369—372. (in Russian)
109. *S. Salman, K. Haupt, K. Ramanathan, B. Danielsson*. Thermometric sensing of fluoride by adsorption on ceramic hydroxyapatite using flow injection analysis. — Analytical Communications, 1997, **34**, № 11, p. 329—332.
110. *A. A. Marakushev, T. A. Stolyarova*. Deficiency of volatile components in the composition of apatite and thermochemistry of fluorapatite. — Geochemistry. Reports of the Academy of Sciences, 1998, **363**, No. 6, p. 811—814. (in Rissian)
111. G. Muralithran, *S. Ramesh*. The effects of sintering temperature on the properties of hydroxyapatite. — Ceramics International, 2000, **26**, №2, p. 221—230.

112. *F. Brunet, D. R. Allan, S. A. T. Redfern, R. J. Angel, R. Miletich, H. J. Reichmann, J. Sergent, M. Hanfland*. Compressibility and thermal expansivity of synthetic apatites, $Ca_5(PO_4)_3X$ with X = OH, F and Cl. — European Journal of Mineralogy, 1999, **11**, № 6, p. 1023—1035.
113. *F. H. Lin, C. J. Liao, K. S. Chen, J. S. Sun*. Thermal reconstruction behavior of the quenched hydroxyapatite powder during reheating in air. — Materials Science & Engineering C. Biomimetic and Supramolecular Systems, 2000, **13**, № 1—2, Sp. Iss. SI, p. 97—104.
114. *A. Ababou, D. Bernacheassollant, M. Heughebaert*. Influence of the calcination conditions on the morphological evolution of hydroxyapatite. — Annales de Chimie — Science des Materiaux, 1994, **19**, № 4, p. 165—175.
115. *K. Yamashita, K. Kitagaki, T. Umegaki.* Thermal instability and proton conductivity of ceramic hydroxyapatite at high temperatures. — Journal of the American Ceramic Society, 1995, **78**, № 5, p. 1191—1197.
116. *J. Cihlar, A. Buchal, M. Trunec*. Kinetics of thermal decomposition of hydroxyapatite bioceramics. — Journal of Materials Science, 1999, **34**, № 24, p. 6121—6131.
117. *N. V. Krivtsov, V. P. Orlovskii, Z. A. Ezhova, E. M. Koval*. Thermochemistry of hydroxyapatite $Ca_{10}(PO_4)_6(OH)_2$. — Zhurnal Neorganicheskoi Khimii, 1997, **42**, № 6, p. 885—887.
118. *E.* Adolfsson*, L. Hermansson*. Phase stability aspects of various apatite-aluminium oxide composites. Journal of Materials Science, 2000, **35**, №22, p. 5719—5723.
119. *H. Fujimori, H. Toya, K. Ioku, S. Goto, M. Yoshimura*. In situ observation of defects in hydroxyapatite up to 1200 degrees C by ultraviolet Raman spectroscopy. — Chemical Physics Letters, 2000, **325**, № 4, p. 383—388.
120. *S. V. Dorozhkin*. Interaction of some calcium phosphates with water at increased temperatures. — Journal of Inorganic Chemistry, 2000, **45**, No. 5, p. 897—904. (in Russian)
121. *P. Gasser, J. C. Voegel, P. Gramain.* Mechanism of action of adsorbed fluoride ions on the dissolution kinetics of apatite powder. — Journal of Colloid and Interface Science, 1994, **168**, № 2, p. 465—472.
122. *R. I. Martin, P. W. Brown*. Effects of sodium fluoride, potassium fluoride and ammonium fluoride solutions on the hydrolysis of $CaHPO_4$ at 37.4 degrees C. — Journal of Crystal Growth, 1998, **183**, № 3, p. 417—426.
123. *A. Lebugle, B. Sallek, A. T. Tai*. Surface modification of monetite in water at 37 degrees C: characterisation by XPS. — Journal of Materials Chemistry, 1999, **9**, № 10, p. 2511—2515.
124. *S. Matsuya, S. Takagi, L. C. Chow*. Hydrolysis of tetracalcium phosphate in H_3PO_4 and KH_2PO_4. — Journal of Materials Science, 1996, **31**, № 12, p. 3263—3269.
125. *S. Shimabayashi, M. Matsumoto*. Effect of sulfate ion and dodecyl sulfate ion on non-stoichiometric dissolution of hydroxyapatite. — Nippon Kagaku Kaishi, 1994, № 1, p. 26—30.
126. *M. R. Christoffersen, J. Dohrup, J. Christoffersen*. Kinetics of growth and dissolution of calcium hydroxyapatite in suspensions with variable calcium to phosphate ratio. — Journal of Crystal Growth, 1998, **186**, № 1—2, p. 283—290.
127. *S.* Koutsopoulos, *E. Pierri, E. Dalas. N. Tzavellas, N. Klouras*. Effect of ferricenium salts on the crystal growth of hydroxyapatite in aqueous solution. — Journal of Crystal Growth, 2000, **218**, N 2—4, p. 353—358.
128. *W. Suchanek, M. Yashima, M. Kakihana, M. Yoshimura*. Hydroxyapatite/hydroxyapatite-whisker composites without sintering additives: Mechanical properties and microstructural evolution. — Journal of the American Ceramic Society, 1997, **80**, № 11, p. 2805—2813.
129. *S. Nicolopoulos, J. M. Gonzalezcalbet, M. P. Alonso, M. T. Gutierrezrios, M. I. Defrutos, M. Valletregi*. Characterization by TEM of local crystalline changes during irradiation damage of hydroxyapatite compounds. — Journal of Solid State Chemistry, 1995, **116**, № 2, p. 265—274.
130. *H. Suda, M. Yashima, M. Kakihana, M. Yoshimura*. Monoclinic-hexagonal phase transition in hydroxyapatite studied by X-ray powder diffraction and differential scanning calorimeter techniques. — Journal of Physical Chemistry, 1995, **99**, № 17, p. 6752—6754.

131. *A. Meldrum, L. M. Wang, R. C. Ewing*. Electron-irradiation-induced phase segregation in crystalline and amorphous apatite: A TEM study. — American Mineralogist, 1997, **82**, № 9—10, p. 858—869.
132. *T. Murata, K. Shiraishi, Y. Ebina, T. Miki*. An ESR study of defects in irradiated hydroxyapatite. — Applied radiation and isotopes, 1996, **47,** № 11/12, p. 1527—1531.
133. *A. Bensaoud, A. Bouhaouss, M. Ferhat*. Ionic conductivity of poorly crystalline apatite: Effect of maturation. — Zeitschrift Für Naturforschung Section A — Journal of Physical Sciences, 2000, **55**, № 11—12, p. 883—886.
134. *V. P. Orlovskii, N. A. Zakharov, A. A. Ivanov*. Structural transition and dielectric characteristics of high-purity hydroxyapatite. — Inorganic Materials, 1996, **32**, № 6, p. 654—656.
135. *J. E. H. Sansom, D. Richings, P. R. Slater*. A powder neutron diffraction study of the oxide-ion-conducting apatite-type phases, $La_{9.33}Si_6O_{26}$ and $La_8Sr_2Si_6O_{26}$ — Solid State Ionics, 2001, **139**, № 3—4, p. 205—210.
136. *P. Serra, L. Cleries, J. L. Morenza*. Analysis of the expansion of hydroxyapatite laser ablation plumes. — Applied Surface Science, 1996, №96—98, p. 216—221.
137. *P. Serra, J. L. Morenza*. Analysis of hydroxyapatite laser ablation plumes in a water atmosphere. — Applied Physics A — Materials Science & Processing, 1998, **67**, № 3, p. 289—294.
138. *P. Serra, J. L. Morenza*. Imaging and spectral analysis of hydroxyapatite laser ablation plumes. — Applied Surface Science, 1998, **129**, p. 662—667.
139. *D. N. Misra*. Interaction of ortho-phospho-L-serine with hydroxyapatite: Formation of a surface complex. — Journal of Colloid and Interface Science, 1997, **194**, № 1, p. 249—255.
140. *N. Spanos, P. G. Koutsoukos*. Model studies of the effect of orthophospho-L-serine on biological mineralization. — Langmuir, 2001, **17**, № 3, p. 866—872.
141. *S. Koutsopoulos, E. Dalas*. Hydroxyapatite crystallization in the presence of serine, tyrosine and hydroxyproline amino acids with polar side groups. — Journal of Crystal Growth, 2000, **216**, № 1—4, p. 443—449.
142. *S. Koutsopoulos, E. Dalas*. The effect of acidic amino acids on hydroxyapatite crystallization. — Journal of Crystal Growth, 2000, **217**, № 4, p. 410—415.
143. *S. Koutsopoulos, E. Dalas*. Inhibition of hydroxyapatite formation in aqueous solutions by amino acids with hydrophobic side groups. — Langmuir, 2000, **16**, № 16, p. 6739—6744.
144. *S. Koutsopoulos, E. Dalas*. The crystallization of hydroxyapatite in the presence of lysine. — Journal of Colloid and Interface Science, 2000, **231**, № 2, p. 207—212.
145. *T. A. Fuierer, M. Lore, S. A. Puckett, G. H. Nancollas*. A mineralization adsorption and mobility study of hydroxyapatite surfaces in the presence of zinc and magnesiumions. — Langmuir, 1994, **10**, № 12, p. 4721—4725.
146. *P. Gasser, Y. Haikel, J. C. Voegel, P. Gramain*. Surface reactions of hydroxyapatite in the presence of fluoride ions. 2. Effects of calcium and phosphate in saturated solutions. — Colloids and Surfaces A. Physicochemical and Engineering Aspects, 1994, **88**, № 2—3, p. 157—168.
147. *K. Schenk-Meuser, H. Duschner*. ESCA-analysis of tin compounds on the surface of hydroxyapatite. — Fresenius Journal of Analytical Chemistry, 1997, **358**, № 1—2, p. 265—267.
148. *Y. L. Chen, X. F. Zhang, Y. D. Gong, N. M. Zhao, T. Y. Zeng, X. Q. Song*. Conformational changes of fibrinogen adsorption onto hydroxyapatite and titanium oxide nanoparticles. — Journal of Colloid and Interface Science, 1999, **214**, № 1, p. 38—45.
149. *K. Kandori, M. Saito, H. Saito, A. Yasukawa, T. Ishikawa*. Adsorption of protein on non-stoichiometric calcium strontium hydroxyapatite. — Colloids and Surfaces A — Physicochemical and Engineering Aspects, 1995, **94**, № 2—3, p. 225—230.
150. *K. Kandori, N. Horigami, H. Kobayashi, A. Yasukawa, T. Ishikawa*. Adsorption of lysozyme onto various synthetic hydroxyapatites. — Journal of Colloid and Interface Science, 1997, **191**, № 2, p. 498—502.

151. *M.* Shirkhanzadeh**,** *G.Q. Liu*. Biocompatible delivery systems for osteoinductive proteins: immobilization of L-lysine in micro-porous hydroxyapatite coatings. — Materials Letters, 1994, **21**, 1. p. 115—118.
152. *D. N. Misra*. Adsorption of potassium N-phenylglycinate on hydroxyapatite: role of solvents and ionic charge. — Colloids and Surfaces A: Physicochemical and Engineering Aspects, 1996, **108**, 2—3, p. 277—285.
153. *D. N. Misra*. Interaction of some alkali metal citrates with hydroxyapatite. Ion-exchange adsorption and role of charge balance. Colloids and Surfaces A — Physicochemical and Engineering Aspects, 1998, **141**, № 2, p. 173—179.
154. *A. Lopez-Macipe, J. Gomez-Morales, R. Rodriguez-Clemente*. The role of pH in the adsorption of citrate ions on hydroxyapatite. — Journal of Colloid and Interface Science, 1998, **200**, № 1, p. 114—120.
155. *Y. Q. Lu, J. Drelich, J. D. Miller*. Oleate adsorption at an apatite surface studied by ex-situ FTIR internal reflection spectroscopy. — Journal of Colloid and Interface Science, 1998, **202**, № 2, p. 462—476.
156. *H. Tanaka, T. Watanabe, M. Chikazawa, K. Kandori, T. Ishikawa*. Surface structure and properties of calcium hydroxyapatite modified by hexamethyldisilazane. — Journal of Colloid and Interface Science, 1998, **206**, № 1, p. 205—211.
157. *H. Tanaka, A. Yasukawa, K. Kandori, T. Ishikawa*. Surface modification of calcium hydroxyapatite with hexyl and decyl phosphates. — Colloids and surfaces A — Physicochemical and Engineering Aspects, 1997, **125**, № 1, p. 53—62.
158. *H. Tanaka, A. Yasukawa, K. Kandori, T. Ishikawa*. Modification of calcium hydroxyapatite using alkyl phosphates. — Langmuir, 1997, **13**, № 4, p. 821—826.
159. *M. Wakamura, K. Kandori, T. Ishikawa*. Surface composition of calcium hydroxyapatite modified with metal ions. — Colloids and surfaces A — Physicochemical and Engineering Aspects, 1998, **142**, № 1, p. 107—116.
160. *S. Sugiyama, T. Minami, H. Hayashi, M. Tanaka, J. B. Moffat*. Surface and bulk properties of stoichiometric and nonstoichiometric strontium hydroxyapatite and the oxidation of methane. — Journal of Solid State Chemistry, 1996, **126**, № 2, p. 242—252.
161. *Y. Matsumura, J. B. Moffat*. Inhibition of CO oxidation on hydroxyapatite by tetrachloromethane. — Catalysis Letters, 1996, **39**, № 3—4, p. 205—208.
162. *S. Sugiyama, K. Abe, T. Minami, H. Hayashi, J. B. Moffat*. A comparative study of the oxidation of methane and ethane on calcium hydroxyapatites with incorporated lead in the presence and absence of tetrachloromethane. — Applied Catalysis A — General, 1998, **169**, № 1, p. 77—86.
163. *S. Sugiyama, Y. Iguchi, H. Nishioka, T. Miyamoto, H. Hayashi, J. B. Moffat*. Effects of incorporated lead and chlorine on the oxidation of ethane on strontium hydroxyapatites. — Journal of Materials Chemistry, 1997, **7**, № 12, p. 2483—2487.
164. *S. Sugiyama, E. Nitta, H. Hayashi, J. B. Moffat*. Alkene selectivity enhancement in the oxidation of propane on calcium-based catalysts. — Catalysis letters, 1999, **59**, № 1, p. 67—72.
165. *S. Sugiyama, E. Nitta, K. Abe, H. Hayashi, J. B. Moffat*. Effect of the introduction of tetrachloromethane into the feedstream for methane oxidation with oxygen and nitrous oxide on thermally stable strontium hydroxyapatites. — Catalysis Letters, 1998, **55**, № 3—4, p. 189—196.
166. *S. Sugiyama, Y. Fujii, K. Abe, H. Hayashi, J. B. Moffat*. Nitrous oxide as oxidant for the oxidation of methane on barium hydroxyapatites in the presence and absence of tetrachloromethane. — Journal of Molecular Catalysis A — Chemical, 2001, **166**, № 2, p. 323—330.
167. *S. Sugiyama, K. Abe, H. Hayashi, J. B. Moffat*. Synergistic effects in the oxidation of methane on strontium and lead hydroxyapatites. — Catalysis Letters, 1999, **57**, № 4, p. 161—165.
168. *K. Yamashita, T. Yagi, T. Umegaki*. Bonelike coatings onto ceramics by reactive magnetron sputtering. — Journal of the American Ceramic Society, 1996, **79**, № 12, p. 3313—3316.

169. *J. G. C. Wolke, K. DeGroot, J. A. Jansen*. Dissolution and adhesion behaviour of radio-frequency magnetron-sputtered Ca-P coatings. — Journal of Materials Science, 1998, **33**, № 13, p. 3371—3376.
170. *P. A. Campbell, H. C. Gledhill, S. R. Brown, I. G. Turner*. Vacuum plasma sprayed hydroxyapatite coatings on titanium alloy substrates: Surface characterization and observation of dissolution processes using atomic force microscopy. — Journal of Vacuum Science & Technology B, 1996, **14**, № 2, p. 1167—1172.
171. *E. Park, R. A. Condrate, D. Lee*. Infrared spectral investigation of plasma spray coated hydroxyapatite. — Materials letters, 1998, **36**, № 1—4, p. 38—43.
172. *W. D. Tong, J. Y. Chen, X. D. Li, J. M. Feng, Y. Cao, Z. J. Yang, X. D. Zhang*. Preferred orientation of plasma sprayed hydroxyapatite coatings. — Journal of Materials Science, 1996, **31**, № 14, p. 3739—3742.
173. *B. C. Wang, E. Chang, C. Y. Yang*. Characterization of plasma-sprayed bioactive hydroxyapatite coatings in vitro and in vivo. — Materials Chemistry and Physics, 1994, **37**, № 1, p. 55—63.
174. *J. L. Arias, M. B. Mayor, J. Pou, B. Leon, M. PerezAmor*. Stoichiometric transfer in pulsed laser deposition of hydroxylapatite. — Applied Surface Science, 2000, **154**, p. 434—438.
175. *L. Torrisi*. Structural investigations on laser deposited hydroxyapatite films. — Thin Solid Films, 1994, **237**, № 1—2, p. 12—15.
176. *S. Hontsu, T. Matsumoto, J. Ishii, M. Nakamori, H. Tabata, T. Kawai*. Electrical properties of hydroxyapatite thin films grown by pulsed laser deposition. — Thin Solid Films, 1997, **295**, № 1—2, p. 214—217.
177. *S. Hontsu, M. Nakamori, N. Kato, H. Tabata, J. Ishii, T. Matsumoto, T. Kawai*. Formation of hydroxyapatite thin films on surface-modified polytetrafluoroethylene substrates. — Japanese Journal of Applied Physics Part 2 — Letters, 1998, **37**, № 10A, p. L1169—L1171.
178. *J. M. FernandezPradas, L. Cleries, E. Martinez, G. Sardin, J. Esteve, J. L. Morenza*. Calcium phosphate coatings deposited by laser ablation at 355 nm under different substrate temperatures and water vapour pressures. — Applied Physics A — Materials Science & Processing, 2000, **71**, № 1, p. 37—42.
179. *J. M. FernandezPradas, L. Cleries, G. Sardin, J. L. Morenza*. Hydroxyapatite coatings grown by pulsed laser deposition with a beam of 355 nm wavelength. — Journal of Materials Research, 1999, **14**, № 12, p. 4715—4719.
180. *M. M. Pereira, A. E. Clark, L. L. Hench*. Effect of texture on the rate of hydroxyapatite formation on gel-silica surface. — Journal of the American Ceramic Society, 1995, **78**, № 9, p. 2463—2468.
181. *C. M. Lopatin, V. Pizziconi, T. L. Alford, T. Laursen*. Hydroxyapatite powders and thin films prepared by a sol-gel technique. — Thin Solid Films, 1998, **326**, № 1—2, p. 227—232.
182. *Y. Fujishiro, A. Fujimoto, T. Sato, A. Okuwaki*. Coating of hydroxyapatite on titanium plates using thermal dissociation of calcium-EDTA chelate complex in phosphate solutions under hydrothermal conditions. — Journal of Colloid and Interface Science, 1995, **173**, № 1, p. 119—127.
183. *J. Majling, S. Svetik, J. Annus, J. Kristin, P. M. Marquis*. Optical transmissivity changes of thin hydroxyapatite sheets on heating. — Chemical Papers — Chemicke Zvesti, 1997, **51**, № 5, p. 268—272.
184. *Y. S.* Hsu*, E. Chang, H. S. Liu*. Hydrothermally-grown monetite ($CaHPO_4$) on hydroxyapatite. — Ceramics International, 1998, **24**, Issue 4, p. 249—254.
185. *Y. Ohba, T. Watanabe, E. Sakai, M. Daimon*. Coating of HAP/CaTiO3 multilayer on titanium substrates by hydrothermal method. — Journal of the Ceramic Society of Japan, 1999, **107**, № 10, p. 907—912.
186. *H. Ishizawa, M. Ogino*. Thin hydroxyapatite layers formed on porous titanium using electrochemical and hydrothermal reaction. — Journal of Materials Science, 1996, **31**, № 23, p. 6279—6284.

187. *R. Damodaran, B. M. Moudgil*. Electrophoretic deposition of calcium phosphates from non-aqueous media. — Colloids and Surfaces A — Physicochemical and Engineering Aspects, 1993, **80**, № 2—3, p. 191—195.
188. *M. Shirkhanzadeh, M. Azadegan, V. Stack, S. Schreyer*. Fabrication of pure hydroxyapatite and fluoridated-hydroxyapatite coatings by electrocrystallisation. — Materials Letters, 1994, **18**, 4, p. 211—214.
189. *J. M. Zhang, C. J. Lin, Z. D. Feng, Z. W. Tian*. Electrochemical preparation for bioactive ceramics coating on Ti-6Al-4V substrate. — Chemical Journal of Chinese Universities — Chinese, 1997, **18**, № 6, p. 961—962.
190. *P. Filip, A. C. Kneissl, K. Mazanec*. Physics of hydroxyapatite plasma coatings on TiNi shape memory materials. — Materials Science and Engineering A — Structural Materials Properties Microstructure and Processing, 1997, **234**, p. 422—425.
191. *A. J. S. Peaker, J. T. Czernuszka*. The effect of electric field on the formation of hydroxyapatite coatings. — Thin Solid Films, 1996, **287**, № 1—2, p. 174—183.
192. *M. A. Barbosa*. Dissolution and deposition processes at metal/apatite interfaces. — Anales de Quimica, 1997, **93**, № 1, Suppl. 1, p. S56—S63.
193. *G. F. Xu, I. A. Aksay, J. T. Groves*. Continuous crystalline carbonate apatite thin films. A biomimetic approach. — Journal of the American Chemical Society, 2001, **123**, № 10, p. 2196—2203.
194. *M. T*. Pham, *M. F. Maitz, W. Matz, H. Reuther, E. Richter, G. Steiner.* Promoted hydroxyapatite nucleation on titanium ion-implanted with sodium. — Thin Solid Films, 2000, **379**, №1—2, p. 50—56.
195. *C. M. Lopatin, T. L. Alford, V. B. Pizziconi, M. Kuan, T. Laursen*. Ion-beam densification of hydroxyapatite thin films. — Nuclear Instruments & Methods in Physics Research Section B — Beam Interactions with Materials and Atoms, 1998, **145**, № 4, p. 522—531.
196. *H. Li, K. A. Khor, P. Cheang*. Effect of the powders melting state on the properties of HVOF sprayed hydroxyapatite coatings. — Materials Science and Engineering A — Structural Materials Properties Microstructure and Processing, 2000, **293**, № 1—2, p. 71—80.
197. *T. Nonami, K. Naganuma, A. Kamiya, T. Kameyama*. Hydroxyapatite granule implantation into superplastic titanium alloy. — Journal of the Ceramic Society of Japan, 1997, **105**, № 8, p. 710—712.
198. *T. Nonami, T. Sonoda, K. Naganuma, A. Kamiya, K. Teraoka, T. Kameyama*. Implantation of hydroxyapatite granules into superplastic Ti alloy substrate with deposited Ti film. — Journal of the Ceramic Society of Japan, 2000, **108**, № 12, p. 1122—1125.
199. *A. J. Ruys, J. A. Kerdic, C. C. Sorrell*. Thixotropic casting of ceramic-metal functionally gradient materials. — Journal of Materials Science, 1996, **31**, № 16, p. 4347—4355.
200. E. Park, R. A. Condrate. Graded coating of hydroxyapatite and titanium by atmospheric plasma spraying. — Materials Letters, 1999, **40**, №5, p. 228—234.
201. *C. L. Chu, J. C. Zhu, Z. D. Yin, S. D. Wang*. Hydroxyapatite-Ti functionally graded biomaterial fabricated by powder metallurgy. — Materials Science and Engineering A — Structural Materials Properties Microstructure and Processing, 1999, **271**, № 1—2, p. 95—100.
202. *V. Craciun, I. W. Boyd, D. Craciun, P. Andreazza, J. Perriere*. Vacuum ultraviolet annealing of hydroxyapatite films grown by pulsed laser deposition. — Journal of Applied Physics, 1999, **85**, № 12, p. 8410—8414.
203. *K. A. Khor, A. Vreeling, Z. L. Dong, P. Cheang*. Laser treatment of plasma sprayed HAp coatings. — Materials Science and Engineering A — Structural Materials Properties Microstructure and Processing, 1999, **266**, № 1—2, p. 1—7.
204. *K. Onuma, A. Ito*. Cluster growth model for hydroxyapatite. — Chemistry of Materials, 1998, **10**, № 11, p. 3346—3351.
205. *A. Oyane, K. Onuma, T. Kokubo, A. Ito*. Clustering of calcium phosphate in the system CaCl2-H3PO4-KCl-H2O. — Journal of Physical Chemistry B, 1999, **103**, № 39, p. 8230—8235.

206. *G. Treboux, P. Layrolle, N. Kanzaki, K. Onuma, A. Ito*. Existence of Posner's cluster in vacuum. — Journal of Physical Chemistry A, 2000, **104**, № 21, p. 5111—5114.
207. *A. Athanasopoulou, D. Gavril, A. Koliadima, G. Karaiskakis*. Study of hydroxyapatite aggregation in the presence of potassium phosphate by centrifugal sedimentation field-flow fractionation. — Journal of Chromatography A, 1999, **845**, № 1—2, p. 293—302.
208. *E. Saw, K. H. Sandhage, P. K. Gallagher, A. S. Litsky*. Near-net-shaped calcium hydroxyapatite by the oxidation of machinable, calcium-bearing precursors (The volume identical metal oxidation, or VIMOX, process). — Journal of the American Ceramic Society, 2000, **83**, № 4, p. 998—1000.
209. *T. Toyama, T. Yasue, Y. Arai*. Formation of a new phase by crystallizing amorphous calcium phosphate and its property. — Journal of the Ceramic Society of Japan, 1997, **105**, № 11. p. 976—980.
210. *A. Rodrigues, A. Lebugle*. Behavior in wet atmosphere of an amorphous calcium phosphate with an atomic Ca/P ratio of 1.33. — Journal of Solid State Chemistry, 1999, **148**, № 2, p. 308—315.
211. *S. N. Vaidya, C. Karunakaran, B. M. Pande, N. M. Gupta, R. K. Iyer, S. B. Karweer*. Pressure-induced crystalline to amorphous transition in hydroxylapatite. — Journal of Materials Science, 1997, **32**, №12, p. 3213—3217.
212. *K. A. Gross, V. Gross, C. C. Berndt*. Thermal analysis of amorphous phases in hydroxyapatite coatings. — Journal of the American Ceramic Society, 1998, **81**, № 1, p. 106—112.
213. *L. M. Yang, W. J. Weber*. Transmission electron microscopy study of ion-beam-induced amorphization of $Ca_2La_8(SiO_4)_6O_2$. — Philosophical Magazine A — Physics of Condensed Matter Structure Defects and Mechanical Properties, 1999, **79**, № 1, p. 237—253.
214. *Y. Ota, T. Iwashita, T. Kasuga, Y. Abe*. Novel preparation method of hydroxyapatite fibers. — Journal of the American Ceramic Society, 1998, **81**, № 6, p. 1665—1668.
215. *W. L. Suchanek, M. Yoshimura*. Preparation of fibrous, porous hydroxyapatite ceramics from hydroxyapatite whiskers. — Journal of the American Ceramic Society, 1998, **81**, № 3, p. 765—767.
216. *K. Teraoka, A. Ito, K. Onuma, T. Tateishi, S. Tsutsumi*. Hydrothermal growth of hydroxyapatite single crystals under natural convection. — Journal of Materials Research, 1999, **14**, № 6, p. 2655—2661.
217. *A. Nakahira, K. Sakamoto, S. Yamaguchi, K. Kijima, M. Okazaki*. Synthesis of hydroxyapatite by hydrolysis of alpha-TCP. — Journal of the Ceramic Society of Japan, 1999, **107**, № 1, p. 89—91.
218. *T. Toyama, A. Oshima, T. Yasue*. Hydrothermal synthesis of hydroxyapatite whisker from amorphous calcium phosphate and the effect of carboxylic acid. — Journal of the Ceramic Society of Japan, 2001, **109**, № 3, p. 232—237.
219. *K. Kato, Y. Eika, Y. Ikada.* In situ hydroxyapatite crystallization for the formation of hydroxyapatite/polymer composites. — Journal of Materials Science, 1997, **32**, № 20, p. 5533—5543.
220. *P. Sepulveda, F. S. Ortega, M. D. M. Innocentini, V. C. Pandolfelli*. Properties of highly porous hydroxyapatite obtained by the gelcasting of foams. — Journal of the American Ceramic Society, 2000, **83**, № 12, p. 3021—3024.
221. *K. Nakamoto* Infrared spectra of inorganic and coordination compounds. — New York: Wiley & Sons, Inc., 1978. — 448 p.
222. *L. D. Kislovsky, R. G. Knubovets.* On the sensitivity of infrared spectra of apatite single crystals to isomorphous substitutions. — The report AS USSR, 1968, **179**, No. 6, p. 1432—1435. (in Russian)
223. *B. Badraoui, R. Thouvenot, H. Debbabi.* X-raypowder diffraction, solid-state P-31-MAS-NMR and IR spectroscopy of cadmium-strontium mixed hydroxyapatites. — Comptes Rendus de L'Academie Des Sciences. Serie II. Fascicule C—Chimie, 2000, **3**, № 2, p. 107—112.
224. *A.P. Shpak, V.L. Karbovskii, O.P. Dimitriev.* The comparative analysis of infrared spectra: influence of the central atom on tetrahedral ion vibrations symmetry. — Physics and Chemistry of Solid State, 2002, **3**, № 1, p. 54—57.

225. *A.P. Shpak, Yu.A. Kunitsky, V. L. Karbivskii*. Cluster and nanostructured materials. — Kiev: Akademperiodika, 2001. — 587 p. (in Russian)
226. *A. P. Shpak, V. L. Karbivskii, V. V. Trachevsky*. Apatite. — Kiev: Akademperiodika, 2002. — 414 p. (in Russian)
227. *A. P. Shpak, V. L. Karbivskii, O. P. Dimitriev, V. V. Trachevskii.* Electron structure features of vanadium hydroxyapatite $Ca_5(VO_4)_3OH$ associated with Ca^{2+} substitution by alkali metals and lanthanum. — Functional Materials, 2001, **8**, № 4, p. 631—634.
228. *V.I. Nefedov*. X-ray photoelectron spectroscopy of chemical compounds. Directory. Moscow: Chemistry, 1984. — 256 p. (in Russian)
229. *M. A. Blokhin*. Methods of X-ray spectral studies. — Moscow: Fizmatgiz, 1959. — 386 p. (in Russian)
230. *A. Maizel, G. Leonhardt, R. Sargan*. X-ray spectra and chemical bond. — Kiev: Naukova Dumka, 1981. — 420 p. (in Russian)
231. *A. P. Shpak, V. L. Karbivskii.* Electronic structure of finely dispersed calcium hydroxyphosphate. — Reports of the Academy of Sciences of Ukraine. Mathematics, science, engineering, 1994, No. 4, p. 88—91.
232. *A. P. Shpak, V. L. Karbivskii, A. G. Vakhnei, O. Yu. Hijun*. On the electronic structure of calcium hydroxyapatite. — Reports of the Academy of Sciences of Ukraine. Mathematics, science, engineering sciences, 2001, No. 2, p. 99—108. (in Russian)
233. *L. Brewer.* Chemical bonding concepts applied to metals and their alloys. — Journal of Materials Education, 1984, **6**, № 5, p. 739—767.
234. *B. B. Kadomtsev, M. B. Kadomtsev*. Colapses of wave functions. — Successes of physical sciences, 1996, **166**, No. 6, p. 651—659. (in Russian)
235. *R. I. Karazia*. The collapse of the orbit of an excited electron and the peculiarities of atomic spectra. — UFN (Progress in Physical Sciences), 1981, **135**, No. 1, p. 79—115. (in Russian)
236. *R. E. Ruus, A. A. Maiste, Yu. A. Maksimov*. Atomic and solid-state effects in L-spectra of absorption of calcium in some compounds. — Izv. AS USSR (Proceedings of the Academy of Sciences of the USSR), 1982, **46**, No. 4, p. 789—796. (in Russian)
237. *A. P. Shpak*. Electronic structure of microheterogeneous systems of cluster type — elements on the basis of *d*-metals: Thesis Doctor of Physical and Mathematical Sciences: 01.04.07 — Kiev, 1990. — 315 p. (in Russian)
238. *V. A. Gubanov, A. L. Ivanovsky, M. V. Ryzhkov*. Quantum chemistry in materials science. — Moscow: Nauka, 1987. — 335 p. (in Russian)
239. *A. P. Shpak, V. L. Karbivskii, Yu. A. Zagorodni, A. G. Vakhney, A. I. Senkevich, V. N. Uvarov*. Spectral and quantum mechanical studies of apatite-like strontium compounds. — Reports of the National Academy of Sciences of Ukraine, 2003, No. 8, p. 86—93. (in Russian)
240. *A. P. Shpak, V. L. Karbovskii, A. G. Vakhney.* Electronic structure of isomorphically substituted strontium apatite. — J. Elec. Spec. and Related Phenomena, 2004, **137—140C**, p. 585—589.
241. *M. I. Sosulnikov, Yu. A. Teterin*. X-ray photoelectron studies of Ca, Sr and Ba and their oxides and carbonates. — Journal of Electron Spectroscopy and Related Phenomena, 1992, **59**, №2, p. 111—126.
242. *W. Harrison*. Electronic structure and the properties of solids. Moscow, 1983. — Volume 1. — 382 p., Volume 2. — 332 p. (in Russian)
243. *J. Zaiman*. Models of disorders. — Moscow: Mir, 1982. — 591 p. (in Russian)
244. *Sh.Myurarka*. Silicides for VLSI. — Moscow: Mir. —1986. — 176 p. (in Russian)
245. *Z.-C. Wu, E. T. Arakawa, J. R. Jimenez, L. J. Schowalter.* Optical properties of epitaxial $CoSi_2$/Si and $CoSi_2$ particles in Si from 0.062 to 2.76 eV. — J. Appl. Phys, 1992, **71**, № 11, p. 5601—5605.
246. *J. Y. Duboz, P. A. Badoz, J. Henz and H. von Kanel.* Near-infrared optical properties of $CoSi_2$ thin films. — J. Appl. Phys., 1990, **68**, № 5, p. 2346—2350.

247. *B. P. Voznyuk, R. Gontarz, J. Dubowik, Yu.V. Kudryavtsev, N.A. Lesnik.* Investigation of changes in the electron structure and in the optical and magnetic properties of amorphous films of $Co_{1-x}W_x$ alloys under conditions of structural relaxation and crystallization by ellipson and NMR spectroscopy methods. — Fizika Tverdogo Tela, 1990, **32**, № 3, p. 694—699.
248. *Yu. V. Kudryavtsev, I. V. Lezhnenko, A. G. Forester*. Optical and electrical properties of amorphous and crystalline $Co_{67}Ge_{33}$ alloy films. — Metallofizika i Noveishie Tekhnologii, 1984, **6**, № 2, p.86—91. (in Russian)
249. *C. Viguier, A. Cros, A. Humbert.* Electronic properties of $CoSi_2$ studied by reflectivity and spectroscopic ellipsometry. — Sol. Stat. Comm., 1986, **60**, № 12, p. 923—926.
250. *N. Ikeo, Y. Iijima, N. Niimura at al.* Handbook of X-ray photoelectron spectroscopy. — Tokyo, Japan: JEOL Ltd, 1991. — 217 p.
251. *B.V. Crist.* Handbook of monochromatic XPS spectra, the elements and native oxides. — USA: XPS International, Inc. 1999. — 548 p.
252. *A. P. Shpak, V. L. Karbivskii, N. A. Kurgan at al.* Electronic structure of calcium hydroxoapatite isomorphically modified by nickel. — Nanosystems, nanomaterials, nanotechnologies, 2004, **2**, №3, p. 945—950. (in Russian)
253. *V. V. Nemoskalenko, V. N. Antonov*. Methods of Computational Physics in Solid State Theory. — Kiev: Naukova Dumka, 1985. — 408 p. (in Russian)
254. *A. P. Shpak, V. V. Trachevsky, V. L. Karbivskii*. Actinides in self-organizing systems. Book 1. Actinoids in technogenesis. — Kiev: Akademperiodika, 2002. — 347 p. (in Russian)
255. *A. P. Shpak, V. V. Trachevsky, V. L. Karbivskii*. Actinides in self-organizing systems. Book 2. Nature of bioactivity of actinides. Kiev: Akademperiodika, 2002. — 317 p. (in Russian)
256. *A. P. Shpak, V. V. Trachevsky, V. L. Karbivskii*. Actinides in self-organizing systems. Book 3. Bioeffects of radiation and toxicological factors of the environment. — Kiev: Akademperiodika, 2003. — 613 p. (in Russian)
257. *A. P. Shpak, V. V. Trachevsky, V. L. Karbivskii*. Physico-chemistry of actinides. — Kiev: Akademperiodika, 2002. — 257 p. (in Russian)
258. *G. Panczer, M. Gaft, R. Reisfeld, S. Shoval, G. Boulon, B. Champagnon.* Luminescence of uranium in natural apatites. — Journal of Alloys and Compounds, 1998, **277,** p. 269—272.
259. *O. Fujino, S. Umetani, E. Ueno, K. Shigeta, T. Matsuda.* Determination of uranium and thorium in apatite minerals by inductively coupled plasma atomic emission spectrometry with solvent extraction separation into diisobutyl ketone. — Analytica Chimica Acta, 2000, **420**, № 1, p. 65—71.
260. *J.V. Bothe, P.W. Brown.* Apatite Formation in the $CaO\text{-}PbO\text{-}P_2O_5\text{-}H_2O$ System at 23 degrees +/– 1 degrees C. — Journal of the American Ceramic Society, 2000, **83**, № 3, p. 612—616.
261. *E. Ordonez-Regil, E. T. R. Guzman, E. O. Regil.* Surface modification in natural fluorapatite after uranyl solution treatment. — Journal of Radioanalytical and Nuclear Chemistry, 1999, **240**, № 2, p. 541—545.
262. *E. A. Hudson, P. G. Allen, L. J. Terminello, M. A. Denecke, T. Reich.* Polarized X-ray-absorption spectroscopy of the uranyl ion: Comparison of experiment and theory. — Phys. Rev, 1996, **B 54,** № 1, p. 156—165.
263. *M. A. Denecke, A. Bauer, J. I. Kim, H. Moll.* Polarization dependent XANES of uranium (VI) sorbed onto smectite. — Workshop "Mineral/Water interactions close to equilibrium". — Germany: Forschungszentrum Karlsruhe GmbH, Karlsruhe, 1999. — p. 35—37.
264. *V. L. Karbivskii, A. G. Vakhnei, R. V. Didenko, A. I. Senkevich, S. S. Smolyak, N. A. Kurgan*. Electronic structure of calcium hydroxoapatite, isomorphically modified by uranium. — Metallofizika i Noveishie Tekhnologii, 2003, **25**, No. 11, p. 1431—1437. (in Russian)
265. *M. I. Sosulnikov, Y. A. Teterin.* X-ray photoelectron studies of Ca, Sr and Ba and their oxides and carbonates. — J. Electron Spectrosc. Relat. Phenom., 1992, **59**, № 2, p. 101—116.

266. *J. Verbist, J. Riga, J.J. Pireaux, R. Caudano.* X-ray photoelectron spectra of uranium and uranium oxides. Correlation with the half-life of ^{235}U. — J. Electron Spectrosc. Relat. Phenom., 1974, **5,** p. 193—205.
267. *A. P. Shpak, V. L. Karbivskii, A. G. Vakhnei, A. Y. Senkevich, V. Kh. Kasiyanenko*. Theoretical and spectral studies of the electronic structure of isomorphically-substituted tetrahedral calcium structures. — Reports of the National Academy of Sciences of Ukraine, 2002, No. 7, p. 88—96. (in Russian)
268. *K. Keiswetter, T.W. Bauer, S.A. Brown, F. Vanlente, K. Merritt.* Characterisation of calcium phosphate powders by ESCA and EDXA. — Biomaterials, 1994, **15**, № 3, p. 183—188.
269. *S. Tougaard, A. Jablonski.* Quantitative XPS: influense of elastic electron scattering in quantification by peak shape analysis. — Surf. Int. Anal., 1997, **25,** p. 404—408.
270. *G. Vereecke, P. G. Rouxhet.* New method to correct for the influence of organic contamination on intensity ratios in quantitative XPS. — Surf. Int Anal., 1999, **27**, p. 761—769.
271. *M. P. Seah.* Quantitative AES and XPS: convergence between theory and experimental databases. — J. Electron Spectrosc. Relat. Phenom., 1999, **100**, p. 55—73.
272. *Y. Suetsugu, K. Hirota, K. Fujii, J. Tanaka.* Compositional distribution of hydroxyapatite surface and interface observed by electron spectroscopy. — J. Mater. Sci., 1996, **31**, № 17, p. 4541—4544.
273. *H. B. Lu, C. T. Campbell, D. J. Graham, B. D. Ratner.* Surface characterization of hydroxyapatite and related calcium phosphates by XPS and TOF-SIMS. — Anal. Chem., 2000, **72**, p. 2886—2894.
274. *S. Sugiyama, T. Moriga, H. Hayashi, J. B. Moffat.* Characterization of calcium, strontium, barium and lead hydroxyapatites: X-ray diffraction, photoelectron, extended X-ray absorption fine structure and MAS NMR spectroscopies. — Bull. Chem. Soc. Jpn, 2001, **74,** p. 187—192.
275. *E. I. Getman, V. I. Marchenko, L. V. Pasichnik, A. P. Shpak, V. L. Karbivskii, O. O. Salnik*. The method of obtaining of fluoride- and chlorapatite of calcium. — Patent on the invention, dated 16.08.04. No. 68775 A (Bulletin No. 8). (in Ukrainian)
276. *J. Mendialdua, R. Casanova, Y. Barbaux.* XPS studies of V_2O_5, V_6O_{13}, V_2O_3. — J. Electron Spectrosc. Relat. Penom, 1995, **71,** p. 249—261.
277. *J. Weber.* Fluorescence and glass lasers. — J. Non-Cryst. Sol., 1982, **47**, № 1, p. 117—133.
278. *K. B. Steinbruegge, T. Henningsen, R. H. Hopkins.* Laser properties of Nd^{3+} and Ho^{3+} doped crystals with the apatite structure. — Appl. Optics., 1972, **11**, № 5, p. 999 —1012.
279. *P. D. Johnson.* Some optical properties of powder and crystals halophosphate phosphors. — J. Electrochem. Soc., 1960, № 108, p. 159.
280. *R. K. Swank.* Color centers in X-irradiated halophosphate crystals. — Phys. Rev., 1964, **135**, № 1A, p. A266—A275.
281. *W. W. Piper, L. C. Kravitz, R. K. Swank.* Axially symmetric paramagnetic color centers in fluorapatite. — Phys. Rev., 1965, **138**, № 6A, p. A1802—A1814.
282. *D. Lapraz, A. Baumer, P. Iacconi.* On the thermoluminescence properties of hydroxyapatie $Ca_5(PO_4)_3OH$. — Phys. Stat. Sol., 1979, № A54, p. 605—613.
283. *D. Lapraz and A. Baumer.* Thermoluminescent properties of synthetic and natural fluorapatite, $Ca_5(PO_4)_3F$. — Phys. Stat. Sol., 1983, № A80, p. 353—366.
284. *D. Lapraz and A. Baumer.* Chloropatite, $Ca_5(PO_4)_3Cl$: Thermoluminescent properties. — Phys. Stat. Sol., 1981, **68**, № 1, p. 309—319.
285. *M. Born, H. Kun*. Dynamic theory of crystal lattices. — Moscow: Publishing house of foreign literature, 1958. — 488 p. (in Russian)
286. *H. Betger*. Principles of the dynamic theory of lattice. — Moscow, 1986. — 52 p. (in Russian)
287. *A. M. Kosevich*. Theory of the crystal lattice. — Kharkov: Vishcha shkola, 1988. — 304 p. (in Russian)
288. *R. S. Halford.* Infrared spectroscopy. — J.Chem.Phys, 1946, **14,** p. 8—29.

289. *A. P. Shpak, V. L. Karbivskii, O. P. Dimitriyev*. Comparative characterization of infrared spectra of apatites: the effect of ion substitutions on the structure of absorption bands. — Scientific News, 2001, No. 6, p. 150—153. (in Ukrainian)
290. *E. I. Getman, V. A. Karmalitsky, Yu.V. Kanyuka, S. N. Loboda, A.V. Ignatov*. Isomorphous substitution in the $Ca_{5-2x}Nd_xNa_x(PO_4)_3OH$ and $Ca_{5-2x}Y_xK_x(PO_4)_3OH$ systems. — Problems of Chemistry and Chemical Technology, 2000, No. 1, p. 24—26. (in Russian)
291. *A. P. Shpak, V. L. Karbivskii, O. P. Dimitriyev, L. P. Klyuenko, V. V. Stonis*. Suppression of oscillations anharmonism in a crystal lattice of apatites of a mixed composition. — Scientific News, 2003, No. 1, p. 151—155. (in Ukrainian)
292. *A. P. Shpak, V. L. Karbivskii, S. S. Smolyak, S. G. Kobzenko*. Thermogravimetric studies of metal-tetrahedral structures. — Nanosystems, nanomaterials, nanotechnologies, 2004, **2**, № 3, p. 927—933. (in Russian)
293. *E. I. Vorob'yev*. The polyphase type of decay of apatite. — Geochemistry. Reports of the Academy of Sciences, 2000, **370**, No. 5, p. 661—664. (in Russian)
294. *R. K. Rascvetaeva, A. P. Khomyakov*. Peculiarities of the structure of a new natural representative of a fluorapatite-delonee series. — Crystallography, 1996, **41**, No. 5, p. 831—834. (in Russian)
295. *F. Stoppa, Y. Liu*. Chemical composition and petrogenetic implications of apatites from some ultra-alkaline Italian rocks. — European Journal of Mineralogy, 1995, **7**, № 2, p. 391—402.
296. *P. Comodi, Y. Liu, F. Stoppa, A. R. Woolley*. A multi-method analysis of Si-, S- and REE-rich apatite from a new find of kalsilite-bearing leucitite (Abruzzi, Italy). — Mineralogical magazine, 1999, **63**, № 5, p. 661—672.
297. *E. A. Perseil, P. Blanc, D. Ohnenstetter*. As-bearing fluorapatite in manganiferous deposits from St. Marcel Praborna, Val d'Aosta, Italy. — Canadian Mineralogist, 2000, **38**, Part 1, p. 101—117.
298. *S. N. Ehrenberg, A. Dalland, P. H. Nadeau, E. W. Mearns, H. E. F. Amundsen*. Origin of chlorite enrichment and neodymium isotopic anomalies in Haltenbanken sandstones. — Marine and Petroleum Geology, 1998, **15**, № 5, p. 403—425.
299. *S. Warner, R. F. Martin, A. F. M. AbdelRahman, R. Doig*. Apatite as a monitor of fractionation, degassing, and metamorphism in the Sudbury Igneous Complex, Ontario. — Canadian Mineralogist, 1998, **36**, Part 4, p. 981—999.
300. *P. I. Karchevsky*. Minerals of Sr and REE in the carbonatites of the Lulecop deposit (Palabora, South Africa). — ZVMO, 2000, No. 1, p. 99—10. (in Russian)
301. *A. R. Faiziev, F. Sh. Iskandarov, F. G. Gafurov*. Mineralogical and genetic peculiarities of carbonatites of the Dunkeldyksky massif of alkaline rocks (Eastern Pamir). — ZVMO, 1998, No. 3, p. 54—57. (in Russian)
302. *S. Ouchani, J. C. Dran, J. Chaumont*. Exfoliation and diffusion following helium ion implantation in fluorapatite: implications for radiochronology and radioactive waste disposal. — Applied Geochemistry, 1998, **13**, № 6, p. 707—714.
303. *K. A. Farley*. Helium diffusion from apatite: General behavior as illustrated by Durango fluorapatite. — Journal of Geophysical Research — Solid Earth, 2000, **105**, № B2, p. 2903—2914.
304. *R. A. Wolf, K. A. Farley, D. M. Kass*. Modeling of the temperature sensitivity of the apatite (U-Th)/He thermochronometer. — Chemical Geology, 1998, **148**, № 1—2, p. 105—114.
305. *D. F. Stockli, K. A. Farley, T. A. Dumitru*. Calibration of the apatite (U-Th)/He thermochronometer on an exhumed fault block, White Mountains, California. — Geology, 2000, **28**, № 11, p. 983—986.
306. *A. E. Blythe, D. W. Burbank, K. A. Farley, E. J. Fielding*. Structural and topographic evolution of the central Transverse Ranges, California, from apatite fission-track, (U-Th)/He and digital elevation model analyses. — Basin Research, 2000, **12**, № 2, p. 97—114.
307. *K. R. Chamberlain, S. A. Bowring*. Apatite-feldspar U-Pb thermochronometer: a reliable, mid-range (Similar to 450 degrees C), diffusion-controlled system. — Chemical Geology, 2001, **172**, № 1—2, Sp. Iss. SI, p. 173—200.

308. *B. Jakni, G. Poupeau, M. Sosson, P. Rossi, J. Ferrandini, P. Guennoc*. Cenozoic denudations in Corsica: an analysis from apatite fission-track thermochronology. — Comptes Rendus de L Academie Des Sciences Serie II Fascicule A — Sciences de La Terre et Des Planetes, 2000, **331**, № 12, p. 775—782.
309. *V. I. Sotnikov, V. A. Ponomarchuk, A. N. Berzina, A. P. Berzina, V. Y. Kiseleva, I. P. Morozova*. Evolution of Sr-87/Sr-86 in erupted rocks of porphyry copper-molybdenum ore clusters (Based on studies of accessory apatite). — Geologiya I Geofizika, 2000, **41**, № 8, p. 1112—1123.
310. *S. J. Mojzsis, G. Arrhenius*. Phosphates and carbon on Mars: Exobiological implications and sample return considerations. — Journal of Geophysical Research. — Planets, 1998, **103**, № E12, p. 28495—28511.
311. *T. F. Cooney, E. R. D. Scott, A. N. Krot, S. K. Sharma, A. Yamaguchi*. Vibrational spectroscopic study of minerals in the Martian meteorite ALH84001. — American Mineralogist, 1999, **84**, № 10, p. 1569—1576.
312. *J. C. Bridges, M. M. Grady*. A halite-siderite-anhydrite-chlarapatite assemblage in Nakhla: Mineralogical evidence for evaporites on Mars. — Meteoritics & Planetary Science, 1999, **34**, № 3, p. 407—415.
313. *V. M. Goldschmidt.* The principles of distribution of chemical elements in minerals and rocks. — J. Chem. Soc., 1937, p. 655 —673.
314. *H. C. Skinner.* In praise of phosphates, or why vertebrates chose apatite to mineralize their skeletal elements. — International Geology Review, 2000, **42**, № 3, p. 232—240.
315. *S. M. Kravchenko*. Calcium-phosphorus ratio in geochemical landscapes and its influence on human health. — Geoecology, No. 1, 1998, p. 30—36. (in Russian)
316. *E. W. White*. Biomaterials innovation: it's a long road to the operating room. — Materials Research Innovations, 1997, **1**, № 1, p. 57—63.
317. *W. F. Le Jong.* La Substance Minerale Dans Les Os. — Rec. Tr. Chim., 1926, **43**, p. 445—448.
318. *A. S. Posner, A. Perloff and A. F. Diorio*. Refinement of the hydroxyapatite structure. — Acta Cryst., 1958, **11**, p. 308—309.
319. *M. I. Kay, R. A. Young, and A. S. Posner*. Crystal structure of hydroxyapatite. — Nature, 1964, **204**, p. 1050—1052.
320. *R. A. Young and J. C. Elliot*. Anomic-scale bases for several properties of apatites. — Arch. Oral. Biol., 1966, **11**, p. 669—707.
321. *R. A. Young.* Dependence of apatites properties on crystal structural details. — Trans. N. Y.Acad. Sci., 1967, **29**, p. 949—959.
322. *J. M. Stutman, J. D. Termine, and A. S. Posner*. Vibrational spectra and structure of the phosphate ion in some calcium phosphates. — Trans. N. Y. Acad. Sci., 1965, **27**, p. 669—675.
323. *H. Wondratschek*. Untersuchungen zur Kristallchemie der Blei-Apatit (Piromorphit). — N. Jahrb. Mineral, 1963, **99**, p. 113—160.
324. *H. Bauer.* Über Cine Apatit-Aruge Verbindung der Formel $Ba_{10}(PO_4)_6(BO_4)_2$. — Angew. Chem., 1959, **71**, 374.
325. *J. S. Stevenson and L. S. Stevenson.* Fluorine content of microsauer teeth from the carboniferous rocks of Joggins, Nova Scotia. — Science, 1966, **154**, p. 1548—1550.
326. *C. A. L. Basset*. Biologic significance of piezoeletricity. — Calc., 1962, Tiss. Res. 1, p. 252—272.
327. *M. H. Shamos and L. S. Lavine*. Physical bases for bioelectrical affects in mineralized tissues. — Clin. Orthoped., 1964, **35**, p. 177—188.
328. *J. E. Eastje.* The chemical composition of bone. In: Biochemists Handbook / Edited By G. Long. Princeton, N. J. Yan. — Nostrand, 1961, p. 715—720.
329. *G. Montel*. Conceptions nouvelles sur la physicochimie des phosphates de structure apatique. — Bull. Soc. Chim., 1968, Special No, p. 1693—1700.
330. *R. Z. Legeros, O. R. Trautz, J. P. Legeros, and E. Kklein*. Carbonate substitution in the apatite structure. In: Collog. Intern. Sur Les Phosphates Mintraux Solidas. — Touluse, 1967, p. 66—72.

331. *J. C. Trombe, G. Bonel and G. Montel*. Influence de la chaux sur la formations d`apatites carbonatecs a haut temperature. — Compl. Rend., 1967, **263**, p. 1113—1116.
332. *G. Bonel and G. Montel*. Etude comparee des apatites carbonatees obtenues par differentes methodes de synthese. In: Redaction of Solids / Edited By G. M. Schwab. — Amsterdam: Elsevier, 1965.
333. *W. F. Neuman and B. J. Mulryan*. Syntetic hydroxyapatite crystals. III. The carbonate system. — Calc. Tiss. Res., 1967, **1**, p. 94—104.
334. *D. Carlstrom*. X-ray crystallographic studies on apatites and calcified strructures. — Acta Radiol., 1955, **121**, p. 1—59.
335. *P. D. Frazier*. X-ray diffraction analyses of human enamel containing different amounts of fluoride. — Arch. Oral. Biol., 1967, **12**, p. 35—42.
336. *C. Wolpers*. Elektronen-microskopie der derivate. — G. Med., 1949, **2**, 327.
337. *Z. Molnar*. Additional observations on bone crystal dimentions. — Clin. Orthoped., 1960, **17**, p. 38—42.
338. *A. Ascenzi and E. Bonucci*. The osteoid calcification as revealed by the electron microscope. In: Calcified Tissues: Proc. Third Europian Symp. on Calcified Tissues / edited by H. Fleisch, J. J. Blackwood and M. Owen. — New York: Springer, 1966.
339. *J. Fernandez-Moran and A. Engstrom*. Electron microscopy and X-ray diffraction of bone. — Biochim. Biophys. Acta, 1957, **23**, p. 260—264.
340. *W. C. Durning*. Submicroscopic structure of frozen-dried epiphysical plate and adjacent spongiosa of the rat. — J. Ultrastruct. Res., 1958, **2**, p. 245—260.
341. *R. A. Robinson and M. L. Watson*. Collagencrystal relationschips in bone as seen in the electron microscope. — Anat. Record, 1952, **114**, p. 383—410.
342. *R. A. Robinson and M. L. Watson*. Cristalcollagen relatonships in bone as observed in the electron microscope. III. Cristal and collagen morphology as a function of age. — Ann. N. Y. Acad. Sci., 1955, **60**, p. 596—628.
343. *E. Johansen and H. F. Parks*. Electron microscopic observation on the three dimensional morphology of apatite crtystallites of human dentin and bone. — J. Biophys. Biohem. Cyttol., 1966, **7**, p. 743—746.
344. *A. S. Posner, E. D. Eanes, R. A. Harper and I. Zipkin*. X-ray diffraction analisis of the affact of fluoride on human bone apatite. — Arch. Oral. Biol., 1963, **8**, p. 549—570.
345. *M. U. Nylen, E. D. Eanes and K. A. Omnel*. Crystal grows in rat enamel. — J. Cell Biol., 1963, **18**, p. 109—123.
346. *A. Engstrom and R. Zetterstrom*. Studies on the ultrustructure of bone. — Exp. Cell. Res., 1951, **2**, p. 2235—2247.
347. *J. B. Finean and A. Engstrom*. The low angle scatter of X-rays from bone tissue. — Biochim. Biophys. Acta, 1953, **11**, p. 178—189.
348. *Z. Molnar*. Development of the parietal bone of young mice. I. Crystals of bone mineral in frozen-dried preparations. — J. Ultrastruct. Res., 1959, **3**, p. 39—45.
349. *J. D. Currey*. Three analogia to explain the mechanical properties of bone. — Biotheology, 1964, **2**, p. 1—10.
350. *J. D. Termine, I. Pullman and A. S. Posner*. Electron spin resonance study of irradiated bone and its constituens. — Arch. Biochem. Biophys., 1967, **122**, p. 318—330.
351. *P. T. Levine, M. J. Glimcher, J. M. Seyer, J. I. Huddleston and J. W. Hein*. Non collagenous naturre of the protein of shark enamel. — Science, 1966, **154,** p. 192— 1194.
352. *J. Menczel, A. S. Posner and R. A. Harper*. Age chenges in the crystallinity of rat bone apatite. — Israel J. Med. Sci., 1965, **1**, p. 251—252.
353. *R. A. Robinson*. The structural organization of bone tissue. In: Structural organization of the skeleton / Edited By D. Bergama and R. A. Mitch. — New York: N. Found. Birth. Defects. Orig. Art. Ser., 1966; **17**, №1, p. 40—44, No. 1.

354. *R. E. Rowland*. Exchangeable bone calcium. — Clin. Orthoped., 1966, **49**, p. 133—248.
355. *W. F. Neuman and M. W. Neuman*. The chemical dynamics of bone mineral. — Chicago: Univ. of Chicago Press, 1958.
356. *R. A. Harper and A. S. Posner*. Measurement of non-crystalline calcium phosphate in bone mineral. — Proc. Soc. Exptl. Biol. Med., 1966, **122**, p. 1137— 1142.
357. *J. D. Termine and A. S. Posner*. Amorphous/crystalline interrelationships in bone mineral. — Calc. Tiss. Res., 1967, **1**, p. 8—23.
358. *J. D. Termine and A. S. Posner.* Infrared analysis of rat bone: age dependency of amorphous and crystalline mineral fractions — Science, 1966, **153**, p. 1523—1525.
359. *M. L. Watson and R. A. Robinson*. Collagen crystal relationships in bone. II. Electron microscope study of basic calcium phosphate crystals. — Am. J. Anal., 1953, **93**, p. 23—60.
360. *E. D. Eanes, I. H. Gillessen and A. S. Posner*. Intermediate states in the precipitation of hydroxyapatite. — Nature, 1965, **208**, p. 365—367.
361. *J. C. Weber, E. D. Eanes and R. J. Gerdes*. Electron microscope study of non crystalline calcium phosphate. — Arch. Biochem. Biophys, 1967, **120**, p. 723—724.
362. *E. D. Eanes, I. H. Gillessen and A. S. Posner*. Mechanism of conversion of non-crystalline calcium phosphate to crystalline Hydroxyapatite. — Crystal Growth, Perganton Press, Oxford, 1967, p. 373—376.
363. *E. D. Eanes, R. A. Harper, I. H. Gillessen and A. S. Posner*. An amorphous component in bone mineral. In: Four European Symp. on Calcified Tissues / Edited By P. J. Gaillared, A. Van Den Hoof, and R. Steendijk. — Amsterdam: Excerpta Med., 1966, p. 24—26.
364. *A. Bienenstock and A. S. Posner*. Calculation of the X—ray intensities from arrays of small crystallites of hydroxyapatite. — Arch. Biochem. Biophys., 1968, **124**, p. 604—607.
365. *E. D. Eanes and A. S. Posner*. Kinetics and mechanism of conversion of non-crystalline calcium phosphate to crystalline hydroxyapatite. — Trans. N. Y. Acad. Sci., 1965, **28**, p. 233—241.

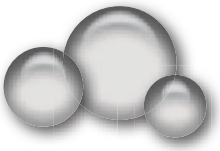

CONTENTS

Монографія присвячена синтезу, електронній структурі, властивостям і застосуванню апатитів та апатитоподібних систем. Містить значний фактичний матеріал з вивчення атомної та електронної будови конкретних систем. Розглянуто сучасні уявлення про структуру кристалічних та невпорядкованих апатитоподібних систем, а також фізико-хімічні, медико-біологічні, екологічні та технологічні аспекти їх застосування. Особливу увагу приділено теоретичним і прикладним розробкам в області функціональних апатитоподібних наноматеріалів.

Для фахівців в області фізики та хімії апатитів, що займаються дослідженням, розробкою та застосуванням нових матеріалів, а також викладачів, аспірантів і студентів відповідних спеціальностей.

Наукове видання

НАЦІОНАЛЬНА АКАДЕМІЯ НАУК УКРАЇНИ
ІНСТИТУТ МЕТАЛОФІЗИКИ
ім. Г.В. КУРДЮМОВА НАН УКРАЇНИ

КАРБІВСЬКА Любов Іванівна
КАРБІВСЬКИЙ Володимир Леонідович

АПАТИТИ І ТЕТРАОКСИДНІ СПОЛУКИ

Англійською мовою

Видається в авторській редакції

Художнє оформлення *Є.О. Ільницького*
Технічне редагування *Т.М. Шендерович*
Комп'ютерна верстка *О.А. Бурдік*

Підп. до друку 13.09.2019. Формат 70 × 100/16.
Гарн. Minion Pro. Ум. друк. арк. 18,85. Обл.-вид. арк. 19,98.
Тираж 300 прим. Зам. № 5722.

Видавець і виготовлювач Видавничий дім "Академперіодика" НАН України
01004, Київ, вул. Терещенківська, 4

Свідоцтво про внесення до Державного реєстру суб'єктів
видавничої справи серії ДК № 544 від 27.07.2001 р.